Thèse de doctorat

Spécialité : Océanographie Physique

présentée par

Rudy Magne

en vue d'obtenir le grade de

Docteur de l'Université du sud Toulon-Var

Réflexion et diffusion des vagues par une topographie sous-marine

soutenue le 26 Septembre 2005 devant le jury composé de :

M. Stephan Grilli	Président du jury	University of Rhode Island, E-U
M. Frédéric Dias	Rapporteur	ENS, Cachan
M. Christian Kharif	Rapporteur	IRPHE, Marseille
M. Ardhuin Fabrice	Directeur scientifique	SHOM/CMO, Brest
M. Vincent Rey	Directeur de thèse	LSEET-LEPI, Toulon

Résumé

A l'approche de la côte la houle est fortement modifiée par la topographie sous-marine. Si la réfraction est souvent le phénomène majeur, il existe d'autres phénomènes moins connus comme la réflexion ou plus généralement la diffusion des vagues par le fond qui peuvent se révéler tout aussi importants. La modélisation des vagues dans ces zones est d'autant plus délicate que les courants peuvent y être importants, ce qui complique la propagation de la houle. La diffusion des vagues par la topographie sous-marine est étudiée par une approche spectrale via un terme de source facilement introduit dans les modèles de vagues spectraux opérationnels. Cette approche peu coûteuse numériquement, représente la topographie par son spectre de variance. Elle se révèle particulièrement précise lorsque les amplitudes du fond sont faibles, et s'applique aussi à des fonds localisés. Pour de grandes amplitudes, comme un canyon sous-marin, l'évolution des vagues est bien représentée avec un modèle elliptique déterministe aux modes couplés, mettant en avant l'importance de la réflexion dans le processus de transmission au-dessus de cet obstacle. L'effet du courant sur la diffusion des vagues est ensuite examiné. Le décalage des fréquences résonantes pour des vagues se propageant au-dessus d'un fond sinusoïdal en présence d'un courant uniforme, calculé théoriquement, est mis en évidence expérimentalement lors d'une campagne de mesure en bassin. La prise en compte du courant dans le terme de source permet la mise en évidence des effets du courant sur la diffusion des vagues par des fonds aléatoires. Des expériences numériques pour des vagues se propageant au-dessus de dunes sous-marines balayées par des courants de marée importants (bathymétrie typique en Mer du Nord) ont montré un décalage important de la direction moyenne de propagation ainsi qu'un fort élargissement du spectre directionnel.

Abstract

Waves entering in shallow water are largely modified by the submarine topography. If refraction plays the major role in this process, other less known phenomena like wave reflection or more generally wave-bottom scattering can be significant. The Modelling of wave propagation in such areas is as much complicated by strong currents, particularly tidal currents. Wave-bottom scattering is investigated from a spectral approach with a source term, easily introduced in operationals spectrals wave models. This numerically efficient approach is found to be accurate, particularly when the bottom amplitudes are small, and is also valid for localized scatterers. For large amplitude topographies, as a submarine canyon, the wave evolution is accurately represented with a deterministic coupled-mode elliptic model, and the importance of the reflection in the transmission process over this obstacle is highlighted. The current effect on the wave-bottom scattering is then investigated. The shift of the resonant wave frequencies for waves propagating over sinusoidal bottom in presence of a uniform current is calculated theoretically, and verified experimentally in the laboratory. A theory for the scattering of waves in the presence of a uniform current is developped for application to the continental shelf. Numerical experiments for waves propagating over sand waves with large tidal currents (typical bathymetry in the North Sea) revealed an important shift for the mean wave direction, and a significant directional broadening for the surface spectrum.

Ma thèse, financée par la DGA, s'est déroulée principalement au SHOM à Brest, mais aussi à Toulon et à Monterey aux Etats-Unis. J'adresse mes remerciements sincères à tous ceux qui ont contribué de près ou de loin à mon travail de thèse :

Merci à Vincent Rey qui a su diriger ma thèse, souvent à distance, mais toujours de manière efficace et pertinente, apportant une vision globale à mon travail. J'ai apprécié aussi le temps passé à Toulon, notamment au cours de l'expérience en bassin à houle pendant laquelle nous avons pu collaborer au quotidien.

Merci à Fabrice Ardhuin qui a su de manière remarquable encadrer mon travail. La qualité de cet encadrement doit être soulignée pour sa richesse scientifique débordante et sa disponibilité au quotidien malgré un emploi du temps parfois surchargé. J'en profite également pour féliciter la qualité de ses prévisions sur le Finistère.

Merci au SHOM, qui en m'accueillant dans ses locaux, m'a offert des conditions de travail de qualité, et à toute l'équipe du CMO, laboratoire dans lequel j'évoluais.

Merci à Tom Herbers qui m'a accueilli à la Naval Postgraduate School à Monterey pendant plusieurs mois. Il m'a apporté l'occasion de participer à l'expérience in situ NCEX à San Diego et m'a éclairé sur mon travail par son recul scientifique.

Merci à Kostas Belibassakis pour sa collaboration scientifique et ses conseils précieux au cours de la campagne NCEX, et aussi tout simplement pour sa personne.

Merci à Paul Jessen, Scott Peak, Steve Lenz, Yves Goyatton, Bill O'Reilly, Steve Elgar, Jim Thomson, l'équipe de Scripps et aussi Patrice.

Merci aux rapporteurs Frédéric Dias et Christian Kharif et le président du jury, Stephan Grilli qui m'ont apporté leur point de vue extérieur et leurs encouragements.

Merci enfin à toutes les personnes qui m'ont entouré pendant cette thèse aussi bien dans le cadre scientifique qu'à l'extérieur. L'équipe brestoise Francois et Mel, Nico et Blanca, Martin, Anita, Emilie, Steven, Philippe, Ben, Steph, JF, Alex, Xavier, Boris, Guillaume et les autres. Mais aussi les extérieurs, Aymeric, Pascale, Régis, Deb, Pierro, JB, Hervé.

Pour conclure, je tiens à réitérer mes remerciements à mes deux encadrants Vincent et Fabrice, pour leurs qualités personnelles, tant au point de vue scientifique qu'au point de vue humain, pour l'intérêt particulier qu'ils ont su me témoigner tout au long de ce riche parcours.

Table des matières

Table des figures

Chapitre 1

Introduction

1.1 Problématique

Les vagues sont communément associées à leur déferlement sur la plage ou sur des rochers. Ce n'est en fait que l'aboutissement de leur périple commencé il y a plusieurs heures, ou plusieurs jours, à des dizaines voire des milliers de kilomètres de là. Le vent, soufflant sur la surface de la mer en exerçant des pressions inégales à cette interface donne naissance aux vagues. Au début infiniment petites, celles-ci croissent avec le temps, en fonction de la force du vent et de la distance sur laquelle celui-ci souffle. Les vagues ainsi formées au large, interagissent entre elles de manière non-linéaire, transférant de l'énergie vers les plus basses fréquences. Commence alors une longue route où ces vagues se propagent "sans contrainte", d'autant plus vite que leur période est importante, induisant à leur passage un mouvement orbital du fluide au-dessous de la surface, jusqu'à une profondeur égale environ à la moitié de la longueur d'onde. A l'approche de la côte ce mouvement est contraint par le fond, réduisant la vitesse de propagation et modifiant la direction de propagation de la houle par réfraction et diffraction. Le fond en fonction de sa nature introduit un effet de frottement induisant une dissipation de l'énergie de la houle. Avant d'arriver sur la plage et de déferler, les propriétés directionnelles des vagues peuvent également être modifiées par diffusion ou réflexion lorsque la bathymétrie change brutalement ou simplement par interactions avec des variations du fond à l'échelle de la longueur d'onde des vagues, comme par exemple les dunes de sable présentes dans les zones à forts courants de marée.

Plusieurs méthodes permettent de représenter la propagation des vagues. L'approche déterministe permet une description du mouvement à l'échelle de la période et de la longueur d'onde, en resolvant la phase des ondes. Une telle description est particulièrement adaptée aux zones littorales. Les modèles d'agitation pour les ports, de propagation de tsunamis ou simplement de propagation de la houle du large vers la côte en sont quelques exemples. Au large, des appareils de mesure permettent de donner des conditions initiales aux modèles déterministes, en calculant à partir de la répartition spectrale de l'énergie, une hauteur et une période significative, ainsi qu'une direction de propagation. L'approche spectrale considère le champ de vagues à des échelles de temps plus grandes, et pour cela fait appel à une moyenne sur la phase des vagues. L'état de mer est alors représenté de manière stochastique par des densités spectrales plutôt que par des dénivellations, perdant alors l'information de phase. Ces modèles, basés sur une équation d'évolution du spectre d'action, représentant la propagation, permettent de traiter de manière plus ou moins efficace par des termes de source, la génération des vagues par le vent, les interactions non-linéaires des vagues, la dissipation des vagues par le fond et en surface. Les modèles de prévisions de vagues de grandes échelles, s'intéressant à une représentation d'ensemble des vagues, utilisent cette dernière approche avec comme données d'entrées les champs de vent ou les spectres de surface.

A l'heure actuelle, le phénomène de réflexion des vagues par la topographie sous-marine est relativement bien connu et surtout étudié avec des modèles déterministes, en particulier en deux dimensions, et avec des modèles de réfraction/diffraction elliptiques. Les modèles spectraux opérationnels ne prennent pas en compte la réflexion des vagues par le fond, ni de manière plus générale, la diffusion des vagues par le fond. L'objet du travail présenté dans ce manuscrit est d'étudier la diffusion des vagues par le fond et son impact sur la propagation des vagues, entre autres, via une approche stochastique qui présente l'avantage de pouvoir être introduite dans les modèles de vagues spectraux. Les zones à fort potentiel de réflexion comme les dunes de sables sous-marines, créées par des forts courants de marée, nous ont conduit également à étudier l'influence d'un courant sur cette diffusion.

Quelques définitions de notions élémentaires sont données dans les paragraphes suivants, avant de faire un état de l'art sur la diffusion de Bragg et de présenter les différentes parties de cette étude.

1.2 Transformations par effets bathymétriques

1.2.1 Réflexion, diffusion, résonance de Bragg

Considérons une topographie bidimensionnelle (2D) présentant des irrégularités suivant une composante horizontale (rides, dunes de sables, barres), et uniforme suivant la deuxième composante horizontale. Si la profondeur est suffisamment faible par rapport à la longueur d'onde des vagues, de l'ordre de la moitié de leur lon-

gueur d'onde ou moins, les vagues vont interagir avec le fond par modification de la vitesse du fluide. En effet, le mouvement des vagues est caractérisé à l'intérieur du fluide par des vitesses orbitales qui décroissent avec la profondeur, et deviennent négligeables pour des profondeurs supérieures à la demi-longueur d'onde des vagues. Les irrégularités du fond sont alors vues par les vagues comme des "obstacles", qui vont réfléchir une partie des vagues incidentes. Cette réflexion est très faible pour des petites irrégularités. Cependant, pour des fonds périodiques, lorsque la longueur d'onde des vagues incidentes est égale à deux fois la longueur d'onde du fond, on observe une amplification de la réflexion. Ce phénomène est connu sous le nom de résonance de Bragg. Il s'explique par une concordance de phase entre l'onde incidente et l'onde réfléchie. Les ondes réfléchies interfèrent alors de manière constructive, ce qui mène à une amplification de la réflexion.
La résonance de Bragg se généralise en trois dimensions (3D), mettant en jeu l'interaction résonante de deux composantes de surface dont les directions sont quelconques, et une composante du fond, satisfaisant la relation $\mathbf{k}' + \mathbf{l} = \mathbf{k}$. Pour un fond irrégulier, le spectre du fond remplit tout l'espace spectral et il existe toujours un ensemble de valeurs de $\mathbf{l}$ permettant une interaction avec tout vecteur $\mathbf{k}$. Les vecteurs $\mathbf{k}'$ participant à cette interaction correspondent à la même fréquence et, en absence de courant, sont donc sur le cercle (k, θ), avec θ l'angle d'incidence de l'onde, représenté sur la figure 1.1 empruntée à Ardhuin et Herbers (2002). Ces vagues sont diffusées par interactions résonantes. On parle alors de diffusion de Bragg. Cette diffusion peut se faire vers l'avant. Le spectre de surface s'en trouve étalé en direction. Pour certaines configurations de fond/surface (k/l proche de 0.5), on peut également observer de la diffusion par l'arrière, correspondant à la réflexion observée en 2D. La figure (1.2) donne un exemple de spectres du fond (Caroline du Nord (DUCK94, Sandy Duck, SHOWEX) et Mer du Nord au large de Dunkerque) intégrés en direction illustrant les différentes échelles de contribution pour la diffusion de Bragg. Les valeurs du spectre du fond sont beaucoup plus importantes pour le fond en Mer du Nord, prédisposant à une plus large diffusion. En particulier, la contribution à l'échelle de la rétro-diffusion ($k/l \simeq 0.5$) est significative, cent fois supérieure aux topographies de Caroline du Nord.

La résonance de Bragg décrite ici ne tient compte que de la diffusion des vagues au premier ordre, c'est-à-dire faisant interagir une composante du fond et deux composantes de surface. Aux ordres supérieurs, on trouve des interactions résonantes impliquant deux composantes de surface et deux composantes du fond (fonds doublement périodiques, Belzons et al., 1991 et Guazzelli et al., 1992 ; Rey et al, 1996), et des interactions résonantes impliquant trois composantes de surface et une com-

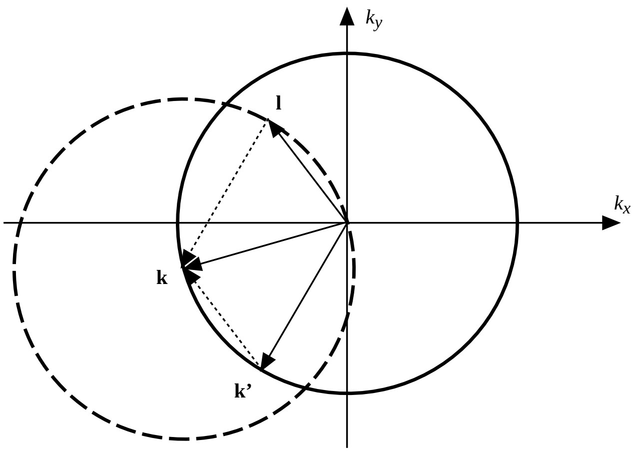

FIG. 1.1 – Condition de résonance pour la diffusion de Bragg du premier ordre vague-topographie. L'interaction entre une vague de vecteur d'onde $\mathbf{k}'$ et une ondulation du fond de vecteur d'onde $\mathbf{l}$ crée une vague diffusée de vecteur d'onde $\mathbf{k} = \mathbf{k}' + \mathbf{l}$. Pour $\mathbf{k}$ fixe, les $\mathbf{k}'$ et $\mathbf{l}$ résonants sont sur les cercles en traits continus et pointillés, respectivement.

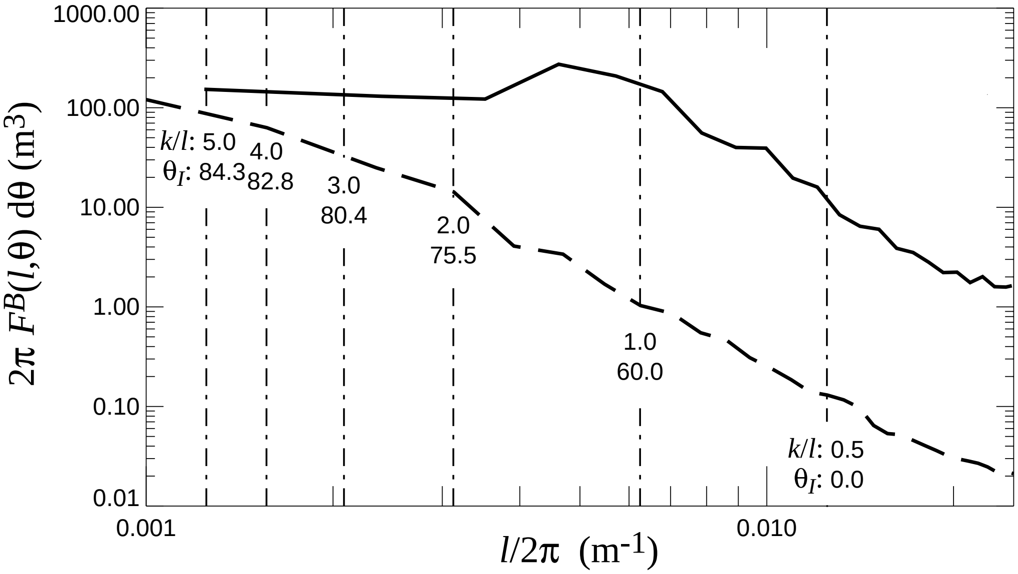

FIG. 1.2 – Exemple de deux spectres du fond (Caroline du Nord en ligne discontinue, et Mer du Nord en ligne continue) intégrés sur les directions. Les lignes verticales indiquent les échelles du fond responsables de la diffusion pour une houle de 0.08Hz, pour différents angles d'incidence θ_I. Figure empruntée à Ardhuin et Herbers (2002) pour le spectre en Caroline du Nord

posante du fond, traduisant la non-linéarité de la surface. Liu et Yue (1998) ont mis en évidence l'importance de ces interactions d'ordres supérieurs. Des détails sur ces interactions d'ordres supérieurs sont donnés à la fin du deuxième chapitre.

1.2.2 Réfraction, diffraction

La réfraction peut être expliquée à la manière de Longuet-Higgins (1967). Comme la vitesse de phase des vagues augmente avec la hauteur d'eau, les parties d'une crête de vague se trouvant au-dessus des eaux plus profondes se propagent plus vite que les parties de la crête de la même vague se trouvant au-dessus des eaux moins profondes. Lors de la propagation, un tel front de vague tourne progressivement vers les eaux moins profondes. Les crêtes des vagues finissent alors leur voyage pratiquement parallèles à la côte en arrivant sur une plage.

Pour des isobathes parallèles, cette caractéristique est décrite par la loi de Snel (suivant l'orthographe hollandaise), $\sin\theta_i/C = cste$, avec θ_i l'angle entre la crête des vagues et les isobathes, et C la vitesse de phase, (figure 1.2.2). Pour des fonds bidimensionnels mais faiblement variables, la théorie des rayons, décrite dans le quatrième chapitre, est utilisée.

La diffraction peut se caractériser par un transfert de l'énergie lorsque le gradient horizontal de la hauteur des vagues est important, comme par exemple à l'entrée d'un port protégé par une digue. La zone se situant derrière la digue reçoit alors de l'énergie des vagues le long des crêtes, se traduisant par un changement de direction de la houle, adaptant ainsi le champ de vagues. Pour des gradients bathymétriques suffisamment importants, comme des monts sous-marins prononcés, la théorie des rayons appliquée à des vagues monochromatiques, prévoit des caustiques, c'est-à-dire des points de convergence des rayons de houle, se traduisant théoriquement par une amplitude de vague localement infinie. La diffraction empêche ces singularités car elle a tendance à lisser les gradients d'amplitude.

Le troisième chapitre de ce manuscrit s'intéresse à la propagation des vagues au-dessus d'un canyon sous-marin. Le changement de profondeur à l'approche du canyon s'apparente au changement d'indice en optique géométrique. Les vagues incidentes, d'angle θ_i par rapport à la normale du canyon, sont en partie réfléchies (θ_r) et en partie transmises (θ_t), voir figure 1.2.2. Il existe un angle critique θ_B, appelé angle de Brewster, tel que, pour $\theta_i > \theta_B$, il n'y a plus de transmission. Pour $\theta_i < \theta_B$, la réfraction correspond alors à l'onde transmise, la réflexion correspondant à l'onde réfléchie. Pour $\theta_i > \theta_B$, toute l'énergie est piégée par le canyon, il n'y a plus que de la réfraction. En réalité la transition autour de cette valeur n'est pas aussi brutale, il existe un peu de transmission au-delà de cet angle critique que l'on peut interpréter

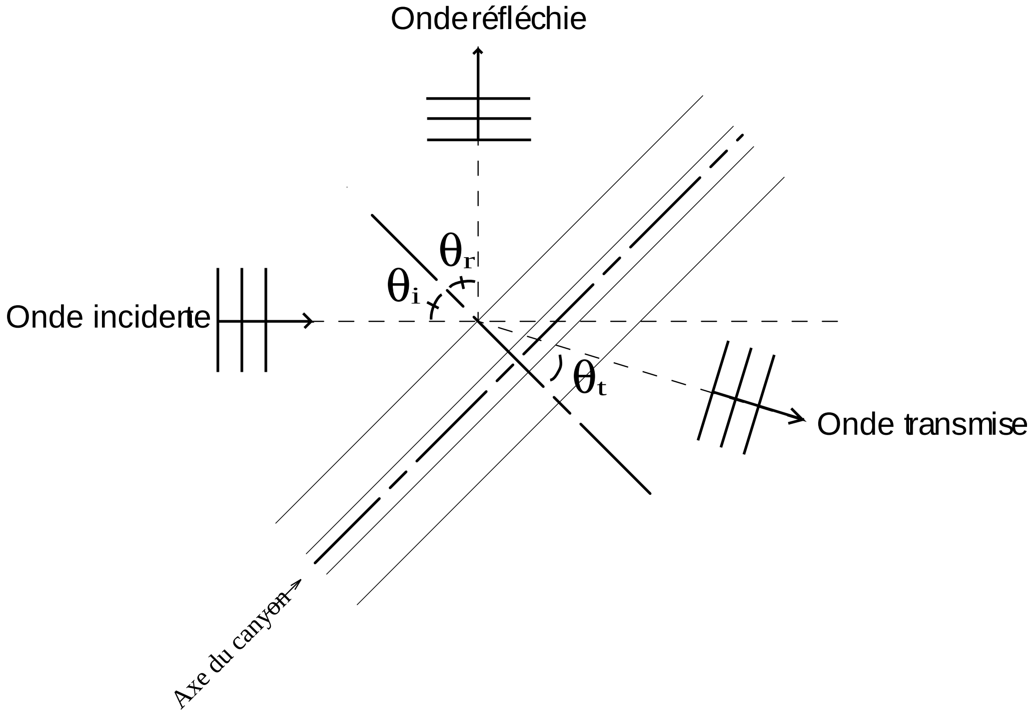

FIG. 1.3 – Définitions

comme le résultat de la diffraction ou d'un effet tunnel, analogue à la transmission d'ondes à travers un puits de potentiel.

1.3 Diffusion de Bragg : Etat de l'art

Hasselmann (1966) proposa une théorie statistique générale pour l'évolution de vagues aléatoires non-linéaires en présence de "forçages" externes comme le vent et la topographie du fond. En supposant des conditions homogènes en espace (c'est-à-dire des vagues et un spectre du fond uniforme), Hasselmann a donné une première expression du taux d'évolution du spectre. A l'ordre le plus faible en pente du fond, deux composantes de vagues avec la même fréquence ω, mais de nombres d'onde différents $\mathbf{k}$ et $\mathbf{k}'$ échangent de l'énergie, par interaction triadique résonante, avec une composante du fond dont le nombre d'onde est la différence $\mathbf{l} = \mathbf{k} - \mathbf{k}'$ (voir figure 1.1). Ce processus de diffusion de Bragg redistribue l'énergie dans le spectre directionnel pour chaque fréquence. Il est donc potentiellement important, au moins pour les propriétés directionnelles des vagues, favorisant la rétro-diffusion pour des rapports k/l proche de 0.5. Long (1973) refit le calcul de Hasselmann pour expliquer la décroissance de la houle observée pendant la campagne JONSWAP de 1969 en Mer du Nord (Hasselmann et al., 1973). Toutefois, Richter et al. (1976) montrèrent grâce à de nouveaux levés hydrographiques, que l'amplitude des perturbations du fond ne permettait pas d'expliquer la décroissance des vagues observée par la réflexion des vagues. Par ailleurs, Ardhuin et Herbers (2002) ont montré que le coefficient de diffusion de Long (1973) était faux, trop grand d'un facteur 4.

Pour une meilleure compréhension du phénomène de diffusion, Davies (1980, 1982) réduisit le problème à deux dimensions, et proposa une théorie déterministe, basée sur un développement en perturbations pour calculer la réflexion de vagues monochromatiques se propageant au-dessus d'un fond sinusoïdal. Motivé par les travaux théoriques de Davies et par les applications possibles en matière de protection du littoral, Heathershaw (1982) a mis en évidence expérimentalement le phénomène de résonance de Bragg pour des barres sinusoïdales, la relation $\mathbf{l} = \mathbf{k} - \mathbf{k}'$ se réduisant en 2D à $2k/l = 1$ (voir aussi Davies et Heathershaw, 1984, pour l'évolution des barres de sable). La méthode par perturbations utilisée par Davies (1982) est limitée à des faibles réflexions. En effet, le coefficient de réflexion théorique est lié linéairement au nombre de barres, et devient donc plus grand que 1 pour un grand nombre de barres, ce qui n'est pas possible car l'énergie doit être conservée. Par un développement aux échelles multiples, Mei (1985) proposa une théorie valide à la résonance, et en accord avec les données expérimentales de Davies et Heathershaw. Kirby (1988) étendit la théorie de Mei en présence de courant, et souligna son influence sur la modification de la relation de résonance, décalant les fréquences résonantes.

Ces études réalisées sur la possibilité d'obtenir de fortes réflexions des vagues par des barres furent motivées par une application en terme de protection du littoral. Cependant, cette protection du littoral envisagée par des barres en amont de plage (Bailard et al. 1990 et 1992 ; observée par Elgar et al., 2003) fut mise en doute par des expériences numériques de O'Hare et Davies (1993b, voir aussi O'Hare et Davies, 1992, 1993a pour la théorie), qui ont révélé que l'amplitude des vagues en aval des barres n'était pas toujours atténuée. En effet, la réflexion de la plage, même faible, peut modifier les conditions de résonance et mener à une amplification de l'amplitude des vagues en aval des barres. Yu et Mei (2000) ont confirmé ces expériences par la théorie.

Sans utiliser un développement en perturbations, Berkhoff (1972) proposa une équation en pente douce du fond, basée sur une intégration verticale de l'équation de Laplace. Cette équation simplifiée aux composantes horizontales, permet de traiter la réfraction et la diffraction, propriété non-intégrée dans les modèles de réfraction classiques. Cette équation, une fois parabolisée (Radder, 1979), se révèle très efficace pour traiter les problèmes de propagation dans les zones littorales tout en incluant des effets de diffraction qui sont importants au voisinage d'ouvrages et dans les ports. Dans sa version elliptique, elle permet également de représenter la réflexion. Cependant, la version originale proposée par Berkhoff ne suffit pas pour représenter la réflexion des vagues par des fonds rapidement variables, et ne donne pas des coefficients de réflexion exacts dans la limite des faibles pentes (Meyer, 1979). Pour traiter la réflexion des vagues par un système de barres, Kirby (1986) étendit cette équation, en décomposant la profondeur en deux échelles de variation, lente et rapide, et permit ainsi de représenter plus précisément la réflexion des vagues au-dessus des fonds tels que des barres sinusoïdales. Pour des fonds plus complexes, comme les fonds doublement périodiques, faisant intervenir la résonance de Bragg aux ordres supérieurs, l'équation de Berkhoff (Berkhoff, 1972 ; Kirby, 1986), et les développements en perturbations et à deux échelles (longueur d'onde et longueur du fond variable) (Mei, 1985) restent peu précis. Ces réflexions de Bragg d'ordres supérieurs furent étudiées par Guazzelli et al. (1992), en confrontant avec succès un algorithme de discrétisation du fond en séries de marches (Rey, 1992) à des données expérimentales (Belzons et al, 1991). Rey et al (1996) ont proposé par la suite un développement faisant intervenir une échelle supplémentaire intermédiaire pour traiter la réflexion sous-harmonique pour les fonds à deux composantes sinusoïdales. Massel (1993) (voir aussi Chamberlain et Porter, 1995 et de nombreux autres auteurs) étendit l'équation de Berkhoff en gardant les termes du fond d'ordres supérieurs (pente du fond au carré et courbure) et les modes évanescents, auparavant négligés. Sans introduire d'échelles multiples comme Kirby (1986), cette équation de Berkhoff étendue permet de représenter les variations rapides comme les fonds sinusoïdaux, mais aussi les fonds doublement périodiques. Ces extensions de l'équation de Berkhoff restent cependant attachées à leur hypothèse de départ, qui suppose un fond localement plat. Enfin, Athanassoulis et Belibassakis (1999) ont proposé un modèle aux modes couplés qui permet de vérifier de façon exacte la condition au fond, en introduisant un terme supplémentaire, appelé "sloping-bottom mode", qui permet de plus d'accélérer la convergence. La généralisation de ce modèle à trois dimensions (Belibassakis et al., 2001) donne d'excellents résultats dans des configurations académiques, pour des topographies du fond très générales. Ainsi, pour des vagues linéaires, c'est une alternative relativement peu coûteuse aux modèles aux éléments frontières pour la résolution de l'équation de Laplace.

La diffusion des vagues par la topographie sous-marine est étudiée dans ce manuscrit avec une orientation vers les applications océanographiques. La présentation est scindée en deux parties. Une première partie est consacrée aux méthodes permettant de représenter correctement ce phénomène pour différents types de topographie. Une présentation générale des méthodes permettant de traiter la diffusion est donnée au chapitre 2. Le terme de source de diffusion de Bragg proposé par Ardhuin et Herbers (2002), calculé pour des fonds aléatoires, corrigeant l'approche spectrale proposée par Hasselmann (1966) est étudié au cours du chapitre 3. Les limites d'applicabilité de ce terme de source sont testées par la confrontation à des théories déterministes, pour différents fonds bi-dimensionnels. Le chapitre 4 étudie l'influence de la réflexion sur la propagation des vagues au-dessus d'un canyon sous-marin par le biais de modèles de réfraction/diffraction et du modèle couplé elliptique de Athanassoulis et Belibassakis (1999). Des mesures effectuées pendant la campagne NCEX permettent une validation de ce modèle. La deuxième partie de notre étude est consacrée à l'effet d'un courant sur la diffusion des vagues. Un bref rappel de l'effet d'un courant sur la propagation des vagues est proposé au chapitre 5. L'influence du courant sur la réflexion des vagues par une topographie sinusoïdale est mise en évidence expérimentalement dans le chapitre 6, confrontant les prédictions de la théorie déterministe de Kirby (1988) aux données mesurées en bassin à houle. Le terme de source (Ardhuin et Herbers, 2002) est étendu en présence d'un courant uniforme dans le chapitre 7. Après une comparaison 2D avec la théorie de Kirby (1988), l'influence de la diffusion des vagues en présence de courant est examinée dans le cas de bathymétries réelles en Mer du Nord, caractérisées par des dunes de sable et des forts courants de marée. Les conclusions générales sont présentées dans le chapitre 8.

Première partie

Influence de la topographie sous-marine

Chapitre 2

Présentation

2.1 Introduction

L'objectif de cette partie est d'étudier l'influence de la bathymétrie sur la diffusion de Bragg, en s'intéressant en particulier aux méthodes permettant de représenter correctement ce phénomène. Une méthode spectrale basée sur un développement en perturbations et échelles multiples est présentée dans le troisième chapitre, offrant une alternative aux approches déterministes. Cette approche spectrale utilisant un terme de source de diffusion de Bragg (Ardhuin et Herbers, 2002) est confrontée à des modèles déterministes (Rey, 1992 ; Mei, 1985) pour différents fonds bidimensionnels, un fond sinusoïdal modulé, une rampe et une marche. Cette étude révèle entre autres que ce terme de source permet une représentation précise et efficace de la réflexion pour des petites amplitudes du fond. Elle permet également de traiter des fonds localisés, montrant que dans la limite des petites amplitudes du fond, la réflexion des vagues est entièrement déterminée par la variance du fond et est insensible aux détails de la forme du fond. Pour des bathymétries accidentées, comme des canyons sous-marins présentant des fortes variations bathymétriques, ce terme de source n'est plus applicable. Le quatrième chapitre propose un modèle de réfraction/diffraction déterministe couplé (Athanassoulis et Belibassakis, 1999) pour représenter la propagation des vagues au-dessus de bathymétries complexes, confrontant les prévisions de ce modèle à des mesures effectuées durant la campagne NCEX à San Diego en 2003. La représentation de la réflexion pour de telles bathymétries est soulignée comme nécessaire pour une correcte description du champ de vagues.

2.2 Approche mathématique

Avant d'étudier en détail le processus de diffusion/réflexion des vagues pour différentes topographies sous-marines, cette partie présente des méthodes ou approches mathématiques utilisées dans la suite de ce manuscrit. Cette partie tente de faire une présentation générale de ces méthodes aussi bien déterministes que stochastiques sans rentrer dans les détails, qui sont présentés dans chacun des chapitres concernés.

2.2.1 Formulation générale

Le mouvement des vagues est supposé irrotationnel, le fluide incompressible et non-visqueux. A partir des équations de Navier-Stockes et de la conservation de la masse, on en déduit pour le potentiel des vitesses ϕ la condition dynamique (Bernoulli) (Eq.2.1) à la surface $z = \zeta$,

$$g\zeta + \frac{\partial \phi}{\partial t} = -\frac{1}{2}\left[|\nabla \phi|^2 + \left(\frac{\partial \phi}{\partial z}\right)^2 \right] \quad \text{sur} \quad z = \zeta, \tag{2.1}$$

et l'équation de Laplace (Eq.2.2) dans tout le fluide,

$$\nabla^2 \phi + \frac{\partial^2 \phi}{\partial z^2} = 0 \quad \text{pour} \quad -H \leq z \leq \zeta, \tag{2.2}$$

avec H(x) la profondeur. En surface, la condition limite cinématique indiquant que la vitesse verticale d'une particule est égale à la vitesse verticale de la surface libre se traduit par,

$$\frac{\partial \phi}{\partial z} = \frac{\mathrm{d}\zeta}{\mathrm{d}t} \quad \text{sur} \quad z = \zeta. \tag{2.3}$$

Au fond, la condition d'imperméabilité est donnée par une vitesse normale nulle,

$$\frac{\partial \phi}{\partial n} = 0 \quad \text{sur} \quad z = -H. \tag{2.4}$$

Enfin, en combinant l'équation (2.1) et (2.3),

$$\frac{\partial^2 \phi}{\partial t^2} + g\frac{\partial \phi}{\partial z} = g\nabla\phi \cdot \nabla\zeta - \nabla\phi \cdot \frac{\partial \nabla \phi}{\partial t} - \frac{\partial \phi}{\partial z}\frac{\partial^2 \phi}{\partial t \partial z} \quad \text{sur} \quad z = \zeta. \tag{2.5}$$

L'équation de Laplace (2.2), les conditions au fond (2.4) et en surface (2.5) constituent les équations de base régissant le mouvement des vagues. A partir de ces équations et en fonction du problème posé, de nombreuses méthodes de résolution existent pour obtenir le potentiel des vitesses.

Pour un milieu homogène (profondeur constante), on cherche des solutions ondulatoires se propageant sans déformation, avec un terme de propagation pour la déformée de la surface libre de la forme $e^{i(\omega t-\mathbf{k}.\mathbf{x})}$, avec ω la pulsation et $\mathbf{k}$ le vecteur d'onde. En linéarisant les conditions de surface libre, on obtient les solutions ondes planes (houles d'Airy ou Stokes au 1er ordre). Par profondeur constante, la prise en compte des termes non-linéaires de la condition de surface libre pour une onde monochromatique modifie la cinématique du fluide, en particulier la déformée de la surface libre qui n'est plus sinusoïdale mais apparaît comme la résultante d'une série d'harmoniques " liés ", car se propageant à la même vitesse que le fondamental. Pour des houles réelles, considérées de la façon la plus simple comme la superposition de composantes de fréquence donnée, correspondant aux solutions d'Airy, les termes non-linéaires sont à l'origine d'interactions entre les différentes composantes de la houle (triadiques ou entre quadruplets par exemple), et donc de transferts d'énergie entre bandes de fréquences dans le cas d'interactions résonantes. Ce transfert d'énergie peut se faire également à cause de la condition d'imperméabilité de fond, qui peut forcer la présence d'une onde par résonance de Bragg lorsque le fond est sinusoïdal, ou décrit comme la superposition de sinusoïdes.

2.2.2 Méthodes en perturbations

Pour résoudre un système d'équations différentielles non-homogènes (2.2, 2.4 et 2.5), dont la solution analytique au système homogène est connue, une solution approchée consiste à exprimer l'inconnue, ici le potentiel des vitesses ϕ, en un développement autour d'un petit paramètre ε, souvent la cambrure des vagues ka,

$$\phi = \varepsilon\phi_1 + \varepsilon^2\phi_2 + \cdots \tag{2.6}$$

La solution du système homogène (linéaire en ϕ) correspond alors au potentiel des vitesses à l'ordre 1, ϕ_1. A cet ordre, la solution peut représenter une onde de cambrure faible (approximation linéaire) se propageant au-dessus d'un fond plat ; c'est la solution d'Airy. L'expression de ϕ_1 est bien connue et donnée au chapitre 3. En fonction du phénomène que l'on veut étudier, on adimensionnalise les équations (2.2), (2.4) et (2.5), également par des petits paramètres caractéristiques des différentes échelles de variations en temps ou en espace. Par exemple, l'amplitude des vagues peut être gouvernée par une variation lente dans l'espace, représentée alors par un petit paramètre, permettant de représenter "shoaling", réfraction ou diffusion. Après un classement de ces petits paramètres entre eux, il "suffit" de calculer les potentiels aux ordres supérieurs. Ces ordres supérieurs apportent ainsi des corrections à la solution onde plane du premier ordre, se rapprochant ainsi de la solution du sytème non-homogène dans la limite des petits paramètres. De telles perturbations permettent de calculer aussi bien des effets de la topographie que des non-linéarités de la surface (Hasselmann, 1962) ou du cisaillement du courant (White, 1999 ; McWilliams et al. 2004).

En décomposant les variables d'espace et de temps en variables rapides et lentes, on peut choisir une échelle de variation de l'amplitude de l'onde plus lente que celle de sa phase. Pour la réfraction, on suppose la longueur d'onde caractéristique des vagues beaucoup plus petite que l'échelle horizontale de variation de la profondeur, le petit paramètre β est alors défini par $\beta = O\left(\nabla h / kh\right)$, où k est le module de $\mathbf{k}$. En s'arrêtant à l'ordre 2 en ε et après un peu de calcul (Mei, 1989), on obtient l'équation de la conservation de l'action (2.7), qui permet de connaître en régime stationnaire la variation de l'énergie des vagues en tout point d'un rayon à partir d'un point de référence connu.

$$\frac{\partial}{\partial t}\left(\frac{E}{\sigma}\right) + \nabla \cdot \left(\frac{E}{\sigma}\mathbf{C_g}\right) = 0, \tag{2.7}$$

avec σ est la fréquence intrinsèque des vagues, définie par $\sigma^2 = gk\tanh(kH)$.

La diffusion des vagues peut également être traitée par une approche en perturbation. Pour traiter le cas de vagues aléatoires sur un fond aléatoire tri-dimensionnel, Ardhuin et Herbers (2002) ont proposé une équation d'évolution de l'énergie incluant un terme de source. La diffusion des vagues par la topographie sous-marine fait intervenir les variations du fond à l'échelle de la longueur d'onde des vagues. La première étape est donc de séparer l'élévation du fond z en une variation lente H, qui prendra en compte les phénomènes de réfraction et de "shoaling", et une variation rapide h traitant la diffusion, tel que $z = -H(\mathbf{x}) + h(\mathbf{x})$. Trois petits paramètres sont introduits, $\varepsilon = ka$ la cambrure des vagues, $\eta = kh$ la pente correspondante à la variation rapide h et β celle de la variation lente H. Les équations adimensionnalisées sont,

$$\nabla^2\phi + \frac{\partial^2\phi}{\partial z^2} = 0 \quad \text{pour} \quad -H + \eta h \le z \le \varepsilon\zeta, \tag{2.8}$$

$$\frac{\partial\phi}{\partial z} = \nabla\phi \cdot (\eta\nabla h - \beta\nabla H) \quad \text{sur} \quad z = -H + \eta h, \tag{2.9}$$

$$\frac{\partial^2\phi}{\partial t^2} + \frac{\partial\phi}{\partial z} = \varepsilon\nabla\phi\cdot\nabla\zeta - \varepsilon\nabla\phi\cdot\frac{\partial\nabla\phi}{\partial t} - \varepsilon\frac{\partial\phi}{\partial z}\frac{\partial^2\phi}{\partial t\partial z} \quad \text{sur} \quad z = \varepsilon\zeta. \tag{2.10}$$

Pour dissocier les différentes échelles de variations, des variables lentes en espace $\bar{\mathbf{x}} = \alpha\mathbf{x}$ et en temps $\bar{\mathbf{t}} = \gamma\mathbf{t}$ sont introduites. h et ϕ sont supposées semi-stationnaires horizontalement en espace et en temps, et sont décomposées en modes de Fourier avec des amplitudes à variation lente. Les petits paramètres sont choisis tels que, $\alpha \approx \beta \approx \gamma \approx \eta^2 \approx \varepsilon^2 \ll 1$, caractéristiques d'une étude sur le plateau continental. Un développement en perturbations pour le potentiel des vitesses ϕ (2.6) est introduit dans les équations (2.2), (2.4) et (2.5). Dans les équations aux frontières de surface et de fond, ϕ est exprimé en $z = -H$ ou $z = 0$ à l'aide d'un développement de Taylor. En conservant alors les termes correspondants aux différents ordres, on obtient des jeux d'équations décrivant les ordres 1, 2, 3..., détaillés au septième chapitre en présence de courant uniforme. La diffusion des vagues intervient à partir de l'ordre 2 en ε pour ϕ, via la condition limite au fond. Une approche statistique est choisie pour décrire l'énergie, utilisant les covariances des potentiels des vitesses aux différents ordres. Il est supposé que la nature aléatoire du fond permet de négliger la part des ondes stationnaires, ce qui conduit à une énergie nulle à l'ordre trois. Il faut donc considérer l'énergie à l'ordre 4, faisant interagir les potentiels des vitesses d'ordre 1 et 3, et 2 et 2 en ε, ce qui mène à une équation d'évolution de l'énergie par combinaison de tous les termes séculaires d'ordre 4.

Pour des fonds sinusoïdaux et des vagues monochromatiques, Mei (1985) proposa une théorie déterministe bi-dimensionnelle basée sur une méthode multi-échelles pour représenter l'évolution et la réflexion des vagues. Le fond est décomposé en une variation lente et rapide, non-aléatoire. Contrairement à Ardhuin et Herbers (2002) qui ont choisi des petits paramètres de différents ordres, Mei les choisit tous égaux, mais le calcul de ϕ_1 et ϕ_2 suit la même démarche. Par ailleurs, Mei ne prend en compte que deux composantes des vagues, qui sont les deux seules pouvant interagir en 2 D une fois la fréquence de l'onde incidente fixée. Une équation d'évolution en amplitude est obtenue pour l'onde incidente et pour l'onde réfléchie en combinant les termes séculaires d'ordre 2. Il s'agit donc de la même démarche, appliquée aux amplitudes plutôt qu'aux énergies. Pour une incidence normale au-dessus d'un champ de barres,

$$\frac{\partial A}{\partial t} + C_g \frac{\partial A}{\partial x} = -i\Omega_0 B, \tag{2.11}$$

$$\frac{\partial B}{\partial t} - C_g \frac{\partial B}{\partial x} = -i\Omega_0 A. \tag{2.12}$$

A et B représentent respectivement l'amplitude de l'onde incidente et réfléchie, la féquence de coupure Ω_0 est définit par $\Omega_0 = (\omega k D)/(2\sinh(2kH))$, avec D l'amplitude des barres. Chacune de ces équations comprend un terme d'amortissement lié à l'onde réfléchie ou incidente respectivement. Par combinaison de ces équations, la conservation de l'énergie est obtenue à l'ordre 3 en énergie, ce qui comprend les corrélations des potentiels des vitesses d'ordre 2 et d'ordre 1. Les interactions incluses dans le terme de source faisant intervenir l'ordre trois en ε sont omises dans le calcul de Mei qui s'intéresse plus à l'amplitude qu'aux énergies.

Pour des fonds aléatoires et des vagues monochromatiques, Mei et Hancock

(2003) ont également proposé une approche monochromatique bi-dimensionnelle en décomposant le fond en une variation lente et rapide. La variation rapide est choisie aléatoire. En utilisant une fonction de Green pour résoudre le système d'ordre 2 pour le potentiel des vitesses, ils obtiennent une équation d'évolution en amplitude avec un terme d'amortissement β. Ce terme d'amortissement est comparé au terme de source dans le chapitre suivant. En se ramenant à une équation d'évolution en énergie en 2D, les deux théories se révèlent cohérentes dans la limite des petites amplitudes du fond (voir le chapitre suivant). La théorie de Mei et Hancock (2003), limitée à l'ordre 2 en ε ne conserve cependant pas l'énergie, qui nécessiterait de prendre en compte des termes d'ordres supérieurs.

2.2.3 Méthode de continuité intégrale aux frontières

Pour connaître l'évolution des vagues au-dessus d'un fond 2D, et en particulier son coefficient de réflexion associé, Rey (1992) proposa un algorithme de continuité intégrale aux frontières. Cette méthode, qui s'applique à des fonds 2D constitués d'une succession de domaines de profondeur constante, consiste à écrire l'expression générale des potentiels des vitesses, puis à trouver leurs expressions exactes par le calcul de coefficients à partir de l'écriture de façon intégrale des conditions de continuité et de pression aux frontières entre domaines successifs. L'expression générale du potentiel des vitesses, donnée au chapitre trois (eq.3.2), s'écrit comme la somme d'une onde plane et de modes locaux appelés évanescents qui permettent d'ajuster le potentiel des vitesses pour des variations rapides du fond ou des discontinuités lorsque l'onde n'est plus plane. Les détails mathématiques de cette méthode sont donnés dans le chapitre suivant. Cette méthode présente l'avantage d'être très précise et d'être applicable à n'importe quel type de fonds uniformes suivant une composante horizontale. Elle ne présente donc aucune limitation quant à la pente ou l'amplitude du fond, sa seule limitation est la linéarité de la surface.

2.2.4 Modèles de réfraction/diffraction, équations en pente douce

Berkhoff (1972) proposa une équation simplifiée pour représenter la réfraction et la diffraction, basée sur une approximation en pente douce, et supposant un fond localement plat. Cette équation est obtenue par intégration sur la verticale de l'équation de Laplace, réduisant alors le problème à deux dimensions. En choisissant un fond uniforme suivant une composante horizontale, cette équation est communément utilisée pour calculer la réflexion des vagues par le fond. Plusieurs méthodes de résolutions (identité de Green, méthode de Galerkin ou formulation variationnelle) ont été proposées pour obtenir l'équation de Berkhoff. On présente ici la méthode de Smith et Sprinks (1975), voir aussi Mei (1989), utilisant l'identité de Green. Pour un fond plat, le potentiel des vitesses est donné par,

$$\phi = -\frac{ig\zeta}{\omega} f, \tag{2.13}$$

avec

$$f = \frac{\cosh k(z+H)}{\cosh kH} \quad \text{et} \quad \omega^2 = gk \tanh kH. \tag{2.14}$$

L'idée consiste à supposer que pour un fond en pente douce, le potentiel des vitesses peut être représenté localement par celui d'un fond plat. En utilisant l'équation de Laplace, la condition en surface linéarisée et la condition au fond $\partial\phi/\partial z = -\nabla h.\nabla\phi$ en $z = -H$, et après intégration par partie, on obtient,

$$\int_{-H}^{0} (k\phi f + f\nabla^2\phi) dz = -(f\nabla.\nabla\phi)_{-H}. \tag{2.15}$$

A partir des équations (2.13), (2.14),

$$\nabla\phi = -\frac{ig}{\omega}\left(f\nabla\zeta + \zeta\frac{\partial f}{\partial H}\nabla H\right), \tag{2.16}$$

$$\nabla^2\phi = -\frac{ig}{\omega}\left(f\nabla^2\zeta + 2\frac{\partial f}{\partial H}\nabla\zeta.\nabla H + \zeta\frac{\partial^2 f}{\partial H^2}(\nabla H)^2 + \zeta\frac{\partial f}{\partial H}\nabla^2 H\right). \tag{2.17}$$

En introduisant (2.16) et (2.17) dans (2.15), et en utilisant le théorème de Leibniz,

$$\begin{aligned} \nabla \quad . \quad & \int_{-H}^{0} f^2\nabla\zeta dz + \int_{-H}^{0} k^2 f^2 \zeta dz = \qquad (2.18) \\ & -f\frac{\partial f}{\partial H}|_-H\zeta(\nabla H)^2 - \int_{-H}^{0}\zeta f\frac{\partial^2 f}{\partial H^2}(\nabla H)^2 dz - \int_{-H}^{0}\zeta f\frac{\partial f}{\partial H}\nabla^2 H dz. \end{aligned}$$

Les termes du membre de droite de l'équation précédente sont les termes d'ordre deux en pente du fond négligés par Berkhoff (1972), proportionnels à la pente au carré et à la courbure du fond. Ils se révèlent importants pour prendre en compte les variations "rapides" du fond. Les modes évanescents intervenant également au deuxième ordre, et négligés ici, doivent aussi être pris en considération pour traiter des fonds rapidement variables. L'équation de Berkhoff modifiée est alors donnée par

$$CC_g\nabla^2\phi + \nabla CC_g.\nabla\phi + \left[\omega^2\frac{C_g}{C} + f_1(kH)\nabla^2 H + f_2(kH)(\nabla H)^2\right]\phi = 0, \tag{2.19}$$

avec $f_1(kH)$ et $f_2(kH)$ les coefficients des termes de courbure du fond $\nabla^2 H$et de pente au carré $(\nabla H)^2$. Ces coefficients ne sont pas détaillés ici (voir par exemple Chandrasekera et Cheung, 1997).

Chapitre 3

La diffusion des vagues par le fond : une approche spectrale

Introduction

La propagation des vagues peut être représentée actuellement sur n'importe quel type de topographies sous-marines par des modèles déterministes, mais souvent très coûteux et peu adaptés aux grands domaines ou aux activités de prévisions opérationnelles. L'approche spectrale de la diffusion des vagues par le fond permet de pallier à ces problèmes, en utilisant un terme de source facilement introduit dans les modèles de vagues opérationnels basés sur une équation d'évolution de l'action. La validité pratique de cette approche est examinée dans ce chapitre, par le biais du terme de source de Ardhuin et Herbers (2002). Les limites d'applicabilités de ce terme de source sont étudiées par confrontation à des modèles déterministes (Rey, 1992 ; Mei 1985).

Topographical scattering of waves : a spectral approach

Rudy Magne(1,2), Fabrice Ardhuin(1), Vincent Rey(2) and Thomas H.C. Herbers(3)

Accepted for publication in Journal of Waterway, Coastal Port and Ocean Engineering (ASCE)
May 2005

(1) *Centre Militaire d'Océanographie, SHOM, BREST, France*
(2) *LSEET-LEPI, Université de Toulon et du Var, La Garde, France*
(3) *Dept. of Oceanography, Naval Postgraduate School, Monterey, CA 93943, USA*

Résumé

La diffusion des vagues par la topographie est étudiée en utilisant une équation spectrale en énergie qui tient compte de la diffusion de Bragg des vagues par le fond au premier ordre. Le modèle représente la topographie du fond et les vagues de surface par des spectres, et évalue un terme de source de diffusion de Bragg, qui est théoriquement valide pour des faibles pentes du fond et de la surface, mais aussi pour des propriétés spectrales à variation lente. La robustesse du modèle est testée pour différentes topographies uniformes le long d'une composante horizontale, incluant un fond sinusoïdal modulé, une rampe linéaire, et des profils de marche. Les résultats sont comparés avec les réflexions calculées utilisant une méthode précise basée sur une décomposition du fond en une succession de marches avec formulation intégrale de continuité aux frontières. Pour les petites amplitudes du fond, le terme de source donne de bonnes estimations de la réflexion, même pour des diffuseurs localisés. Ce résultat est prouvé pour les petites amplitudes du fond h, relatif à la profondeur moyenne H. La réflexion des vagues par des petites amplitudes du fond dépend donc essentiellement de la variance de l'élévation du fond aux échelles de la résonance de Bragg, et est insensible aux détails de la forme du fond, représentés par les phases de composantes de Fourier, ignorées ici. Les erreurs relatives sur les coefficients de réflexion en énergie sont de l'ordre de $2h/H$.

Abstract

The topographical scattering of gravity waves is investigated using a spectral energy balance equation that accounts for first order wave-bottom Bragg scattering. This model represents the bottom topography and surface waves with spectra, and evaluates a Bragg scattering source term that is theoretically valid for small bottom and surface slopes and slowly varying spectral properties. The robustness of the model is tested for a variety of topographies uniform along one horizontal dimension including nearly sinusoidal, linear ramp and step profiles. Results are compared with reflections computed using an accurate method that applies integral matching along vertical boundaries of a series of steps. For small bottom amplitudes, the source term representation yields accurate reflection estimates even for a localized scatterer. This result is proved for small bottom amplitudes h relative to the mean water depth H. Wave reflection by small amplitude bottom topography thus depends primarily on the bottom elevation variance at the Bragg resonance scales, and is insensitive to the detailed shape of the bottom profile. Relative errors in the energy reflection coefficient are found to be typically $2h/H$.

CE DATABASE Subject Headings

Surface waves, scattering, wave reflection, spectral analysis.

3.1 Introduction

Wave propagation over any bottom topography can now be predicted with boundary element methods or other accurate numerical techniques. However, wave forecasting relies to a large extent on phase-averaged spectral wave models based on the energy or action balance equation (Gelci et al. 1957) . For large bottom slopes waves can be reflected and this reflection is currently not represented in these models, while the significance of this process is still poorly known (Long 1973 ; Richter et al. 1976 ; Ardhuin et al. 2003). For waves propagating over a sinusoidal seabed profile, a maximum reflection or resonance is observed when the seabed wavenumber is twice as large as the surface wave wavenumber (Heathershaw 1982). Davies and Heathershaw (1984) proposed a deterministic wave amplitude evolution equation for normally incident waves over a sinusoidal seabed, based on a perturbation expansion for small bottom undulations. This theory was shown to be in good agreement with experimental data but overestimates reflection at resonance. Mei (1985) developed a more accurate approximation that is valid at resonance using a multiple scale theory. This approach was further extended to random bottom topography in one dimension (Mei and Hancock, 2003). The Bragg resonance theory can be extended to any arbitrary topography in two dimensions, that is statistically uniform(Hasselmann 1966). Ardhuin and Herbers (2002) further included slow depth variations. The resulting spectral energy balance equation contains a bottom scattering source term S_{bscat}, which is formally valid for small surface and bottom slopes and slowly varying spectral properties. S_{bscat} is readily introduced into existing energy-balance-based spectral wave models, and was numerically validated with field observations (Ardhuin et al. 2003). While this stochastic theory is in a good agreement with deterministic results for small amplitude sinusoidal topography (Ardhuin and Herbers 2002), the assumed slowly varying bottom spectrum is not compatible with isolated bottom features, and the limitations and robustness of the source term approximation for realistic continental shelf topography are not well understood. The limitations of the stochastic source term model are examined here through comparisons with a deterministic model for arbitrary one-dimensional ($1D$) seabed topography that is uniform along the second horizontal dimension. We review the random Bragg scattering model, and investigate the applicability limits of the source term for a variety of seabed topography. Predicted reflection coefficients are compared with results based on Rey's (1992) model, which approximates the bottom profile as a series of steps. Examples include modulated sinusoidal topography that is well within the validity constraints of the source term approximation as well as a steep ramp and a step that violate the assumption of a slowly varying bottom spectrum and thus provide a simple test of the robustness of the source term approximation.

3.2 Theoretical background

3.2.1 Matching boundary solution

We use Rey's (1992) algorithm, based on the theory of Takano (1960) and Kirby and Dalrymple (1983). It uses a decomposition of the bottom profile in a series of N steps with integral matching along vertical boundaries between each pair of adjacent steps. A coordinate frame is defined with the horizontal x coordinate in the direction of the incident waves and the vertical z coordinate pointing upwards relative to the mean water level. The velocity potential is described by a sum of flat bottom propagating and evanescent modes. Evanescent modes are included in the matching condition to ensure a consistent treatment of the wave field (Rey 1992). The general solution of the velocity potential for a step (p) of depth H_p is given by the following equations :

$$\Phi_p(x,z,t) = \phi_p(x,z)\mathrm{e}^{-\mathrm{i}\omega_p t} \quad \text{for} \quad p = 1, N, \tag{3.1}$$

with,

$$\phi_p(x,z) = \underbrace{A_p^{\pm} e^{\pm ikx}\chi_p(z)}_{\text{propagating modes}} + \underbrace{\sum_{q=1}^{Q} B_{p,q}^{\pm} e^{\pm k_q x}\psi_{p,q}(z)}_{\text{evanescent modes}}, \tag{3.2}$$

where (χ_p, $\psi_{p,q} \quad q = 1, Q$) define a complete orthogonal set for each step region (p) :

$$\chi_p(z) = \cosh k_p(H_p + z), \tag{3.3}$$

$$\psi_{p,q}(z) = \cos k_{p,q}(H_p + z). \tag{3.4}$$

k_p and $k_{p,q}$ satisfy the following dispersion relations :

$$\frac{\omega_p^2}{g} = k_p \tanh(k_p H_p), \tag{3.5}$$

$$\frac{\omega_p^2}{g} = -k_{p,q} \tan(k_{p,q} H_p). \tag{3.6}$$

where g is the acceleration of gravity.

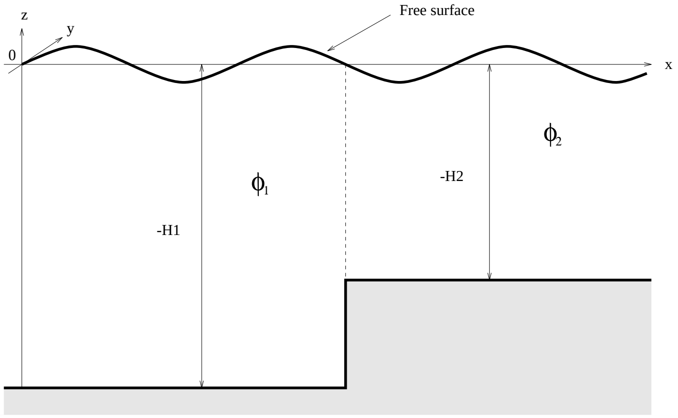

FIG. 3.1 – Stepwise approximation

Across each step (p), matching conditions between two domains (labelled $p = 1$ and $p = 2$ in figure 3.1) must be applied to ensure continuity of the fluid velocity and surface elevation.

$$\phi_1 = \phi_2,\ \frac{\partial \phi_1}{\partial x} = \frac{\partial \phi_2}{\partial x} \quad \text{for} \quad -H_2 < z < 0, \tag{3.7}$$

$$\frac{\partial \phi_1}{\partial x} = 0 \quad \text{for} \quad -H_1 < z < -H_2. \tag{3.8}$$

The integral formulation of these conditions (for $H_1 > H_2$) leads to :

$$\begin{aligned}
\int_0^{H_2} \phi_1 \cdot \chi_2 dz &= \int_0^{H_2} \phi_2 \cdot \chi_2 dz, && (3.9)\\
\int_0^{H_2} \phi_1 \cdot \psi_{2,q} dz &= \int_0^{H_2} \phi_2 \cdot \psi_{2,q} dz \quad \text{for} \quad q = 1, Q, && (3.10)\\
\int_0^{H_1} \frac{\partial \phi_1}{\partial x} \cdot \chi_1 dz &= \int_0^{H_2} \frac{\partial \phi_2}{\partial x} \cdot \chi_1 dz, && (3.11)\\
\int_0^{H_1} \frac{\partial \phi_1}{\partial x} \cdot \psi_{1,q} dz &= \int_0^{H_2} \frac{\partial \phi_2}{\partial x} \cdot \psi_{1,q} dz \quad \text{for} \quad q = 1, Q. && (3.12)
\end{aligned}$$

The orthogonality of the set functions largely simplifies these equations. In order to solve the problem numerically, the number of evanescent modes q are truncated to $q = Q$. Practically, only a few evanescent modes are needed to ensure convergence. For N steps, $2N(Q + 1)$ equations are solved to obtain the $2N(Q + 1)$ complex coefficients $A_p^{\pm}$ and $B_{p,q}^{\pm}$. At the boundaries (p=0 and p=N), the reflection coefficient is given by :

$$K_r = \frac{|A_0^+|}{|A_0^-|} \tag{3.13}$$

This method has the advantage that it is valid for arbitrary $1D$ topography.

3.2.2 Bragg scattering theory

We consider random waves propagating over a 2D irregular bottom with a slowly varying mean depth H and small-scale topography h. The bottom elevation is given by $z = -H(\underline{\mathbf{x}})+h(\underline{\mathbf{x}})$, with $\underline{\mathbf{x}}$ the horizontal position vector. The free surface position is $\zeta(\underline{\mathbf{x}}, t)$.

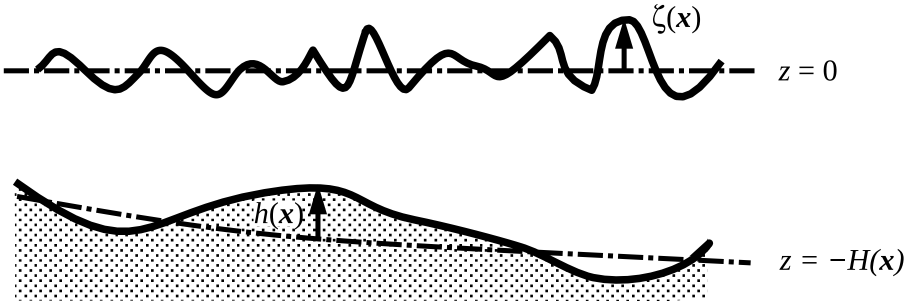

Fig. 3.2 – Definitions

Considering an irrotational flow for an incompressible fluid, we have the governing equations and boundary conditions for the velocity potential ϕ :

$$\nabla^2\phi + \frac{\partial^2\phi}{\partial z^2} = 0 \quad \text{for} \quad -H+h \leq z \leq \zeta, \tag{3.14}$$

$$\frac{\partial\phi}{\partial z} = \underline{\nabla}\phi \cdot \underline{\nabla}(h-H) \quad \text{at} \quad z = -H+h, \tag{3.15}$$

$$\frac{\partial\zeta}{\partial t} = \frac{\partial\phi}{\partial z} \quad \text{at} \quad z = \zeta, \tag{3.16}$$

$$g\zeta + \frac{\partial\phi}{\partial t} = -\frac{1}{2}[|\underline{\nabla}\phi|^2 + (\frac{\partial\phi}{\partial z})^2] \quad \text{at} \quad z = \zeta, \tag{3.17}$$

where $\underline{\nabla}$ and ∇^2 are the horizontal gradient and Laplacian operators. The equations (7.1), (7.2), (3.16) and (3.17) are respectively the Laplace's equation, free surface and bottom boundary conditions, and Bernoulli's equation. Combining these two last equations, we obtain :

$$\frac{\partial^2\phi}{\partial t^2} + g\frac{\partial\phi}{\partial z} = g\underline{\nabla}\phi\cdot\underline{\nabla}\zeta - \underline{\nabla}\phi\cdot\frac{\partial\underline{\nabla}\phi}{\partial t} - \frac{\partial\phi}{\partial z}\frac{\partial^2\phi}{\partial t\partial z} \quad \text{at} \quad z = \zeta. \tag{3.18}$$

Assuming that the surface and the small-scale bottom slopes are of the same order ε, and the large scale bottom slope is of order ε^2, a perturbation expansion of ϕ up to the third order in ε yields the following spectral energy balance equation (details are given in Ardhuin and Herbers 2002) :

$$\frac{dE(\underline{\mathbf{k}},\mathbf{x},t)}{dt} = S_{\mathrm{bscat}(\underline{\mathbf{k}},\underline{\mathbf{x}},t)}, \tag{3.19}$$

where

$$S_{\mathrm{bscat}}\left(\underline{\mathbf{k}},\underline{\mathbf{x}},t\right) = K\left(k,H\right)\int_0^{2\pi}\cos^2\left(\theta-\theta'\right)F^B\left(\underline{\mathbf{k}}-\underline{\mathbf{k}}',\underline{\mathbf{x}}\right)\left[E\left(\underline{\mathbf{k}}',\underline{\mathbf{x}},t\right)-E\left(\underline{\mathbf{k}},\underline{\mathbf{x}},t\right)\right]\,\mathrm{d}\theta', \tag{3.20}$$

with

$$K\left(k,H\right) = \frac{4\pi\omega k^4}{\sinh\left(2kH\right)\left[2kH+\sinh\left(2kH\right)\right]}. \tag{3.21}$$

$E(\underline{\mathbf{k}},\underline{\mathbf{x}},t)$ is the surface elevation spectrum and $F^B(\underline{\mathbf{k}},\underline{\mathbf{x}})$ is the small-scale bottom elevation spectrum. These spectra are slowly varying functions of $(\underline{\mathbf{x}},t)$ and $\underline{\mathbf{x}}$ respectively. $\underline{\mathbf{k}}$ is the wavenumber vector defined by $\underline{\mathbf{k}} \equiv (k\cos\theta, k\sin\theta) \equiv (k_x,k_y)$, where θ defines the angle with the x-axis. The spectral densities E and F^B are defined such that the integral over the entire $\underline{\mathbf{k}}$-plane equals the local variance,

$$< h^2(\underline{\mathbf{x}}) >= \int_{-\infty}^{+\infty}\int_{-\infty}^{+\infty} F^B(\underline{\mathbf{k}},\underline{\mathbf{x}})dk_xdk_y. \tag{3.22}$$

The frequency ω is given by the dispersion relation :

$$\omega^2 = gk\tanh(kH). \tag{3.23}$$

Here we consider a steady wave field in one dimension with incident and reflected waves propagating along the x-axis. After integration over k_y, k_x becomes k and (3.19) reduces to

$$C_g\frac{\partial E(k,x)}{\partial x} + C_k\frac{\partial E(k,x)}{\partial k} = S_{\mathrm{bscat}}(k,x), \tag{3.24}$$

with a source term

$$S_{\mathrm{bscat}}(k,x) = K(h,H)\frac{F^B(2k,x)}{k}\left[E(-k,x)-E(k,x)\right]. \tag{3.25}$$

The first term of Eq.(3.24) represents advection in physical space with the group velocity defined by

$$C_g = \frac{dx}{dt} = \frac{\partial\omega}{\partial k}, \tag{3.26}$$

and the second term describes the effect of shoaling on the wavenumber

$$C_k = \frac{dk}{dt} = -C_g \cdot \frac{2k^2}{2kh + \sinh(2kh)} \cdot \frac{\partial H}{\partial x}. \tag{3.27}$$

3.3 Reflection by modulated sinusoidal bottom topography

The source term approximation was validated by Ardhuin and Herbers (2002) for random waves reflecting from a sinusoidal seabed, by integrating S_{bscat} analytically across the wave spectrum in the limit of weak reflection ($E(-k) << E(k)$, with positive and negative wavenumbers corresponding to the incident and reflected waves, respectively). A comparison with Dalrymple and Kirby's (1986) solution gave good agreement, even for only a few bars. For stronger reflection, equation (3.24) is not readily evaluated analytically, and numerical integration is not feasible since a sinusoidal bottom has an infinitely narrow spectrum (a Dirac distribution), and thus cannot be represented with a finite bottom discretization Δk_b.

We consider instead a bottom spectrum with a finite width that corresponds to a modulated sinusoidal bottom profile.

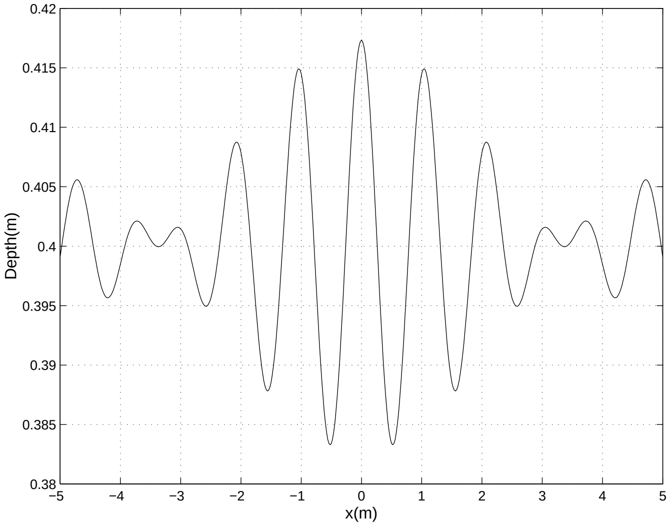

FIG. 3.3 – Modulated seabed (m=3), $bk_{b,0} = 0.06$

The modulated seabed is represented by a sum of cosines :

$$h(x) = \Sigma_{i=-(m-1)/2}^{i=(m-1)/2} b_i cos[(k_{b,0} + i\Delta k_b)x] \tag{3.28}$$

The slowly varying depth (H), defined in part 2 is taken constant while the perturbation (h) represents the modulated seabed. We define the root mean square (r.m.s.)

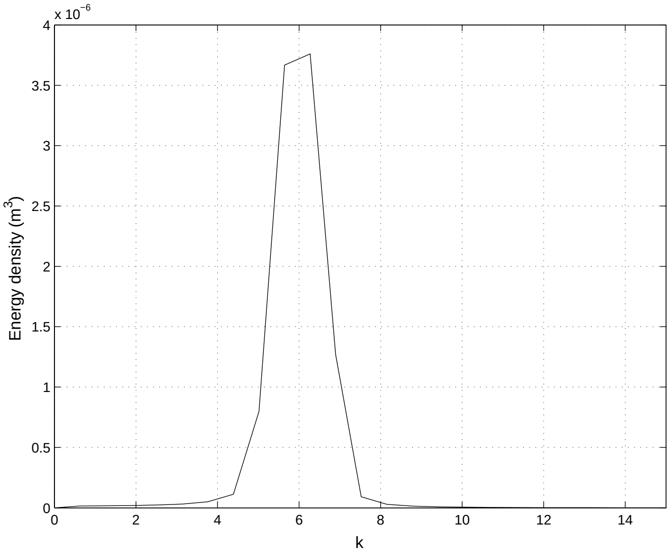

Fig. 3.4 – Modulated seabed spectrum (m=3)

bar amplitude b from the bottom variance, $b = \sqrt{< h^2 >}$, and a representative bottom slope $\varepsilon = bk_{b,0}$. The reflected wave energy is calculated for the bed profile shown in figure 3.3, with the peak bottom wave number $k_{b,0} = 6\mathrm{m}^{-1}$ ($\lambda_{b,0} = 1.04\mathrm{m}$), and a short modulation length with $m = 3$, and equal amplitudes (b_i) for all bottom components. The length of the bed is 1.5 modulation lengths, giving the bottom spectrum shown in figure 3.4. The reflection from this modulated sinusoidal bottom was evaluated for an incident Pierson-Moskowitz spectrum, with a peak at k_0 satisfying the Bragg resonance condition $2k_0 = k_{b,0}$ (Fig.3.5). Spectral results for Rey's model were obtained by evaluating reflection coefficients for monochromatic waves over a range of frequencies and integrating the reflected energy across the spectrum. 70 steps are used to resolved the bathymetry. Results for various values of b are displayed in the form of reflection coefficients R (Fig.3.6) as a function of the slope $bk_{b,0}$. R is defined by the ratio of the reflected and incident energies : $R = (\Sigma_{k<0}E)/\ (\Sigma_{k>0}E)$. Predictions based on the source term method (R_{Smod}) and the matching boundary model using 5 evanescent modes (R_{MBmod}) agree well over a wide range of bottom slopes. The solutions gradually diverge for large bottom slopes where the source term under-predicts the reflection. Even for $bk_0 = 0.3$ ($b/\lambda_0 = 0.05$), differences are less than 10% confirming the robustness of the source term method for steep topography.

To evaluate the effect of the spectral width on the reflection coefficient, figure 3.6 also includes predictions for sinusoidal topography (m=0) with the same variance. Results for sinusoidal topography were obtained using Mei's (1985) analytical approximation and Rey's (1992) algorithm. The resulting reflection coefficients R_{Mei} and R_{MBsin}, respectively, agree for small bottom slopes (Fig.3.6) and diverge for

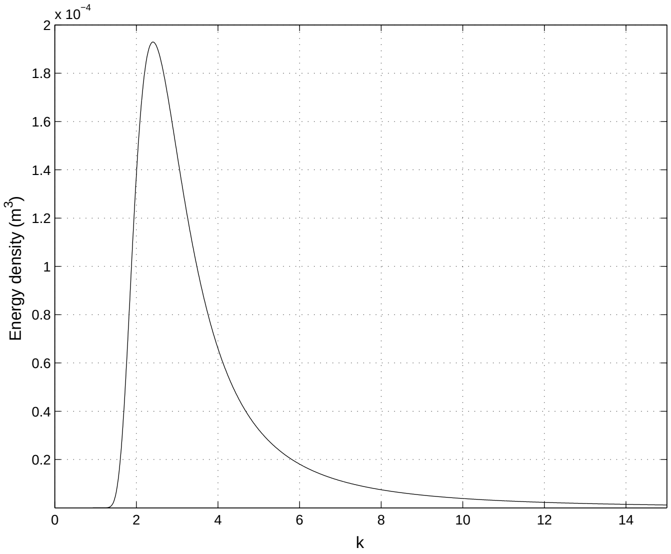

FIG. 3.5 – Incident wave spectrum

larger slopes as already shown by Rey (1992). Indeed, R_{Mei} was derived for small bottom slopes while the matched boundary solution converges to the exact reflection for any bottom profile when the number of evanescent modes goes to infinity. What may seem surprising is that the reflection coefficient for the sinusoidal and modulated sinusoidal topographies R_{MBmod} and R_{MBsin} agree for small slopes although bottom profiles are quite different. Apparently, for small bottom slopes and narrow bottom spectra the reflection is only a function of the total bottom elevation variance b^2 and does not depend on the phases of its components. This result is obvious from the viewpoint of the source term theory that was derived for small bottom slopes, and does not retain the phases of the bottom spectrum components. The predicted reflection depends on the convolution of the wave spectrum with the bottom spectrum at the Bragg resonance wavenumber (the integral of (3.25) over all wavenumbers). If the bottom spectrum is narrow compared with the wave spectrum then the total source term depends only on the total bottom variance and the surface spectral density at the Bragg resonance wavenumber.

3.4 Reflection by a linear ramp

To investigate the robustness of the variance-based source term model for reflection induced by localized topography, we consider the linear ramp problem used in previous studies to test the mild slope equation (Booij 1983). In the source term approximation, wave scattering is the result of interactions between surface waves and bottom variations at the scale of the surface wavelength. The scattering model

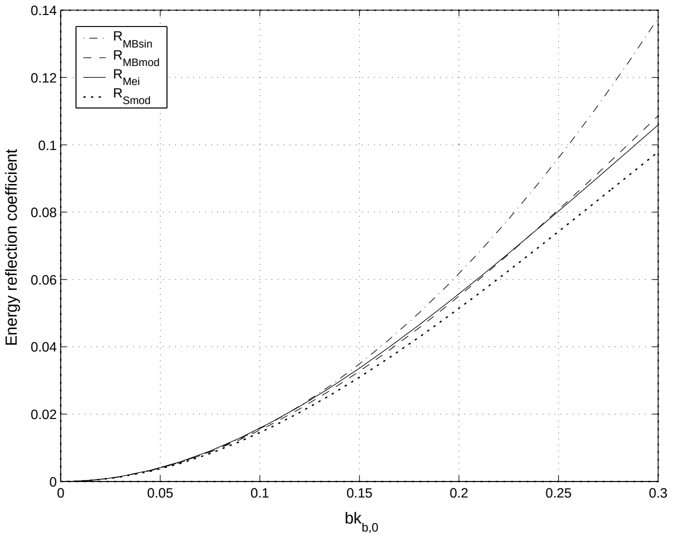

FIG. 3.6 – Wave reflection by modulated sinusoidal bottom

is thus based on a decomposition of the topography into a slowly varying depth H and a perturbation h (small scale topography), which corresponds to a separation between refraction and shoaling that occurs over the slowly varying depth H and scattering at these short scales. For practical applications, it is desirable to have a perturbation h that is zero outside of a finite region, so that the spectrum of h is well defined. Once the two criteria that the slope of H does not exceed a given threshold and h is zero outside of a region of radius nL are satisfied, the choice of the depth decomposition in h and H is fairly arbitrary and does not affect the following results. For simplicity we take a piecewise linear function for $H(x)$, so that the perturbation $h(x)$ takes the form of a triangular wave (Fig.3.7).

The ramp profile is defined by the fixed water depths H_1, H_2, while the ramp slope α is varied by adjusting its length $2L$ (Fig.3.7). To ensure that $H(x)$ is slowly varying, γ has to be small. This is achieved by extending the domain to a length $2nL$ with $n > 1$ (Fig.3.7). The slope of H is then given by $\tan\ \gamma = (\tan\ \alpha)/n$, with several values of n tested below.

3.4.1 First test case : small depth change

We first consider a ramp with a small depth transition from $H_1 = 0.5\text{m}$ to $H_2 = 0.3\text{m}$. The incident wave spectrum is represented by the same Pierson-Moskowitz spectrum that was used in the previous section with the peak wavenumber in deep water $k_0 = 3\text{m}^{-1}$ (Fig.3.5), so that $k_0 H_1 = 1.5$ and $k_0 H_2 = 0.9$. In order to investigate the source term applicability limits, the linear ramp slope $\tan\alpha$ is varied from 0.01 to 2.9. For each value of α, several values of γ are tested, with n varying from

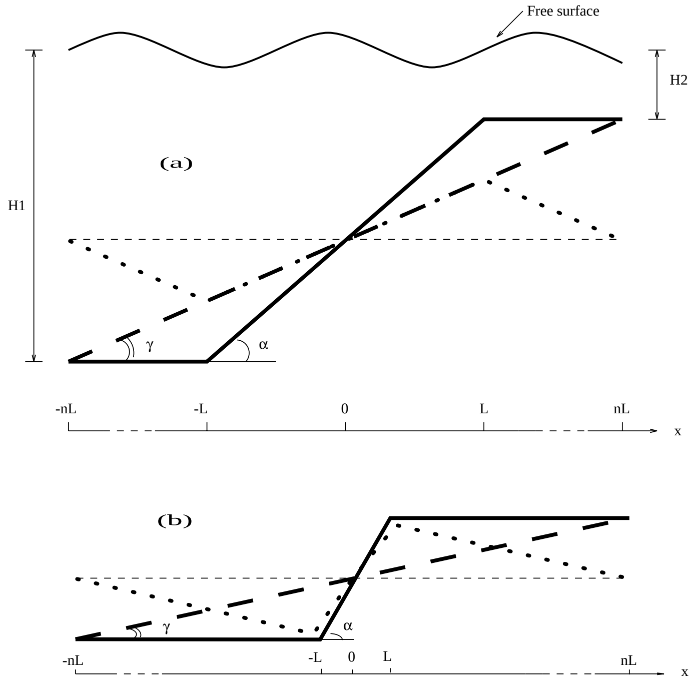

FIG. 3.7 – Decomposition of linear ramp (solid line) into a slowly varying depth H (dashed line) and residual h (dotted line). (a) and (b) for small and large n respectively

5 to 50. The reflection coefficient R_{S} (source term reflection due to the residual) is compared with the "exact" computation R_{MB} (matching boundary algorithm) in figure 3.8 and the relative error $(R_{\mathrm{S}} - R_{\mathrm{MB}})/R_{\mathrm{MB}}$ is shown in figure 3.9. In our calculations, for slopes of H such as $\tan\alpha < 0.4$, $R_{\mathrm{S},n=5}$ is within 30% of the exact value R_{MB}. For larger values of $\tan\alpha$, $R_{\mathrm{S},n=5}$ decreases and tends to zero (Fig.3.8), while the exact solution R_{MB} converges to the reflection over a vertical step as $\tan\alpha$ goes to infinity. The value $\tan\alpha = 0.4$ corresponds to $\tan\gamma$ $(= \tan\alpha/5)$ equal to 0.08. For larger n the slope of H is reduced and $R_{\mathrm{S},n}$ is valid for a wider range of ramp slopes.

We notice that for all values of n shown in figure 3.8, the model gives reasonable results for $\tan\gamma$ $(= (\tan\alpha)/n)$ up to about 0.08. The ramp slope does not appear to be a limiting factor (as it was assumed in the theory). For $\tan\gamma$ larger than 0.08 the reflection is increasingly underestimated probably because of the contribution of the large scale profile $H(x)$ to the reflection. As n increases h approaches the slope of the actual ramp and $R_{\mathrm{S},n}$ converges to $R_{\mathrm{S},\infty}$ which is about 10% larger than R_{MB} for all ramp slopes. As discussed below, the accuracy of the model is apparently not limited by the ramp slope.

It may seem surprising that $R_{\mathrm{S},n}$ actually converges for large n while the bottom spectrum does not. In the case of a vertical step of height h in the middle of a

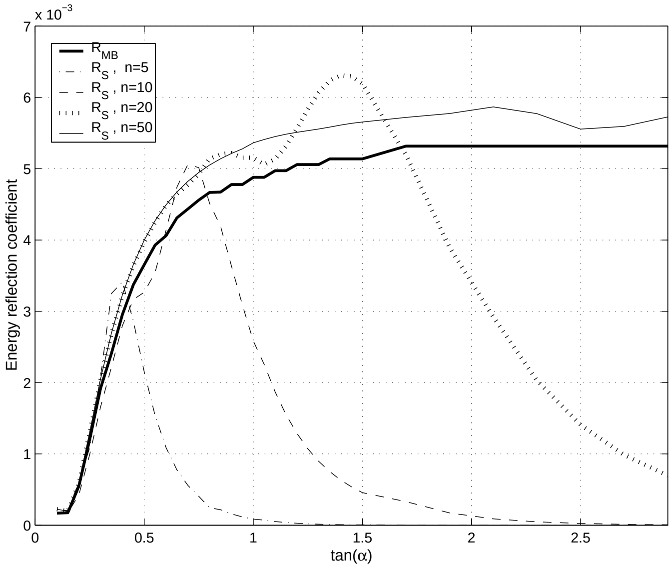

FIG. 3.8 – Wave reflection by a ramp

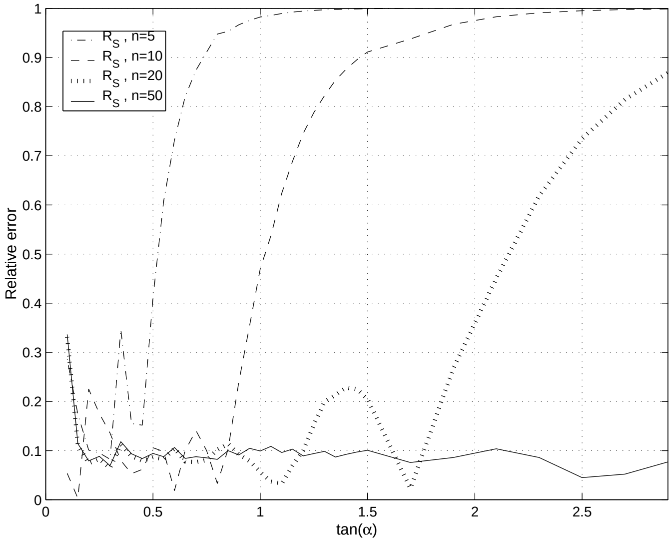

FIG. 3.9 – Relative errors in wave reflection by a ramp

domain of length $2nL$, the spectral density $F^B(k)$ of a discrete variance spectrum of the residual is proportional to $h^2/2nLk^2$ and tends to zero (except around $k = 0$) as n goes to infinity. However the source term formulation represents scattering as uniformly distributed along the bottom, and the integration of the source term along the wave propagation path yields a reflection that is proportional to $2nL\ F^B(k)$ and thus converges when n goes to infinity. The use of infinite support for H and h (taking the limit $n \rightarrow \infty$) to compute the reflection over a localized ramp is counterintuitive. It represents a physically localized scattering with a mathematically distributed source. In practice, the bottom spectrum is obtained by discrete Fourier Transform of the bottom, and it only tends to continuous power spectrum in the limit $n \rightarrow \infty$. Further, it should be realized that the bottom power spectrum is the Fourier transform of the bottom auto-correlation function used by Mei and Hancock (2003, see Appendix).

For a non-random bottom such as the ramp here, one may use intermediate results by Mei and Hancock (2003) where the hypothesis that the bottom is random only comes in for discarding nonlinear wave effects (which are not taken into account here). It thus appears that our rather surprising result for the convergence as $n \rightarrow \infty$ is justified by the convergence of the discrete spectrum to the continuous power spectrum and the theory of Mei and Hancock (2003) applied to non-random bottoms (see Appendix). It shows that the far field scattered energy by small amplitude depth variations only depends on the power spectrum of the scatterers at the Bragg scale, and not on its localization in space, as long as the bottom amplitude remains small.

3.4.2 Booij's ramp : larger depth change

This approach should clearly break down for finite bottom amplitudes, in particular because sub-harmonic scattering was observed (Belzons et al. 1991) while it is not explained by the present theory. Such a limit should be tested to see whether our present approach has some practical applicability. We therefore take a second test case with a larger ramp from Booij (1983) with water depths $H_1 = 4.97$m, $H_2 = 14.92$m and an incident wave peak period $T = 10$s. The corresponding peak wavenumber in deep water $k_0 = 0.04\text{m}^{-1}$ so that $k_0 H_1 = 0.6$ and $k_0 H_2 = 0.2$. Results for ramp slopes $\tan\alpha$ ranging from 0.001 to 2.9, and n=10 and 50 are shown in figure 3.10.

We notice again that $R_{\mathrm{S},n}$ converges for large n, provided that $(\tan\alpha)/n < 0.08$. However, in this case the relative error is larger than in the first test case, up to about 30%. The two tests have the same ramp slopes but different ratio of water depths at the edges of the ramp $H_1/H_2 = 3$ here versus $H_1/H_2 = 1.7$ in the previous

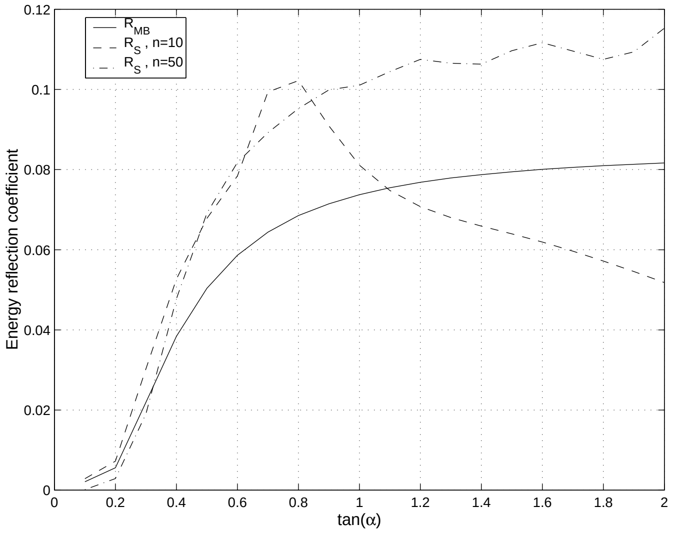

FIG. 3.10 – Wave reflection by Booij's ramp

case. The two cases suggest that the source term is more sensitive to the amplitude than the slope of the bottom perturbation h. Formally, the bottom amplitude only appears in the bottom boundary condition (7.2), which is linearized at $z = -H$ using the following Taylor series expansion ;

$$\Phi|_{z=-H+h} = \Phi|_{z=-H} + h\frac{\partial \Phi}{\partial z}|_{z=-H} + \frac{h^2}{2}\frac{\partial^2 \Phi}{\partial z^2}|_{z=-H} + O(h^3). \qquad (3.29)$$

Ardhuin and Herbers(2002) use a representative length scale $1/k_0$ to non-dimensionalize (3.29) as,

$$\tilde{\Phi}|_{\tilde{z}=-H+h} = \tilde{\Phi}|_{\tilde{z}=-H} + \eta\frac{\partial \tilde{\Phi}}{\partial \tilde{z}}|_{\tilde{z}=-H} + \frac{\eta^2}{2}\frac{\partial^2 \tilde{\Phi}}{\partial \tilde{z}^2}|_{\tilde{z}=-H} + O(\eta^3), \qquad (3.30)$$

where $\tilde{z} = k_0 z$, $\eta = k_0 h$, η corresponding to the scales that cause wave scattering. The validity of the Taylor expansion requires that η is small and also that the first and second derivative of $\tilde{\phi}$ with respect to $\tilde{z}$ are of order 1. In this approximation (3.30) is limited by the small-scale slope $k_0 h$. However one may also take H_0 as the representative length which leads to the same equation (3.30) with $\eta = h/H_0$, limited then by the water depth ratio h/H_0. The choice of the representative length was arbitrary and can be justified only a posteriori, by evaluating the scale of variation of Φ and thus the magnitude of $\partial\tilde{\Phi}/\partial\tilde{z}$ and $\partial^2\tilde{\Phi}/\partial\tilde{z}^2$. The numerical results presented here show that the source term is more sensitive to the water depth change h/H_0 than the small-scale slope $k_0 h$. Booij (1983) had found that the standard mild slope equation (Berkhoff 1972) gave errors less than 10% for $\tan\alpha$ up to 1/3. Our results suggest that the Bragg scattering model can be as accurate as the mild slope equation for computing reflection, but only for $\Delta h/H_0$ less than 0.2.

3.5 Reflection by a step

Now that the effect of h/H_0 is well established, one may question the importance of other parameters. We thus evaluate source term predictions of broad and narrow surface wave spectra over steps of varying height to gain further insight into the limitations of the source term approximation for localized topography. Reflection of waves by a rectangular step has been investigated analytically and experimentally in numerous studies (Neuman 1965a,b ; Miles 1967 ; Mei and Black 1969 ; Mei 1983 and Rey, Belzons and Guazzelli 1992) and is well understood. The step is defined in figure 3.11, where $2L$ is the step-length, h the height and $2nL$ the size of the entire computational domain.

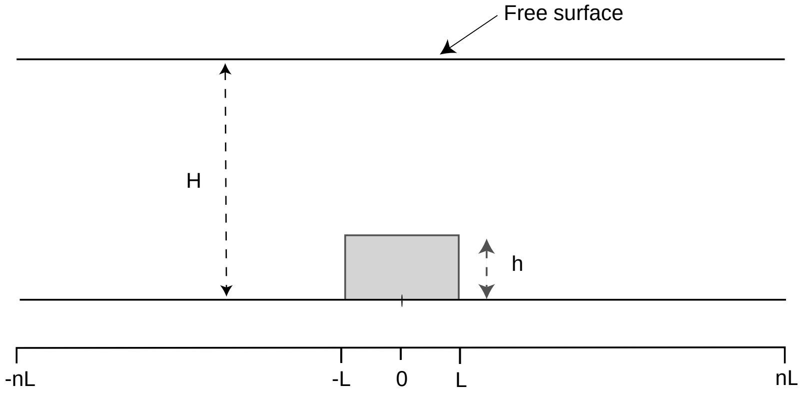

FIG. 3.11 – Sketch of the step

3.5.1 Numerical set-up

The spectral density of the bottom $F^B(k)$ is proportional to $h^2/2nLk^2$. Hence, integration of the source term along the wave propagation path yields a reflection that is proportional to $2nLF^B(k) \sim h^2/k^2$, independent of n. Although the domain length has no effect on real waves in the absence of bottom friction, it influences the discretization of the bottom spectrum ($\Delta k = 2\pi/2nL$), and thus it may have an impact on the numerical results. However $2nF^B(n)$ converges as n goes to infinity (Fig.3.12), so that the domain length does not change the results for large enough values of n. A large domain with $n = 8$ was used here.

The step width ($2L$) is taken to be half the wavelength of the surface waves for a spectrum peak $k_{0p} = 0.06\text{m}^{-1}$ ($L_0 = 104\text{m}$) in a water depth of 15m. Two different wave spectra are used here (bold lines in figure 3.12) : a wide spectrum (solid) with a classic Pierson-Moskowitz shape, typical of wind seas, and the narrow swell-like spectrum (dashed) with a Gaussian shape. Once the shape of wave spectrum is

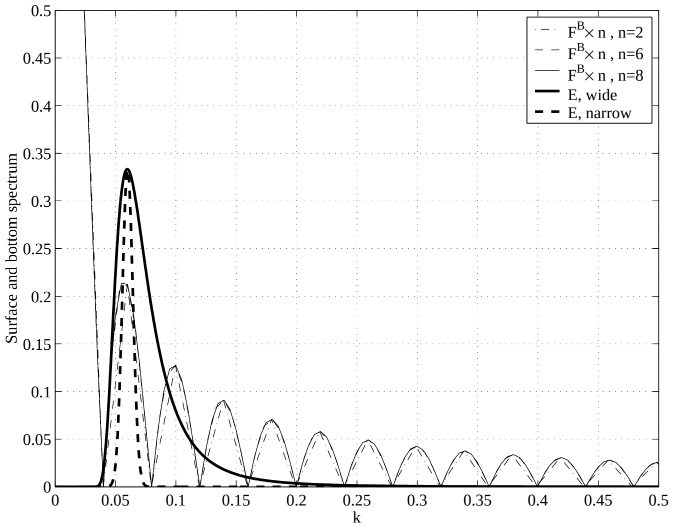

FIG. 3.12 – Wide and narrow surface wave spectra superposed on the bottom spectrum for domain sizes $n = 2, 6$ and 8. The bottom spectrum is rescaled by the surface wavenumber $(F^B(k/2))$ to show the resonant bottom and surface components.

chosen, the solution is a function of three non-dimensional variables : the step height h/H, the water depth $k_{0p}H$, and the relative step width $k_{0p}L$.

3.5.2 Influence of the height of the step

The accuracy of the source term for a range of non-dimensional step heights h/H is evaluated in intermediate and shallow water through comparison with the "exact" matching boundary algorithm (Fig.3.13). Energy reflection coefficients are compared for two different water depths, $k_{0p}H = 0.1$ and $k_{0p}H = 0.6$, representative of shallow and intermediate depths. The incident wave spectrum has a Pierson-Moskowitz shape.

As expected from previous calculations, the error in the source term increases with the step amplitude h/H. For $h/H < 0.05$ the error in the predicted reflection coefficients is less than 10%. These results provide further confirmation that the height of the localized scatterer is a limiting factor for the source term computation, but not its slope, which is infinite here, and this result holds for very shallow water.

3.5.3 Influence of the width of the step and the wave spectrum

Here we consider the dependence of the reflection coefficient on the width of the step and the width of the wave spectrum for a small amplitude step ($h/H = 0.02$) in shallow water ($k_{0p}H = 0.1$). The non-dimensional step width $k_{0p}L$ is varied,

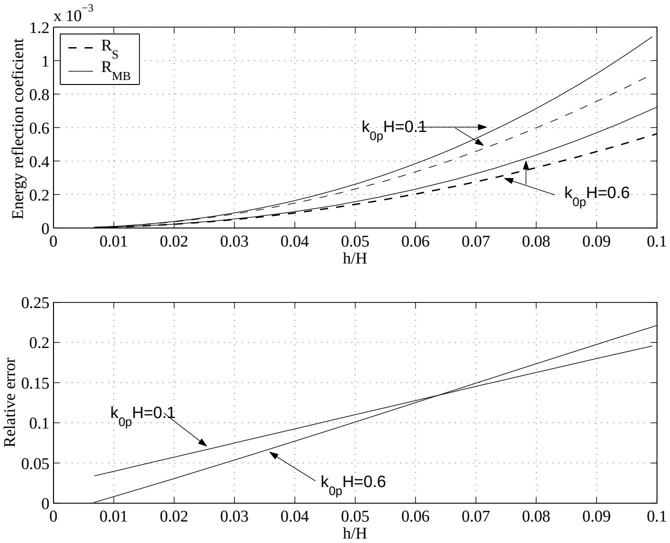

Fig. 3.13 – Reflected energy computed with the source term (dash-line) and with the matching boundary algorithm (full-line), for intermediate depth ($k_{0p}H = 0.6$) and shallow water ($k_{0p}H = 0.1$), and relative error of the source term.

effectively changing the position of the wave spectrum peak relative to the bottom spectral peaks (see Fig.3.12). Results are shown in figures 3.14 and 3.15 for wide and narrow wave spectra, respectively.

The same computation is done for the narrow spectrum (Fig.3.15).

For both wide and narrow surface wave spectra, the source term yields accurate results, and the errors do not appear to be sensitive to the width of the step. Oscillations in the reflection coefficient with varying $k_{p0}L$ represent an interference phenomenon that has been described in numerous previous studies. When a monochromatic incident wave runs up the leading edge of the step at $x = -L$, it is partly reflected and partly transmitted. As the transmitted component passes the rear edge of the step at $x = L$, it is again partially reflected and partially transmitted. If the reflected waves originating from the front and rear edges of the step are in phase we have a constructive interference which amplifies the reflection. Conversely, destructive interference occurs if the two reflected wave trains are 180 degrees out of phase and cancel out, yielding zero reflection. For long waves, maximum reflection occurs when $\sin^2 2k_{p0}L = 1$ (Mei, 1983), where k_{p0} is the incident wave wavenumber. This condition is met when :

$$2k_{0p}L = (2n-1)\frac{\pi}{2}, \qquad n = 1, 2, 3, \cdots \tag{3.31}$$

The corresponding values of $k_{p0}L$ are $k_{p0}L = \pi/4 \simeq 0.78,\ 3\pi/4 \simeq 2.35,\ 5\pi/4 \simeq 3.93 \cdots$ These values match with the reflection peaks observed in the figures (3.14,3.15) both for the source term and the matching boundary algorithm. In the wide spec-

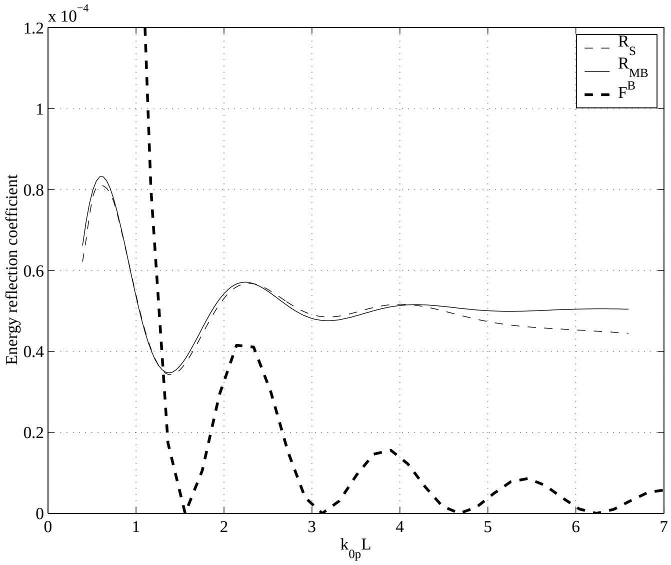

FIG. 3.14 – Reflected energy computed with the source term (dash-line) and with the matching boundary algorithm (full-line) for a wide wave spectrum. The bottom spectrum (F^B) is also indicated, scaled by the normalized resonant surface wavenumber to indicate the resonant response (bold dash-line). Other parameters are $h/H = 0.02$ and $k_{0p}H = 0.1$.

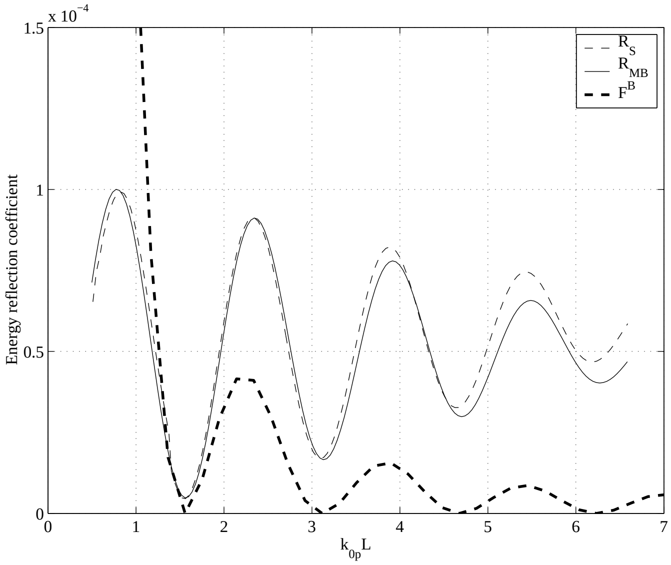

FIG. 3.15 – Same as Fig.3.14 but for a narrow wave spectrum.

trum case (Fig.3.14) these oscillations are suppressed and for high values of $k_{p0}L$, the reflection tends to a constant value. Using Bragg scattering, this is explained by the fact that in the limit of large step width $k_{p0}L$ the wave spectrum is wider than the side lobes of the bottom spectrum (see Fig.3.12) and the effects of constructive and destructive interferences for different spectral component average out. The reflection coefficient is a convolution of the bottom spectrum and the surface wave spectrum, and thus the reflection is insensitive to bottom spectral details with scales finer than the wave spectrum width.

3.6 Conclusions

Predictions of the scattering of surface waves by bottom topography based on a spectral energy balance equation that includes a wave-bottom Bragg scattering source term (Ardhuin and Herbers 2002) are compared with exact results based on a matching boundary algorithm (Rey 1992). The source term yields accurate reflection predictions for modulated sinusoidal topography. In the limit of small bottom amplitudes h compared to the water depth H, the two models yield identical results, confirming that the far-field scattered wave is determined entirely by the variance spectrum of the bottom and does not depend on the phases of its components. This finding also holds for localized topography, a result that can be justified by the approach of Mei and Hancock (2003) using their intermediate results for non-random bottoms. In that case, the bottom spectrum must be carefully calculated over a large enough domain in order to resolve the important bottom scales. Using Discrete Fourier Transforms, one may use an artificial gently sloping extension of the area covered by scatterers. However, it is found that it also holds for very steep topography, such as a single step, for a variety of water depths and wave spectrum shapes, as long as $h < H$ is small. In our calculations, relative errors in the energy reflection coefficient are found to be typically $2h/H$, or h/H for the amplitude reflection coefficient. These results show that the Bragg scattering source term is a reasonably accurate method for representing wave reflection in spectral wave models, for a wide range of small amplitude bottom topographies found on continental shelves. The source term approach is also very efficient compared to the elliptic models such as proposed by Athanassoulis and Belibassakis (1999). An extension of the source term to higher order (e.g. following Liu and Yue 1998) may reduce errors for larger values of h/H, that are shown here to be the limiting factor in practical applications. Results for $1D$ bottom profiles are expected to hold for practical $2D$ applications of the source term approximation.

Acknowledgements

This research is supported by a joint grant from Centre National de la Recherche Scientifique (CNRS) and Délégation Générale pour l'Armement (DGA). Additional funding is provided by the U.S. Office of Naval Research, and the U.S. National Science Foundation in the framework of the 2003 Nearshore Canyon Experiment (NCEX). Fruitful discussions with Kostas Belibassakis are gratefully acknowledged.

3.7 APPENDIX.A : Reconciliation of random and deterministic wave theories

Mei and Hancock (2003) considered the same problem of a wave train propagating over an arbitrary topography of small amplitude h. In their scaling h is small compared to the wavelength $2\pi/k$, but, as discussed in this paper, the scaling for the bottom perturbation could also be the mean water depth H. These authors further assume that h is a random function that is stationary with respect to the fast coordinate x, and introduce a slow coordinate x_1 for variations in the statistics of h. This two-scale approach is similar to that used by Ardhuin and Herbers (2002). Mei and Hancock (2003) obtained an amplitude evolution equation in which the topography acts as a linear damping with a coefficient β_i given by their equation (B8) as

$$\beta_i = \frac{\omega (k\sigma)^2 k (\hat{\gamma}(2k) + \hat{\gamma}(0))}{4 \cosh^2 kH (\omega^2 H/g + \sinh^2 kH)}, \tag{3.32}$$

where $\sigma^2(x_1)\gamma$ is the auto-correlation function of the bottom topography, decomposed in a slowly-varying local variance $\sigma^2(x_1)$ and a normalized auto-covariance γ. $\hat{\gamma}$ is the Fourier Transform of γ. Although Mei and Hancock's (2003) result does not conserve energy (which requires the introduction of higher order terms, see Ardhuin and Herbers 2002), it is rather general as far as the bottom is concerned. The essential difference with Ardhuin and Herbers (2002) is that there is no need for a large number of bottom undulations to obtain an expression for the scattering, and the "number of undulations" is properly defined by the scale over which the bottom auto-covariance goes to zero.

Naturally the two theories are consistent, and we can obtain from β_i the damping coefficient β_E for the energy, which is twice that for the wave amplitude A since $\partial(AA^\star)/\partial t = -2\beta_i AA^\star = -\beta_E AA^\star$, with $A^\star$ the complex conjugate of A. Re-writing (3.32) one has,

$$\beta_E = \frac{2k^3 \omega \sigma^2 (\hat{\gamma}(2k) + \hat{\gamma}(0))}{\sinh 2kH \left[2kH + \sinh 2kH\right]}. \tag{3.33}$$

For a zero-mean stationary process the Fourier transform of the auto-covariance function is simply 2π times the power spectral density F^B (e. g. Priestley 1981, theorem 4.8.1 p 211), so that, for $F^B(0) = 0$, we get

$$\beta_E = \frac{4\pi k^3 \omega F^B(2k)}{\sinh 2kH \left[2kH + \sinh 2kH\right]}, \tag{3.34}$$

which is the linear part of the bottom scattering source term (3.25) in one dimension,

$$S_{\mathrm{bscat}}(k) = \beta_E \left(E(-k) - E(k)\right). \tag{3.35}$$

Interestingly the hypothesis of randomness for h is not important for the value of β_i when averaged over the entire field of scatterers (however, it does impact the real part of β_i, i.e. the phase of the waves). Following Mei and Hancock's (2003) derivation, one may define a β_i that is also a function of the fast coordinate x using their equation (2.36), and in that case the derivation is identical, replacing $\sigma^2(x_1)\gamma$ by $h(x)h(x-\xi)$, all the way to their equations (B1)–(B3). Then one may define a mean value, which, in the case of a finite region with scatterers between $-nL$ and nL reads,

$$\overline{\beta_i} = \frac{1}{2nL} \int_{-nL}^{nL} \beta_i(x) \mathrm{d}x. \tag{3.36}$$

Taking the imaginary part of their equations (B1)–(B3) we have,

$$\overline{\beta_i} = \omega \frac{k^2}{2\cosh^2(kH)} \left\{ \frac{I_0}{\omega^2 H/g + \sinh^2(kH)} + \sum_{n=1}^{\infty} \frac{k I_n}{k_n \left[\omega^2 H/g + \sin^2(k_n H)\right]} \right\} \tag{3.37}$$

with

$$I_0 = -\Re \left\{ \frac{1}{2nL} \int_{-nL}^{+nL} \int_{-\infty}^{+\infty} \left(\frac{\mathrm{d}^2}{\mathrm{d}\xi^2} - \mathrm{i}k \right) \left(h(x)h(x-\xi) \right) \mathrm{e}^{\mathrm{i}k\xi + ik|\xi|} \mathrm{d}\xi \mathrm{d}x \right\} \tag{3.38}$$

and

$$I_n = -\Im \left\{ \frac{1}{2nL} \int_{-nL}^{+nL} \int_{-\infty}^{+\infty} \left(\frac{\mathrm{d}^2}{\mathrm{d}\xi^2} - \mathrm{i}k \right) \left(h(x)h(x-\xi) \right) \mathrm{e}^{\mathrm{i}k\xi + ik_n|\xi|} \mathrm{d}\xi \mathrm{d}x \right\} \tag{3.39}$$

Switching the order of the integrals, 3.38-3.39 are identical to their equations (B2)–(B3), provided that we redefine γ as the full auto-covariance function

$$\gamma(\xi) = \frac{1}{2nL} \int_{-nL}^{+nL} h(x)h(x-\xi) \mathrm{d}x. \tag{3.40}$$

In this case γ is obviously real and even and we obtain (3.34) for $\overline{\beta_i}$.

We have thus proved that in one dimension and in the limit of small bottom amplitudes the scattering source term applies to non-random bottoms. In these conditions, the linear part of the source term represents the damping of the incident waves (and thus also the scattered wave energy) averaged over the area covered by scatterers.

3.8 APPENDIX.B

3.8.1 Notations

A = propagating modes amplitude ;
b = root mean square amplitude from the bottom variance ;
B = evanescent modes amplitude ;
Cg = group velocity ;
Ck = spectral advection velocity ;
E = surface elevation spectral density ;
F^B = small-scale bottom elevation spectrum ;
h = bottom perturbation height ;
H = water depth ;
k = surface wavenumber ;
k_0 = peak wavenumber in deep water ;
k_{0p} = peak wavenumber ;
$k_{b,0}$ = peak bottom wavenumber ;
K = Source term coefficient ;
Kr = amplitude reflection coefficient ;
L = half-length of the ramp ;
L_0 = peak wavelength ;
n = mild slope inclination parameter ;
m = modulation parameter ;
R = energy reflection coefficient ;
R_{MB} = Matching Boundary energy reflection coefficient ;
R_{Mei} = Mei energy reflection coefficient ;
R_S = Source term energy reflection coefficient ;
S_{scat} = bottom scattering source term for the wave energy spectrum ;
T_0 = peak period ;
α = ramp inclination ;
γ = mild slope inclination ;
ε = representative bottom slope ;
ζ = free surface position ;
η = small parameter ;
Φ = velocity potential ;
χ, ψ_n = complete orthogonal set of functions ;
ω = wave radian frequency ;
Δk_b = discretization of the bottom spectrum ;

3.8.2 Subscripts

$\tilde{}$ = non-dimensionalized variable ;

3.9 Compléments : d'autres classes de résonance de Bragg

L'étude précédente (confrontation du terme de source à des cas 2D) a montré, que la principale limitation du terme de source est l'amplitude des perturbations du fond, et non sa pente (hypothèse initiale de calcul dans Ardhuin et Herbers, 2002). Le terme de source, valide théoriquement pour des fonds aléatoires, est en pratique applicable à des fonds localisés dans la limite des petites amplitudes du fond, distribuant alors la variance des perturbations uniformément sur le fond. Dans la limite des petites amplitudes du fond, la réflexion ne dépend pas de la forme du fond mais simplement de sa variance. Cette propriété est démontrée dans le cas 2D dans l'appendice de l'article précédent en utilisant les travaux de Mei et Hancock (2003). Si le terme de source est bien adapté pour représenter les effets de diffusion des vagues par la topographie dans les modèles de vagues spectraux, il se révèle également efficace pour des applications plus académiques, comme le calcul de coefficient de réflexion pour différents profils du fond (voir septième chapitre).

La diffusion des vagues par le fond calculée par le terme de source repose sur l'interaction entre deux composantes de surface ($\mathbf{k_1}$ et $\mathbf{k_2}$) et une composante de fond $\mathbf{l}$, soit la relation, $\mathbf{k_1} = \mathbf{k_2} + \mathbf{l}$, avec $\omega_1 = \omega_2$. Cette relation constitue la relation classique de diffusion de Bragg.

Belzons et al. (1991), puis Guazzelli et al. (1992) ont mis en évidence expérimentalement la diffusion de Bragg aux ordres supérieurs en utilisant un fond doublement périodique 2D (de nombres d'onde l_1 et l_2). Pour des vagues se propageant suivant une composante k, la relation de Bragg au premier ordre est caractérisée par $k = l_1/2$ et $k = l_2/2$. Au deuxième ordre, les conditions de résonance sont réalisées pour $k = l_1$, $k = l_2$, $k = (l_2+l_1)/2$ et $k = (l_2-l_1)/2$. Les études précédemment citées ont révélé une forte réflexion au niveau du pic sous-harmonique $k = (l_2 - l_1)/2$, du même ordre de grandeur que les pics principaux, et ce même pour des amplitudes du fond relativement petites. Les résultats expérimentaux ont été confrontés avec succès à la méthode des potentiels avec décomposition du fond en série de marches (Rey 1992, Rey et al. 1992) utilisée dans l'article précédent. Rey et al. (1996) ont étendu l'approche multi-échelles de Mei (1985) au deuxième ordre, rajoutant ainsi un terme à la condition au fond,

$$\frac{\partial \phi}{\partial z} = \varepsilon \frac{\partial}{\partial x}\left(\delta \frac{\partial \phi}{\partial x}\right) + \varepsilon^2 \frac{\partial}{\partial x}\left(\frac{\delta^2}{2}\frac{\partial^2 \phi}{\partial x \partial z}\right). \tag{3.41}$$

Cette approche multi-échelles a été validée dans la limite des petites amplitudes du fond (δ) par les expériences de Belzons et al. (1991) et Guazzelli et al. (1992).

Liu et Yue (1998) ont généralisé les conditions de diffusion de Bragg des vagues par le fond (Phillips 1960). Ils classent les résonances de Bragg en trois catégories. La classe I considère les interactions entre deux composantes de surface $\mathbf{k_1}$ et $\mathbf{k_2}$ et une composante de fond $\mathbf{l}$, c'est celle étudiée ici,

$$\text{Classe I} \quad \begin{cases} \mathbf{k_1} - \mathbf{k_2} \pm \mathbf{l} & = 0, \\ \omega_1 - \omega_2 & = 0. \end{cases} \tag{3.42}$$

La classe II met en jeu la non-linéarité du fond indiquant la résonance de deux composantes de surface et de deux composantes de fond.

$$\text{Classe II} \quad \begin{cases} \mathbf{k_1} - \mathbf{k_2} - (\mathbf{l_1} \pm \mathbf{l_2}) & = 0, \\ \omega_1 - \omega_2 & = 0. \end{cases} \tag{3.43}$$

Les signes $-/+$ indiquent la résonance sub-/super-harmonique respectivement.

La Classe III est le résultat de non-linéarité de surface impliquant trois composantes de surface et une composante de fond.

$$\text{Classe III} \quad \begin{cases} \mathbf{k_1} \pm \mathbf{k_2} \pm \mathbf{k_3} \pm \mathbf{l} & = 0, \\ \omega_1 \pm \omega_2 \pm \omega_3 & = 0. \end{cases} \tag{3.44}$$

Dans l'état actuel, le terme de source permet de représenter seulement la résonance de Bragg de Classe I. En poussant le calcul du terme de source à des ordres supérieurs en pente du fond, les Classes II et III pourraient être prises en compte. Le terme de source est en pratique limité par le rapport h/H, le coefficient de réflexion en amplitude est estimé avec une erreur en h/H. Pousser le calcul du terme de source aux ordres supérieurs pourrait permettre de réduire l'erreur relative en $(h/H)^2$, et étendre ainsi le domaine de validité de ce terme de source.

Chapitre 4

Evolution des vagues au-dessus d'un canyon sous-marin, influence de la réflexion

Introduction

Le chapitre précédent nous a permis de mieux connaître et comprendre les limitations du terme de source S_{bscat}. Cette pré-étude fut menée initialement dans l'objectif d'appliquer ce terme de source au cas réaliste d'un canyon sous-marin, le Canyon de Scripps (Fig. 4.1) qui présente une topographie très complexe et est sujet à d'importants effets de réfraction/diffraction/réflexion. A l'approche de ce canyon, les vagues sont réfractées de manière brutale, ce qui provoque des variations importantes de l'énergie des vagues le long de la côte (photo 4.2). Les vagues sont focalisées, en particulier à l'extrémité nord du Canyon de Scripps, emplacement réputé pour son spot de surf "Black's beach". Ce canyon est depuis longtemps l'objet

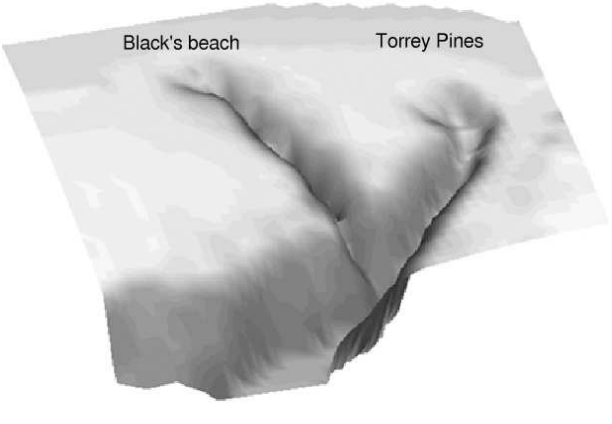

Fig. 4.1 – Canyons de Scripps et La Jolla

Fig. 4.2 – Variations importantes de l'énergie des vagues le long de la côte

d'études sur la propagation des vagues et la circulation dans la zone de surf. Munk et Traylor (1947) ont mené une campagne de mesures concentrant leurs efforts sur le phénomène de réfraction. La plage de Torrey Pines fut aussi le lieu de la première expérience côtière de grande ampleur : Nearshore Sediment Transport Study (NSTS). A l'automne 2003, une nouvelle campagne de mesures, Nearshore Canyon Experiment (NCEX), fut réalisée dans le but, entre autres, de mieux comprendre et modéliser la propagation des vagues pour des bathymétries aussi abruptes et complexes. L'objectif initial était de traiter les processus de diffusion et réflexion dans le cas de ce canyon sous-marin à l'aide du terme de source, cependant le terme de source s'est révélé inapplicable pour ce type d'étude. Les variations de profondeurs de ce canyon sont très importantes allant de 15 à 140m, plus grandes que la profondeur moyenne. On s'éloigne alors du cadre d'application du terme de source limité aux petites variations du fond. De plus, ce canyon très profond fait intervenir une variance du fond énorme dans le calcul du terme de source. En pratique les plus grandes profondeurs de ce canyon n'influencent pratiquement plus les vagues, bien qu'elles influencent grandement la valeur du terme de source par sa variance, surdimensionnant ainsi la réflexion.

Il a donc fallu s'orienter vers d'autres moyens pour traiter la propagation des vagues au-dessus de ce canyon sous-marin, et mettre en évidence les processus de réfraction et réflexion. Le choix s'est porté vers un modèle elliptique de réfraction/diffraction (Athanassoulis et Belibassakis 1999, Belibassakis et al. 2001, Gerostathis 2004) qui permet de traiter les bathymétries à fortes pentes. Afin de mettre en évidence l'importance des fortes pentes du fond qui sont totalement intégrées dans ce modèle, les résultats sont comparés à deux modèles de références qui supposent une pente douce : un modèle de réfraction/diffraction parabolique, et un modèle spectral de réfraction basé sur le tracé de rayons inverses.

4.1 Quelques mots sur les modèles

4.1.1 Modèle couplé

Le modèle elliptique de réfraction/diffraction couplé (Athanassoulis et Belibassakis, 1999) est présenté en détail dans l'article suivant et n'est donc pas repris dans ce paragraphe. Seul un exemple de modélisation est donné pour une houle venant de l'ouest et de période 15s (Fig.4.3). La grille de calcul est tournée de 45° pour obtenir une condition limite plus homogène au large, dans l'axe du canyon. On distingue clairement les zones de focalisation de la houle aux extrémités des canyons.

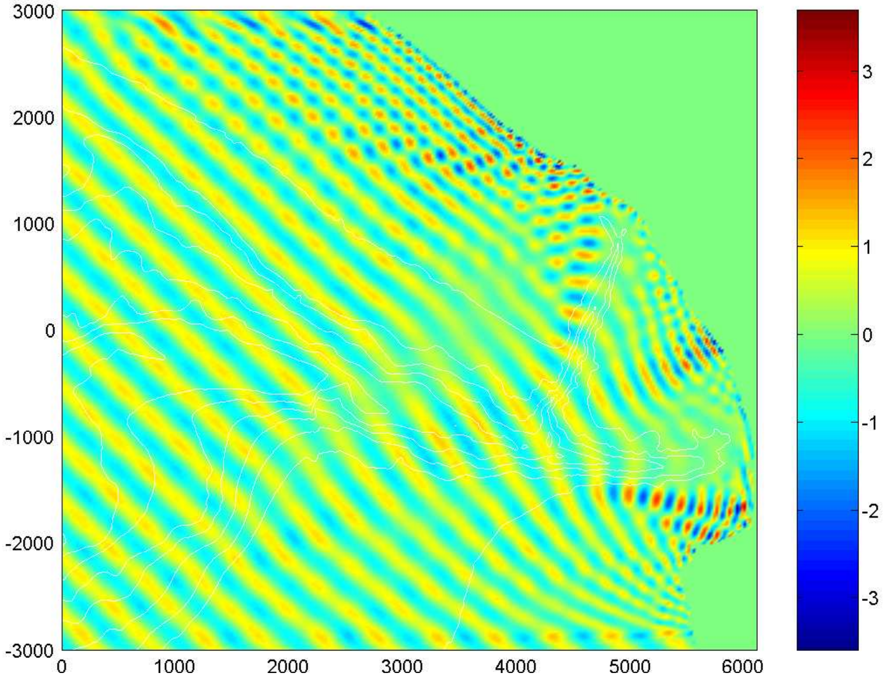

Fig. 4.3 – Partie réelle du potentiel des vitesses pour une houle de direction ouest et de période 15s

4.1.2 Modèle de réfraction

Pour des isobathes parallèles, la réfraction peut être caractérisée par la loi de Snel. Pour des bathymétries réelles, la réfraction des vagues peut être évaluée par la théorie des rayons, construction de lignes orthogonales (rayons) aux crêtes des vagues qui décrivent le chemin de propagation des vagues. Munk et Arthur (1952) ont développé une technique pour le tracé de rayon en partant des eaux profondes vers les eaux peu profondes. Les équations des rayons sont,

$$\frac{dx}{ds} = \cos(\theta), \tag{4.1}$$

$$\frac{dy}{ds} = \sin(\theta), \tag{4.2}$$

$$\frac{d\theta}{ds} = \frac{1}{C}\left(\sin\theta\frac{dC}{dx} - \cos(\theta)\frac{dC}{dy}\right), \tag{4.3}$$

avec x, y, θ la position et direction des vagues en un point du rayon, s la distance le long d'un rayon et C la vitesse de phase.

Le tracé de ces rayons permet de représenter de manière visuelle la transformation des vagues par la réfraction. Le flux d'énergie entre 2 rayons étant constant (voir eq.2.7), une convergence des rayons indique une zone d'amplification des vagues tandis qu'une divergence indique une zone de réduction de l'amplitude des vagues. Pour décrire qualitativement la réfraction de la houle au-dessus du Canyon de Scripps et La Jolla, lieu de la campagne NCEX, des rayons sont calculés et tracés pour une houle typique de direction ouest avec une période de 16s (Fig.4.4, empruntée à Peak 2004). Les vagues arrivant du Nord du Canyon de Scripps sont réfractées vers le nord, menant à une zone de focalisation importante au nord de la tête du Canyon correspondant à "Black's beach".

Lorsque les rayons se croisent (caustique), la théorie de la réfraction prévoit des amplitudes infinies pour des vagues monochromatiques. Pour palier à ce problème une solution consiste à utiliser le tracé des rayons de manière inverse, pour l'ensemble du spectre. En supposant les effets de diffraction négligeables, la relation entre un spectre incident homogène dans l'espace E_0 (conditions au large), et un spectre en eau peu profonde E est donnée par Longuet-Higgins (1957),

$$E(f,\theta) = \frac{k}{k_0}\frac{C_{g0}}{C_g}E_0(f,\theta_0). \tag{4.4}$$

Cette équation est valable le long d'un rayon, et la relation entre θ et θ_0 est obtenue en réfractant vers l'arrière une palette directionnelle de rayons à partir d'un point près de la côte. Cette méthode utilisée dans la suite de ce chapitre est illustrée par la figure 4.5, (empruntée à Peak 2004).

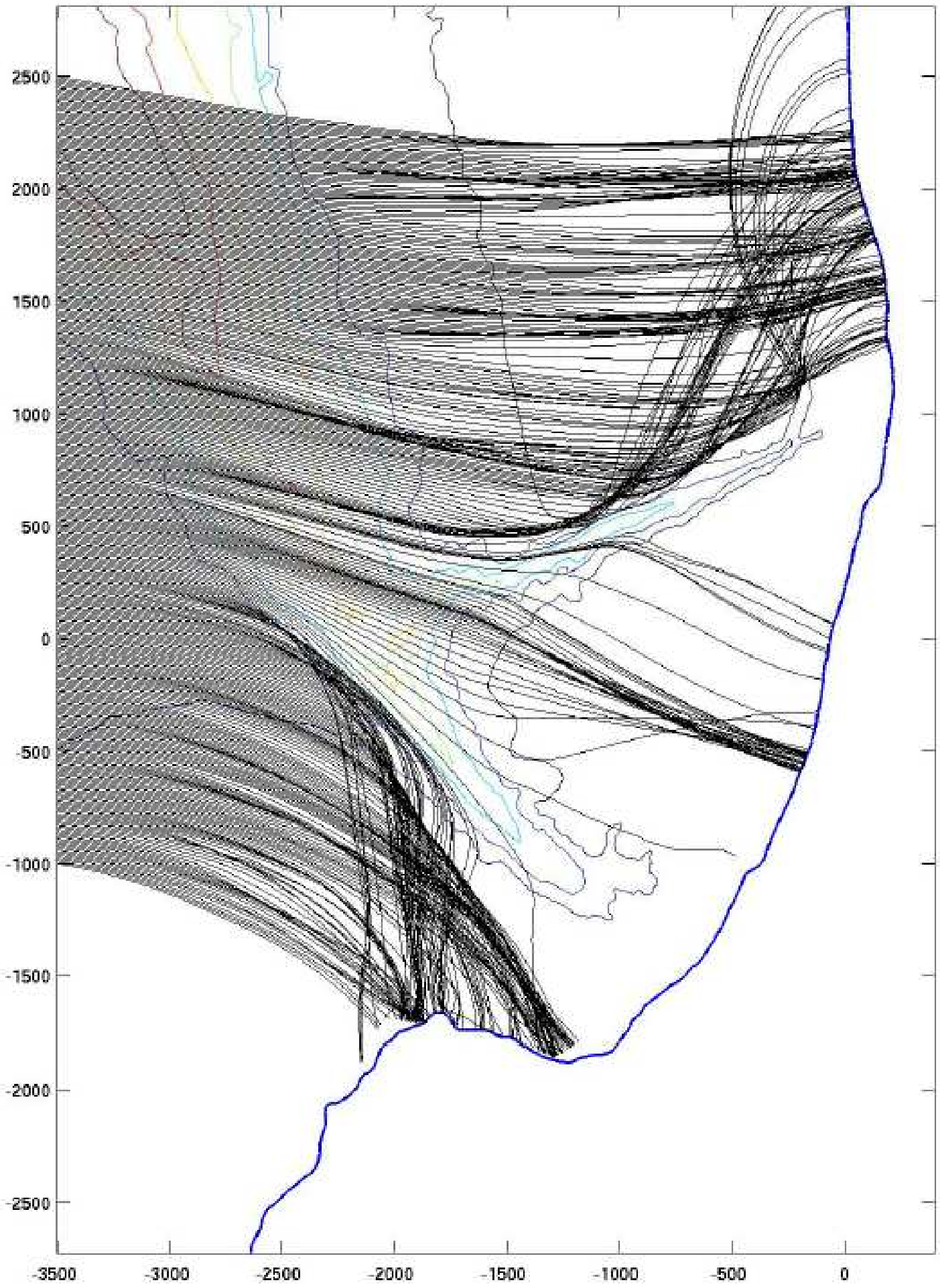

FIG. 4.4 – Rayons tracés pour une houle de direction ouest et de période 16 s. L'espace entre deux rayons sur la frontière au large est de 10m.

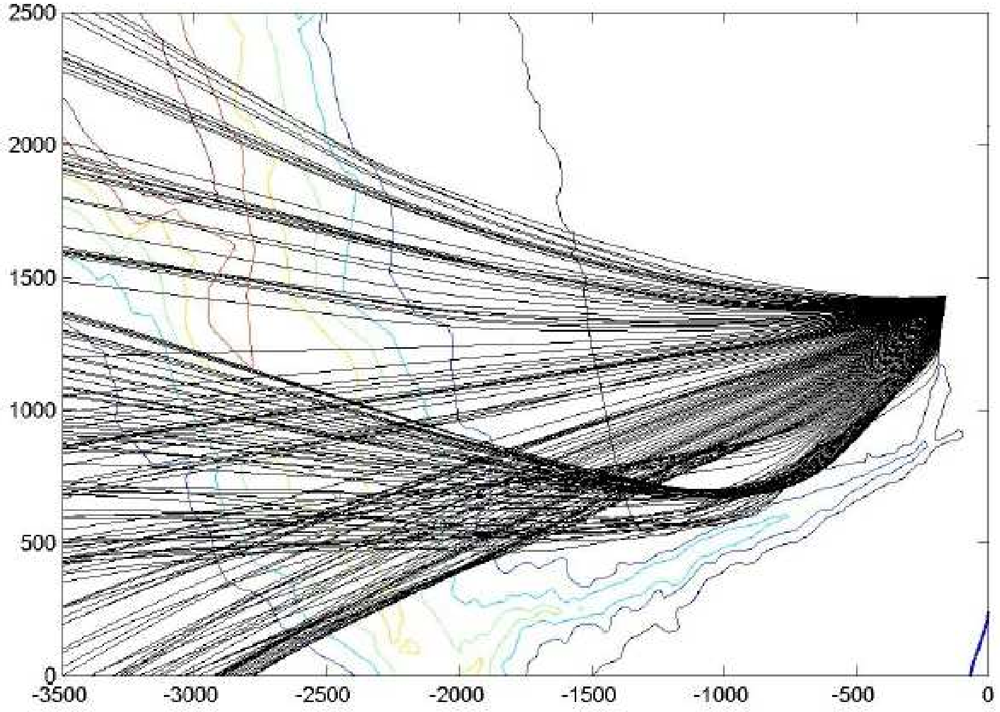

FIG. 4.5 – Rayons tracés de manière inverse pour une houle de 14 s réfractée vers un point situé au nord de la tête du Canyon de Scripps à partir du large (eau profonde), résolution angulaire de 0.5°.

Evolution of surface gravity waves over a submarine canyon

Rudy Magne(1,2), Kostas Belibassakis(3), Fabrice Ardhuin(1),
Thomas H.C. Herbers(4), Bill O'Reilly(5) and Vincent Rey(2)

Submitted to Journal of Geophysical Research
May 2005
Revised version for Journal of Geophysical Research
July 2005

(1) *Centre Militaire d'Océanographie, SHOM, BREST, France*
(2) *LSEET-LEPI, Université de Toulon et du Var, La Garde, France*
(3) *Department of Naval Architecture and Marine Engineering, National Technical University of Athens, Athens, Greece*
(4) *Dept. of Oceanography, Naval Postgraduate School, Monterey, California, USA*
(5) *Integrative Oceanography Division, Scripps Institution of Oceanography, La Jolla, California, USA*

Résumé

Les effets d'un canyon sous-marin sur la propagation des vagues sont examinés à l'aide d'un modèle couplé tridimensionnel de propagation des vagues pour des bathymétries présentant des fortes pentes. Tandis que l'approximation en optique géométrique classique prédit une transition brutale d'une transmission totale pour des angles d'incidence faible à un piégeage pour des angles importants, le modèle utilisé prédit une transition plus douce avec une réflexion/transmission partielle, sensible à la géométrie du canyon et contrôlée par les modes évanescents. Les résultats du modèle sont comparés avec les données des bouées à houle directionnelles déployées autour du bord et au-dessus du Canyon de Scripps, près de San Diego, en Californie, pendant la campagne Nearshore Canyon Experiment (NCEX). Les houles observées approchent le bord du canyon avec des angles obliques, et les hauteurs de vagues décroissent au travers du canyon par un facteur 5 sur une distance plus courte que le longueur d'onde. Un modèle spectral de rayon prédit même une réduction plus importante d'un facteur 10, car les composantes basses féquences ne peuvent traverser le canyon dans l'approximation de l'optique géométrique. Le modèle couplé mène à des résultats précis au-dessus et en aval du canyon. Ces résultats montrent que, bien que la plupart de l'énergie des vagues est piègée par réfraction en amont du bord du canyon, une petite fraction de l'énergie des vagues traverse le canyon par effet tunnel. Les simplifications du modèle qui se réduit en mild slope equation et modified mild slope equation donnent également des bon résultats, indiquant que l'effet des modes évanescents et des termes d'ordre supérieur en pente du fond sont d'importance mineure pour le spectre de surface en élévation, lorsque les vagues aléatoires se propagent à travers des variations de profondeur pour des angles d'incidence oblique.

Abstract

The effects of a submarine canyon on the propagation of ocean surface waves are examined with a three-dimensional coupled-mode model for wave propagation over steep topography. Whereas the classical geometrical optics approximation predicts an abrupt transition from complete transmission at small incidence angles to no transmission at large angles, the full model predicts a more gradual transition with partial reflection/transmission that is sensitive to the canyon geometry and controlled by evanescent modes for small incidence angles and relatively short waves. Model results are compared with data from directional wave buoys deployed around the rim and over Scripps Canyon, near San Diego, California, during the Nearshore Canyon Experiment (NCEX). Observed swells approach the canyon walls at large oblique angles, and wave heights are observed to decay across the canyon by a factor 5 over a distance shorter than a wavelength. Yet, a spectral ray model predicts an even larger reduction by a factor 10, because low frequency components cannot cross the canyon in the geometrical optics approximation. The coupled-mode model yields accurate results over and behind the canyon. These results show that although most of the wave energy is refractively trapped on the offshore canyon rim of the canyon, a small fraction of the wave energy ‘tunnels’ across the canyon. Simplifications of the model that reduces it to the standard and modified mild slope equations also yields good results, indicating that evanescent modes and high order bottom slope effects are of minor importance for the surface elevation spectrum when random waves propagate across the depth contours at large oblique angles.

4.2 Introduction

Waves are strongly influenced by the bathymetry when they reach shallow water areas. *Munk and Traylor* [1947] conducted a first quantitative study of the effects of bottom topography on wave energy transformation over Scripps and La Jolla Canyons, near San Diego, California. Wave refraction diagrams were constructed using a manual method, and compared to visual observations. Fairly good agreement was found between predicted and observed wave heights. Other effects such as diffraction were found to be important for sharp bathymetric features (e.g. harbour structures or coral reefs), prompting *Berkhoff* [1972] to introduce an equation that represents both refraction and diffraction. Berkhoff's equation is based on a vertical integration of the Laplace equation and is valid in the limit of small bottom slopes. It is widely known as the mild slope equation (MSE). A parabolic approximation of this equation was proposed by *Radder* [1979], and further refined by *Kirby* [1986] and *Dalrymple and Kirby* [1988].

O'Reilly and Guza [1991, 1993] compared *Kirby*'s [1986a, 1986b] refraction-diffraction model to a spectral refraction model using backward ray tracing, based on the theory of *Longuet-Higgins* [1957]. The two models generally agreed in simulations of realistic swell propagation in the Southern California Bight. However, both models assume a gently sloping bottom, and their limitations in regions with steep topography are not well understood. *Booïj* [1983], showed that the MSE is valid for bottom slopes as large as 1/3. To extend its application to steeper slopes, *Massel* [1993 ; see also *Chamberlain and Porter*, 1995] modified the MSE by including terms of second order in the bottom slope, that were neglected by *Berkhoff* [1972]. This modified mild slope equation (MMSE) includes terms proportional to the bottom curvature and the square of the bottom slope. *Chandrasekara and Cheung* [1997] observed that the curvature terms significantly change the wave height behind a shoal, whereas the slope-squared terms have a weaker influence. *Lee and Yoon* [2004] noted that the higher order bottom slope terms change the wavelength, which in turn affects the refraction. In spite of these improvements, an important restriction of these equations is that the vertical structure of the wave field (the wave potential) is given by a pre-selected function, corresponding to Airy waves over a flat bottom. Hence the MMSE cannot describe the wave field accurately over steep bottom topography. Thus, *Massel* [1993] also introduced an infinite series of local modes ('evanescent modes' or 'decaying waves'), that allows a local adaptation of the wave field [see also *Porter and Staziker*, 1995], and converges to the exact solution of Laplace's equation, except at the bottom interface. Indeed, the vertical velocity at the bottom is still zero, and is discontinuous in the limit of an infinite number of modes. Recently, *Athanassoulis and Belibassakis* [1999] added a 'sloping bottom mode' to the local mode series expansion, which properly satisfies the Neuman bottom boundary condition. This idea was further explored by *Chandrasekara and Cheung*, [2001] and *Kim and Bai*, [2004]. Although this sloping-bottom mode yields only small corrections for the wave height, it significantly improves the accuracy of the velocity field close to the bottom. Moreover, this mode enables a faster convergence of the series of evanescent modes, by making the convergence mathematically uniform.

As these steep topography models are becoming available, one may wonder if this level of sophistication is necessary to accurately describe the transformation of ocean waves over natural continental shelf topography. It is expected that if such models are to be useful anywhere, it should be around submarine canyons, such as Scripps canyon, off La Jolla, California, with bottom slopes $\alpha > 70°$ corresponding to $\tan\alpha > 3$. Nevertheless, a much simpler and widely used refraction model based on geometrical optics was found to yield accurate predictions of swell transformation over Scripps canyon [*Peak*, 2004], although its limitations for large bottom slopes are not well established.

The goal of the present paper is to understand the propagation of waves over the realistic bottom topography of a submarine canyon, including the practical limitations of geometrical optics theory. Numerical models will be used to sort out the relative importance of refraction and reflection. Observations of ocean swell transformation over Scripps and La Jolla Canyons, collected during the Nearshore Canyon Experiment (NCEX), are compared with predictions of the three-dimensional (3D) coupled-mode model. This model is called NTUA5 because its implementation will be limited in practice to a total of 5 modes [*Belibassakis et al.*, 2001]. This is the first verification of a NTUA-type model with field observations, as previous model validations were done with laboratory data. Further details on the latest software developments for NTUA and comparison with results of the SWAN model [*Booij et al.*, 1999] for the same NCEX case are given by *Gerosthathis and al.* [2004]. This application of NTUA5 is not straightforward since the model is based on the extension of the two-dimensional (2D) model of *Athanassoulis and Belibassakis* [1999], and requires special care in the position of the offshore boundary and the numerical damping of scattered waves along the boundary.

Here, model results are compared with two earlier models which assume a gently sloping bottom. These are a parabolic refraction/diffraction (Ref-dif) model [*O'Reilly and Guza*, 1993 adapted from *Kirby*, 1986], applied in a spectral sense, and a spectral refraction model based on backward ray tracing [*Dobson*, 1967 ; *O'Reilly and Guza*, 1993]. A brief description of the coupled-mode model and the problems posed by its implementation in the NCEX area is given in section 2. Although our objective is the understanding of complex 3D bottom topography effects in the NCEX observations, this requires some prior analysis, performed in section 3, of reflection and refraction patterns over idealized 2D canyons. Results are presented for realistic transverse canyon profiles, including a comparison with the 2D analysis of infragravity wave observations reported by *Thomson and al.* [2005]. Comparisons of 3D models with field data are presented in section 4 for a representative westerly swell event observed during NCEX. Conclusions follow in section 5.

4.3 Numerical Models

The fully elliptic 3D model developed by *Belibassakis et al.* [2001] is based on the 2D model of *Athanassoulis and Belibassakis* [1999]. These authors formulate the problem as a transmission problem in a finite subdomain of variable depth $h_2(x)$ (uniform in the lateral y-direction), closed by the appropriate matching conditions at the offshore and inshore boundaries. The offshore and inshore areas are considered as incidence and transmission regions respectively, with uniform but different depths (h_1, h_3), where complex wave potentials amplitudes φ_1 and φ_3 are represented by complete normal-mode series containing the propagating and evanescent modes.

The wave potential φ_2 associated with h_2 (region 2), is given by the following local mode series expansion :

$$\varphi_2(x,z) = \varphi_{-1}(x)Z_{-1}(z;x) + \varphi_0(x)Z_0(z;x) + \sum_{n=1}^{\infty} \varphi_n(x)Z_n(z;x), \tag{4.5}$$

where $\varphi_0(x)Z_0(z;x)$ is the propagating mode and $\varphi_n(x)Z_n(z;x)$ are the evanescent modes. The additional term $\varphi_{-1}(x)Z_{-1}(z;x)$ is the sloping-bottom mode, which permits the consistent satisfaction of the bottom boundary condition on a sloping bottom. The modes allow for the local adaptation of the wave potential. The functions $Z_n(z;x)$ which represent the vertical structure of the n^{th} mode are given by,

$$Z_0(z,x) = \frac{\cosh[k_0(x)(z+h(x))]}{\cosh(k_0(x)h(x))}, \tag{4.6}$$

$$Z_n(z,x) = \frac{\cos[k_n(x)(z+h(x))]}{\cos(k_n(x)h(x))}, \quad n = 1,2,..., \tag{4.7}$$

$$Z_{-1}(z,x) = h(x)\left[\left(\frac{z}{h(x)}\right)^3 + \left(\frac{z}{h(x)}\right)^2\right], \tag{4.8}$$

where k_0 and k_n are the wavenumbers obtained from the dispersion relation (for propagating and evanescent modes), evaluated for the local depth $h = h(x)$:

$$\omega^2 = gk_0 \tanh k_0 h = -gk_n \tan k_n h, \tag{4.9}$$

with ω the angular frequency

As discussed in *Athanassoulis and Belibassakis* [1999], alternative formulations of Z_{-1} exist, and the extra sloping-bottom mode controls only the rate of convergence of the expansion (7.5) to a solution that is indeed unique. The modal amplitudes φ_n are obtained by a variational principle, equivalent to the combination of the Laplace equation, the bottom and surface boundary conditions, and the matching conditions at the side boundaries, leading to the coupled-mode system,

$$\sum_{n=-1}^{\infty} a_{mn}(x)\varphi_n^{''}(x) + b_{mn}(x)\varphi_n^{'}(x) + c_{mn}(x)\varphi_n(x) = 0, \qquad (m = -1, 0, 1, ...), \tag{4.10}$$

where a_{mn}, b_{mn} and c_{mn} are defined in terms of the Z_n functions, and the appropriate end-conditions for the mode amplitudes φ_n ; for further details, see *Belibassakis et al.* [2001]. The sloping-bottom mode ensures absolute and uniform convergence of the modal series. The rate of decay for the modal function amplitude is proportional to (n^{-4}). Here, the number of evanescent modes is truncated at $n = 3$, which ensures satisfactory convergence, even for bottom slopes exceeding 1.

This 2D solution is further extended to realistic 3D bottom topographies by *Belibassakis et al.* [2001]. In 3D, the depth h_2 is decomposed into a background parallel-contour surface $h_i(x)$ and a scattering topography $h_d(x, y)$. The 3D solution is then obtained as the linear superposition of appropriate harmonic functions corresponding to these two topographies. There is no limitation on the shape and amplitude of the bottom represented by $h_d(x, y)$ except that $h_d > 0$, which can always be enforced by a proper choice of h_i, for further details see *Belibassakis et al.* [1999]. The wave potential solution over the 2D topography (h_i) is governed by the equations described previously. The wave potential associated with the scatterers (h_d) is obtained as the solution of a 3D scattering problem. The decomposition of the topography in h_d and h_i is not uniquely defined by the constraints that h_i is invariant along y and $h_d > 0$, and there is thus no simple physical interpretation of the scattered field which corresponds to both reflection and refraction effects. The main benefit of that decomposition is that the scattered wave field propagates towards the outside of the model domain all along the boundary, which greatly simplifies the specification of the horizontal boundary conditions.

In practice we chose

$$h_i(x) = \min \{h(x,y) \quad \text{for} \quad y \in [y_{\min}, y_{\max}]\} \,. \tag{4.11}$$

Further, the bathymetry $h_i + h_d$ is modified by including a transition region for $y < y_{\min}$ and $y > y_{\max}$ in which h_d goes to zero at the model boundary, so that no scattering sources are on the boundary and waves actually propagate out of the domain. This modification of the bathymetry does not change the propagation of the incoming waves, provided that the offshore boundary is in uniform water depth, as in the test cases described by *Belibassakis et al.* [2001], or in deep enough water so that a uniform water depth can be prescribed without having an effect on the waves. Solutions are obtained by solving a coupled-mode system, similar to Eq.(4.10), but extended to two horizontal dimensions (x, y), and coupled with the boundary conditions ensuring outgoing radiation. The spatial grid for the scattered field is extended with a damping layer all around the boundary [*Belibassakis et al.*, 2001].

Both 2D and 3D implementations of this model called NTUA5 are used here to investigate wave propagation over a submarine canyon. If we neglect the sloping-bottom mode and the evanescent modes, and retain in the local-mode series only the propagating mode $\varphi_0(x,y)$, this model (NTUA5) exactly reduces to MMSE,

$$\nabla^2\varphi_0(x,y) + \frac{\nabla(CC_g)}{CC_g} \cdot \nabla\varphi_0(x,y) + \left[k_0^2 + f_1\dot{\nabla}^2 h + f_2\dot{(}\nabla h)^2\right]\varphi_0(x,y) = 0, \tag{4.12}$$

where $f_1 = f_1(x,y)$ and $f_2 = f_2(x,y)$ are respectively functions dependent on the bottom curvature and slope-squared terms. From Eq.(4.12), the MSE is obtained by further neglecting the curvature and slope-squared terms.

In the following sections, these two formulations (MSE and MMSE) will be compared to the full 5-mode model to examine the importance of steep bottom slope effects, which are fully accounted for in this model. The MSE and MMSE solutions are obtained by exactly the same scattering method described above with the same computer code in which the high order bottom slope terms and/or evanescent modes are turned off. For 3D calculations, our use of a regular grid sets important constraints on the model implementation due to the requirements to have the offshore boundary in deep water and sufficient resolution to resolve the wavelength of waves in the shallowest parts of the model domain. These constraints put practical limits on the domain size for a given wave period and range of water depths. Here a minimum of 7 points per wavelength in 10 m depth was enforced, in a domain that extends 4–6 km offshore. Such a large domain with a high resolution leads to memory intensive inversion of large sparse matrices. However, the NTUA, MSE and MMSE models are linear, and thus the propagation of the different offshore wave components can be performed separately, sequentially or in parallel.

Before considering the full complexity of the 3D Scripps-La Jolla Canyon system, we first examine the behaviour of these models in the case of monochromatic waves propagating over 2D idealized canyon profiles (transverse sections of the actual canyons). We consider both normal incidence, for which many studies have been published including a recent study of infragravity wave reflection by La Jolla Canyon [*Thomson et al.* 2005], and oblique incidence, which is relevant to observed swell propagation over Scripps Canyon.

4.4 Idealized 2D Canyon profiles

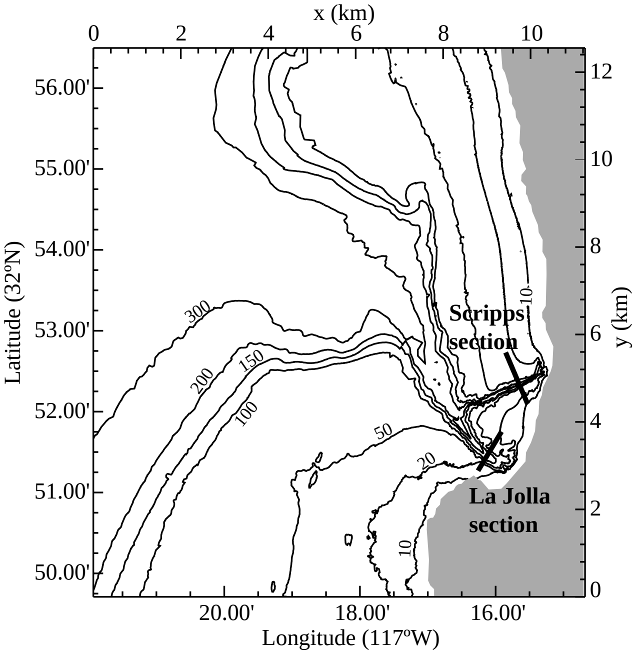

FIG. 4.6 – Bathymetry around La Jolla and Scripps canyons, and definition of transverse sections for idealized calculations.

4.4.1 Transverse section of La Jolla Canyon

We investigate monochromatic waves propagating at normal incidence over a transverse section of the La Jolla Canyon (Figures 4.6,4.7), which is relatively deep (120 m) and wide (350 m). Oblique incidence will not be considered for this canyon because results similar to Scripps canyon are obtained for these angles, and less data is available around La Jolla Canyon. Reflection coefficients R for the wave

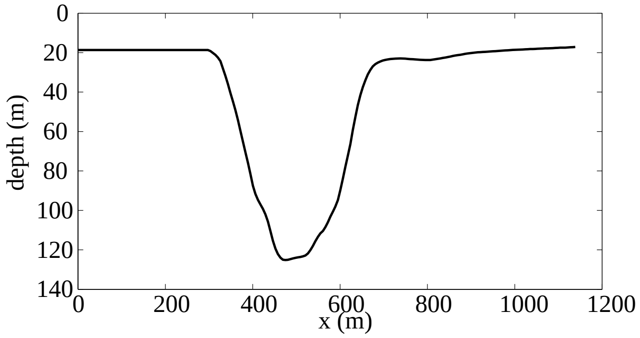

FIG. 4.7 – Water depth across the La Jolla canyon section

amplitude are computed using the MSE, the MMSE, and the full coupled-mode model NTUA5. R is easily obtained using the natural decomposition provided by the scattering method, and it is defined as the ratio between the scattered wave potential amplitude, up-wave of the topography, and the amplitude of the imposed propagating wave. In addition, a stepwise bottom approximation model developed by *Rey* [1992], based on the matching of integral quantities at the boundaries of adjacent steps, is also used to evaluate R [see *Takano*, 1960 ; *Miles*, 1967 ; *Kirby and Dalrymple*, 1983]. This model is known to converge to the exact solution of Laplace's equation, and will be used as a benchmark for this study. 70 steps were found to be enough to obtain a converging result and are thus used to resolved the canyon profile. The predicted values of R as a function of wave frequency f (Figure 4.8), are characterized by maxima and minima, which are similar to the rectangular step response shown in *Mei and Black* [1969], *Kirby and Dalrymple* [1983a], and *Rey et al.* [1992]. The spacing between the minima or maxima is defined by the width of the step or trench, which imposes resonance conditions, leading to constructive or destructive interferences. Both the MSE and MMSE models are found to generally overestimate the reflection at high frequencies, whereas the NTUA5 model is in good agreement with the benchmark solution. The sloping-bottom mode included in NTUA5 has a negligible impact on the wave reflection in this and other cases discussed below. The only other difference between the NTUA5 and the MMSE models is the addition of the evanescent modes which, through their effect on the near wave field solution modify significantly the far field, including the overall reflection and transmission over the canyon.

The influence of the bottom slope on the reflection and the limitations of the models are investigated using idealized profiles of the La Jolla Canyon. A 120 m deep and 350 m wide rectangular trench was smoothed to obtain three profiles with the same cross section (comparable to the La Jolla Canyon, Figure 4.7), but different maximum slopes $\tan\alpha_{\max} = 0.25$, 0.75 and 2.47 (Figure 4.9). As expected

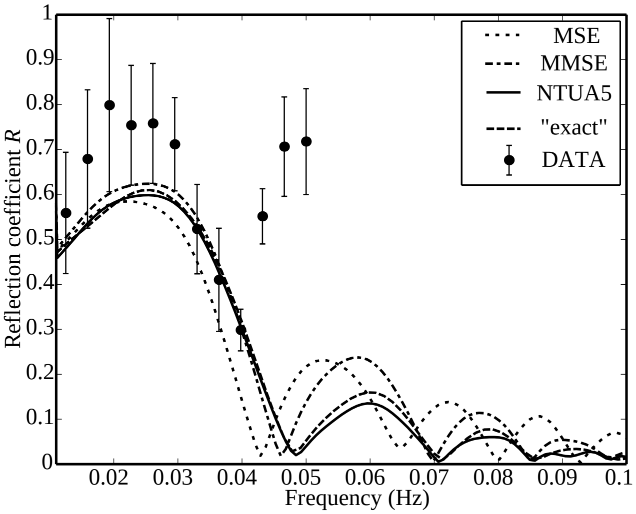

FIG. 4.8 – Amplitude reflection coefficient R for waves propagating at normal incidence over the La Jolla canyon section (figure 4.7) using several numerical models, and observed infragravity reflections for near-normal incidence angles [*Thomson et al.*, 2005]

.

from theory, MMSE and NTUA5 converge to the benchmark solution in the limit of mild slopes. In particular, general agreement between the models is found for a profile with a relatively mild slope ($\tan \alpha_{\max} = 0.25$, figure 4.9b), except for some over-prediction of the MSE and (to a lesser degree) the MMSE at low frequencies.

A well known limitation of the MSE was demonstrated found for large slopes by *Booij* (1983) who, based on finite element models, concluded that the MSE is inaccurate for bottom slopes exceeding 1/3. Yet, *Suh et al.* [1997], *Lee et al.* [1998] and *Benoit* [1999] have also noticed errors of the MSE for bottom profiles with slopes smaller than 1/3 but rapid slope variations in space (i.e. with relatively large curvature). This results highlight the importance of the bottom curvature and slope squared terms that are necessary to obtain accurate wave propagation properties, even in the limit of small bottom slopes. More generally, the error of the MSE in the limit of small slopes is related to the fact that, in general, the reflection coefficient over a gently sloping bottom, even with zero curvature, cannot be approximated with a polynomial function of the bottom slope [*Meyer*, 1979]. This author and others have described this peculiarity as a 'WKB paradox'.

For moderate slopes ($\tan \alpha_{\max} = 0.75$, Figure 4.9c), both the MSE and MMSE models do not reproduce correctly the amplitude of the reflection. It is interesting to notice that the reflection coefficient pattern with MSE is slightly shifted to lower frequencies, whereas MMSE still yields relatively good estimates of the frequencies where reflection maxima and minima occur. For the steepest ($\tan \alpha_{\max} = 2.47$)

slope case (Figure 4.9d), this shift is more pronounced, especially for the MSE model which predicts zero reflection where maxima occur according to the benchmark. The NTUA5 model is in good agreement with the benchmark solution. The evanescent modes apparently shit to larger values the resonant wavenumbers where R reaches maxima. That shift is consistent with results by *Kirby and Dalrymple* [1983] in the case of a rectangular trench.

Thomson et al. [2005] investigated the transmission of infra-gravity waves with frequencies in the range 0.006–0.05 Hz across this same canyon. Based on pressure and velocity time series at two points located approximately at the ends of the La Jolla section these authors estimated energy reflection coefficients as a function of frequency. In a case of near-normal incidence they observed a minimum of wave reflection at about 0.04 Hz, generally consistent with the present results for our choice of a canyon section (figure 4.8). *Thomson et al.* [2005] further found a good fit of their observations to the theoretical reflection across a rectangular trench as given by *Kirby and Dalrymple* [1983] in the limit of long waves, and neglecting evanescent modes. This approximation is appropriate for the long infragravity band for which the effects of evanescent modes are relatively weaker. The observations of *Thomson et al.* [2005] also agree well with the various NTUA models applied here to the actual canyon profile (figure 4.8). At higher swell frequencies ($f > 0.05$ Hz), the MSE, MMSE and NTUA model results diverge for normal incidence (figure 4.8). However, contrary to the beach-generated infragravity waves, swell arrives from the open ocean and thus always reaches this canyon with at a large oblique angle, for which the differences between these models are small (not shown). This is also true for Scripps canyon, further discussed below, as if the bottom has a smaller 'effective slope', closer to the bottom slope in the direction of the wave orbital motion. This convergence of various models for large incidence angles, corresponding to relative weak evanescent modes effects on the reflection, was also found by *Kirby and Dalrymple* [1983] over a rectangular trench.

4.4.2 Transverse section of Scripps Canyon

Normal incidence

The north branch of the canyon system, Scripps Canyon, provides a very different effect due to a larger depth (145 m) and a smaller width (250 m). Scripps Canyon is also markedly asymmetric with different depths on either side. A representative section of this canyon is chosen here (Figure 4.10). Reflection coefficient predictions for waves propagating at normal incidence over the canyon section are shown in Figure 4.11. R decreases with increasing frequency without the pronounced side lobe

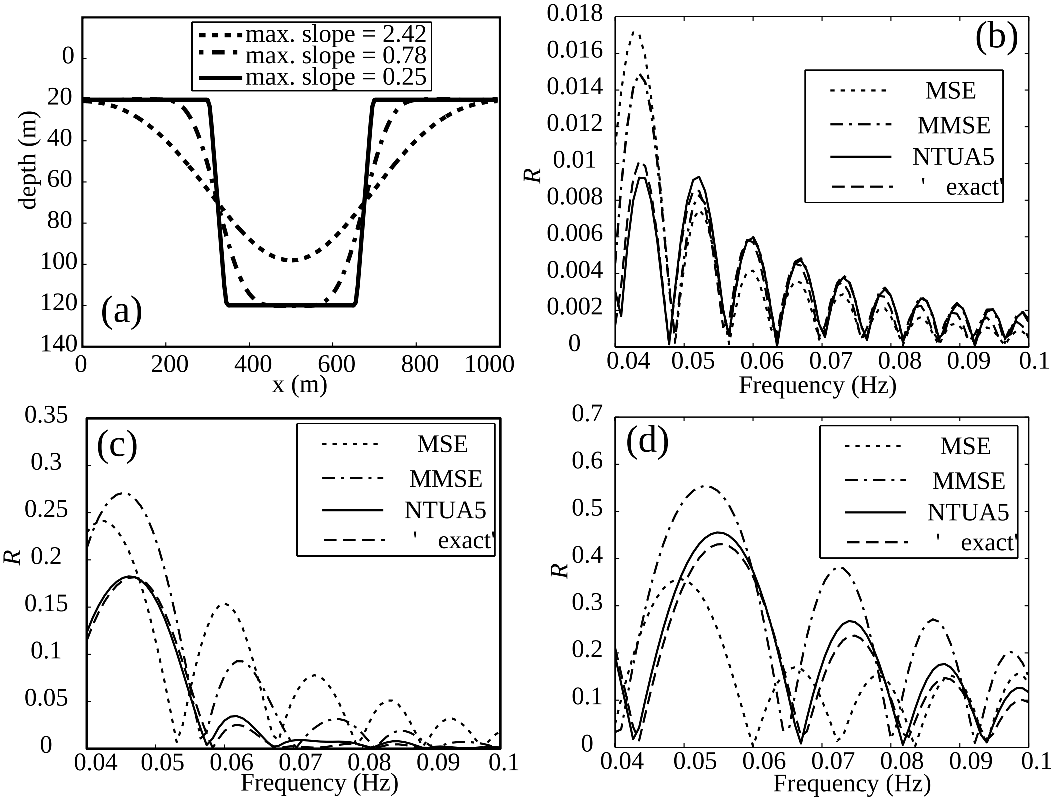

FIG. 4.9 – (a) idealized sections of La Jolla Canyon and wave amplitude reflection coefficients R calculated with various models and for maximum bottom slopes of (a) 0.25, (b) 0.74, and (c) 2.47

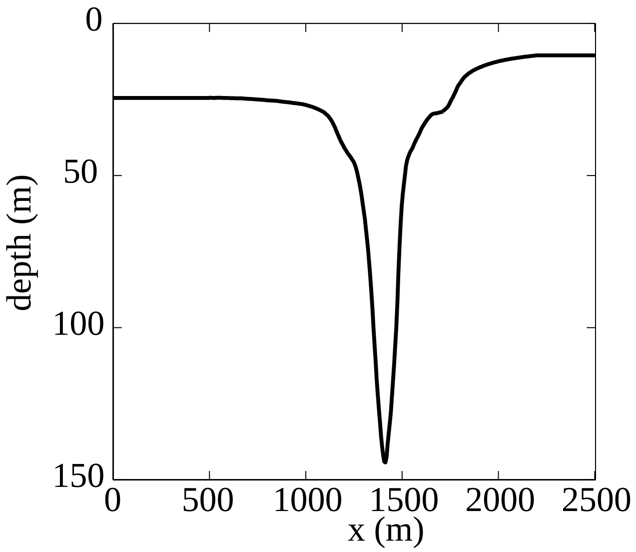

FIG. 4.10 – Water depth across the Scripps canyon section

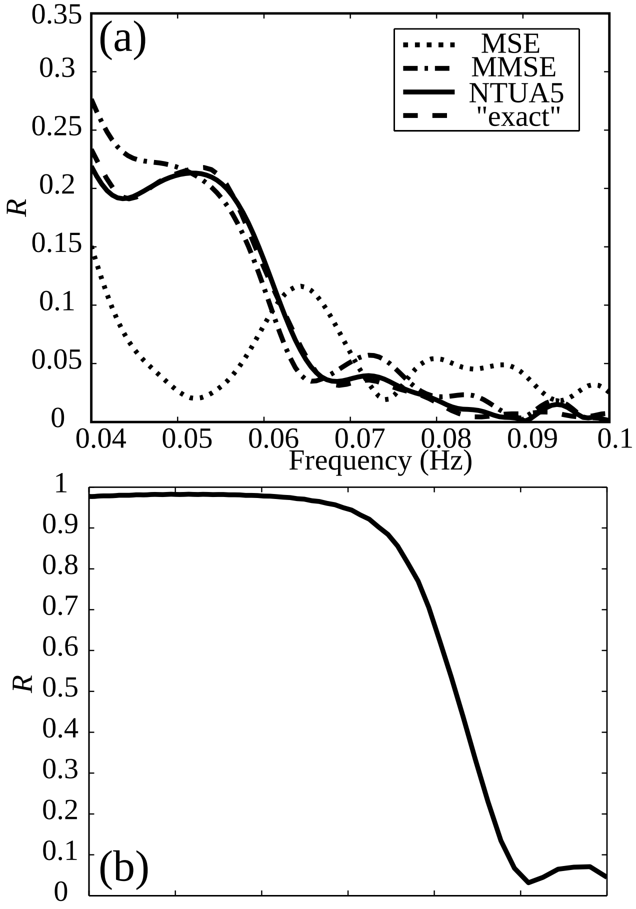

FIG. 4.11 – Reflection coefficient for waves propagating at (a) normal incidence over the Scripps canyon section, (b) for $\theta_i = 45°$. All models collapse on the same curve in (b).

pattern predicted for the La Jolla Canyon section. Again, the NTUA5 results are in excellent agreement with the exact solution. The MSE dramatically underestimates R at low frequencies, and overestimates R at high frequencies. However, the MMSE is in fairly good agreement with the benchmark solution in this case, suggesting that the higher order bottom slope terms are important for the steep Scripps Canyon profile reflection, while the evanescent modes play only a minor role.

Oblique incidence

The swell observed near Scripps Canyon generally arrives at a large oblique angle at the offshore canyon rim. To examine the influence of the incidence angle θ_i, a representative swell frequency $f = 0.067$ Hz was selected, and the reflection coefficient was evaluated as a function of θ_i. The amplitude reflection coefficient R is very weak when θ_i is small, and as θ_i increases, R jumps to near-total reflection within a narrow band of direction around 35° (Figure 7). Indeed, for a wave train propagating through a medium with phase speed gradient in one dimension only, geometrical optics predicts that beyond a threshold (Brewster) angle θ_B, all the wave energy is trapped, and no energy goes through the canyon. This sharp transition does not depend at all on the magnitude of the gradient which may even be infinite, and for a shelf depth H_1 and maximum canyon depth H_{max}, this threshold angle is given by

$$\theta_B = \arcsin\left(\frac{C_1}{C_{\max}}\right) \tag{4.13}$$

where C_1 and $C_{\max}$ are the phase speeds for a given frequency corresponding to the depths H_1 and $H_{\max}$. Thus θ_B increases with increasing frequency as the phase speed ratio diminishes at high frequencies. For Scripps Canyon , at $f = 0.067$ Hz, $H_1 = 24$ m, and $H_{\max} = 145$ m, and θ_B is 38°. As a result, for $\theta_i < \theta_B$, no reflection is predicted by refraction theory (dashed line), and all the wave energy is transmitted through the canyon. This threshold value separates distinct reflection and refraction (trapping) phenomena, respectively occurring for $\theta_i < \theta_B$ and $\theta_i > \theta_B$.

The elliptic models that account for diffraction predict a smoother transition. For $\theta_i < \theta_B$, weak reflection is predicted. For $\theta_i > \theta_B$, a fraction of the energy is still transmitted through the canyon. This transmission of wave energy across a deep region where $\sin\theta_i/C_{\max}$ exceeds $1/C_1$, violates the geometrical optics approximation. This transmission is similar to the tunneling of quantum particles through a barrier of potential in the case where the barrier thickness is of the order of the wavelength or less [*Thomson et al.*, 2005]. The wave field near the turning point of wave rays in the canyon decays exponentially in space on the scale of the wavelength [e.g. *Chao and Pierson*, 1972], and that decaying wave excites a propagating wave on the other side of the canyon. This coupling of both canyon sides generally decreases as the canyon width or the incidence angle increase [*Kirby and Dalrymple*, 1983 ; *Thomson at al.*, 2005]. The significant differences between MSE and MMSE at small angles $\theta_i < \theta_B$ are less pronounced for $\theta_i > \theta_B$.

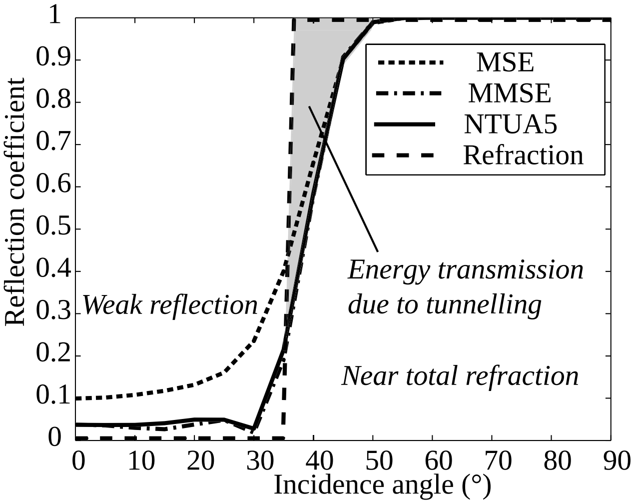

FIG. 4.12 – Reflection coefficient for waves of period $T = 16$ s propagating over the Scripps Canyon section as a function of the wave incidence angle θ_i (0 corresponds to waves travelling perpendicular to the canyon axis).

These two regimes are illustrated by the evolution of the wave potential amplitude over the Scripps canyon section. In figure 4.13, results of various elliptic models (MSE, MMSE and NTUA5) are compared with a parabolic approximation of the MSE (the 'Ref-dif' model used by *O'Reilly and Guza* [1993], based on *Kirby* [1986]). It should be noted that this 2D version of Ref-dif model does not have the very large angle approximation of *Dalrymple et al.* [1989], and that the model grid orientation is chosen with the main axis along the wave propagation direction (different grids are used for different incidence angles), on order to minimize large angle errors due to the parabolic approximation. For $\theta_i = 30° < \theta_B$, weak reflection (about 10%) is predicted by the MMSE and NTUA5 (figure 8a). MSE considerably overestimates the reflection, and thus underestimates the transmitted energy down-wave of the canyon section. A partial standing wave pattern is predicted up-wave of the canyon as a result of the interference of incident and reflected waves. The largest amplitudes, about 20% larger than the incident wave amplitude, occur in the first antinode near the canyon wall. These oscillations are not predicted by Ref-dif, because the parabolic approximation, by construction, does not allow wave reflection in directions

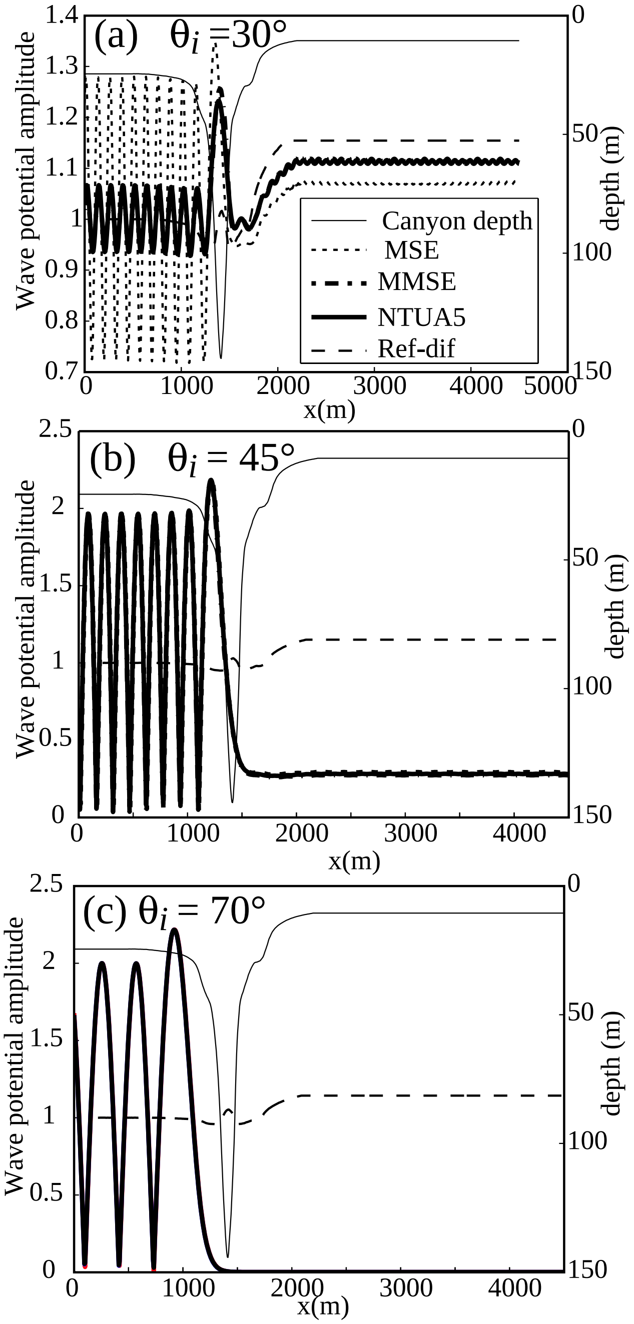

Fig. 4.13 – Wave amplitude over the Scripps Canyon section, for $T = 16$ s and different incident angles (a) $\theta_i = 30°$, (b) $\theta_i = 45°$, and (c) $\theta_i = 70°$. The canyon depth profile is indicated with a thin dashed line. The MMSE result cannot be distinguished from that of NTUA5 in all panels, and all models except for Ref-dif give the same results in (b) and (c).

more than 90° away from the main axis of the grid. As a result, the present implementation of Ref-dif overestimates the transmitted wave energy on the other side of the canyon. However, improved reflection can be obtained with a different grid orientation.

For a larger wave incidence angle (e.g. $45° > \theta_B$), an almost complete standing wave pattern is predicted by the elliptic models up-wave of the canyon, with an exponential tail that extends across the canyon to a weak transmitted component. Finally, transmission is extremely weak for $\theta_i = 70°$ (figure 4.13.c). The parabolic model Ref-dif does not predict the trapping and the associated standing wave pattern, up-wave of the canyon and strongly overestimates the transmitted wave amplitude downwave of the canyon.

4.5 West Swell Over Scripps Canyon

The models used in the previous section (MSE, MMSE, NTUA5, Ref-dif, refraction) are now applied to the real 3D bottom topography of the Scripps-La Jolla Canyon system, and compared with field data from directional wave buoys deployed around the rim and over Scripps Canyon during NCEX.

4.5.1 Models Set-up

The implementations of MSE, MMSE, NTUA5, and Ref-dif use two computational domains with grids of 275 by 275 points (Figure 4.14). The larger domain is used for wave periods longer than 15 s and the grid has a resolution of 21 m. The smaller domain, with a higher resolution of about 15 m, is used for 15 s and shorter waves. The y-axis of the grid is rotated 45° relative to the North to place the offshore boundary in the deepest region of the domain. Models were run for many sets of incident wave frequency and direction $(f,\ \theta)$. The CPU time required for one (f, θ) wave component calculation with the NTUA5 model (with 3 evanescent modes) is about 120s on a Linux computer with 2Gb of memory and a 3 GHz processor. The wave periods and offshore directions used in the computation range from 12 to 22 s and 255 to 340 degrees respectively, with 0.2 s and 2° increments. The minimum period 12 s corresponds to the shortest waves that can be resolved with 7 points per wavelength in 10 m depth. Shorter waves are not considered here because they may be affected by local wind generation, not represented in the models used here, and are also generally less affected by the bottom topography.

Transfer functions between the local and offshore wave amplitudes were evaluated at each of the buoy locations and used to transform the offshore spectrum. The backward ray-tracing refraction model directly evaluates energy spectral transfer functions between deep water, where the wave spectrum is assumed to be uniform, and each of the buoys located close to the canyon, based of the invariance of the wavenumber spectrum along a ray [*Longuet-Higgins*, 1957]. A minimum of 50 rays was used for each frequency-direction bin (bandwidth 0.005 Hz by 5 degrees), computed over the finest available bathymetry grid, with 4 m resolution. The model is identical to the CREST model described by *Ardhuin et al.* [2001] with the energy source term set to zero.

4.5.2 Model-Data Comparison

Long swell from the west was observed on 30 November 2003, in the absence of significant local winds. In the present analysis we use only data from Datawell Directional Waverider buoys. The Torrey Pines Outer Buoy is permanently deployed by the Coastal Data Information Program (CDIP), and located about 15 km offshore of Scripps Canyon. That buoy provided the deep water observations, in the form of frequency-direction spectra, necessary to drive the wave models. The directional distribution of energy for each frequency was estimated from buoy cross-spectra using the Maximum Entropy Method [*Lygre and Krogstad*, 1986]. The NCEX observations were made at six sites around the head of Scripps Canyon (figure 4.16). All spectra used in the comparison, including the offshore boundary condition, were averaged from 13 :30 to 16 :30 UTC, so that the almost continuous record yields about 100 degrees of freedom for each frequency band with a width of 0.005 Hz.

The observed narrow spectrum has a single peak with a period of 14.5 s, and a mean direction of 272 degrees, corresponding to an incidence angle θ_i (relative to the Scripps Canyon axis) of 65° (Figure4.15). The model hindcasts are compared with observations in Figure 4.17. Significant wave heights were computed from the measured and predicted wave spectra at each instrument location, including only the modelled frequency range,

$$H_s = 4\left(\int_{f_1}^{f_2}\int_{\theta_1}^{\theta_2} M(f,\theta)E(f,\theta)df d\theta\right)^{1/2}, \tag{4.14}$$

where $E(f,\theta)$ is the offshore frequency-directional spectrum and $M(f,\theta)$ is the ratio between the local and offshore wave energies for the frequency f and offshore direction θ, as computed with the models. Observations show a dramatic variation in wave height on a very short scale across the canyon (figure 4.17) . The offshore wave height is slightly increased at site 33 and 34, in water depths of 34 and 23 m respectively, along the North side of the Canyon, and slightly reduced on the shelf

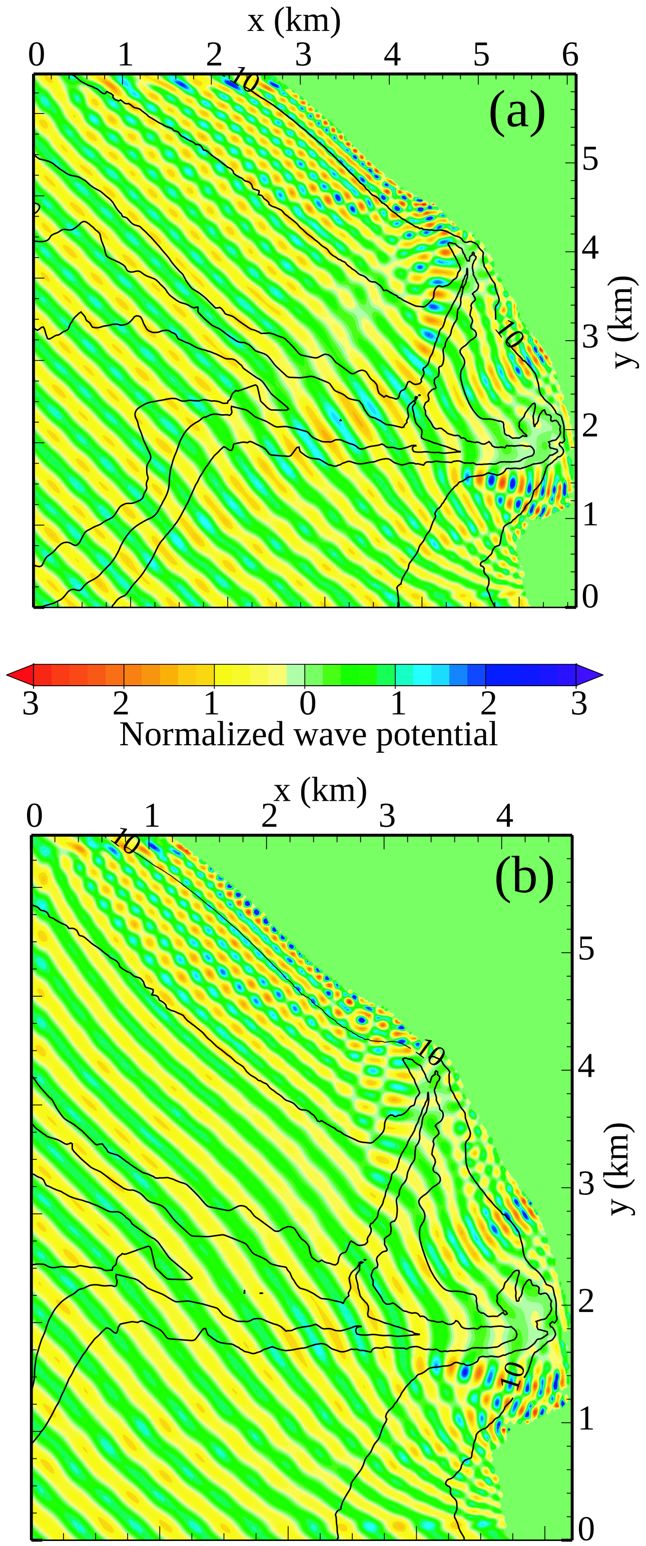

FIG. 4.14 – Computational domain for (a) $T > 15$ s, and (b) $T \leq 15$ s. Also shown are the NTUA5 solution for the real part of the wave potential amplitude in the case offshore waves from 270° and (a) $T = 16$ s, or (b) $T = 15$ s, together with the 10, 30, 100, 200, and 300 m depth contours.

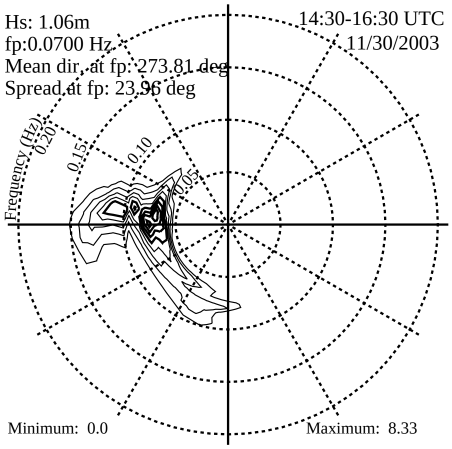

FIG. 4.15 – Directional wave spectrum at Torrey Pines Outer Buoy at 15 :00 UTC on 30 November 2003. The contour lines are logarithmically spaced from 0.1 to 10, with thicker contours for values larger than 1.

North of the Canyon at site 35, in 34 m depth. The most dramatic observed feature is the sharp reduction of wave heights at sites 36, 37 and 32, over the Canyon and on the south side, where the water depths are 11, 49 and 24 m, respectively. Between buoys 34 and 36 the wave height drops by a factor 5 although the distance is only 150 m, compared to a wavelength of 216 m at the peak frequency for the shallowest of the two sites. Such a pattern is generally consistent with refraction theory as illustrated by forward ray-tracing. Whereas rays crossing the shelf north of the canyon show the expected gradual bending towards the shore, rays that reach the canyon northern wall are trapped on the shelf, and reach the shore in a focusing region north of the canyon (Black's beach). From that offshore direction, and an offshore ray spacing of 15 m, no rays are predicted to cross the canyon, so that the south side of the canyon is very effectively sheltered from 16 s Westerly swells, in agreement with the observed extremely low wave heights (figure 4.17, see also *Peak* [2004]).

Up-wave of the canyon (instruments 33, 34, 35), all models are found to be in fairly good agreement with the observations. Over and down-wave of the canyon (instruments 32, 36, 37), the wave height predicted by MSE, MMSE and NTUA5 agree reasonably well with the observations, whereas Ref-dif overestimates the wave height. The version of Ref-dif used here is based on a small angle approximation [*Kirby*, 1986], that do not accurately account for waves scattered by the canyon at large angles relative to the grid orientation. This refraction pattern is very sensitive to the wave period, with a sharp cut-off in the predicted wave spectrum at a frequency of about 0.06 Hz (e.g. comparing results at sites 35 and 37 in Figure 4.18). For $f < 0.06$ Hz very few rays can cross the canyon and the energy predicted by the

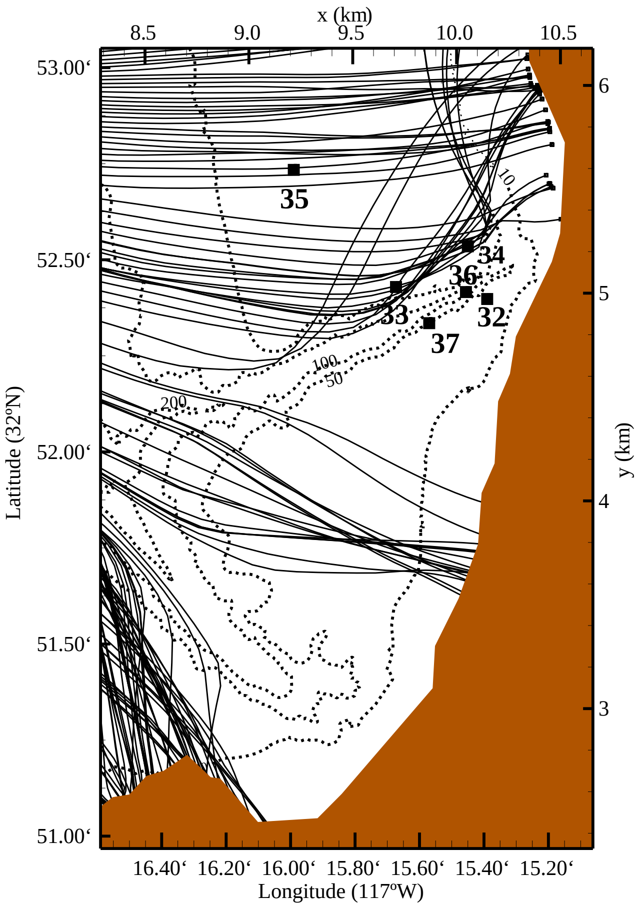

FIG. 4.16 – Location of directional wave buoys at the head of the Scripps canyon, and wave rays for an offshore direction of 272° and a period of 15.4 s, corresponding to a frequency just below the peak of the observed swell on November 30. Contrary to the backward ray tracing model used for estimating the wave spectrum at near-shore sites, rays were integrated forward from parallel directions and equally spaced positions at 15 m intervals along the offshore boundary at $x = 0$, 10 km to the West of the buoys, practically in deep water.

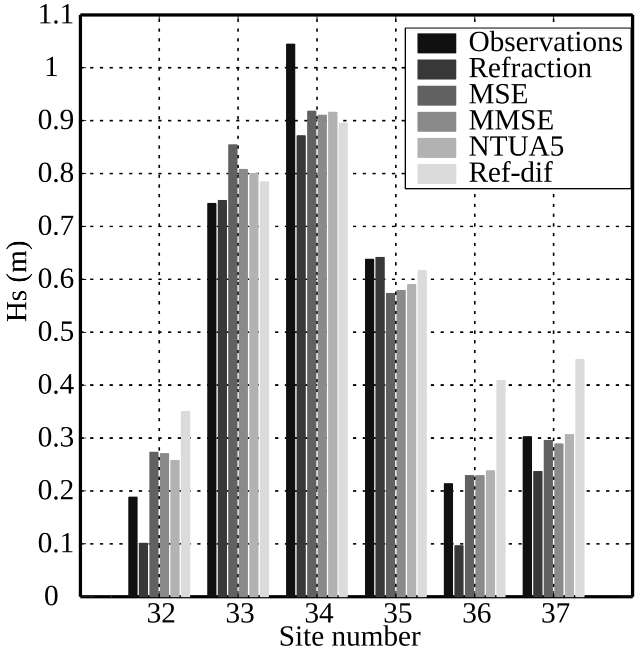

FIG. 4.17 – Comparison of predicted and observed significant wave height at the location of instruments shown on figure 4.16

refraction model is extremely low, so that the total energy is predicted to decrease by a factor 10 between sites 34 and 36. Clearly, such a strong variation of wave heights on very short scales is reduced by diffraction, which is not taken into account in this ray-tracing, and the refraction model underestimates the wave height at sites 32, 36 and 37.

The inclusion of diffraction effects in the models based on the MSE and its extensions leads to a tunneling of wave energy across the canyon in these models and better results in the simulated wave heights and wave spectra at sites 32, 36 and 37 (figures 4.17, 4.18). The differences between NTUA5, MSE and MMSE model predictions are very small and thus only NTUA5 results are shown in figure 4.18. It may appear surprising that the wave height behind the canyon is still 20% of the offshore wave height whereas the 2D simulations with comparable incidence angles yield wave heights much less than 5%. However, the real canyon is neither infinitely long nor exactly regular along its axis. This three-dimensional nature of the topography apparently reduces its blocking effect on long period swells.

4.6 Summary

Observations of the evolution of long period swell across a submarine canyon were compared with various mild-slope models and the coupled-mode model NTUA5 va-

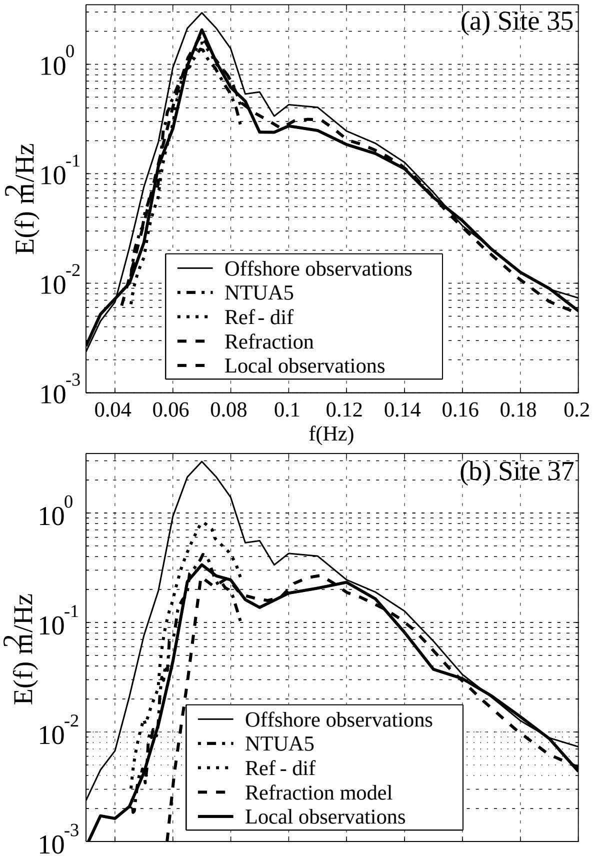

FIG. 4.18 – Comparison of predicted and observed frequency spectra at (a) site 35, and (b) site 37.

lid for arbitrary bottom slope [*Athanassoulis and Belibassakis*, 1999 ; *Belibassakis et al.*, 2001]. A simple refraction model, that is also used here, gave predictions for the entire experiment that are in good agreement with observations [*Peak*, 2004], demonstrating that refraction is the dominant process in swell transformation across Scripps Canyon. Yet, for waves longer than 12 s, the refraction model underestimates the energy levels behind the canyon, and more accurate results were obtained with the NTUA5 model and other more simple elliptic mild slope equation models. These differences were clarified with 2D simulations using representative transverse profiles of La Jolla and Scripps Canyons, showing the behavior of the far wave field as a function of the incidence angle. The underestimation by the refraction model may be interpreted as the result of wave tunneling, i.e. a transmission of waves to water depths greater than allowed by Snel's law, for obliquely incident waves. This tunneling effect cannot be represented in the geometrical optics approximation that is used for ray-tracing. That is, the refraction model predicts that all wave energy is trapped for large incidence angles relative to the depth contours, while a small fraction of the wave energy is in fact transmitted across the canyon. Although different from the classical diffraction effect behind a breakwater [e.g. *M*ei 1989], this tunneling is a form of diffraction in the sense that it prevents a sharp spatial variation of wave amplitude, and induces a leakage of wave energy in areas forbidden by geometrical optics. Besides, observations were also compared with a parablic refraction-diffraction model that is known to be inaccurate for large wave directions relative to the numerical grid, and is shown here to overestimate the amplitude of waves transmitted across the canyon. Finally, depending on the bottom profile and incidence angle, higher order bottom slope and curvature terms (incorporated in modified mild slope equations and NTUA5), as well as evanescent and sloping-bottom modes (included in NTUA5) can be important for an accurate representation of wave propagation over a canyon at small incidence angles. For large incidence angles, that are more common for natural canyons across the shelf break, the standard mild slope equation (MSE) gives a correct representation of the variations in surface elevation spectra that is similar to that of the full NTUA model. Yet, further analysis of NCEX bottom velocity and pressure measurements may show that the MSE or MMSE is not accurate enough for these bottom properties, as also discussed by *Athanassoulis et al.* [2003].

acknowledgments

The authors acknowledge the Office of Naval Research (Coastal Geosciences Program) and the National Science Foundation (Physical Oceanography Program) for their financial support of the Nearshore Canyon Experiment. Steve Elgar provided bathymetry data, Julie Thomas and the staff of the Scripps Institution of Oceanography deployed the wave buoys, and Paul Jessen, Scott Peak, and Mark Orzech assisted with the data processing. Analysis results of the infragravity reflections across La Jolla Canyon were kindly provided by Jim Thomson.

4.7 Compléments et perspectives

Dans la partie précédente, il a été démontré l'importance des termes du fond d'ordre supérieur (pente au carré $(\nabla h)^2$ et courbure du fond $\nabla^2 h$), ainsi que les modes évanescents pour une représentation correcte de la propagation des vagues au-dessus du canyon pour les angles d'incidences faibles. En particulier, les termes de courbure du fond se sont révélés importants même pour les pentes faibles, contrairement aux résultats énoncés par Booij (1983). Ce résultat également observé par d'autres auteurs peut s'expliquer par le paradoxe WKB discuté dans Mahony (1967) et Meyer (1979). Les méthodes par perturbations reposent sur un comportement asymptotique en puissance de ε, alors que le coefficient de réflexion à un comportement asymptotique différent pour des fonds en pente douce.

Dans la dernière partie de l'article, les comparaisons aux mesures effectuées, révèlent des différences significatives entre les différents modèles, le modèle réfraction/diffraction parabolique, le modèle de réfraction basé sur le tracé de rayons et le modèle couplé elliptique. La sur- et sous-estimation respective de la hauteur des vagues derrière le canyon du modèle parabolique et du modèle de réfraction révèle l'importance du processus de réflexion/diffraction pour une modélisation correcte de la propagation des vagues dans cette étude.

Les différences de hauteurs significatives des vagues prévues par les différents modèles elliptiques (MSE, MMSE et NTUA5), qui permettent la représentation du processus de réflexion, se sont révélées peu importantes aux angles élevés considérés dans le cas 3D (en accord avec les cas test 2D). Il semble qu'un modèle elliptique MSE classique, représentant la réflexion, suffise pour prédire de façon précise le champ de vagues en surface au-dessus des canyons sous-marins arrivant près des côtes, généralement orientés perpendiculaires au littoral. Les modes évanescents, ainsi que le mode "sloping-bottom" ajouté par Athanassoulis et Belibassakis (1999) modifient la structure verticale du potentiel des vitesses, et ce notamment au fond pour le mode "sloping-bottom". Afin d'établir de manière plus complète l'influence de ces modes, en particulier sur le champ de vitesses à l'intérieur du fluide, il serait intéressant de comparer directement les observations aux valeurs de pressions prévues au fond par les différents modèles elliptiques.

Deuxième partie

Influence du courant

Chapitre 5

Présentation

5.1 Introduction

L'influence du courant sur la diffusion des vagues est étudiée dans cette partie. Tout d'abord, au cours du sixième chapitre, l'influence du courant sur la réflexion des vagues au-dessus d'un fond sinusoïdal considéré bi-dimensionnel (uniforme suivant une composante horizontale) est observée lors d'une expérience en bassin à houle, comparant les observations à la théorie de Kirby (1988). Théorie et observations suggèrent un décalage des fréquences résonantes en présence de courant. Le septième chapitre propose une extension du terme de source présenté dans la partie précédente en présence d'un courant uniforme. Ce terme de source est confronté avec succès à la théorie de Kirby (1988) pour le cas de fonds bi-dimensionnels sinusoïdaux, tant au niveau du décalage des fréquences résonantes que sur les amplitudes de réflexions. Une application tri-dimensionnelle est ensuite proposée pour des vagues se propageant au-dessus de dunes sous-marines balayées par des forts courants de marée. Une diffusion importante des vagues est prédite, fortement influencée par le courant.

Les différentes études réalisées dans cette partie considèrent un courant uniforme. Cette approche est cohérente avec une variation lente du courant par rapport à la longueur d'onde des vagues. Lorsque des vagues se propagent sur un courant variable horizontalement, celles-ci sont réfractées et réfléchies par modification de leur vitesse de phase. Pour un courant cisaillé verticalement, la colonne d'eau est affectée par des vitesses de courant différentes suivant la profondeur. Pour conserver une structure verticale cohérente, les vagues se déplacent avec une vitesse de phase correspondant à une pondération du profil de courant sur la verticale. Biesel (1950) a donné une expression analytique de cette pondération. Pour un courant variant linéairement de U_{-D} au fond à U_0 en surface. Dans la limite $kH << 1$, la vitesse de phase est alors,

$$C = \left[\left(\frac{U_0 - U_{-D}}{2} \right)^2 + gH \right]^{1/2}. \tag{5.1}$$

Pour un profil plus général, et une profondeur quelconque, Kirby et Chen (1989) ont donné une solution approchée dans la limite où les variations de U sur la verticale sont faibles devant σ/k,

$$C = \frac{\sigma}{k} + 2\int_{-D}^{0} \mathbf{k}.\mathbf{U}\frac{\cosh(2kz + 2kH)}{\sinh(2kH)}dz. \tag{5.2}$$

5.2 Influence d'un courant uniforme sur les vagues et effet Doppler

Dans un référentiel fixe, une onde progressive se définit par la relation suivante (Mei, 1989),

$$e^{i(\mathbf{k}.\mathbf{x}-\omega t)}. \tag{5.3}$$

En présence de courant, après la transformation,

$$\mathbf{x}' = \mathbf{x} - \mathbf{U}t, \tag{5.4}$$

$$e^{i(\mathbf{k}.\mathbf{x}-\omega t)} = e^{i[\mathbf{k}.\mathbf{x}'-(\omega-\mathbf{k}.\mathbf{U})t]}. \tag{5.5}$$

La fréquence intrinsèque dans le référentiel en mouvement s'écrit,

$$\sigma = \omega - \mathbf{k}.\mathbf{U} = \omega - kU\cos\alpha, \tag{5.6}$$

avec α l'angle entre $\mathbf{k}$ et $\mathbf{U}$. La fréquence intrinsèque σ est alors inférieure ou supérieure à la fréquence absolue ω en fonction de la valeur de α, et donc de la direction et du sens des vagues par rapport au courant. On retrouve alors l'effet Doppler.

En orientant notre système de coordonnées tel que $\mathbf{k} = (k, 0)$, avec $k > 0$. La relation de dispersion s'écrit alors,

$$\omega - kU\cos\alpha = \pm\sigma(k) = \pm(gk\tanh kh)^{1/2}. \tag{5.7}$$

Elle peut être résolue graphiquement par intersection de la ligne $y = \omega - kU\cos\alpha$ et des courbes $y = \pm\sigma(k)$ (voir figure 5.2). Lorsque les vagues et le courant sont perpendiculaires ($\alpha = \pm\pi/2$), le courant n'a pas d'effet sur le nombre d'onde des vagues (voir point E).

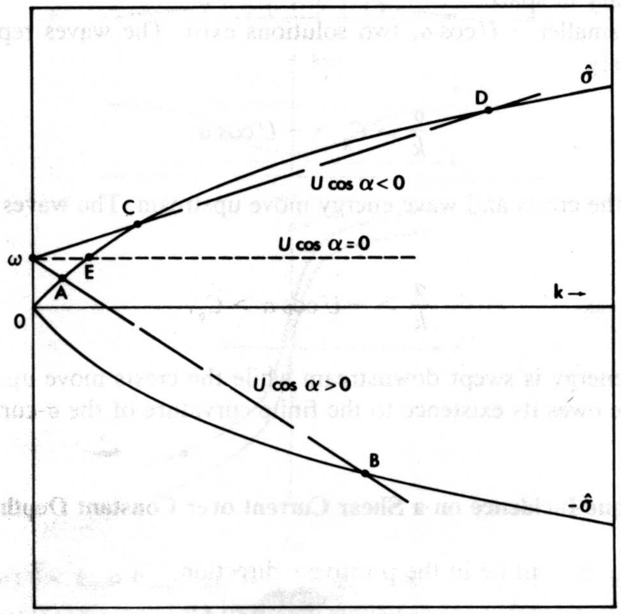

FIG. 5.1 – Solution graphique de l'Eq.(5.7), figure empruntée à Mei (1989)

Pour $U\cos\alpha > 0$, il y a deux solutions correspondant aux points A et B. Par comparaison avec les vagues sans courant (point E), les vagues représentées par A sont plus longues et plus rapides. C'est l'opposé pour les vagues représentées par B. Leurs vitesses de groupe et de phase (intrinsèque) sont négatives, mais toutes deux inférieures à $U\cos\alpha$. Les crêtes et l'énergie des vagues continuent de se propager dans le sens du courant.

Pour $U\cos\alpha < 0$, le courant a une composante opposée aux vagues. Si $-U\cos\alpha > (gh)^{1/2}$, aucune solution n'est possible. Pour des valeurs plus faibles de $-U\cos\alpha$ il y a un seuil tel qu'une seule solution existe pour une fréquence ω. Ce seuil correspond à l'annulation de la vitesse de transport de l'énergie des vagues,

$$C_g + U\cos\alpha = 0. \tag{5.8}$$

Bien que les crêtes des vagues se propagent contre le courant ($\sigma/k > 0$), l'énergie est stationnaire dans l'espace. Pour des plus petites valeurs de $-U\cos\alpha$, deux solutions existent. Les vagues représentées par le point C satisfont

$$\frac{\sigma}{k} > C_g > -U\cos\alpha, \tag{5.9}$$

donc les crêtes et l'énergie des vagues se propagent contre le courant. Les vagues représentées par D satisfont

$$\frac{\sigma}{k} > -U\cos\alpha > C_g. \tag{5.10}$$

L'énergie des vagues est maintenant dans le sens du courant alors que les crêtes sont toujours opposées au courant.

De façon plus simpliste, un courant colinéaire et dans le sens des vagues, allongera les vagues et diminuera l'amplitude. Un courant contraire engendrera des vagues plus courtes et plus amples, donc aussi plus raides. Ces effets du courant sont représentés sur les figures 5.2 et 5.3 empruntées à Brevik et Aas (1980).

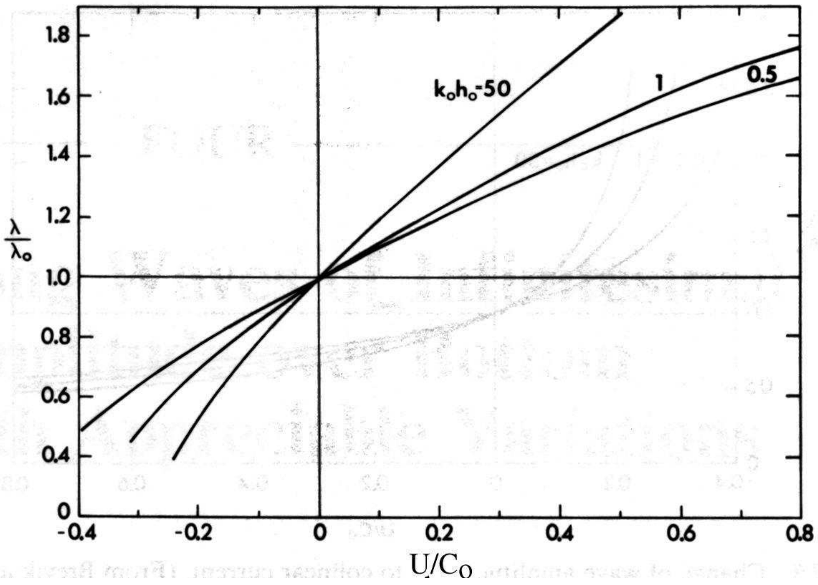

FIG. 5.2 – Changement de longueur d'onde dû à un courant colinéaire, figure empruntée à Mei (1989)

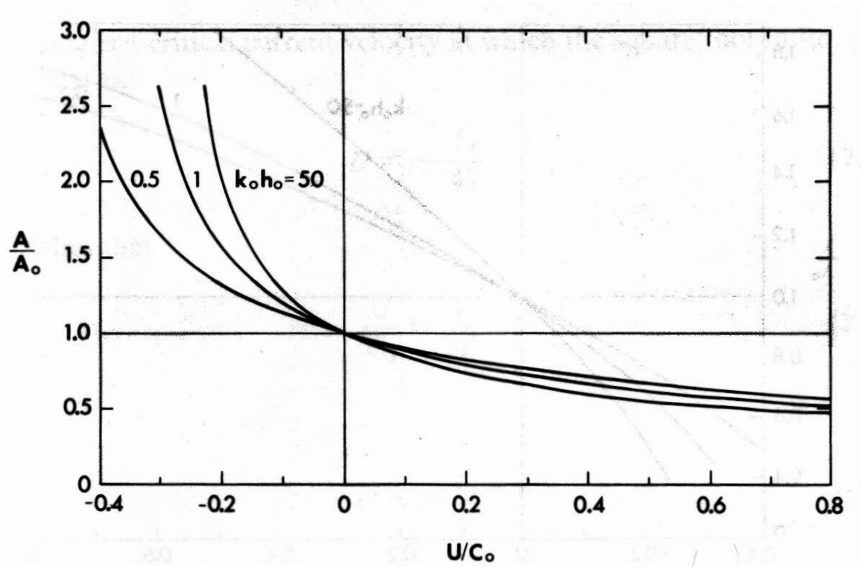

FIG. 5.3 – Changement de l'amplitude des vagues dû à un courant colinéaire, figure empruntée à Mei (1989)

Chapitre 6

Effet d'un courant sur la réflexion des vagues par une topographie sinusoïdale 2D, mise en évidence expérimentale

Introduction

Pour des vagues monochromatiques se propageant au-dessus d'un fond sinusoïdal 2D, le phénomène de résonance de Bragg (de Classe I) étudié dans le chapitre précédent intervient lorsque le nombre d'onde du fond est égal à deux fois celui des vagues incidentes. Cette amplification de la réflexion est due à un accord de phase entre l'onde incidente et l'onde réfléchie (interférences constructives). En présence de courant, le nombre d'onde des vagues incidentes et réfléchies n'est plus le même (effet Doppler). Les fréquences résonantes sont alors décalées, et la relation de résonance $2k/l = 1$ n'est donc plus valable. Ce décalage Doppler des fréquences résonantes de Bragg est étudié et mis en évidence expérimentalement dans ce chapitre. Le dispositif expérimental utilisé est illustré par des photographies dans l'annexe de ce chapitre.

Measurement of wave scattering by topography in presence of currents

Rudy Magne(1,2), Vincent Rey(2) and Fabrice Ardhuin(1)

Submitted to Physics of FLuids
January 2005
Revised version for Physics of Fluids
September 2005

(1) *Centre Militaire d'Océanographie, SHOM, BREST, France*
(2) *LSEET-LEPI, Université de Toulon et du Var, La Garde, France*

Résumé

La réflexion des vagues par un fond sinusoïdal en présence d'un courant ambiant est examinée expérimentalement. Les vagues sont générées dans un bassin à houle avec et sans courant, et propagées au-dessus d'un fond constitué de 5 barres sinusoïdales avant de se dissiper sur une plage. Le décalage Doppler des fréquences de Bragg résonantes et l'amplification de la réflexion des vagues due au courant sont observés expérimentalement. Des faibles réflexions au-dessus de la plage peuvent avoir une influence significative sur la réflexion des vagues au-dessus des barres.

Abstract

Wave scattering over a sinusoidal bottom in the presence of an ambient current is investigated experimentally. Waves were generated in a flume with and without current and propagated over a patch of 5 sinusoidal bars before dissipating on a beach. A Doppler shift of resonant Bragg frequencies and an amplification of the wave reflection are observed in the presence of the current. Weak reflections over the beach are found to have a significant influence on the wave reflection over the bars.

6.1 Introduction

Wave reflection by periodical topography was widely studied, particularly for the possible role in coastal protection (Bailard et al., 1990 ; Heathershaw, 1982). Davies (1982) and Davies and Heathershaw (1984) showed theoretically and experimentally in the 2D case that waves can be strongly reflected by a series of bars when their wavenumber k is half the bottom wavenumber l, according to the triad wave-wave-bottom resonance condition $k-(-k)=l$. This phenomenon, well known in solid-state physics, is called Bragg resonance. Their theory, not valid at the resonance, was first improved by Mei (1985) and followed by numerous authors (Kirby, 1986 ; Hara and Mei, 1987 ; Guazzelli et al., 1992 ; Rey, 1992 ; Rey et al.,1996). Considering the application of this phenomenon to coastal protection, effects of partial reflection from the shore were also studied (Kirby and Anton, 1990 ; O'Hare and Davies, 1993 ; Yu and Mei, 2000). Kirby and Anton (1990) found numerically that in the presence of a vertical wall at the shore, wave amplitude downwave from the patch could be dramatically amplified by possible resonance between the end of the patch and the wall. O'Hare and Davies (1993) found numerically that wave amplitude could decrease or increase shoreward over the bars depending on the (standing-)wave envelope location in relation to the bar crests. More recently, Yu and Mei (2000) confirmed and generalized these findings analytically, introducing the phase relation between the bars and the shoreline reflection. In the presence of a steady current U, a wave of given frequency f in a fixed frame propagates with a higher celerity in the current direction, and with a lower celerity in the opposite direction, corresponding wavenumbers are then $k^-$and k^+ respectively. Extending the theory of Mei (1985) in the presence of an ambient current, Kirby (1988) found analytically a shift of the resonant frequencies and an amplification of the wave reflection. Although currents are essentially oriented alongshore in the surf zone, the influence of currents may be significant for continental shelf areas where large sand-waves are generated by tidal currents (Knaapen and Hulsher, 2002 ; Schmitt et al., 2004) and should cause strong scattering (Ardhuin et al., 2003).

This study investigates experimentally the effect of an ambient current on the Bragg scattering phenomenon, particularly on wave reflection over a sinusoidal bottom. Both regular and irregular waves are studied since real sea states are to be considered for *in situ* applications. The experiment is carried out in the Ocean Engineering Basin BGO-FIRST, La Seyne sur Mer, France. After a description of the experimental set-up in section 2, section 3 presents observed reflection coefficients for both regular and irregular waves with and without current. Conclusions follow in section 4.

6.2 Experimental techniques

6.2.1 Experimental set-up

The BGO-FIRST flume has a useful length of 24 m, and an effective width of 16 m (see Fig. 6.1). Its maximum water depth is 5 m, with a central pit of 10 m water depth that is not used in the present study. It is equipped with a current generator, a wavemaker over the entire width and an $X-Y$ carriage, working in a Cartesian coordinate system. At the end of the tank is a permeable wave absorber of parabolic shape of total length 3 m, enabling tests with a current that goes through this "beach". The bottom can be moved vertically to adjust the water depth. However, this depth cannot be shallower than 1.9 m due to the tank design. For the investigation of Bragg scattering, the resonant bottom wavelength should thus be larger than 3.8 m, so that wave are influenced by the bottom. Thus, regarding the length of the tank, only 5 bottom wavelengths could be constructed. Finally, the amplitude of the bars has to be large enough to produce a significant reflection. For this study, the maximum water depth is fixed to 1.9 m, and a sinusoidal topography $h(x)$ made of marine plywood is installed on the bottom. The ripple amplitude is $a = 0.4$ m, and thus the mean water depth over the sinusoidal patch is $H = 1.5$m, with a wavelength $\lambda = 2.5$ m. The patch is 10 m long including 4 wavelengths, plus a 3 m long adaptor ramp at the beginning and at the end of the patch, to avoid discontinuities. The width of the patch is 9 m centered within the 16 m width of the tank (Fig. 6.1b).

The wavemaker, composed of horizontally oscillating cylinders, allows regular and irregular waves to be generated with a maximum height of 0.8 m for periods between 0.7 and 3.4 s. Both regular and irregular waves are investigated. Regular wave periods range from 1.4 to 2.9 s with a wave amplitude $A = 0.05$ m. Irregular waves with Jonswap ($\gamma = 3.3$) shapes have a peak period of 1.813 s and significant wave height about 0.12 m without current and 0.10 m with current. Current generation is provided by pumps. Our studies were executed with current velocities U of 0 and 0.32 m.s^{-1} upstream from the ramp in 1.9m water depth, collinear with the wave direction. It follows, that the non-dimensional bars height a/H equals 0.26, the maximum bottom slope $2\pi a/\lambda$ equals 1, the wave steepness kA varies from 0.032 to 0.1 and, kH from 1.2 to 3.9. These parameters may be too large for a strict application of the theories (based on an expansion of the bottom slope (Kirby, 1988) and on linear waves (Rey, 1992) that are used in the following sections to interpret the measurements.

Regular wave measurements were carried out with nine capacitive synchronous wave

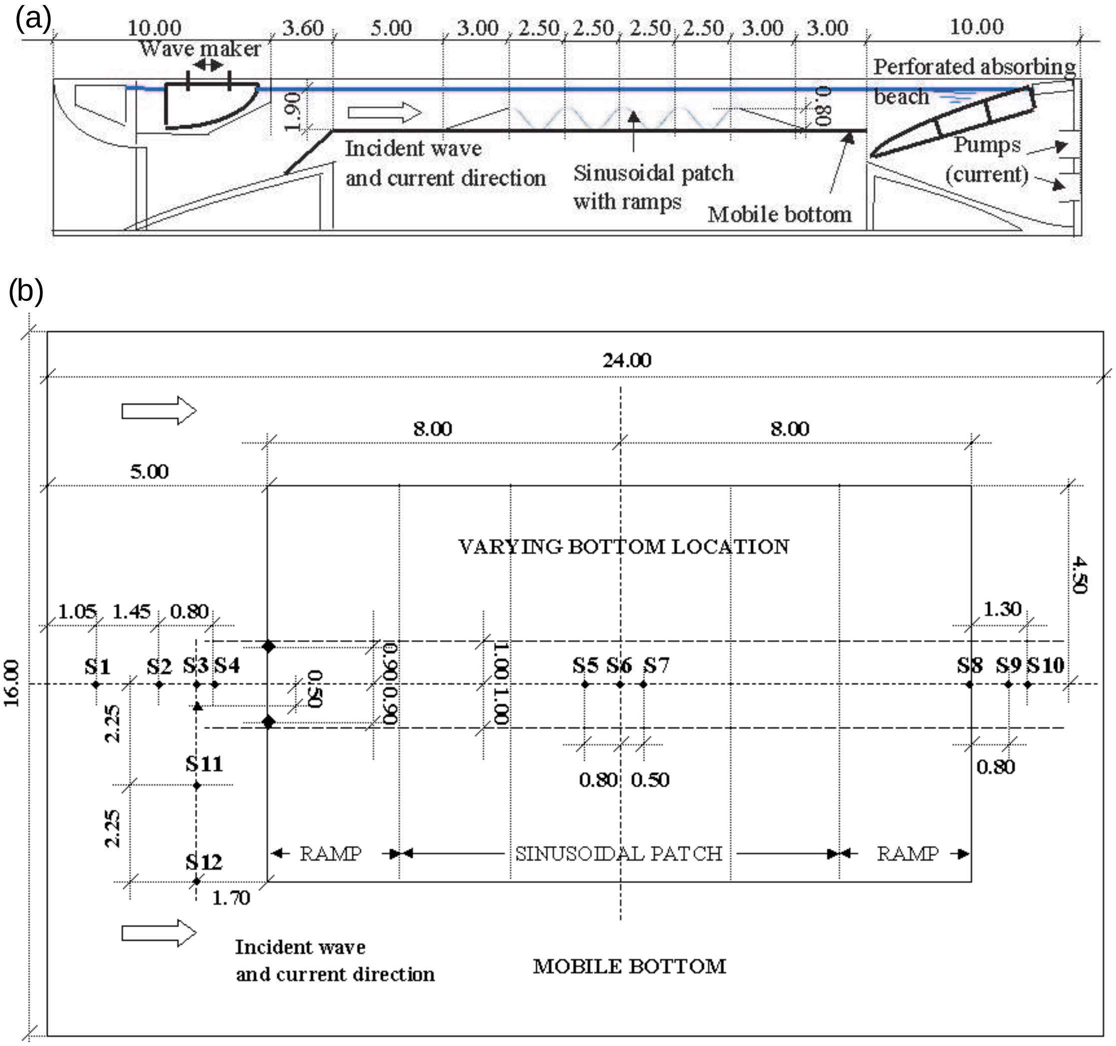

FIG. 6.1 – Sketch of the experimental set-up, (a) cross section, (b) view from above. For regular waves, gauges locations are G1-G4, G6, G8, G10-G12, micro-propellers are M1 and M2, ADV is A1. For irregular waves, gauges locations are G1-G3, G4 (but 0.05cm downstream as indicated in Fig.1b), G5-G9, G10 (but 0.05cm upstream as indicated in Fig.1b), G11-G12, micro-propellers are M1 and M3, ADV is A1. For the current measurements along the tank (without waves, —-), $y = 1$m for the Micro-propeller, $y = -1$m for the ADV.

probes, and velocity measurements with two micro-propellers and an ADV (Acoustic Doppler Velocimeter). Four probes ahead of the structure (G1-G4, see Fig. 6.1), one in the middle (G6) and two behind (G8-G10) made it possible to measure both incoming and transmitted waves. Two more (G11, G12) were added along the y-axis to measure possible transversal variations, that proved to be negligible upwave from the bars. For irregular wave measurements two more probes (G5, G7) were added in the middle of the patch and one other more (G9) at the end.
The experimental procedure in the presence of current is as follows. At time $t0 = 0$s starts the data acquisition. The current is generated at $t1 = 10$s. The wave maker is activated at $t2 = 130$s. For regular wave measurements, the wave maker is stopped at $t3 = 310$s. For irregular wave measurements it is stopped at $t3 = 730$s.

6.2.2 Wave reflection measurement

The technique used to separate the irregular incident and reflected wave and then calculate the reflection for each wave frequency component is based on a least squares method using linear wave theory applied to three probes (Rey et al., 2002). In the following, probes are labelled 1, 2 and 3 for simplicity, they are located at $x = x_i$, $i = 1, 2, 3$.

The surface elevation $\eta(x,t)$ for a wave (or wave component) of frequency $f = \omega/2\pi$ resulting from two plane waves, traveling in opposite directions along the x-axis is of the form :

$$\eta(x,t) = \left\{ a^- e^{-ik^- x} + a^+ e^{+ik^+ x} \right\} e^{i\omega t} \tag{6.1}$$

where a^- and a^+ are complex amplitudes. $k^\mp$ are the wavenumbers of the incident and reversed running waves, given by

$$(\omega \pm U k^\pm)^2 = \left(\sigma^\pm\right)^2 = g k^\pm \tanh(k^\pm H) \tag{6.2}$$

where H is the water depth, and $\sigma^\pm$ are the relative frequencies in a coordinate system, traveling with velocity U. The theoretical expression for the free surface at the position of probe G_n based on Airy waves is given for an arbitrary choice of time zero by :

$$\eta_n = \left\{ a_i e^{-i(k^- x_1 + \Delta n^-)} + a_r e^{+i(k^+ x_1 + \Delta n^+ + \varphi)} \right\} e^{i\omega t} \tag{6.3}$$

with $\Delta_n^- = k^-(x_n - x_1)$ and $\Delta_n^+ = k^+(x_n - x_1)$, a_i and a_r are the amplitudes of the incident and reflected wave and φ the phase lag of the reflected wave. The component of frequency f of the elevation of the free surface as measured by probe G_n $(n = 1, 2, 3)$ is of the form :

$$\eta_n^{(m)} = A_n e^{i(\omega t - \varphi_n)} \tag{6.4}$$

where superscript (m) indicates the measured values. The amplitude and phase A_n and φ_n are determined from a Fourier analysis of the signal measured by probe G_n. Application of the method of least squares to data from probes G_1 through G_3 leads to the determination of the moduli of the amplitudes of the incident and reflected waves components a_i and a_r

$$|a_i| = \left|\frac{s_2 s_3 - s_{12} s_4}{s_5}\right| \tag{6.5}$$

$$|a_r| = \left|\frac{s_1 s_4 - s_{12} s_3}{s_5}\right| \tag{6.6}$$

with

$$s_1 = \sum_{n=1}^{3} e^{-2i\Delta_n^-};\ s_2 = \sum_{n=1}^{3} e^{+2i\Delta_n^+};\ s_{12} = \sum_{n=1}^{3} e^{+i(\Delta_n^+ - \Delta_n^-)}; \tag{6.7}$$

$$s_3 = \sum_{n=1}^{3} A_n e^{-i(\Delta_n^- + \varphi_n)};\ s_4 = \sum_{n=1}^{3} A_n e^{+i(\Delta_n^+ - \varphi_n)};\ s_5 = s_1 s_2 - s_{12}^2 \tag{6.8}$$

If irregular waves can be considered as a linear superposition of Airy waves of frequency f_p, discrete energy density spectra (EDS) for both incident and reflected waves can be defined by $E_{i,r}(f_p) = \frac{1}{2} a_{i,r}^2(f_p)$ (in m^2/Hz). The smooth estimate of the spectral density function is then

$$W(f_p) = \frac{1}{2m+1} \sum_{j=-m}^{j=+m} E(f_{p+j}) \tag{6.9}$$

where $m = 10$ for the present study.

For monochromatic waves, frequency wave is also calculated through Fast Fourier Transform and the reflection coefficient R is given by $R = \frac{|a_r|}{|a_i|}$. For the reflection measurement upwave the patch, the above three gauges method is used. For the beach reflection measurement, only two probes were available for regular waves, and a two probes method was used.. The amplitudes of the incident and reflected waves components a_i and a_r are as follows

$$|a_i| = \frac{1}{2\left|\frac{\sin(\Delta_2^+ + \Delta_2^-)}{2}\right|}\sqrt{A_1^2 + A_2^2 - 2A_1A_2\cos(\varphi_2 - \varphi_1 + \Delta_2^+)} \qquad (6.10)$$

$$|a_r| = \frac{1}{2\left|\frac{\sin(\Delta_2^+ + \Delta_2^-)}{2}\right|}\sqrt{A_1^2 + A_2^2 + 2A_1A_2\cos(\varphi_2 - \varphi_1 - \Delta_2^-)} \qquad (6.11)$$

where labels 1 and 2 correspond to probes 1 and 2.

In the following sections, results concerning reflection are presented versus $2k/l$, in accordance to the well-known Bragg resonance condition for triad resonant interaction between two waves of wavenumber k propagating in opposite direction in a homogeneous medium of spatial periodicity $\lambda = 2\pi/l$. Here k is the wave wavenumber corresponding to the mean water depth $H = 1.5$ m for a gravity wave of frequency f without current. l is the bottom wavenumber such that $l = 2\pi/\lambda$, with λ the distance between two bottom crests. The corresponding wave period for the Bragg condition is $T = 1.831s$.

6.3 Experimental results

6.3.1 Current variability across the tank

The current variability analysis, across and along the tank, is presented in this section before going further into the presentation and the interpretation of the measurements. Current measurements were realized without waves along the x-axis upstream and above the modulated bottom, using an ADV with immersion depths 0.50 m and 0.90 m and a micro-propeller with immersion 1 m. The averaged currents and their standard deviation (not shown for the ADV at water depth 0.90 m for clarity) are represented in Fig. 6.2, including standard deviation, indicated by an error bar. The ADV also measured the transverse (v) and vertical (w) velocity that were found to be smaller than 1cm.s^{-1} on average, with a standard deviation less than 5cm.s^{-1}. The measurement area, upwave from the bars shows a quite homogeneous current both in intensity in the horizontal direction (low values of the standard deviation) and in vertical direction (almost constant). We can see an increase of the horizontal velocity over the ramp, larger at the ”bottom” (1m) than at the ”surface” (0.50 m), followed by a decrease beyond the ramp, in particular for the ”bottom” velocities. The mass flux over the modulated seabed is smaller and smaller downstream, which means that a part of the current is canalized by the topography and flows around the modulated bottom (the tank is 16m wide while the modulated bottom is 9m wide

within the 16 m, see Fig. 6.1). During reflection measurements with regular waves, no current measurement was made over the patch, but, an ADV (A1, see Fig. 6.1) located 1.3m upwave from the bottom and 0.50 m deep, and two micro-propellers (M1, M2) at 1m depth, located 1m on either side from the longitudinal axis at the beginning of the ramp ($x = 0$) allowed verification of the homogeneity of the current in this area, in transverse and vertical directions, of intensity 0.32 m/s. For instance for $T = 1.812s$, current measurements gave respectively 0.322, 0.317 and 0.319 m/s with standard deviation 0.013, 0.006 and 0.006 m/s. During irregular wave measurements, the current was measured over the patch with a micro-propeller (M3) and an ADV located up-wave from the bars (A1). By comparison with measurements without waves (Fig. 6.2), the current is more intense in the presence of waves on the middle of the patch as shown in Fig.6.3. The current intensity is closer to the one given by the mass flux conservation, i.e. 0.32cm.s^{-1} in 1.9m deep up-wave and 0.40cm.s^{-1} in 1.5m depth over the modulated bottom. The wave induced fluid oscillations strongly limitate the development of instabilities at the origin of the current variabilities observed during experiments without waves.
We can also observe that ADV measurements are somewhat noisy even with only current (before $t = 130s$) because of overly clean water in the basin for a good backscattering of the ultrasonic beams.

6.3.2 Monochromatic waves

The amplitude reflection coefficient with and without current as a function of the normalized resonant wavenumber $2k/l$ is presented in Fig. 6.4 . Experimental results are compared with the following theories. Kirby (1988)'s approximation provides reflection coefficient with and without current for a purely sinusoidal topography, and thus cannot represent the effects of the ramps at the beginning and at the end of the sinusoidal patch. Rey (1992)'s model is based on the matching of integral quantities at the boundaries of adjacent steps, converging to the exact reflection for an infinite number of steps. Computations with Rey's model are done without current for the real topography, including the adjusting ramps. The effects of both the ramp and the evanescent modes (computation are done with the Rey algorithm including $P = 0$ and $P = 3$ evanescent modes) on the reflection coefficient versus k are presented in Fig. 6.5.

Without ramp, a small shift still exists between Kirby and Rey computations. This shift is due to the "non-linearity" of the dispersion law (Eq.6.2). Indeed, differences in the wave phase evolution over a patch are observed using either the integration of the local value of the wavenumber or its patch-mean value as is done

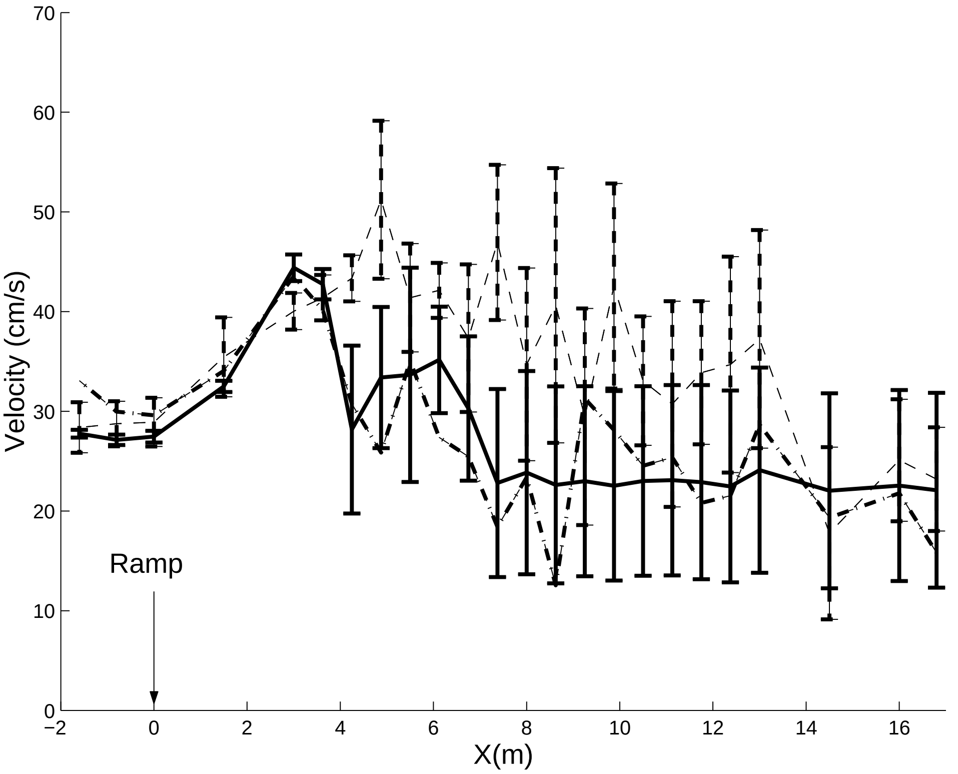

FIG. 6.2 – Velocity upstream and above the modulated bed, (—) Micro-propeller (1m), (-.-.) ADV (0.9m), (- -) ADV (0.5m). Error bars indicate standard deviation.

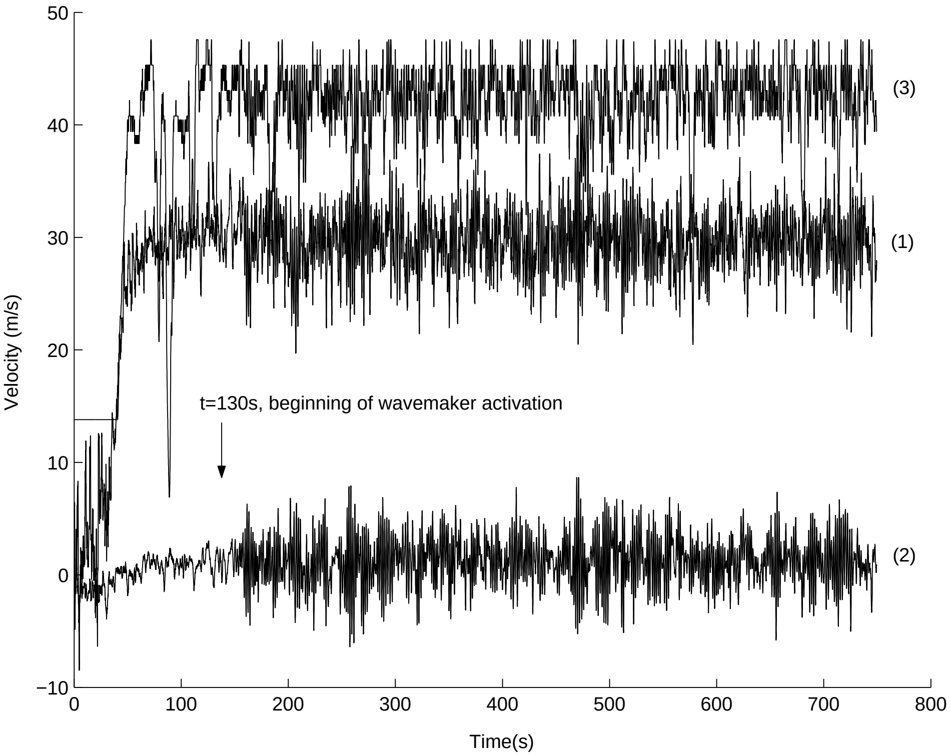

FIG. 6.3 – Velocity measurements : (1) along x-axis with ADV at X=-1.3m, (2) along z-axis with ADV at X=-1.3m, (3) along x-axis with Micro-propeller at X=8m.

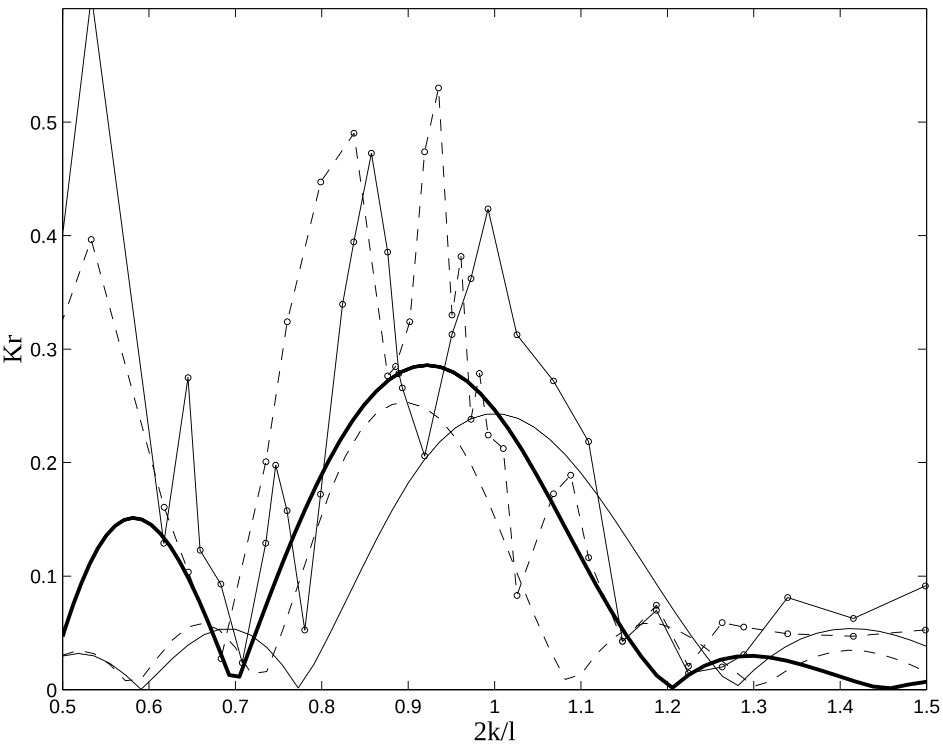

FIG. 6.4 – Reflection coefficient for the wave amplitude. The measurements are represented with 'o' markers. Full and dashed line correspond to reflection with and without current respectively. Kirby's approximations are plotted with (full) and without (dashed) current. Rey's model (without current) including evanescent modes is the bold full line.

in the asymptotic theories. This shift tends to zero when the bottom amplitude tends to zero. The reflection coefficient including the effect of adjusting ramp is shifted again towards the low frequencies. The evanescent modes are found to increase the reflection coefficient, and thus explain the difference of magnitude found (Fig.6.4) between Kirby's theory (not including the evanescent modes) and stepwise computations.

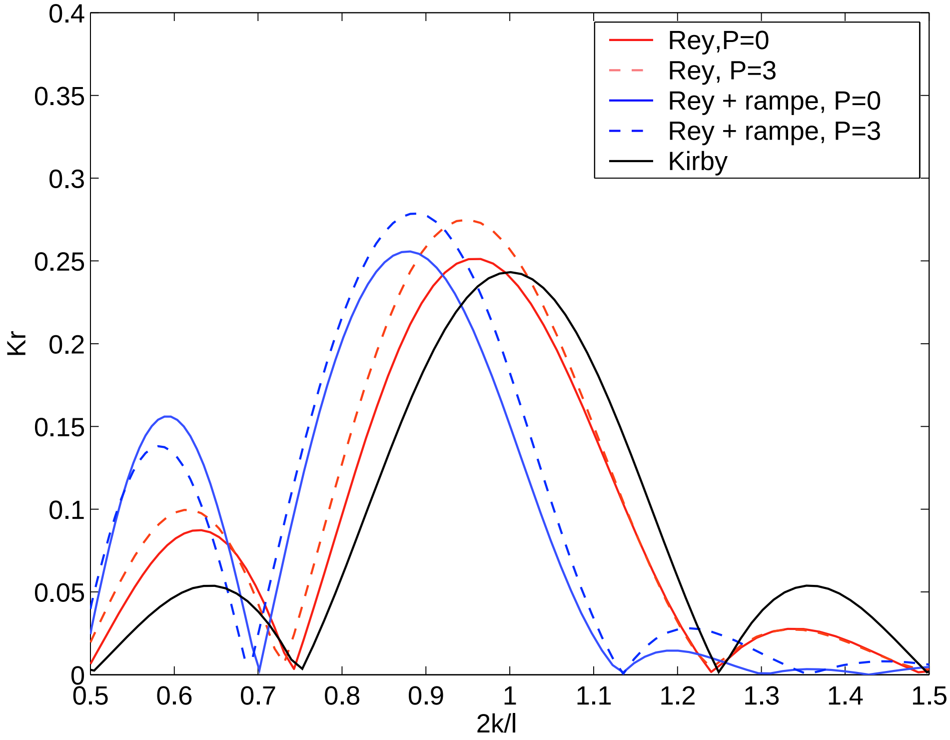

FIG. 6.5 – Reflection coefficient with and without adjusting ramp.

Bragg resonance

Bragg resonance corresponds to a phase matching between incident and reflected wave, implying constructive interferences which increase the reflection. For the case of a nearly flat bottom, it appears when the wave wavenumber is twice the bottom wavenumber. Using the linear dispersion relation (Eq.6.2), the round trip integral δ of the wave of frequency f over one bottom wavelength λ is defined by,

$$\delta(f) = \int_0^\lambda k^- dx + \int_\lambda^0 k^+ dx. \tag{6.12}$$

Resonance occurs at the frequency such that $\delta(f) = 2\pi$. For a sinusoidal topography, because of the "non-linearity" of the dispersion relation (Eq.6.2), δ is not exactly 2π and the Bragg resonance condition slightly differs (Rey, 1992) from $2k/l = 1$. The exact resonant frequency (with and without current) can be found by solving numerically $\delta(f) = 2\pi$. Without current, we observe a maximum of reflection centered on the main resonant peak around $2k/l = 0.9$ instead of $2k/l = 1$, that is explained by the presence of the ramps (Fig.6.5).

The shift due to the adjusting ramp is also consistent with a spectral analysis of the Bragg scattering (Ardhuin and Herbers, 2002; Mei and Hancock, 2003), in which wave reflection is found to be linearly linked with the bottom spectrum, even for steep topography. The inclusion of adjusting ramps at the edges of the patch also shifts the peak of the bottom spectrum as shown in figure (6.6), from $2k/l = 1$ to $2k/l = 0.9$. Bragg resonance does not take place exactly at the spectral component l corresponding to the spacing between two bars λ, but at the peak of the total bottom spectrum including the ramps.

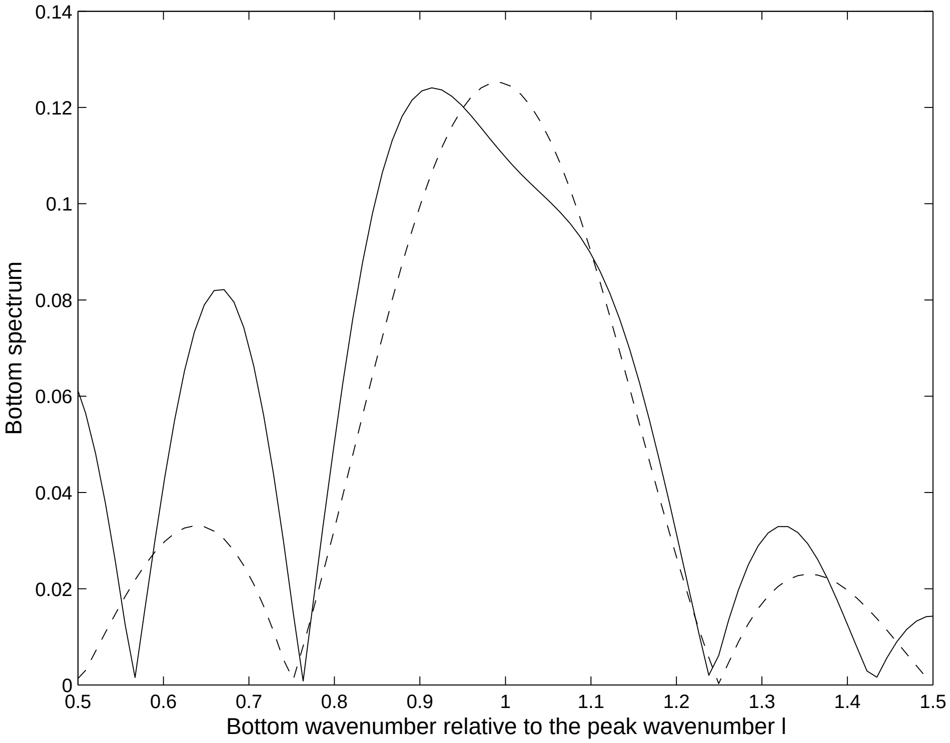

FIG. 6.6 – Bottom spectrum with (full line) and without (dashed line) adjusting ramp.

The two theories for linear waves (Rey, 1992; Kirby, 1988) underestimate the observed main resonant peak of the reflection coefficient Kr. Kirby's theory is limited to small ripples amplitude and thus may not represent accurately conditions with a non-dimensional bottom amplitude of 0.26. However, Rey's theory is not limited by the bottom amplitude, and it also underestimates reflection. The reflection over the bars must therefore be influenced by other parameters.

Beach reflection and 3-D homogeneity

Yu and Mei (2000) showed that the beach reflection, more precisely the phase relation between the bars and the shoreline reflection has a significant influence on the reflection by sinusoidal bars and "contribute to qualitative difference in the final steady states of Bragg resonance". Concerning the reflection measurement upwave from the modulated bed, a reflection from the beach of coefficient Kr_b leads to an uncertainty of $\pm Kr_b$ on the measured reflecting power of the patch. During laboratory experiments on sandy bar formation under partially standing waves, Belzons and Rey (1996) found a good agreement between the measured reflected wave versus frequency and the linear theory (Rey, 1992) taking into account both amplitude Kr_b and phase ϕ_b of the beach reflection, obtained from the measured wave enveloppe. Beach reflection was introduced in Rey's model by defining the coefficient for the reflected wave in the downstream domain as $|Kr_b| \cos \phi_b T$ where T is the computed coefficient for the transmitted wave. In the present experiments, phase is estimated through the synchronized down wave gauges $G8$ and $G9$. Using measured values of Kr_b and ϕ_b (which largely depend on the frequencies, see Fig.6.7 and 6.8) in Rey's model to correct the reflection coefficient leads to Fig.6.9, where the dashed line is the corrected reflection coefficient. A better agreement is found for non-resonant high and low frequency waves, matching the oscillations of the measured reflection coefficient, but results in magnitude near the resonant peak are not significantly improved. When waves are reflected by the beach, a part is re-reflected by the bars, trapping energy between the bars and the beach, as shown by Kirby and Anton (1990). It follows an observed transmission coefficient Kt (Fig.6.9), computed by the ratio of the measured incident wave amplitude downwave and upwave from the patch, larger than 1 at low frequency, corresponding to constructive phase matching between the bars and the beach. However, the observed reflection Kr is still dramatically larger than expected around the resonant peak, and lower exactly at resonance (Fig.6.9).

A 3D numerical model was then used to investigate the effect of the limited width of the bars. To test the 3-D homogeneity of the wave field downwave from the bars (not available by measurements), computations were done with an elliptical refraction-diffraction model based on the modified mild slope equation. A 'numerical wave tank' was set-up with the same characteristics as the experimental wave tank. 180 points were used both for the x- and y-axis. Absorbing boundary layers were imposed to avoid spurious reflections on the wave maker, beach and side-walls (see Belibassakis et al., 2001). A "transmission" coefficient, was thus computed (Fig.6.10), defined as the ratio of the wave amplitudes upwave and downwave from the bars,

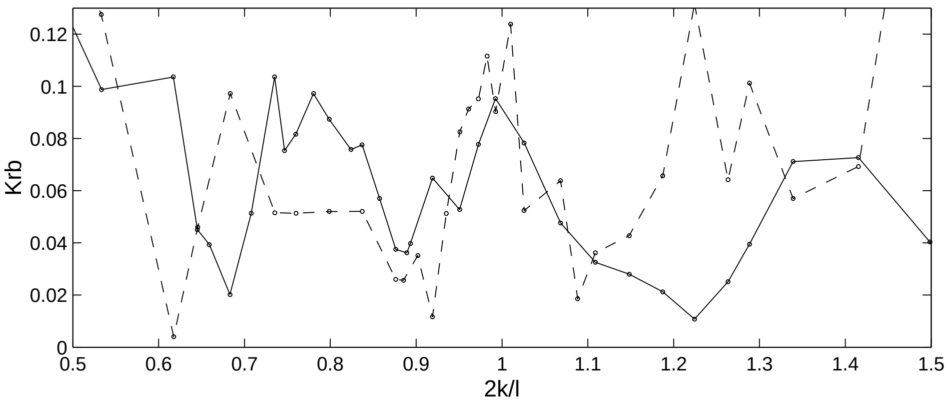

FIG. 6.7 – Beach reflection observation without (full) and with (dashed) current.

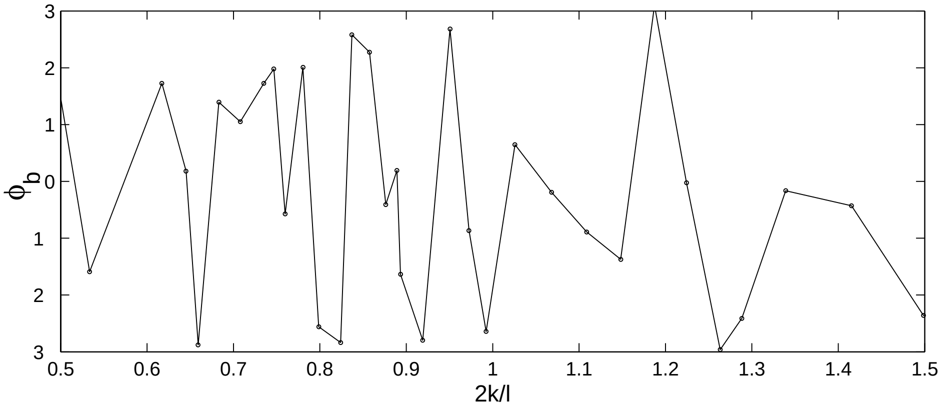

FIG. 6.8 – Beach reflection wave phase at X=16m.

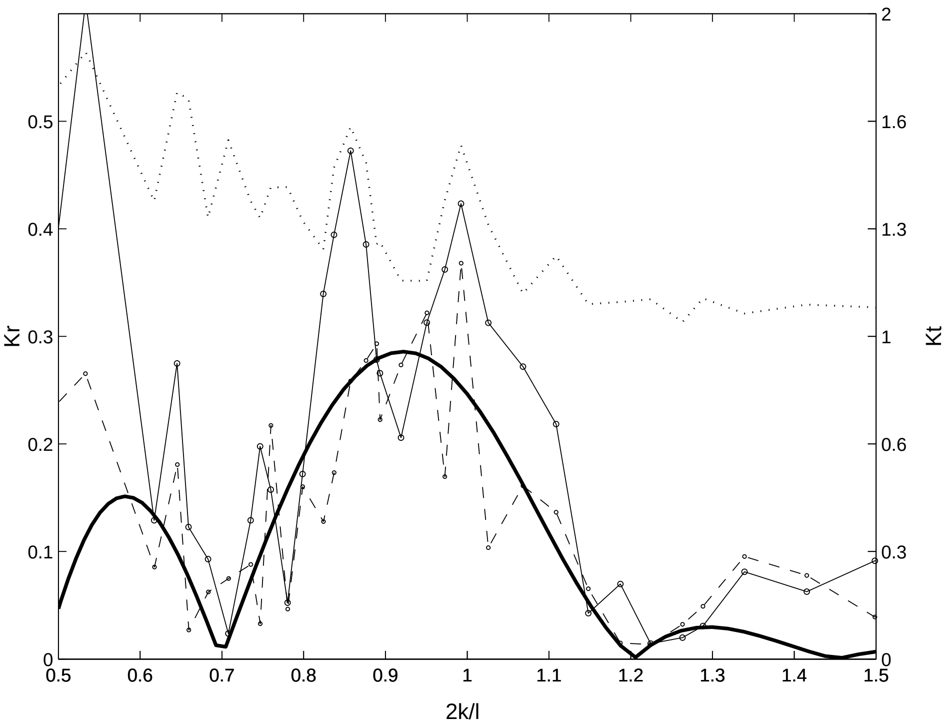

FIG. 6.9 – Reflection coefficient (K_r) without current, corrected with the beach reflection (dashed), transmission coefficient (K_t) in dotted line, same legend elsewhere.

corresponding exactly to the beginning ($x = 0$m) and to the end ($x = 16$m) of the adjusting ramps respectively and centered in the transverse direction ($y = 0$m). Wave amplitude used to compute this ratio slightly differs from the one used for the experimental data set in the sense that incident and reflected waves are not dissociated and treated separately. Comparisons cannot thus be done in a rigorous physical sense, and no direct comparison with the measurements will be given, but this transmission coefficient can give an interesting estimate for the underestimation predicted by the theories. The shape of the transmission coefficient obtained as a function of $2k/l$ reveals a frequency modulation, similar to the two lobes (or the gap) observed for the main resonant peak in the reflection coefficient (Fig. 6.4, 6.9). This large modulation around the resonant peak ($2k/l = 0.9$) may thus be explained by the wave refraction over the bars which leads to 3D non-homogeneity downwave in the tank, also correlated with a weak transverse variation of the wave field upwave from the bars. To illustrate the level of complexity involved, a spatial pattern of the scattered wave field is represented (Fig.6.11) for the monochromatic case $2k/l = 1$.

Influence of the current on wave reflection

In the presence of a current the reflection peak is shifted towards the low wavenumbers and the reflection is enhanced (Fig.6.4). Although Kr predicted by Kirby's

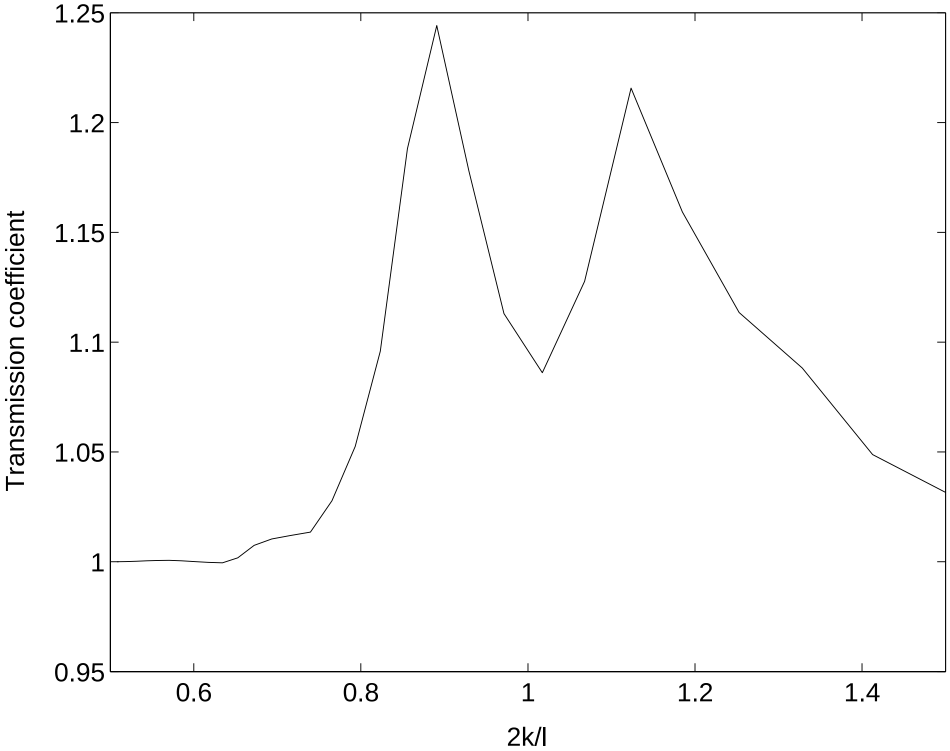

Fig. 6.10 – Transmission coefficient.

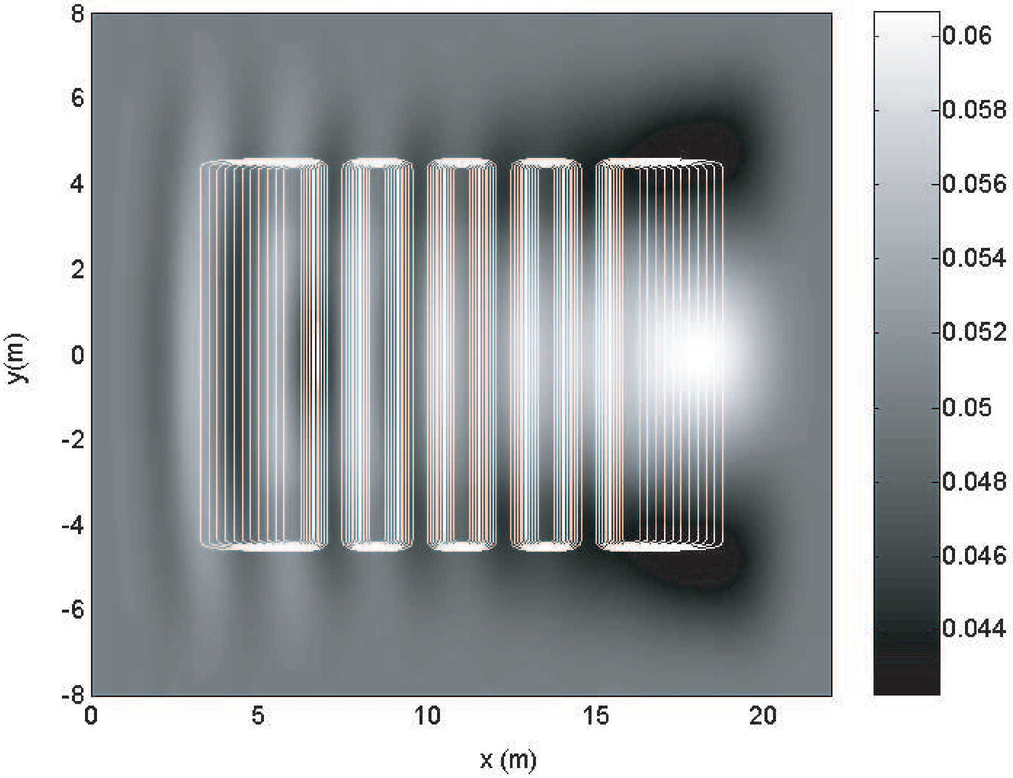

Fig. 6.11 – Spatial pattern of the scattered wave field, $2k/l = 1$.

theory (1988) cannot be compared with the measured values because of the adjusting ramps, there is a good agreement between general observed and predicted shifts Δk to lower wavenumbers. The experimental shift $\Delta k \simeq 0.08.l/2 \pm 10\%$ is in agreement with Kirby (1988)'s theory ($\Delta k = 0.085.l/2$). This shift due to the current can be estimated by considering the modification of the wave-bottom resonant condition. The frequency shift due to the current computed from (Eq.6.12) ($\Delta k = 0.09.l/2$) is consistent with the observed value. We can observe in particular that the current variability over the patch has little influence on the reflected wave energy, which is correctly determined by use of the averaged current.

6.3.3 Irregular waves

Bragg scattering and current influence

The Fig.6.12a-f present incident and reflected energies as a function of the normalized resonant wavenumber $2k/l$ with and without current for three locations over the patch : upwave, over (at half-length) and downwave from the patch, as is shown in Fig. 6.1. The observations are compared with the linear theory of Kirby (1988) (with and without current), applied to each component of the observed incident spectrum. After Fast Fourier Transform of the data set, the algorithm for reflection calculation is applied to each of the frequency components. The obtained spectra for incident and reflected wave are then averaged in frequency (with the 10 nearest neighbors) to get the final wave spectra.

The incident wave spectrum follows a Jonswap shape, with a peak period of $T =$ 1.813 s (corresponding to a wavelength of $4.91m$ for $h = 1.5m$) near the "theoretical" Bragg resonance conditions. The significant wave height is about 0.12 m without current, and 0.10 m with current, that correctly fits to the ratio of about 0.6 between incident energies with and without current. Without current, the observed reflection peak is centered about $2k/l = 0.95$, slightly different from the monochromatic case, but explained by an incident energy non uniform over a large band around the spectral peak . The rate of reflected energy near resonance of about 10% corresponds to amplitude ratio of 0.3, as in the monochromatic case. In the presence of current, the reflected peak is shifted toward lower wavenumbers, and its relative amplitude with respect to the incident wave is increased, as already found for monochromatic waves. Kirby's theory underestimates the reflection but follows the measurement tendencies. The incident spectrum (Fig.6.12a) presents a gap centered around the resonant frequency due 3D effects already discussed in the previous section.

With and without current, the reflection decreases over the patch, and vanishes downwave as predicted by the linear theory. In the presence of current, the reflected spectrum is shifted toward the low wavenumbers. For the same incident signal provided by the wavemaker it is also interesting to note that the wave reflection is larger in the presence of current following the waves, as was found for regular waves.

Nonlinear Bragg scattering

Moderately steep waves may behave differently due to higher order Bragg scattering. Liu and Yue (1988) classified the Bragg resonances and present a new class (III), involving resonant interaction among one bottom and three surface wave components, that may have the same order of magnitude as class I (wave-wave-bottom) and class II (wave-wave-bottom-bottom ; Guazzelli et al., 1992) scattering. In order to investigate the possible effects of the surface nonlinearity on Bragg resonance, we compared the reflection coefficient computed directly from the incident and reflected energy (corresponding to Fig.6.12a) with a reflection coefficient computed by convolution of this incident spectrum with the reflection coefficient obtained from the linear measurements. They are represented in Fig.6.13 with dashed and dotted line respectively. The small differences observed are not significant compared to the uncertainties of the measurements, in particular the modification of beach response to a wave spectrum compared to a single wave. The general agreement of the observed spectral response and the superposition of the linear results suggest that wave nonlinearities play a very minor role, if any, in our experiment, suggesting that class I Bragg scattering dominates the reflection (compared to class III).

Conclusion

Effect of currents on the scattering of surface gravity waves over a sinusoidal bottom was investigated in this study for regular and irregular gravity waves. Theories by Rey (1992), including evanescent modes, and Kirby (1988), including current effects were used for the analysis of the experimental results. For regular waves, the location of the main resonant peak without current is well predicted by Rey's theory. Kirby's theory only computes the reflection over the sinusoidal bars without including the adjusting ramp and thus, the predicted main resonant peak location with and without current is slightly shifted in comparison with the measurements. However, the observed shift of the reflection peak due to the current, agrees with the effect predicted by Kirby. Concerning the magnitude of the reflection, significant differences are observed between theory and measurements. The beach reflection and its phase are found to significantly modify the reflection coefficient at the low and

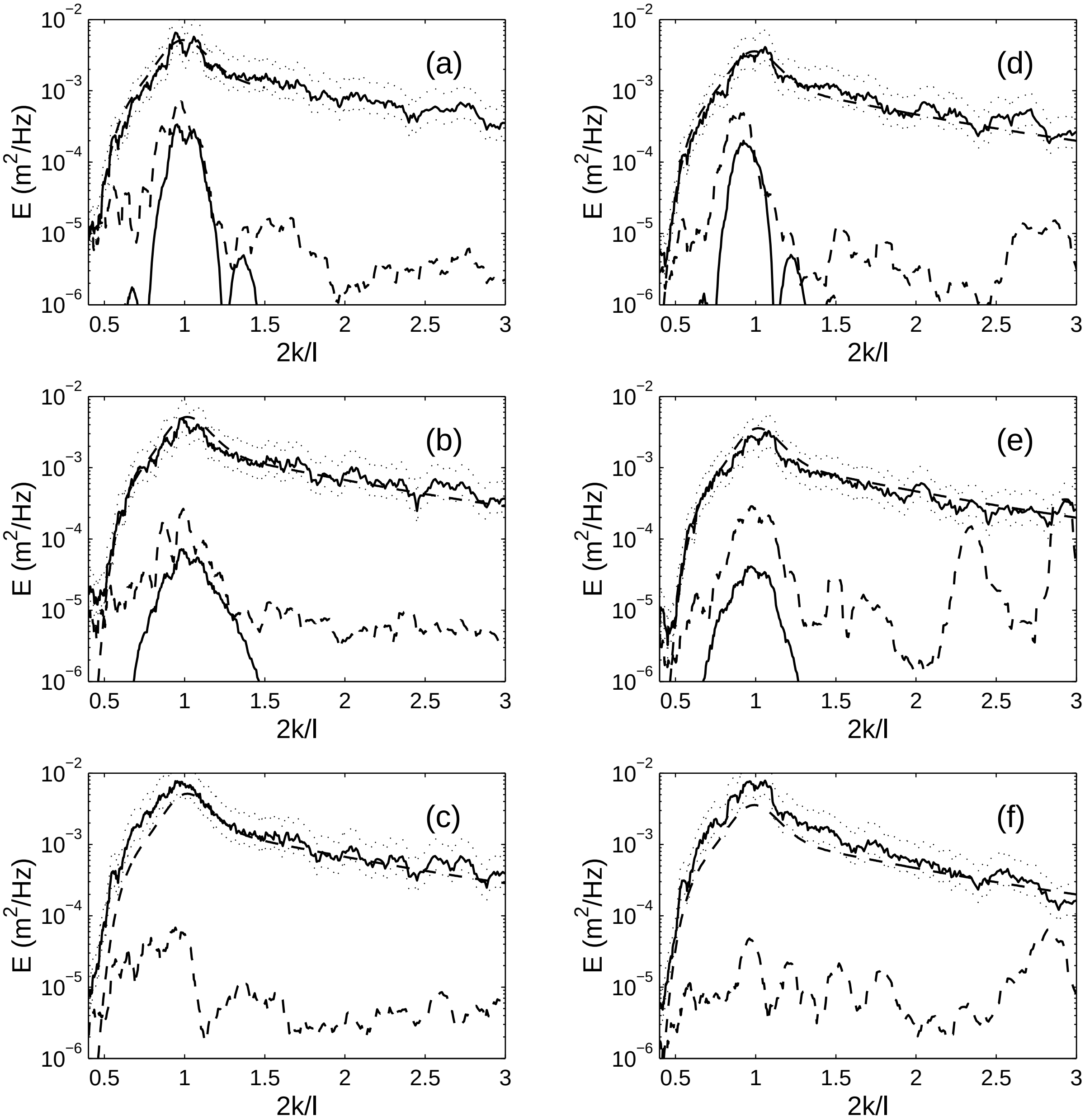

Fig. 6.12 – Wave spectrum evolution (y-log scale) up-wave(a,d) , over (at half length)(b,e), and down-wave the patch(c,f), with and without current (respectively right panels, $d - f$, and left panels, $a - c$), for a $T = 1.813$ s peak period. The upper full and dashed lines are respectively the observed incident spectrum and the theoretical incident spectrum generated by the wavemaker. The lower dashed line is the measured reflected energy. The lower full line is the theory, Kirby (1988), with and without current. The 95% confidence interval is represented by two limit spectra in grey dotted line.

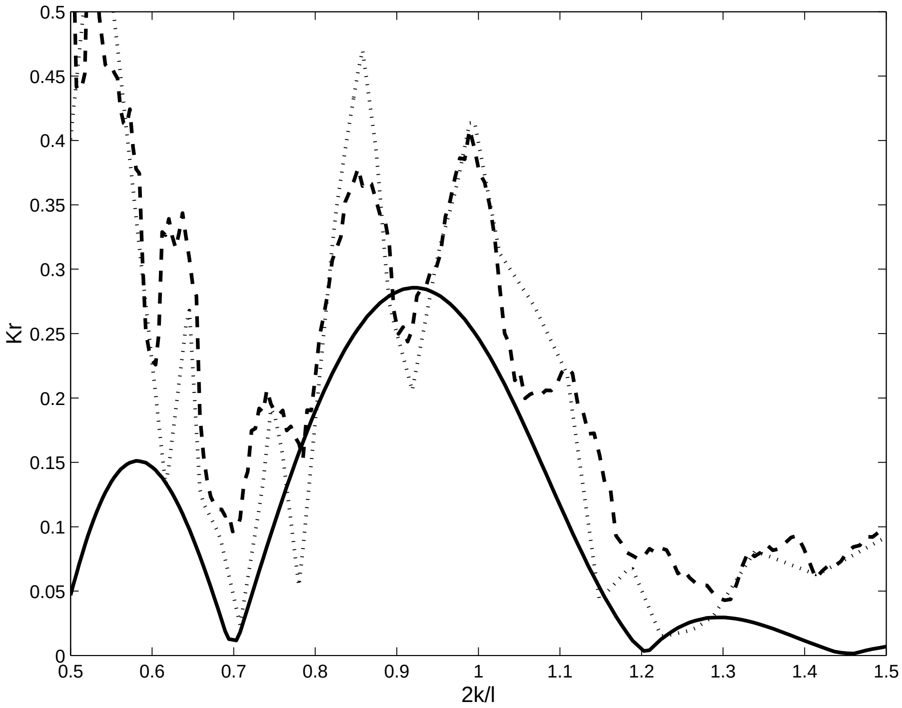

FIG. 6.13 – Reflection coefficient, $T = 1.813$ s, $U = 0$ m.s^{-1}, up-wave of the bars.

high frequencies while the refraction (and 3D effects) modify the reflection around the resonant wavenumbers ($2k/l = 1$). In addition, the wave measurement techniques assume linear plane waves, which is correctly but not strictly verified for larger waves upwave from the patch since gauges are located over a flat bed domain of limited extent (5 m), and over the patch where water depth strongly varies around its mean value. These effects may explain the underestimation predicted by the models, as well as the modulation observed nearby the peak of reflection. For irregular waves, the shift of the main resonant peak and the amplification of the reflection due to the current are also observed through spectral analysis based on a linear superposition of independant waves. The good agreeement with theory that assumes that wave components behave as independant waves confirm the linearity of the process since it is well described by a linear approach. The non-homogeneous current has no significant influence, since results are in good agreement with the theories based on uniform current. These two observations give strenght to the linear approach which remains consistent even when nonlinearities arising from steep slopes, wave-wave and wave-current interactions and inhomogeneous current may be present.

Acknowledgements

The authors acknowledge the Conseil Général du Var for its financial support for the experiments carried out in the wave basin BGO FIRST in the framework of the GIS HYDRO.

6.4 Compléments : analyse de la variabilité du courant au-dessus du fond modulé

Pour appuyer les résultats concernant l'influence du courant sur la réflexion des vagues, une analyse de comportement du courant au-dessus du fond modulé est réalisée. Deux profils de courant sont effectués au-dessus du fond modulé, en l'absence de houle, à l'aide d'un micro-moulinet et d'un ADV (Acoustic Doppler Velocimeter). La profondeur d'immersion du micro-moulinet est fixée à 1 m pour les deux profils. Pour l'ADV, une profondeur de 50 cm est choisie pour le premier profil, et 90 cm pour le second. Ces profils sont moyennés sur 10 s et représentés sur les figures 6.14ab, incluant un calcul d'écart type indiqué par une barre d'erreur. L'ADV renseigne également sur les vitesses transversales et verticales (figures 6.15ab). La zone de mesure de la réflexion, en amont du fond modulé, présente un courant assez homogène, tant en intensité, puisque l'écart type est faible, qu'en profil vertical, quasiment constant. On observe ensuite une accélération sur la rampe plus forte au "fond" (1 m) qu'en "surface" (50 cm), le profil s'inverse après au-dessus du fond modulé. Par ailleurs, le flux de masse au-dessus du fond modulé est plus faible qu'en amont, ce qui signifie qu'une partie du courant est canalisée par les sinusoïdes et s'écoule de part et d'autre du fond modulé (le bassin a une largeur de 24 m et le fond modulé n'est disposé que sur 16 m). Ceci est corrélé avec une augmentation de la dispersion pour le micro-moulinet et l'ADV, et confirmé par les vitesses transversales et verticales de l'ADV (figures 6.15 ab).

Lors des mesures de réflexion avec la houle régulière, aucune mesure de courant n'était disponible au-dessus du fond, par contre, un ADV placé 1.3 m en amont du fond et deux micro-moulinets à 1 m de part et d'autre de l'axe longitudinal, au niveau du début de la rampe ($x = 0$) avaient pour but de vérifier l'homogénéité du courant dans cette zone, dans les directions verticales et transversales de part et d'autre de l'axe longitudinal. Pour la période $T = 1.812$ s, en amont, le courant est assez homogène en direction et en intensité sur la verticale (figure 6.16 a), et de part et d'autre de l'axe médian du bassin (figure 6.16 b). Une panne d'un des deux micro-moulinets pendant les expériences n'a pas permis de vérifier l'homogénéité pour toutes les fréquences d'étude, mais au vu de l'exemple précédent ($T = 1.812$ s), on peut supposer qu'elle est correcte.

Pour les essais en houle irrégulière (ici représentée avec trois périodes pic 1.3, 1.8 et 2.047 s respectivement par les figures 6.17, 6.18, 6.19), l'information de courant au-dessus du fond était disponible, à l'aide d'un micro-moulinet placé au milieu du fond ($x = 8$ m) et à 1 m de profondeur. Cette information était également disponible pour les essais sans houle (figure 6.20). Un ADV placé en amont du fond permet également de connaître l'intensité du courant au niveau des mesures amont. Par comparaison avec les mesures sans houle (figures 6.20 et 6.14), le courant est plus intense en présence de houle au milieu du fond, et sa variabilité d'autant plus faible que la période de la houle est importante. Ainsi, le courant semble mieux "dirigé" avec une houle plus longue, l'intensité moyenne du courant se rapprochant de celle donnée par la conservation du débit, c'est à dire 0.32 cm/s en amont par 1.5 m de fond et 0.40 m/s au-dessus par 1.5 m en moyenne.

La variabilité assez importante observée au-dessus du fond pour les deux profils de courant en l'absence de houle semble correspondre aux résultats les plus pessimistes en termes de variabilité du courant, la houle ajoutée par-dessus ayant tendance à homogénéiser le courant. De plus, la zone en amont du fond, lieu des mesures de réflexion, est bien homogène en intensité et direction, ce qui conforte les résultats sur les mesures de réflexion présentés dans l'article.

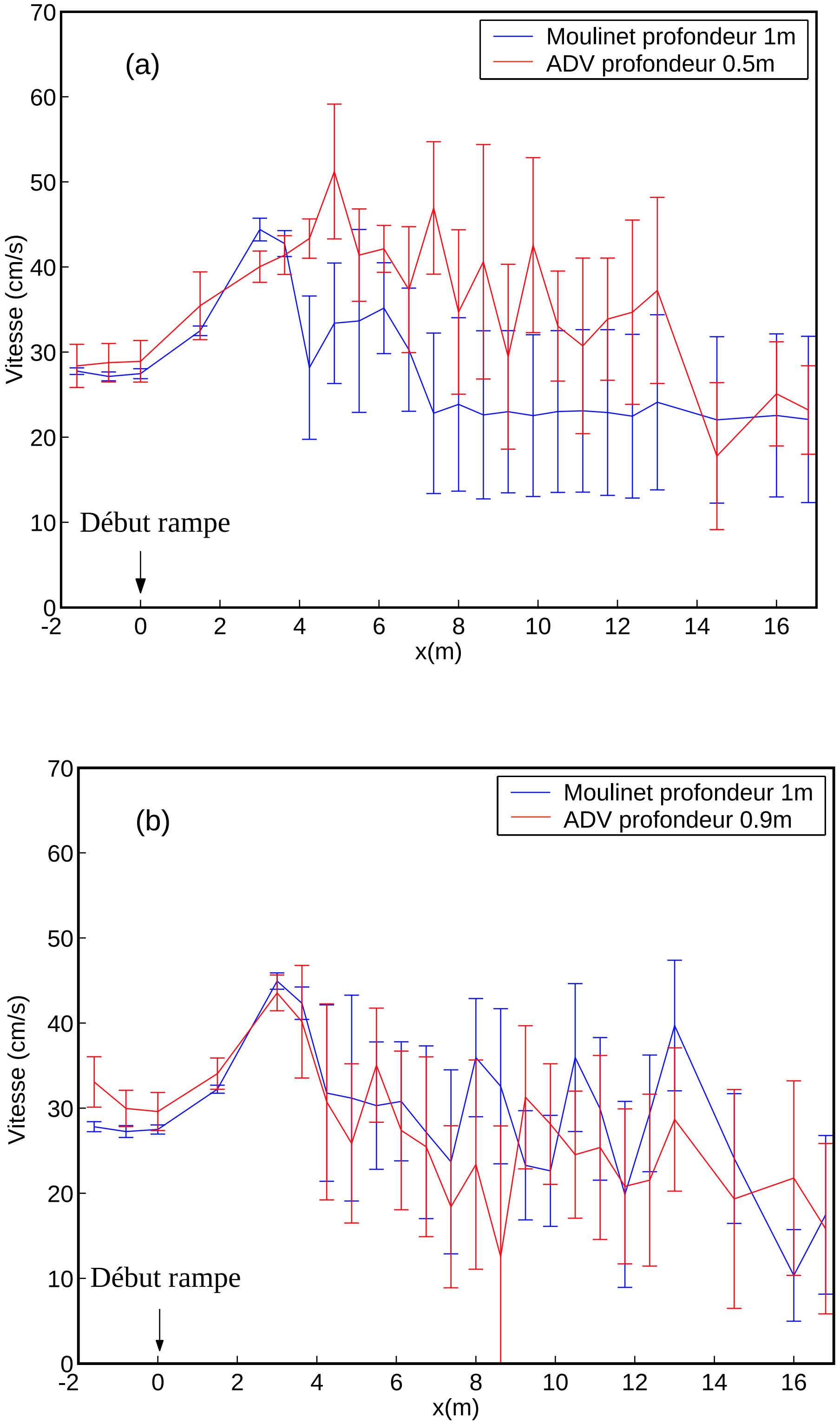

FIG. 6.14 – Profils de courant (a, b) réalisés au-dessus du fond avec un micro-moulinet immergé à 1 m, et un ADV immergé à 50 cm pour le premier profil (a) et 90 cm pour le deuxième profil (b).

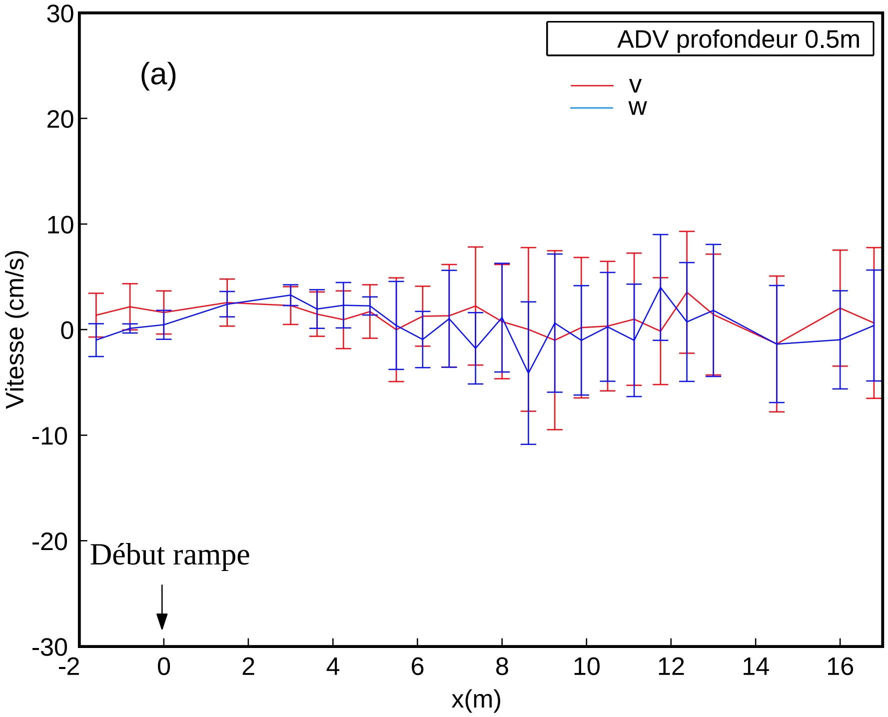

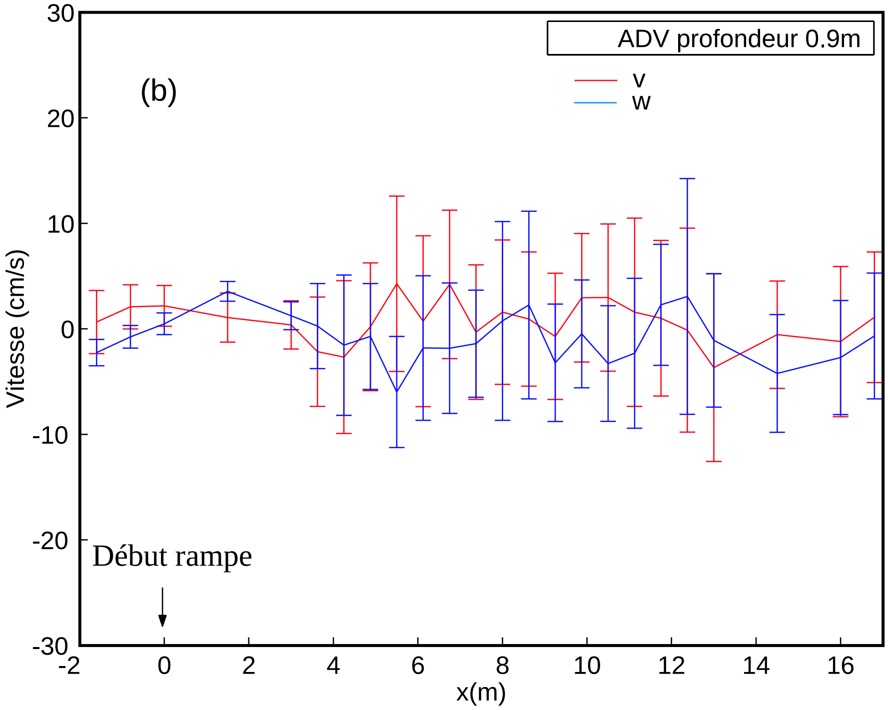

FIG. 6.15 – Profils de courant (a, b), vitesses transversales (v) et verticales (w) réalisés au-dessus du fond avec un ADV immergé à 50 cm pour le premier profil (a) et 90 cm pour le deuxième profil (b).

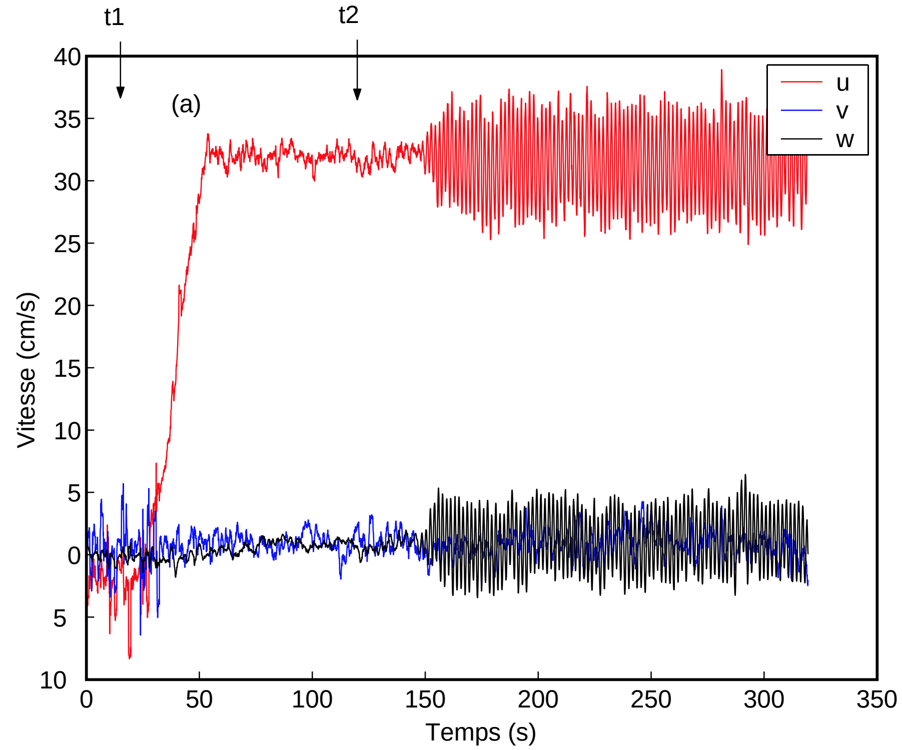

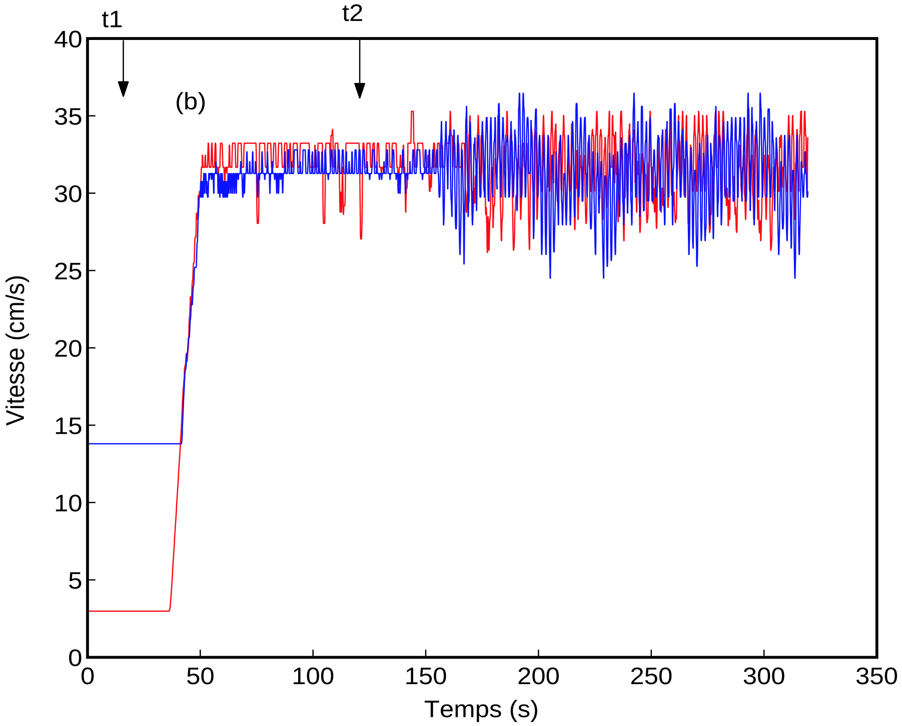

FIG. 6.16 – (a) Mesure de courant avec ADV en amont ($x = -1.3$ m) immergé à 50 cm pour une houle régulière de période pic $T = 1.812$ s. Les données sont moyennées sur 1 s. (b) Mesure de courant avec les micro-moulinets de part et d'autre de l'axe longitudinal, au niveau du début de la rampe, immergés à 1 m. Les données sont moyennées sur 1 s. t1=10s : mise en route du courant, t2=130s : mise en route des batteurs.

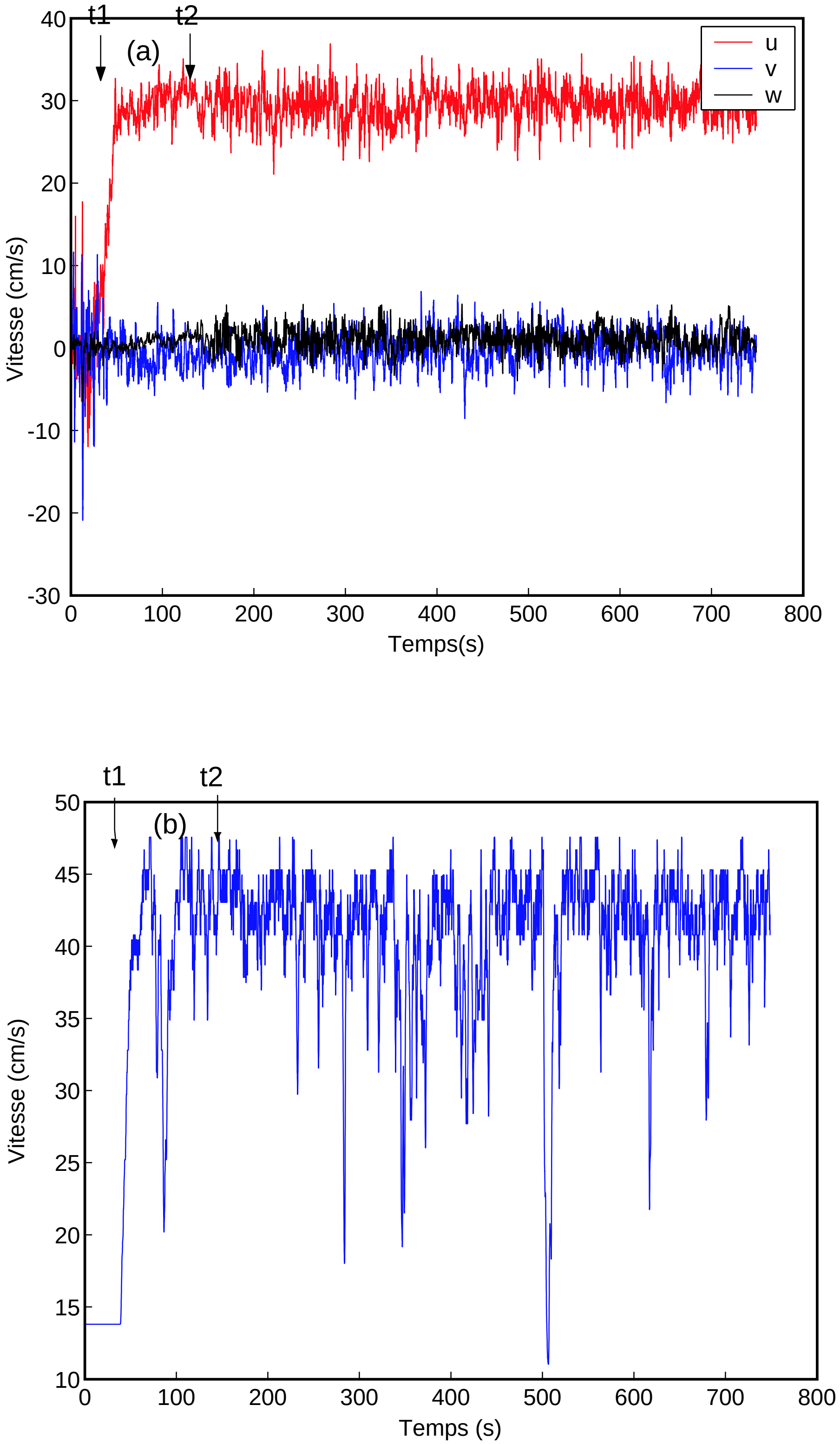

FIG. 6.17 – (a) Mesure de courant avec ADV en amont ($x = -1.3$ m) immergé à 50 cm pour une houle irrégulière (Jonswap) de période pic $T = 1.3$ s. Les données sont moyennées sur 1 s. (b) Mesure de courant avec le micro-moulinet au milieu du fond, immergé à 1 m. Les données sont moyennées sur 1 s. t1=10s : mise en route du courant, t2=130s : mise en route des batteurs.

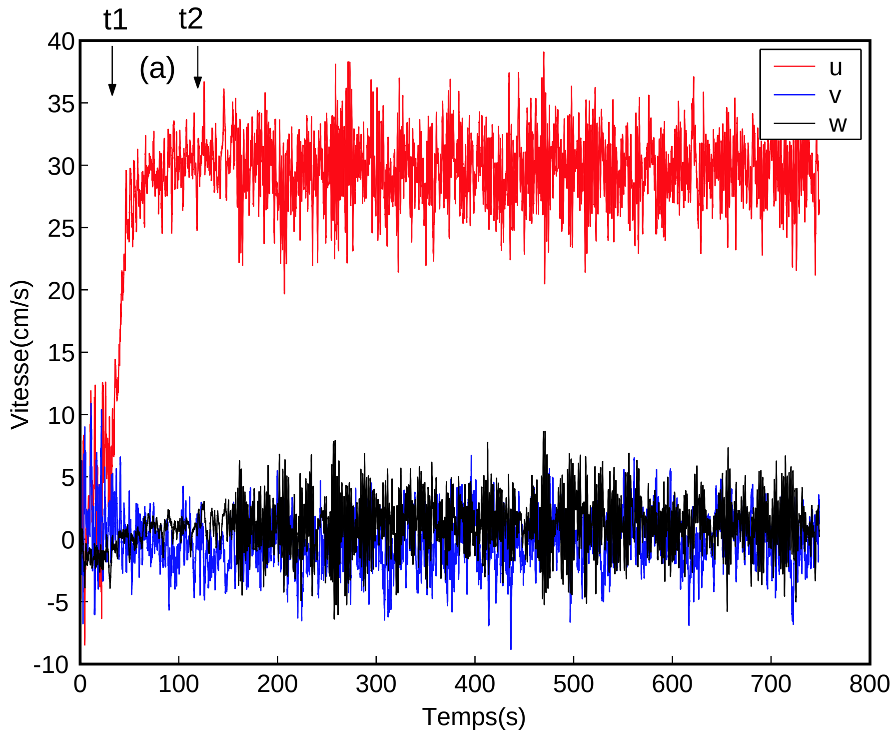

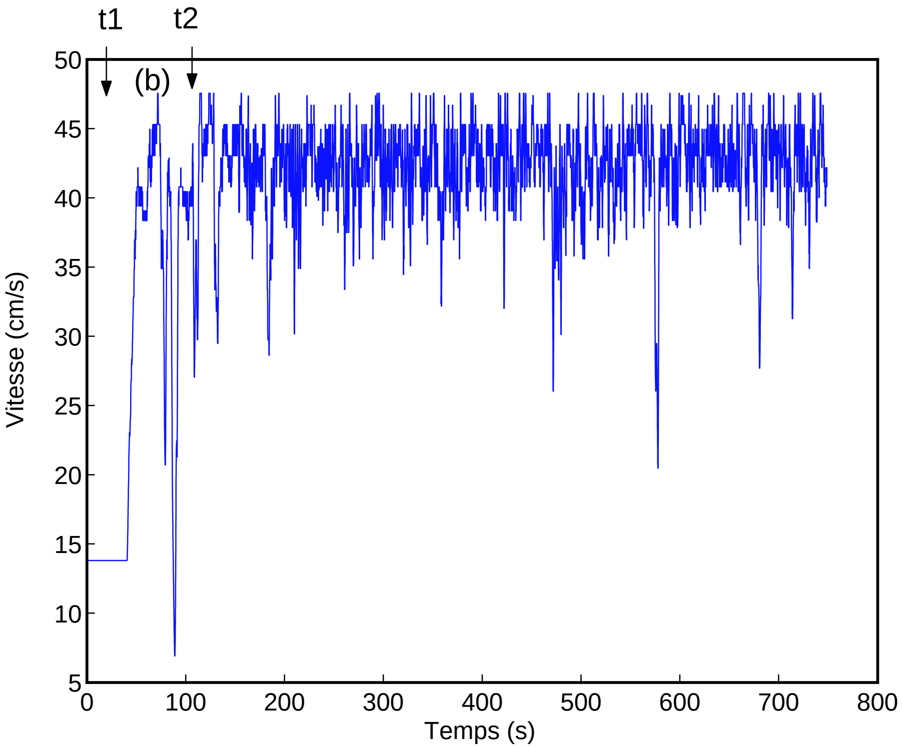

FIG. 6.18 – (a) Mesure de courant avec ADV en amont ($x = -1.3$ m) immergé à 50 cm pour une houle irrégulière (Jonswap) de période pic $T = 1.813$ s. Les données sont moyennées sur 1 s. (b) Mesure de courant avec le micro-moulinet au milieu du fond, immergé à 1 m. Les données sont moyennées sur 1 s. t1=10s : mise en route du courant, t2=130s : mise en route des batteurs.

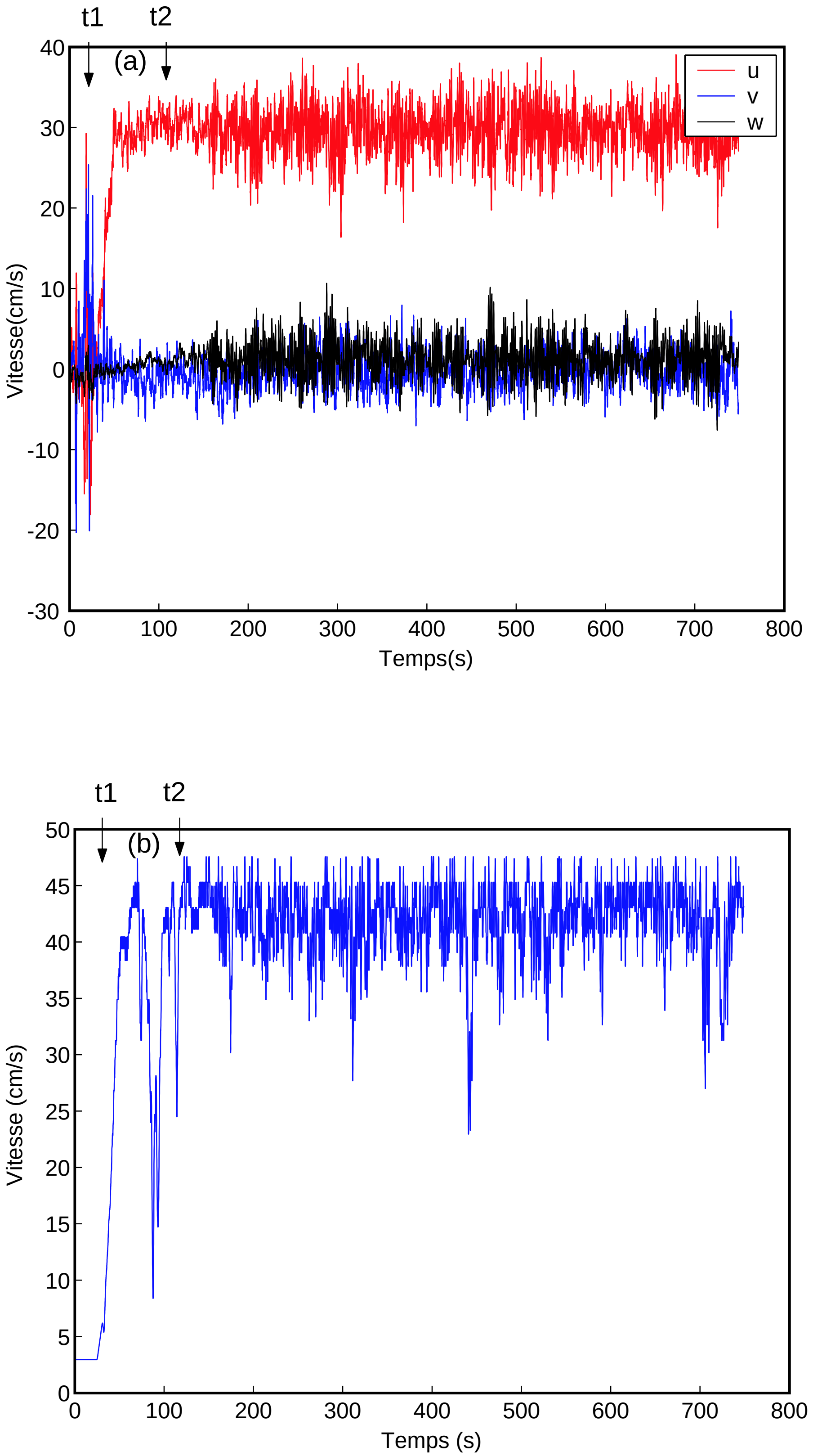

FIG. 6.19 – (a) Mesure de courant avec ADV en amont ($x = -1.3$ m) immergé à 50 cm pour une houle irrégulière (Jonswap) de période pic $T = 2.047$ s. Les données sont moyennées sur 1 s. (b) Mesure de courant avec le micro-moulinet au milieu du fond, immergé à 1 m. Les données sont moyennées sur 1 s. t1=10s : mise en route du courant, t2=130s : mise en route des batteurs.

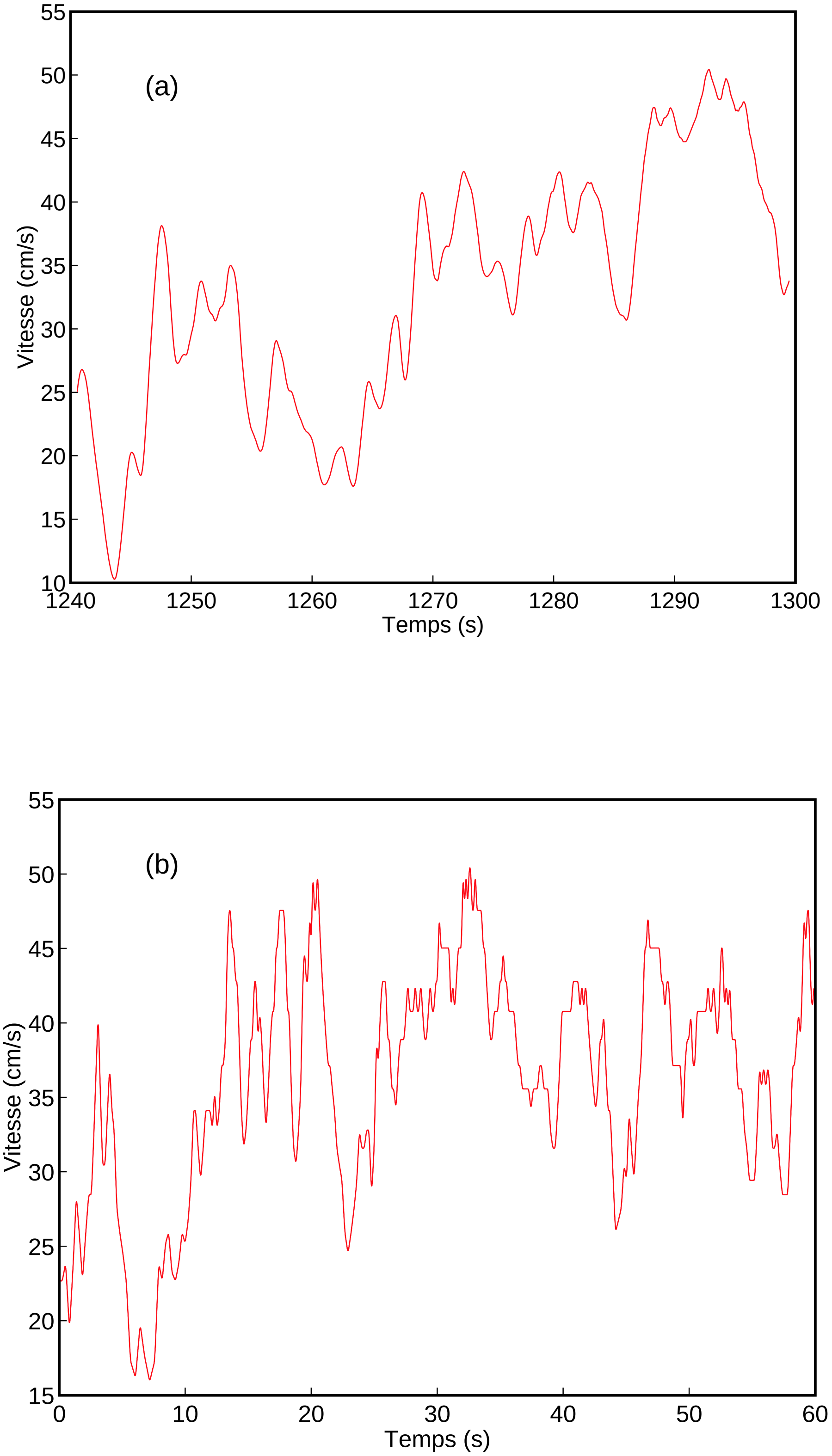

FIG. 6.20 – Mesures de courant sans houle effectuées au cours les deux profils (a, b) réalisés au-milieu du fond ($x = 8m$) avec un micro-moulinet immergé à 1 m, moyennées sur 1s

6.5 Annexe : illustrations du dispositif expérimental

FIG. 6.21 – Fond sinusoïdal

FIG. 6.22 – Sondes à houles

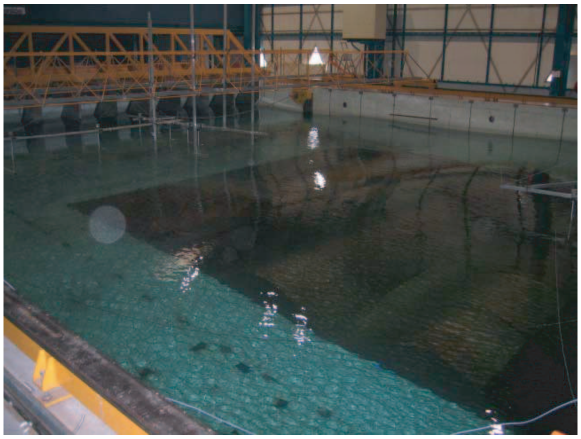

FIG. 6.23 – Bassin à houle

Chapitre 7

Effet d'un courant sur la diffusion des vagues par une topographie 3D, l'approche spectrale

Introduction

Le chapitre précédent s'est intéressé à mettre en évidence expérimentalement le décalage des fréquences résonantes en présence d'un courant ambiant, en confrontant les résultats expérimentaux à une théorie (Kirby, 1988), capable de représenter l'effet d'un courant sur la diffusion de Bragg pour un fond sinusoïdal 2D. Pour des fonds réalistes 3D, Ardhuin et Herbers (2002) et Ardhuin et al. (2003a) ont montré par la confrontation du terme de source (S_{bscat}) à des observations in situ (plateau continental en Caroline du Nord), que la diffusion de Bragg des vagues par le fond peut expliquer l'élargissement de l'étalement directionnel du spectre des vagues incidentes. Les échelles de longueur d'onde caractéristiques du fond dans cette zone sont de l'ordre du kilomètre. Cette échelle favorise des interactions, pour des longueurs d'onde de surface de 2 à 4 fois plus petites que celles du fond ($k/l = 2$ à 4) menant à une diffusion directionnelle du spectre vers l'avant. En mer du Nord, certaines zones sont caractérisées par des échelles de variation plus petites, comme des dunes de sable, plus propices à la réflexion des vagues intervenant autour de $k/l = 0.5$. De plus, la variance du fond pour de telles zones est beaucoup plus importante que celle rencontrée en Caroline du Nord, suggèrant un effet plus prononcé du phénomène de diffusion. Pour traiter la diffusion des vagues dans de telles zones, balayées par de forts courants de marée, le terme de source (Ardhuin et Herbers, 2002) est étendu en présence d'un courant uniforme, et appliqué à des fonds réalistes en Mer du Nord.

Surface gravity wave scattering over a bottom topography with uniform currents

Rudy Magne(1,2) and Fabrice Ardhuin(1)

In preparation

(1) *Centre Militaire d'Océanographie, SHOM, BREST, France*
(2) *LSEET-LEPI, Université de Toulon et du Var, La Garde, France*

Résumé

La diffusion des vagues aléatoires par une topographie aléatoire est étudiée en présence d'un courant uniforme utilisant un développement en perturbations de l'action au deuxième ordre en puissance de l'amplitude du fond. Ce problème est pertinent pour la propagation des vagues sur les plateaux continentaux peu profonds où les courants de marée sont souvent importants. Cette théorie mène à une équation d'évolution de l'action avec un terme de source de diffusion qui donne le taux d'évolution du spectre d'action. La diffusion par le fond résulte d'un échange de l'action des vagues entre les composantes des vagues qui ont la même fréquence absolue. Avec et sans courant, le terme de diffusion donne des coefficients de réflexion pour les amplitudes des vagues qui convergent, dans la limite des petites amplitudes dues fond et des petits nombres de Froude, vers les résultats des précédentes théories pour des vagues monochromatiques se propageant dans une dimension au-dessus de barres sinusoïdales. A la résonance, des petites différences entre les théories déterministes et la présente approche apparaissent pour des amplitudes du fond finies dues au couplage de phase entre l'onde incidente et réfléchie avec la phase de la topographie du fond. A partir de calculs numériques pour des barres sinusoïdales, ce bispectre fond-surface est probablement insignifiant pour des conditions océaniques. Au-dessus de plateaux continentaux sableux, les courants de marée sont connus pour générer des dunes de sable avec des échelles comparables à celles des vagues. L'application de la théorie à des topographies réalistes suggère que le courant peut affecter de manière importante la diffusion des vagues sélectionnant différentes échelles du fond, comme le nombre d'onde k change pour une fréquence absolue fixée.

Abstract

Scattering of random surface gravity waves by small amplitude topography is investigated in the presence of a uniform current, using a perturbation expansion of the wave action to second order in powers of the bottom amplitude. This problem is relevant to ocean waves propagation on shallow continental shelves where tidal currents are often significant. The present theory yields a wave action balance equation with a scattering source term that gives the rate of change of the wave action spectrum. Bottom scattering results in an exchange of wave action between wave components that have the same absolute frequency. With and without current, the scattering term yields reflection coefficients for the amplitudes of waves that converge, in the limit of small bottom amplitudes and small Froude numbers, to the results of previous theories for monochromatic waves propagating in one dimension over sinusoidal bars. At resonance, small differences between deterministic theories and the present approach arise for finite bottom amplitudes due to a phase coupling of incident and reflected waves with the phase of the bottom topography. Based on numerical calculations for sinusoidal bars, this mixed surface-bottom bispectrum is unlikely to be significant in oceanic conditions. Over sandy continental shelves, tidal currents are known to generate sandwaves with scales comparable to those of surface waves. Application of the theory to a realistic topography suggests that the current may strongly influence surface gravity wave scattering by selecting different bottom scales, as the surface wavenumber k changes for a fixed absolute frequency.

7.1 Introduction

Following the early observations of Heathershaw (1982), a considerable body of knowledge has been accumulated on the scattering of small amplitude surface gravity waves by periodic bottom topography. An accurate theory that could reproduce the observed scattering of monochromatic waves over a few sinusoidal bars was put forward by Mei (1985), leading to practical phase-resolving equations that may be used to model this phenomenon for more general bottom shapes (Kirby 1986). For sinusoidal bottoms of wavenumber l, Mei (1985) proposed an approximate analytical solution. In two dimensions (one horizontal and the vertical) this solution yields simple expressions for the wave amplitude reflection coefficient R, as a function of the mismatch between the wavenumber of the surface waves k and the resonant value $l/2$, for which Bragg resonance leads to the maximum reflection. Beyond a cut-off value of that mismatch, it was found that the incident and reflected wave amplitudes oscillate in space instead of decreasing monotonically from the incident region. In three dimensions the Bragg resonance condition becomes $\boldsymbol{k} = \boldsymbol{l} + \boldsymbol{k}'$ and $k = k'$, with k, k', and l the norms of the horizontal wave-vectors $\boldsymbol{k}$, $\boldsymbol{k}'$, and $\boldsymbol{l}$. A uniform current was later introduced by Kirby (1988). The resonant condition is modified in that case, with $k \neq k'$ if incident and reflected waves propagate at different angles relative to the current direction. Other contributions have shown that higher-order theories are necessary to represent the sub-harmonic resonance observed over a bottom that is a superposition of two components of different wavelengths (Guazzelli, Rey & Belzons 1992). Such sub-harmonic resonance was found to have as large an effect as the lowest order resonance for bottom amplitudes of only 25% of the water depth, due to a general stronger coupling of relatively longer waves. However, these methods are still prohibitively expensive for investigating the propagation of random waves over distances larger than about 100 wavelengths, and the details of the bottom are typically not available over large areas, while the details of the wave field on the scale of a wavelengths are often not of interest. Besides, a consistent phase-averaged wave energy evolution equation is also necessary for the investigation of the long waves associated with short wave groups (Hara & Mei 1987).

The large scale behaviour of the wave field may rather be represented by the evolution of the wave action spectrum assuming random phases. Such an approach was already proposed by Hasselmann (1966) for wind-wave propagation, and Elter & Molyneux (1972) for the calculation of tsunami propagation. A proper theory for the evolution of the spectrum can be obtained from a solvability condition for the wave spectrum, in a way similar to the work of Mei (1985) and Kirby (1988) for the wave amplitudes. In the absence of currents the correct form of that equation was first obtained by Ardhuin & Herbers (2002, hereinafter referred to as AH) using a two scale approach. They decomposed the water depth $H - h$ in a slowly varying depth H, that causes shoaling and refraction, and a rapidly varying perturbation h with zero mean, that causes scattering. The resulting scattering was shown to be consistent with the dramatic increase of the directional width of the wave spectra observed on the North Carolina continental shelf. (Ardhuin *et al.* 2003a, 2003b). Recently, Magne *et al.* (2005, hereinafter referred to as MAHR) showed that AH's theory gives the same damping of incident waves as a Green function solution applied to any two dimensional topography (random or not) of small amplitude (see also Pihl, Mei & Hancock 2002, Mei & Hancock 2003). Investigated the applicability limits of the scattering term of AH, MAHR also performed numerical calculations, comparing AH's theory to the accurate matched-boundary model of Rey (1995) that uses a decomposition of the bottom in a series of steps, including evanescent modes. The numerical results show that AH's theory is generally limited by the relative bottom amplitude $\max(h)/H$ rather than the bottom slope.

The resulting expression of the scattered energy as a Bragg scattering term is consistent with results for scattering of acoustic and electromagnetic waves obtained by the small perturbation method, valid in the limit of small $k \max(h)$ with k the wavenumber of the propagating waves (Rayleigh 1896, see Elfouhaily & Guerin 2004 for a review of this and other approximations). Since there is no scattering for $kH >> 1$, in that case the waves do not 'feel' the bottom, the small parameter $\max(h)/H$ may be used in our context, instead of the more general $k \max(h)$. The scattering strength is thus entirely determined by the bottom elevation variance spectrum at the bottom scales resonant with the incident waves. Based on these results it follows that Mei's (1985) theory should yield the same reflection coefficient as AH's theory in the limit of small bottom amplitudes. Yet, AH predict that the wave amplitude in 2D would decay monotonically, which is not compatible with the oscillatory nature of Mei's theory for large detunings from resonance. Further, outside of the surf zone and the associated multiple bar systems, the application of AH's theory is most relevant in areas where the bottom topography changes significantly on the scale of the wavelengths of swells. This often corresponds, over sand, to the presence of sandwaves. These sandwaves are generated by currents, and particularly by tidal currents (e.g. Dalrymple Knoght & Lambiase 1978, Idier, Erhold & Garlan 2002). It is thus logical to seek a theory for the scattering of waves in the presence of currents. A first theory was proposed by Kirby (1988), in the form of an extension of Mei (1985), with waves in a uniform current over a sinusoidal bottom.

The present paper thus provides an extension of AH for the case of uniform currents in § 2, and a detailed discussion of the differences between this theory and those of Mei (1985) and Kirby (1988) in § 3. Finally the oceanographic effects of the current are investigated in § 4 using a spectral phase-averaged numerical model, predicting the evolution of the wave action spectrum, and detailed measurements of the topography in the Southern North Sea. Conclusions follow in § 5.

7.2 Theory

7.2.1 General formulation

The variation in the action spectral density due to wave-bottom scattering is derived following the method of AH, now including the effect of a uniform current in the wave scattering source term. We consider weakly nonlinear random waves propagating over an irregular bottom with a constant mean depth H and random small-scale topography $h(\mathbf{x})$, so that the bottom elevation is given by $z = -H + h(\mathbf{x})$ where z is the elevation relative to the mean water level. The free surface is at $z = \zeta(\mathbf{x}, t)$. Extension to current and mean depth variations on a large scale is expected to follow from a two-scale approximation, similar to the effect of large scale depth variation (AH). When the depth varies in the flow direction, the current should also vary so that the flows remains non-divergent. Perturbations of the current should thus be of the order of ηU with $\eta = \max\{h/H\}$, and may scatter waves (Bal & Chou 2002). As far as this and other effects do not modify the wave-bottom resonance, they should only contribute separate source terms and shoaling and refraction terms. Further, for depth-varying current U should be regarded as the wave advection velocity (Andrews & McIntyre 1978, see Kirby & Chen 1989 for practical approximate expressions).

The solution is obtained in a frame of reference moving with the current so that only the bottom boundary condition changes. The maximum surface slope is caracterized by ε and we shall assume that $\varepsilon^3 \ll \eta^2$ so that the contributions to the wave energy to order η^2 are much larger than the resonant non-linear four wave interactions (Hasselmann 1962) and may be neglected. For shallow water waves, $kH << 1$, a stricter inequality is needed to prevent triad wave-wave interactions to enter the energy evolution equation at the same order as bottom scattering. In the frame of reference moving with the current, the governing wave equations are given by Laplace's equation for the wave potential, the bottom kinematic boundary conditions and a combination of Bernouilli's equation with the free surface kinematic

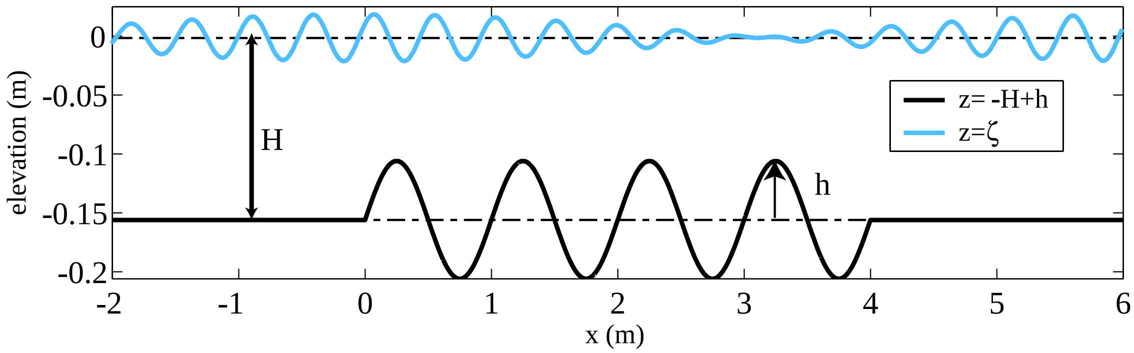

FIG. 7.1 – Definition sketch of the mean H water depth and relative bottom elevation h, in the particular case of the sinusoidal bottom used in § 3.

boundary condition,

$$\nabla^2\Phi + \frac{\partial^2\Phi}{\partial z^2} = 0 \quad \text{for} \quad -H+h \leq z \leq \zeta, \tag{7.1}$$

$$\frac{\partial \Phi}{\partial z} = \frac{\partial h}{\partial t} + \nabla\Phi\cdot\nabla h \quad \text{at} \quad z = -H+h, \tag{7.2}$$

$$\frac{\partial^2\phi}{\partial t^2} + g\frac{\partial\phi}{\partial z} = g\nabla\phi\cdot\nabla\zeta - \nabla\phi\cdot\frac{\partial\nabla\phi}{\partial t} - \frac{\partial\phi}{\partial z}\frac{\partial^2\phi}{\partial t\partial z} \quad \text{at} \quad z = \zeta. \tag{7.3}$$

The symbol ∇ represents the usual gradient operator restricted to the two horizontal dimensions.

Following Hasselmann (1962) we shall approximate h and ϕ with discrete sums, and take the limit to continuous integrals after deriving expressions for the evolution of the phase average wave energy. The current $\mathbf{U}$ introduced a transformation of the horizontal coordinates $\mathbf{x}' = \mathbf{x} + \mathbf{U}t$, where $\mathbf{x}$ is the coordinate in the moving frame, and

$$h(\mathbf{x}) = \sum_{\mathbf{l}} G_l \mathrm{e}^{\mathrm{i}\mathbf{l}.[\mathbf{x}+\mathbf{U}\mathbf{t}]}. \tag{7.4}$$

We look for a velocity potential solution in the form

$$\phi(\mathbf{x},z,t) = \sum_{\mathbf{k},s}\Phi^s_{\mathbf{k}}(z,\alpha t)\mathrm{e}^{\mathrm{i}[\mathbf{k}.\mathbf{x}-(s\omega-\mathbf{k}.\mathbf{U})t]} = \sum_{\mathbf{k},s}\Phi^s_{\mathbf{k}}(z,\alpha t)\mathrm{e}^{\mathrm{i}[\mathbf{k}.\mathbf{x}-s\sigma t]}, \tag{7.5}$$

where $\mathbf{l}$ and $\mathbf{k}$ are the bottom and surface wavenumber, respectively, s is a sign index equal to 1 or -1, and $s\sigma = s\omega - \mathbf{k}.\mathbf{U}$. In the moving frame of reference, components with $s=1$ propagate in the direction of the vector $\mathbf{k}$, while components with $s=-1$ propagate in the opposite direction. The amplitudes $\Phi^s_{\mathbf{k}}$ are slowly modulated in time, with a slowness defined by the small parameter α. Because ϕ is a real quantity we also have $\overline{\Phi^s_{\mathbf{k}}} = \Phi^{-s}_{-\mathbf{k}}$.

Numerical calculations by MAHR showed that the reflection coefficient predicted by AH were accurate for any bottom slope but appeared to be limited by the relative bottom amplitude $\eta = h/H$. We thus chose to expand the bottom boundary condition and wave potential in powers of η,

$$\phi = \phi_0 + \eta\phi_1 + \eta^2\phi_2 + \cdots \tag{7.6}$$

The boundary conditions (7.3) and (7.2) are expressed at $z = 0$ and $z = -H$, respectively, using Taylor series of ϕ about $z = -H$ and $z = 0$.

The spectral statistics of free wave components can be expressed in terms of covariances $F^{\Phi}_{i,j,k}$ of the velocity potential amplitudes,

$$F^{\Phi}_{i,j,k} = \langle \Phi^{+}_{i,\mathbf{k}} \Phi^{-}_{j,-\mathbf{k}} + \Phi^{-}_{i,-\mathbf{k}} \Phi^{+}_{j,\mathbf{k}} \rangle. \tag{7.7}$$

The contribution of the complex conjugate pairs of components $(\mathbf{k}, +)$ and $(-\mathbf{k}, -)$ are combined in (7.7) so that $F^{\Phi}_{i,j,k}$ is the covariance of all waves with wavenumber magnitude k propagating in the direction of $\mathbf{k}$. In the limit of small wavenumber separation, a continuous slowly-varying cross-spectrum can be defined (e.g. Priestley 1981, ch.11 ; see also AH),

$$F^{\Phi}_{i,j}(\mathbf{k}) = \lim_{|\Delta k| \to 0} \frac{F^{\Phi}_{i,j,k}}{\Delta k_x \Delta k_y}. \tag{7.8}$$

The definition of all spectral densities are chosen so that the integral over the entire wavenumber plane yields the total covariance of ϕ_i and ϕ_j. The bottom elevation spectrum in discrete form is given by $F^{G}_{\mathbf{l}} = \langle G_{\mathbf{l}} G_{-\mathbf{l}} \rangle$ and in continuous form by

$$F^{B}(\mathbf{l}) = \lim_{|\Delta l| \to 0} \frac{F^{G}_{\mathbf{l}}}{\Delta l_x \Delta l_y}, \tag{7.9}$$

and verifies[1],

$$\int_{-\infty}^{\infty} \int_{-\infty}^{\infty} F^{B}(\mathbf{l}) \mathrm{d}l_x \mathrm{d}l_y = \lim_{L \to \infty} \frac{1}{L^2} \int_{-L/2}^{L/2} \int_{-L/2}^{L/2} h(x,y)^2 \mathrm{d}x \mathrm{d}y \tag{7.10}$$

$N_{i,j}(\mathbf{k})$ is defined as the $(i+j)^{\text{th}}$ order depth-integrated wave action contribution from correlation between i^{th} and j^{th} order components with wavenumber k. For freely propagating waves, and following the common usage in non-accelerated reference frames the gravity g is left out, so that the action has units of meters squared times second. Accurate to second order in ε and η (Andrews & McIntyre 1978), $N_{i,j}$ is

---

[1] This expression only applies to bottom perturbations h with finite supports. F^B generalizes to the Fourier transform of the auto-covariance function for random bottoms, see Magne *et al.* (2005).

given from the velocity potential by the linear relation,

$$N_{i,j}(\mathbf{k}) = \frac{k}{g\sigma} F^{\Phi}_{i,j}(\mathbf{k}) \tanh(kH). \tag{7.11}$$

The spectral wave action is thus,

$$N(\mathbf{k}) = \sum_i N_i(\mathbf{k}) = \sum_i \sum_j N_{i,i-j}(\mathbf{k}). \tag{7.12}$$

We shall now solve for the velocity potential in the frame of reference moving with the current.

7.2.2 Zeroth-order solution

The governing equations for ϕ_0 are unchanged from the case with a current, thanks to the moving reference frame, i.e.

$$\phi_0 = \sum_{\mathbf{k},s} \frac{\cosh(k(z+H))}{\cosh(kH)} \Phi^s_{0,\mathbf{k}} \mathrm{e}^{\mathrm{i}[\mathbf{k}.\mathbf{x} - s\sigma t]}. \tag{7.13}$$

The intrinsic frequency σ is the positive root of the linear dispersion relation,

$$\sigma^2 = gk \tanh(kH). \tag{7.14}$$

7.2.3 First-order solution

The equations at order η are

$$\begin{aligned}
\nabla^2 \phi_1 + \frac{\partial^2 \phi_1}{\partial z^2} &= 0 \quad \text{for} \quad -H \leq z \leq 0, && (7.15)\\
\frac{\partial \phi_1}{\partial z} &= -h \frac{\partial^2 \phi_0}{\partial z^2} + \frac{\partial h}{\partial t} + \nabla \phi_0 \cdot \nabla h \qquad \text{at} \qquad z = -H, && (7.16)\\
\frac{\partial^2 \phi_1}{\partial t^2} + g \frac{\partial \phi_1}{\partial z} &= NL_2 \qquad \text{at} \qquad z = 0, && (7.17)
\end{aligned}$$

where the non-linear terms NL_2 force a bound wave solution ϕ_1^{nl} (Hasselmann 1962) that will be neglected here because it does not modify our second order wave energy balance. The small-scale variation h that causes scattering now appears in the bottom boundary condition. A general solution for the (unchanged) Laplace equation (7.15) is given by the following superposition of free and bound wave components, with amplitudes $\Phi_{2,\mathbf{k}}^{s_3}$ and $\Phi_{1,\mathbf{k}}^{si,s_3}$ respectively,

$$\phi_1 = \sum_{\mathbf{k},s_3=-1,0,1} \left[\frac{\cosh(k(z+H))}{\cosh(kH)} \Phi_{1,\mathbf{k}}^{s_3}(t) + \frac{\sinh(k(z+H))}{\cosh(kH)} \Phi_{1,\mathbf{k}}^{si,s_3}(t) \right] \mathrm{e}^{\mathrm{i}\mathbf{k}.\mathbf{x}}. \tag{7.18}$$

Bottom condition

Substitution of (7.18) in the bottom boundary condition (7.16) yields

$$\frac{k}{\cosh(kH)} \Phi_{1,\mathbf{k}}^{si,s}(t) = -\sum_{\mathbf{k}'} \frac{\mathbf{k}' \cdot \mathbf{k}}{\cosh(k'H)} \Phi_{1,\mathbf{k}'}^{s} G_{\mathbf{k}-\mathbf{k}'} \mathrm{e}^{\mathrm{i}[(\mathbf{k}-\mathbf{k}')\cdot\mathbf{U}-s\sigma']t}, \tag{7.19}$$

for $s = \pm 1$. The amplitude of the $s_3 = 0$ term forced by the $\partial h/\partial t$ term in (7.16) is given by

$$\Phi_{1,\mathbf{k}}^{si,0}(t) = i\mathbf{k} \cdot \mathbf{U} \frac{\cosh(kH)}{k} G_{\mathbf{k}} \mathrm{e}^{\mathrm{i}\mathbf{k}.\mathbf{U}t}. \tag{7.20}$$

Surface boundary condition

Replacing now (7.18) in the surface boundary condition (7.17), yields an equation for $\Phi_{1,\mathbf{k}}^{s_3}$,

$$\left(\frac{d^2}{dt^2} + \sigma^2 \right) \Phi_{1,\mathbf{k}}^{s}(t) = \sum_{\mathbf{k}'} M^s(\mathbf{k},\mathbf{k}') \Phi_{1,\mathbf{k}'} G_{\mathbf{k}-\mathbf{k}'} \mathrm{e}^{\mathrm{i}[(\mathbf{k}-\mathbf{k}')\cdot\mathbf{U}-s\sigma']t}, \tag{7.21}$$

for $s = \pm 1$, with

$$M^s(\mathbf{k},\mathbf{k}') = \left[gk - \left[(\mathbf{k}-\mathbf{k}') . \mathbf{U} - s\sigma' \right]^2 \tanh(kH) \right] \frac{\mathbf{k}' \cdot \mathbf{k}}{k} \frac{\cosh(kH)}{\cosh(k'H)}. \tag{7.22}$$

For the $s_3 = 0$ component we have,

$$\left(\frac{d^2}{dt^2} + \sigma^2 \right) \Phi_{1,\mathbf{k}}^{0}(t) = C(\mathbf{k}) G_{\mathbf{k}} \mathrm{e}^{\mathrm{i}\mathbf{k}\mathbf{U}t} \tag{7.23}$$

with

$$C(\mathbf{k}) = \mathrm{i}\mathbf{k} \cdot \mathbf{U} \left[\frac{(\mathbf{k} \cdot \mathbf{U})^2}{k} \sinh(kH) - g\cosh(kH) \right]. \tag{7.24}$$

The free wave amplitude $\Phi_{1,\mathbf{k}}^{s}$ is forced by the harmonic oscillator equation (7.21). The resolution of this equation (see Appendix A for a definition of f_1) leads to

$$\Phi_{1,\mathbf{k}}^{s}(t) = \sum_{\mathbf{k}'} M^s(\mathbf{k},\mathbf{k}') \Phi_{0,\mathbf{k}'}^{s} G_{\mathbf{k}-\mathbf{k}'} f_1(\sigma, \mathbf{l}.\mathbf{U} - s\sigma'), \tag{7.25}$$

and

$$\Phi_{1,\mathbf{k}}^{0}(t) = C(\mathbf{k}) G_{\mathbf{k}} f_1(\sigma, \mathbf{k}\mathbf{U}). \tag{7.26}$$

The components of amplitude $\Phi^0_{1,\mathbf{k}}$ and $\Phi^{si,0}_{1,\mathbf{k}}$ corresponds to stationary waves such as generated by the bottom topography in rivers (e.g. Fredsøe, 1974). These components do not give rise to resonant interaction except at the critical Froude number, when the current is equal to the phase speed of the waves. This solution is identical to equation (2.9) in Kirby (1988) for monochromatic waves. The second term gives rise to scattered waves and reduces to the form given by AH when U goes to zero.

First order energy

The lowest order perturbation of the wave energy by scattering involves ϕ_1 and because it is a quadratic term it is found in the first order covariance

$$F^{\Phi}_{1,0,\mathbf{k}} + F^{\Phi}_{0,1,\mathbf{k}} = 4\mathrm{Re}\left(\langle \Phi^{+}_{0,\mathbf{k}} \Phi^{-}_{1,-\mathbf{k}} \rangle\right), \tag{7.27}$$

with Re denoting the real part. Including only the non-bounded terms, we get

$$F^{\Phi}_{1,0,\mathbf{k}} + F^{\Phi}_{0,1,\mathbf{k}} = 4\mathrm{Re}\left(\sum_{\mathbf{k}'} M^{+}(\mathbf{k},\mathbf{k}') \langle \Phi^{+}_{0,\mathbf{k}'} \Phi^{-}_{0,-\mathbf{k}} G_{\mathbf{k}-\mathbf{k}'} \rangle f_1(\sigma, \mathbf{l}.\mathbf{U} - \sigma') \mathrm{e}^{\mathrm{i}\sigma t}\right). \tag{7.28}$$

Although this term was assumed to be zero in AH, it is non zero for sinusoidal bottoms and becomes significant at resonance due to the function f_1. At this order, another term is needed to balance this energy transfer. In uniform conditions, the time evolution of the wave field requires that the non-stationarity must come into play so that $\alpha \approx \eta$, the non-stationary term is given by AH (appendix D),

$$\frac{\partial\left[N^{\mathrm{ns}}_{1,0}(\boldsymbol{k}) + N^{\mathrm{ns}}_{0,1}(\boldsymbol{k})\right]}{\partial t} = -\frac{\partial N_0(\boldsymbol{k})}{\partial t}. \tag{7.29}$$

In order to simplify the discussion, we shall briefly assume that there is no current and that the waves are unidirectional. In that case, $\mathbf{k}' = -\mathbf{k}$ and $M(\mathbf{k},\mathbf{k}') = gk^2/\cosh^2(kH)$. Replacing (7.28) in (7.11) and combining it with (7.29) yields the action balance

$$\frac{\partial N_{0,\mathbf{k}}}{\partial t} = \frac{\partial}{\partial t}\left[\frac{k}{\sigma}\tanh(kH)\left(F^{\Phi}_{1,0,\mathbf{k}} + F^{\Phi}_{0,1,\mathbf{k}}\right)\right] = \mathrm{Im}\left(\frac{4k\sigma^2}{g^2\sinh(2kH)}\langle \Phi^{+}_{0,\mathbf{k}} \Phi^{-}_{0,\mathbf{k}} G_{-2k} \rangle\right), \tag{7.30}$$

with Im denoting the imaginary part.

For a real bottom (e.g. random or consisting of a finite series of sinusoidal bars), the evaluation of (7.28) is not simple. Indeed, for directionally spread random waves and with a current, using $N(\mathbf{k}) = N_0(\mathbf{k})\left[1 + O(\eta)\right]$ and taking the limit to continuous surface and bottom spectra yields

$$\frac{\partial N(\mathbf{k})}{\partial t} = S_1(\mathbf{k}) = \int_{-\infty}^{\infty}\int_{-\infty}^{\infty} \frac{4\mathbf{k}\cdot\mathbf{k}'}{2g\cosh(kH)\cosh(k'H)} \mathrm{Im}\left(Z(\mathbf{k},\mathbf{k}')\right)\mathrm{d}k'_x \mathrm{d}k'_y, \qquad (7.31)$$

The mixed surface bottom bispectrum is defined by

$$Z(\mathbf{k},\mathbf{k}') = \lim_{\Delta \boldsymbol{k}\rightarrow\infty} \langle \frac{\Phi^{+}_{1,\mathbf{k}}\Phi^{-}_{1,-\mathbf{k}'}G_{-k-k'}}{(\Delta \boldsymbol{k})^2}\rangle, \qquad (7.32)$$

with $\mathbf{k} = k(\cos\theta, \sin\theta)$ and $\mathbf{k}' = k(\cos\theta', \sin\theta')$. Z is identical to a classical bispectrum (e.g. Herbers *et al.* 2003) with one surface wave amplitude replaced by a bottom amplitude, and a similar expression is fond for a non-zero current. Since we have neglected non-linear effects the only waves that have the same absolute frequency interact. Thus the phase coupling of all other wave component pairs is random and the bispectrum is zero for $\sigma' \neq \sigma + \mathbf{l}\cdot\mathbf{U}$. The energy balance (7.31) is not closed, and requires the knowledge of the wave phases that are not available in a phase-averaged model. This contribution of the mixed bispectrum will thus be evaluated below to investigate in which cases it may be neglected or parameterized. It is expected that S_1 is generally negligible because MAHR have found a good agreement of the second order energy balance, neglecting S_1, with an exact numerical solution of Laplace's equation.

Second order energy

At the next order one of the contributions from the covariance of the velocity potential amplitudes is given by,

$$F^{\Phi}_{1,1,\mathbf{k}} = 2\langle \Phi^{+}_{1,\mathbf{k}}\Phi^{-}_{1,-\mathbf{k}}\rangle. \qquad (7.33)$$

Equation (7.25) yields

$$\frac{F^{\Phi}_{1,1,\mathbf{k}}}{\Delta\mathbf{k}} = 2\sum_{\mathbf{k}'}\left|M^{+}(\mathbf{k},\mathbf{k}')\right|^2 \frac{\langle\left|\Phi^{+}_{0,\mathbf{k}'}\right|^2\rangle}{\Delta\mathbf{k}'}\frac{\langle\left|G_{\mathbf{k}-\mathbf{k}'}G_{-\mathbf{k}+\mathbf{k}'}\right|^2\rangle}{\Delta\mathbf{k}}\left|f_1(\sigma,\mathbf{l}.\mathbf{U}-\sigma')\right|^2\Delta\mathbf{k}' \qquad (7.34)$$

One also has

$$\langle f_1(\sigma,\mathbf{l}.\mathbf{U}-\sigma')f_1(\sigma,-\mathbf{l}.\mathbf{U}+\sigma')\rangle = \frac{\pi t}{2\sigma^2}\delta\left[\sigma'-(\sigma+\mathbf{l}.\mathbf{U})\right]+O(1), \qquad (7.35)$$

where δ is the one-dimension Dirac distribution, infinite where the argument is zero. Taking the limit of (7.34) when $\Delta\mathbf{k}\rightarrow 0$ and changing variables from (k'_x, k'_y) to

(σ', θ') yields

$$F_{1,1}^{\Phi}(t, \mathbf{k}) = \frac{\pi t}{2\sigma^2} \int_{\theta'} \int_{\sigma'} \left| M^{+}(\mathbf{k}, \mathbf{k}') \right|^2 F_{1,1}^{\Phi}(\mathbf{k}') F^{B}(\mathbf{k}-\mathbf{k}') \frac{k'}{C_g'} \delta \left[\sigma' - (\sigma + \mathbf{l}.\mathbf{U})\right] d\sigma' \mathrm{d}\theta' + O(1), \tag{7.36}$$

Only the terms for which $\sigma' = \sigma + \mathbf{l}.\mathbf{U}$ contribute to the integral. Thus $M^s(\mathbf{k}, \mathbf{k}') = M(\mathbf{k}, \mathbf{k}')$, with

$$\begin{aligned} M(\mathbf{k}, \mathbf{k}') &= \left[gk - \sigma^2 \tanh(kH)\right] \frac{\mathbf{k}' \cdot \mathbf{k}}{k} \frac{\cosh(kH)}{\cosh(k'H)}, \\ &= \frac{g\mathbf{k}.\mathbf{k}'}{\cosh(kH)\cosh(k'H)}. \end{aligned} \tag{7.37}$$

Using the relation between velocity potential and action given by (7.11), and evaluating the integral over σ', one obtains

$$N_{1,1}(t, \mathbf{k}) = \frac{\pi t}{2} \int_{\theta'} M^2(\mathbf{k}, \mathbf{k}') \frac{N_{0,0}(\mathbf{k}')}{\sigma\sigma'} F^{B}(\mathbf{k} - \mathbf{k}') \frac{k'}{C_g'} d\theta' + O(1). \tag{7.38}$$

7.2.4 Second order solution

Because we have computed one second order energy term, we now have to compute all other second order terms in (7.12) to obtain the solvability condition. This requires solving for the second order potential ϕ_2, that is a solution of

$$\nabla^2 \phi_2 + \frac{\partial^2 \phi_2}{\partial z^2} = 0 \qquad \text{for} \qquad -H \le z \le 0, \tag{7.39}$$

$$\frac{\partial \phi_2}{\partial z} = -h \frac{\partial^2 \phi_1}{\partial z^2} - \frac{h^2}{2} \frac{\partial^3 \phi_0}{\partial z^3} + \nabla \phi_1 \cdot \nabla h + \nabla \left(h \frac{\partial \phi_0}{\partial z}\right) \cdot \nabla h \qquad \text{at} \qquad z = -H, \tag{7.40}$$

that simplifies because odd vertical derivatives of ϕ_0 are zero at $z = -H$,

$$\frac{\partial \phi_2}{\partial z} = -h \frac{\partial^2 \phi_1}{\partial z^2} + \nabla \phi_1 \cdot \nabla h \qquad \text{at} \qquad z = -H, \tag{7.41}$$

and

$$\frac{\partial^2 \phi_2}{\partial t^2} + g \frac{\partial \phi_2}{\partial z} = \mathrm{i} \sum_{\boldsymbol{k}, s} 2s\sigma \frac{\partial \Phi_{0,\mathbf{k}}^{s}}{\partial t} \mathrm{e}^{\mathrm{i}(\boldsymbol{k} \cdot \boldsymbol{x} - s\omega t)} + NL_3 \qquad \text{at} \qquad z = 0. \tag{7.42}$$

The solution ϕ_2 is given by the following form,

$$\phi_2 = \phi_2^{\mathrm{ns}} + \sum_{\mathbf{k}, s_3 = -1,0,1} \left[\frac{\cosh(k(z+H))}{\cosh(kH)} \Phi_{2,\mathbf{k}}^{s_3}(t) + \frac{\sinh(k(z+H))}{\cosh(kH)} \Phi_{2,\mathbf{k}}^{si,s_3}(t) \right] \mathrm{e}^{\mathrm{i}\mathbf{k}.\mathbf{x}}. \tag{7.43}$$

The non-stationarity term ϕ_2^{ns} is defined as the solution of the second order equations forced by only the first term on the right-hand side of (7.41) and is given by AH. Following the method used at first order, substitution of (7.43) in the bottom boundary condition (7.41) leads to, for $s = \pm 1$,

$$\Phi^{si,s}_{2,\mathbf{k}}(t) = -\sum_{\mathbf{k}'} \frac{\mathbf{k}'\cdot\mathbf{k}}{k}\frac{\cosh(kH)}{\cosh(k'H)}\Phi^{s}_{1,\mathbf{k}'}(t)G_{\mathbf{k}-\mathbf{k}'}\mathrm{e}^{\mathrm{i}\mathbf{l}\cdot\mathbf{U}t}. \tag{7.44}$$

After calculations detailed in Appendix B (see Magne 2005 for further details), ϕ_2 yields the following contribution to the wave action,

$$N_{2,0}(\mathbf{k}) + N_{0,2}(\mathbf{k}) = -\frac{\pi t}{4\sigma}\int_0^{2\pi} M^2(\mathbf{k},\mathbf{k}')F^B(\mathbf{k}-\mathbf{k}')\frac{N_0(\mathbf{k})}{\sigma\sigma'}\frac{k'}{C_g}\frac{C_g+\mathbf{k}.\mathbf{U}}{C_g'+\mathbf{k}'.\mathbf{U}}\mathrm{d}\theta' + O(1), \tag{7.45}$$

in which $\sigma' = \sigma - \mathbf{l}.\mathbf{U}$, $\sigma'^2 = gk'\tanh(kH)$ and $C_g' = \sigma'(1/2 + k'H/\sinh(2k'H))/k'$.

7.2.5 Action and momentum balances

The solvability condition for the spectral wave action at second order imposes that all secular terms cancel. Neglecting the first order energy contribution S_1 given by (7.31), and using $N(\mathbf{k}) = N_0(\mathbf{k})\left[1 + O(\eta)\right]$ one has,

$$\frac{\mathrm{d}N(\mathbf{k})}{\mathrm{d}t} = S_{\mathrm{bscat}}(\mathbf{k}), \tag{7.46}$$

with the spectral action source term,

$$S_{\mathrm{bscat}}(\mathbf{k}) = \frac{\pi}{2}\int_{\theta'}\frac{M^2(\mathbf{k},\mathbf{k}')}{\sigma\sigma'}F^B(\mathbf{k}-\mathbf{k}')\left[N(\mathbf{k}')\frac{k'}{C_g'} - N(\mathbf{k})\frac{k'^2\left(kC_g+\mathbf{k}.\mathbf{U}\right)}{kC_g\left(k'C_g'+\mathbf{k}'.\mathbf{U}\right)}\right]\mathrm{d}\theta', \tag{7.47}$$

where $\sigma' = \sigma + \mathbf{l}\cdot\mathbf{U}$ and $\mathbf{k} = \mathbf{k}' + \mathbf{l}$. This interaction rule was already given by Kirby (1988). The only waves that can interact share the same absolute frequency $\omega = \sigma + \mathbf{k}\cdot\mathbf{U} = \sigma' + \mathbf{k}'\cdot\mathbf{U}$. For a given $\mathbf{k}$ and without current, resonant wavenumbers are described by geometric properties, the resonant $\mathbf{k}'$ and $\mathbf{l}$ lie on circles (see AH). The current slightly modifies this geometric property. For $U << C_g$ the circles become ellipses (see Appendix C).

For a given value of ω, one may obtain the source term integrated over all directions,

$$S_{\mathrm{bscat}}(\omega) \quad = \quad \int_\theta kS_{\mathrm{bscat}}(\mathbf{k})\frac{\partial k}{\partial\omega}\mathrm{d}\theta \tag{7.48}$$

$$= \int_{\theta}\int_{\theta'} \frac{\pi}{2}\frac{M^2(\mathbf{k},\mathbf{k}')}{\sigma\sigma'}F^B(\mathbf{k}-\mathbf{k}')\left[\frac{k'k}{C_g'}\frac{\partial k}{\partial \omega}N(\mathbf{k}') - \frac{k'k}{C_g}\frac{\partial k'}{\partial \omega}N(\mathbf{k})\right]d\theta' \mathrm{d}\theta.$$

This expression is fully symmetric and is thus unchanged when θ and θ' are exchanged. Thus $S_{\mathrm{bscat}}(\omega)$ is a substraction of two equal terms, so that for any bottom and wave spectra $S_{\mathrm{bscat}}(\omega) = 0$. In other words, the 'source term' is rather an 'exchange term', and conserves the wave action at each absolute frequency. This conservation is consistent with the general wave action conservation theorem proved by Andrews & McIntyre (1978), which states that there is no flux of action through an unperturbed boundary (here the bottom).

S_{bscat} may be re-written in a form close to that in AH,

$$S_{\mathrm{bscat}}(\mathbf{k}) = \int_{\theta'} K(k,k',H)\cos^2(\theta-\theta')F^B(\mathbf{k}-\mathbf{k}')\left[N(\mathbf{k}') - N(\mathbf{k})\frac{k'C_g'\left(kC_g + \mathbf{k}.\mathbf{U}\right)}{kC_g\left(k'C_g' + \mathbf{k}'.\mathbf{U}\right)}\right]d\theta', \tag{7.49}$$

with

$$K(k,k',H) = \frac{4\pi\sigma k k'^3}{\sinh(2kH)[2k'H + \sinh(2k'H)]}. \tag{7.50}$$

Finally, we may also write the evolution equation for the wave pseudo-momentum $\mathbf{M}^w = \rho_w g \int \boldsymbol{k}N(\boldsymbol{k})\mathrm{d}\boldsymbol{k}$ (see Andrews & McIntyre 1978b), where ρ_w is the density of sea water. For slow medium and wave field variations, that do not interfere with the scattering process, except by probably reducing the surface-bottom bispectrum Z, one has an extension of the equation of Phillips (1977)

$$\frac{\partial M_\alpha^w}{\partial t} + \frac{\partial}{\partial x_\beta}\left[(U_\beta + C_{g\beta})M_\alpha^w\right] = T_\alpha^{\mathrm{bscat}} - M_\beta^w\frac{\partial U_\beta}{\partial x_\alpha} - \frac{M_\alpha^w}{k_\alpha}\frac{k\sigma}{\sinh 2kD}\frac{\partial D}{\partial x_\alpha}, \tag{7.51}$$

with the dummy indices α and β denoting dummy horizontal components, and the scattering stress vector,

$$\mathrm{T}^{\mathrm{bscat}} = \rho_w g \int \boldsymbol{k} S_{\mathrm{bscat}}\mathrm{d}\mathbf{k}. \tag{7.52}$$

This stress has dimensions of force per unit length and corresponds to the force necessary to compensate for the divergence of the wave pseudo-momentum flux. Based on the results of Longuet-Higgins (1967) and Hara & Mei (1987) this force does not contribute to the mean flow equilibrium with a balance of the radiation stresses divergence by long waves (or wave set-up in stationary conditions) contrary to the initial proposition of Mei (1985). This force is thus provided by a mean pressure on the bottom that must arise from the pressure under partial standing waves locked in phase with the bottom undulations.

7.3 Wave scattering in two dimensions

Before considering the full complexity of the 3D wave-bottom scattering in presence of current, we first examine the behavior of the source term in the case of 2D sinusoidal seabeds. MAHR have investigated the applicability limits of the source term with $U = 0$, using 2D test cases. They showed that for small bottom amplitudes the source term yields accurate reflection estimates even for localized scatterers. It is thus expected that this also holds for $U \neq 0$, and that the present theory should conform to Kirby's (1988) theory in the limit of small reflection coefficients.

7.3.1 Wave evolution equation in 2D

We consider here a steady wave field in two dimension with incident and reflected waves propagating along the x-axis. We shall consider in particular the case of m sinusoidal bars of amplitude b and height $2b$, defined by,

$$\begin{aligned} h(x) &= b \sin(m l_0 x) \quad \text{for} \quad 0 < x < L \\ h(x) &= 0 \quad \text{otherwise.} \end{aligned} \tag{7.53}$$

This form is identical to that of the bottom profile chosen by Kirby (1988) but differs, for $0 < x < L$, by a $\pi/2$ phase shift from the bottom profile chosen by Mei (1985). The bottom spectrum is thus

$$F^B(l_x, l_y) = F^{B2D}(l_x)\delta(l_y), \tag{7.54}$$

For this particular bottom

$$F^{B2D}(l) = \left(\frac{1}{2\pi}\int_{-\infty}^{\infty} h(x)\mathrm{e}^{-\mathrm{i}lx}\mathrm{d}x\right)^2 = \frac{2b^2 l_0^2}{\pi L}\frac{\sin^2(lL/2)}{(l_0^2 - l^2)^2}, \tag{7.55}$$

with

$$F^{B2D}(l_0) = \frac{nb^2}{4l_0} = \frac{b^2 L}{8\pi}. \tag{7.56}$$

Please note that this is a double-sided spectrum, with only half of the bottom variance contained in the range $l > 0$. For a generic bottom, for which $h(x)$ does not go to zero at infinity, the spectrum is obtained using standard spectral analysis method, for example, from the Fourier transform of the bottom auto-covariance function (see MAHR).

First, replacing (7.54) in (7.46) removes the angular integral of the source term.

Taking $\mathbf{k} = (k, 0)$, we have $l_y = -k'_y$, and

$$S_{\mathrm{bscat}}\left(\mathbf{k}, x\right) = K(k', k, H) \frac{F^{B2D}(\mathbf{k} - \mathbf{k}')}{k'} \left[N(\mathbf{k}') - N(\mathbf{k}) \frac{k' C'_g}{k C_g} \frac{k C_g + \mathbf{k}.\mathbf{U}}{k' C'_g + \mathbf{k}'.\mathbf{U}} \right]. \quad (7.57)$$

Second, assuming now that waves propagate only along the x-axis, the wave spectral densities are of the form

$$N(k_x, k_y) = N^{2D}(k_x) \delta(k_y). \quad (7.58)$$

Integrating over k_y removes the singularities on k_y, and assuming a steady state one obtains,

$$\left[\frac{k_x}{k} C_g + U_x \right] \frac{\partial N}{\partial x} \left(k_x, x\right) = S_{\mathrm{bscat2D}}\left(k_x, x\right), \quad (7.59)$$

with

$$S_{\mathrm{bscat2D}}\left(k_x, x\right) = K(k', k, H) \frac{F^{B2D}(\mathbf{k} - \mathbf{k}')}{k'} \left[N(k'_x, x) - N(k_x, x) \frac{k' C'_g}{k C_g} \frac{k C_g + \mathbf{k}.\mathbf{U}}{k' C'_g + \mathbf{k}'.\mathbf{U}} \right]. \quad (7.60)$$

Finally, for monochromatic waves the incident wave spectrum is $N(k, x) = N(x)\delta(k - k_0)$ and the reflected wave spectrum is $N(k', x) = N'(x)\delta(k' - k'_0)$. The resulting evolution equation is, omitting the 0 subscripts on k and k',

$$\begin{aligned} \left[\frac{k_x}{k} C_g + U_x \right] \quad & \frac{\partial N}{\partial x} \\ & = K(k', k, H) \frac{F^{B2D}(\mathbf{k} - \mathbf{k}')}{k'} \left[N' \frac{k}{k'} \frac{k' C'_g + \mathbf{k}'.\mathbf{U}}{k C_g + \mathbf{k}.\mathbf{U}} - N \frac{k' C'_g}{k C_g} \frac{k C_g + \mathbf{k}.\mathbf{U}}{k' C'_g + \mathbf{k}'.\mathbf{U}} \right], \end{aligned} \quad (7.61)$$

with a similar equation for N', exchanging C_g and C'_g, and k' and k, from which it is easy to verify that the total action is conserved.

For a uniform mean depth H and bottom spectrum F^B, as considered here, the stationary evolution equation only couples two wave components $N(k)$ and $N(k')$. We thus have a linear system of two differential equations, that may be written in matrix form for any $k > 0$,

$$\frac{\mathrm{d}}{\mathrm{d}x} \begin{pmatrix} N(k) \\ N(k') \end{pmatrix} = Q \begin{pmatrix} N(k) \\ N(k') \end{pmatrix}, \quad (7.62)$$

The general solution is thus

$$\begin{pmatrix} N(k,x) \\ N(k',x) \end{pmatrix} = \mathrm{e}^{Qx} \begin{pmatrix} N(k,0) \\ N(k',0) \end{pmatrix}, \tag{7.63}$$

and the reflection coefficient for the wave action is found using the boundary condition expressing the absence of incoming waves from beyond the bars, $N(k',L)=0$, giving,

$$R_N = \frac{N(k',0)}{N(k,0)} = -\left(\mathrm{e}^{Qx}\right)_{2,1} / \left(\mathrm{e}^{Qx}\right)_{2,2}. \tag{7.64}$$

A reflection coefficient for the modulus of the wave amplitude predicted by the source term is thus,

$$R_S = \left[\frac{\sigma' N(-k',0)}{\sigma N(k,0)}\right]^{1/2} = -\left\{\sigma' \left(\mathrm{e}^{Qx}\right)_{2,1} / \left[\sigma \left(\mathrm{e}^{Qx}\right)_{2,2}\right]\right\}^{1/2} \tag{7.65}$$

7.3.2 Analytical solution for $U = 0$

If $U=0$ then $k'=-k$, and

$$q = -Q_{1,1} = Q_{1,2} = -Q_{2,1} = Q_{1,1} = K(k,H)\frac{F^B(2k)}{C_g k}, \tag{7.66}$$

with $Q_{i,j}$ the (i,j) component of Q. Q is not diagonalizable, which would allow a simple way of evaluating the matrix exponential e^{Q}. However $Q^2=0$ so that $\mathrm{e}^{Qx} = (\mathbf{Id}+Q)\,x$, where **Id** is the identity matrix. The solution is thus simply,

$$N(k,x) = N(k,0)\left[\frac{-q\,(x-L)+1}{1+qL}\right] \tag{7.67}$$

$$N(-k,x) = N(k,0)\left[\frac{-q\,(x-L)}{1+qL}\right]. \tag{7.68}$$

An example of spatial variation of the wave spectrum from $x=0$ to $x=L$ is shown in Figure 7.2, for $U=0$. The reflected wave energy (at $k<0$ in figure 7.2.a) compensates the loss of energy in the transmitted spectrum (at $k>0$ in figure 7.2.b).

At resonance, in the limit of small bar amplitudes (7.56) yields

$$R_S = (qL)^{1/2} + O(qL) = \frac{k^2 bL}{2kH + \sinh(2kH)} + O(qL) \tag{7.69}$$

which is identical to Mei's (1985) equation (3.21)–(3.22) for exact resonance, in the limit of $qL \ll 1$, and also converges to the result of Davies & Heathershaw (1984)

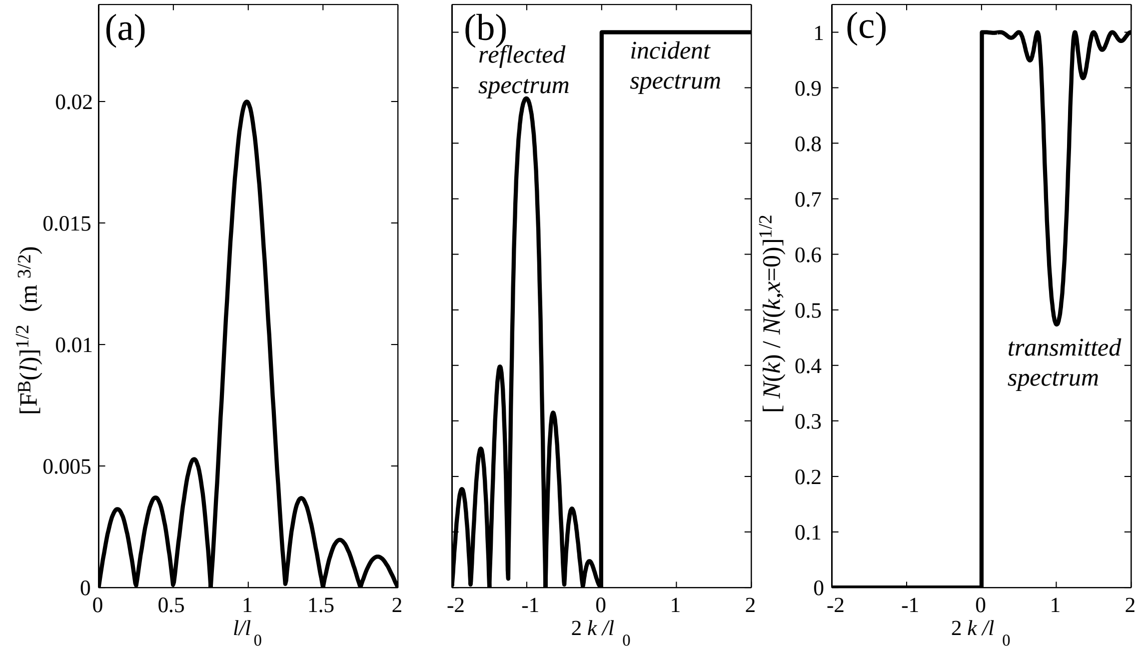

FIG. 7.2 – Bottom spectrum and evolution of a surface wave spectrum along a field of sinusoidal bars for $U = 0$, $b = 0.05$ m, $H = 0.156$ m, so that $b/H = 0.32$, and $l_0 = 2\pi$, $n = 4$, so that $L = 4\ m$ (bottom shown in figure 1). (a) square root of the bottom spectrum, (b) and (c) normalized square root wave spectrum upwave (at $x < 0$) and downwave (at $x > L$) of the bars, respectively. The incident spectrum ($k > 0$ at $x = 0$) is specified to be white (unform in wavenumbers).

for that same limit. For large bar amplitudes, our analytical solutions for a uniform bottom spectrum show that the reflection is significant if the bars occupy a length L longer than the localization length $1/q$. However, the reflection coefficient for the wave amplitude only increases with L as $[qL/(1+qL)]^{1/2}$, which is slower than the exponential asymptote given by Mei (1985) for sinusoidal bars, and that predicted by (Belzons *et al.* 1988) for a random bottom from the lowest-order theory. Our use of higher-order correction may be thought as the representation of multiple reflections that tend to increase the penetration length in the random medium.

A deeper understanding of this question is provided by the comparison of numerical estimations of the reflection coefficients for the wave amplitudes R. A benchmark estimation for linear waves is provided by the step-wise model of Rey (1995) using integral matching conditions for the free propagating waves and three evanescent modes at the step boundaries. This model is known to converge to the exact solution of Laplace's equation and the boundary conditions in the limite of an infinite number of steps and evanescent modes. Calculations are performed here with 70 steps. This number is chosen because a larger number of steps gives indistinguishable results in figure 7.3. An analytical expression R_{Mei} is given by Mei (1985). And R for the present second order theory is given by R_S in (7.65).

We further compare these estimates to the reflection coefficient $R_{S1,\mathrm{Mei}}$ that is deduced from the energy evolution given by Hara & Mei (1987) using the approximate solutions of Mei (1985, his equations 3.8–3.23). One may prefer to reformulate the energy evolution from the amplitude evolution equations of Kirby (1988) because he used a continuous water depth $h = \sin(ml_0)$, instead of Mei's $h = \cos(ml_0)$ and $h = 0$ for $x < 0$ or $x > L$, which is discontinuous at $x = 0$ and $x = L$[2]. Yet both Mei's and Kirby's equations lead to the same energy exchange between the incident and reflected components. Using Mei's (1985) notations, the amplitudes of the incident waves, reflected waves, and bottom undulations are $A = 2\sigma\Phi^{+}_{0,\mathbf{k}}/g$, $B = 2\sigma\Phi^{-}_{0,\mathbf{k}}/g$, and $D = -2\mathrm{i}G_{-2k}$, and the 'cut-off' frequency is

$$\Omega_0 = \frac{\sigma k D}{2\sinh(2kH)}. \tag{7.70}$$

The energy evolution of waves propagating over sinusoidal bars along the x-axis,

---

[2] Such a discontinuous bottom has a markedly different spectrum at low and high frequencies. The present theory, confirmed by calculations with Rey's (1995) numerical model that converges to the exact solution of Laplace's equation, yield very different reflection coefficients for waves much shorter and much longer than the resonant waves

towards $x > 0$ is given by Hara & Mei (1987) for the reflected wave energy is

$$\frac{\partial}{\partial t}\left(\frac{BB^\star}{2}\right) - C_g\frac{\partial}{\partial x}\left(\frac{BB^\star}{2}\right) = S_{1,\mathrm{Mei}} = \mathrm{Re}\left(\mathrm{i}\Omega_0 B^\star A\right), \tag{7.71}$$

where $B^\star$ denotes the complex conjugate of B. This is identical to (7.30) for a *monochromatic* bottom except that the imaginary part replaced by a real part.

Equation (7.71) yields a corresponding energy reflection coefficient, given by the fraction of energy lost by the incoming waves,

$$R_{E,S1\mathrm{Mei}} = -\frac{1}{C_g}\int_0^L S_{1,\mathrm{Mei}}(x)\mathrm{d}x. \tag{7.72}$$

Simple analytical expressions can be obtained at resonance, where Mei's (1985) eq. (3.20)–(3.21) give,

$$\frac{AB^\star}{A_0} = \frac{-\mathrm{i}\sinh\left(2\tau(1-x/L)\right)}{2\cosh^2\tau} \tag{7.73}$$

so that

$$R_{E,S1\mathrm{Mei}} = \frac{\cosh 2\tau - 1}{4\cosh^2\tau} = \frac{1}{2}\tanh^2\tau = \frac{1}{2}R^2_{\mathrm{Mei}}, \tag{7.74}$$

and

$$R_{S1,\mathrm{Mei}} = 2^{-1/2}R_{\mathrm{Mei}}. \tag{7.75}$$

It is not surprising that the energy transfer thus computed differs from the energy computed from the amplitude evolution equations. This is a typical of small perturbation methods, and was discussed by Hasselmann (1962), among others. Yet, it is remarkable that the ratio of the two is exactly one half. The transfer of energy given by $\mathrm{i}\Omega_0 B^\star A$ in (7.71) thus correspond to an amplitude reflection coefficient $R_{S1,\mathrm{Mei}}$ that is smaller by a factor $2^{-1/2}$, at resonance, compared to R_{Mei} (figure 3). This underprediction of the the reflexion of the energy by (7.74) also has consequences for the analysis and calculation of wave set-up due to wave group propagation over a reflecting bottom. Indeed, the estimation of the scattering stress (7.52), that contribute to the driving of long waves, was analyzed by Hara & Mei (1987) using (7.74), which is a factor 2 too small. This may explain in part their under-prediction of the observed water level in the long wave travelling with the incident wave group.

7.3.3 Effects of wave and bottom relative phases

At resonance and for $U = 0$, it can be seen that the product $\Phi^+_{0,\mathbf{k}}\Phi^-_{0,\mathbf{k}}G_{-2k}$ that arises in (7.30) is equal to $\mathrm{i}AB^\star D/8$, in the limit of a large number of bars. Based on Mei's (1985) approximate solution, this quantity is purely real so that its imaginary part is zero and the corresponding reflection coefficient R_{S1} is zero. For $U \neq 0$ this property remains as can be seen by replacing Mei's (1985) solution with Kirby's (1988). Further, away from resonance but for small values of the scattering strength parameter $\tau = (qL)^{1/2} = \Omega_0 L / C_g$, with Ω_0 defined by (7.70), the imaginary part of $\Phi^+_{0,\mathbf{k}} \Phi^-_{0,\mathbf{k}} G_{-2k}$ is an order $(qL)^{1/2}$ smaller than the real part and thus contributes a negligible amount to the reflexion.

7.3.4 Source term and deterministic results for sinusoidal bars

For large bar amplitudes, such as $b/H = 0.32$ (figure 3a), all theories with linearized bottom boundary conditions fail to capture the shift of the reflection pattern to lower wavenumbers. This effect was discussed by Rey (1992) and attributed to the non-linear nature of the dispersion relation and the rapid changes in water depth. However reflection coefficients are still relatively well estimated. For these large amplitudes Mei's (1985) approximate solution is found to be more accurate at resonance compared to the source term. As expected from MAHR, R_{Mei} and R_S become identical as b/H goes to zero (figure 7.3.b), which provides a verification that the first order term S_1 only accounts for a small fraction of the reflection, a fraction that goes to zero as h/H goes to zero. It is also found that for all bottom amplitudes but away from resonance, the source term expression provides a simple solution that is more accurate than Mei's (1985) approximate solutions (see the sidelobes in figure 3).

7.3.5 Effects of currents

The basic feature of the solutions with currents is the modification of the resonant condition from $k = k'$ and $l = 2k$ to $\sigma' = \sigma + lU$ and $l = k + k'$ (notations here assume that $\boldsymbol{k}$ is in the direction of the current and $\boldsymbol{k}'$ is opposite to the current). Yet, the introduction of the current makes the solution much more complex. It is striking that Kirby's (1988) solution involve a modified cut-off parameter $\Omega_c = \Omega_{0c} + \Omega_{1c}$ that would be analytically similar to our source term result except for the rather complicated Ω_{1c} term. At resonance, Kirby (1988) found that the transmission losses $1 - T$ differ from the case without current. In the long-wave limit this difference is a increase by a factor $\left(1 - Fr^2\right)^{-1}$ (his equation 5.29). However, the present theory predicts an increase by a factor $1 + Fr$. Thus both theories only agree in the limit $Fr \to 0$. To our knowledge there is unfortunately no simple numerical method to arrive at an independent solutions. Besides, observations of that effect require to test relatively large Froude numbers. Some first observations of the shift in resonant

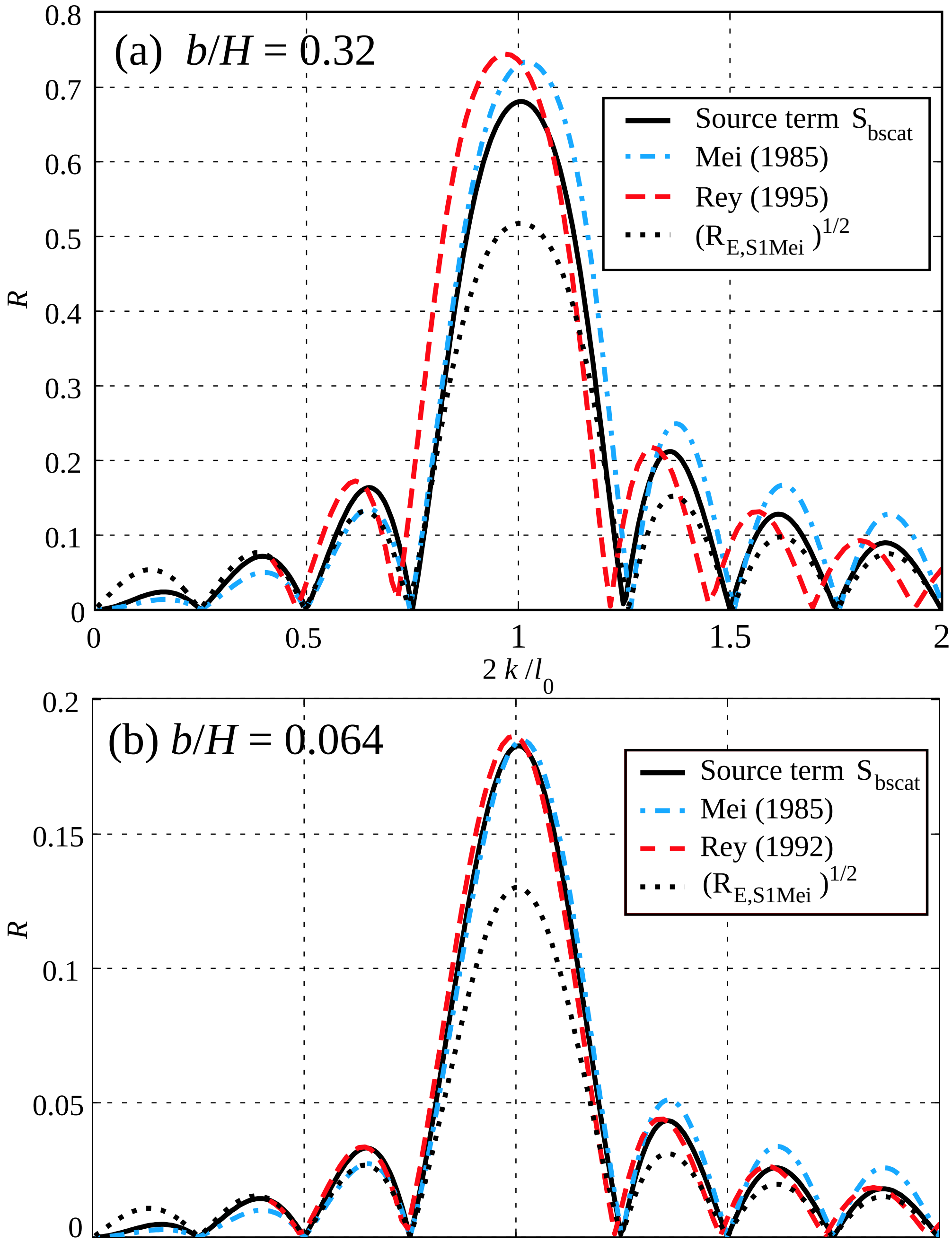

FIG. 7.3 – Reflection coefficients for the wave amplitudes for $U = 0$, $H = 0.156$ m, $l_0 = 2\pi$, $n = 4$. In (a) $b = 0.05$ so that $b/H = 0.32$, corresponding to one of the experiments of Davies & Heathershaw (1984), and in (b), $b = 0.01$, so that $b/H = 0.064$.

frequencies in the presence of currents were only performed at relatively low Froude numbers and are not accurate enough to test these predictions (Magne, Rey & Ardhuin manuscript submitted to Physics of Fluids).

We now compare reflection coefficients for monochromatic waves as obtained with the source term using (7.61) and with Kirby's (1988) analytical approximate solutions for near-resonant waves. An approximation to the reflection coefficient (7.65) corresponding to the solution of (7.61) is obtained with a fourth order Taylor expansion of the matrix exponential. For oceanographic conditions with a water depth of 20 m, a strong 2 m s^{-1} current corresponds to a Froude number of 0.17 only. For such a low value the difference in peak reflection for $b/H = 0.065$ is of 8% only between the two theories, while the reflection coefficient is largely increased due to the general conservation of the wave action flux. The reflection coefficient for the wave amplitude can thus be larger than 1 for currents following the incident waves because it is enhanced by the factor $\{\sigma(Cg+U)/\left[\sigma'(Cg'-U)\right]\}^{1/2}$ compared to the amplitude transmission losses. The overall increase in amplitude reflection for following waves amounts to about 60% for $Fr = 0.17$ for the laboratory sinusoidal bars of Davies & Heathershaw (1984) shown before (figure 4). The horizontal density of reflected wave energy is thus multiplied by a factor 2.5 in this case, for a Froude number of only 0.17.

Both theory agree reasonably well and we thus expect the source term to represent accurately the scattering of waves over bottom topographies in cases of uniform currents and with h/H of the order of 0.3 or less. The present method has the advantage of a large economy in computing power. This method is also well adapted for natural sea beds for which continuous bathymetric coverage is only available in restricted areas, and thus only the statistical properties of the bottom topography are accessible, assuming homogeneity.

7.4 Scattering with current on a realistic topography

7.4.1 Sandwaves in the North Sea

A real ocean topography, at least on the continental shelf, generally presents a continuous and broad bottom elevation spectrum. Given this bottom spectrum, simple solutions are available for uniform conditions as the scattering source term is a linear function of the directional spectrum at a given value of the absolute frequency ω (see AH for numerical methods). However, practical situations rather correspond

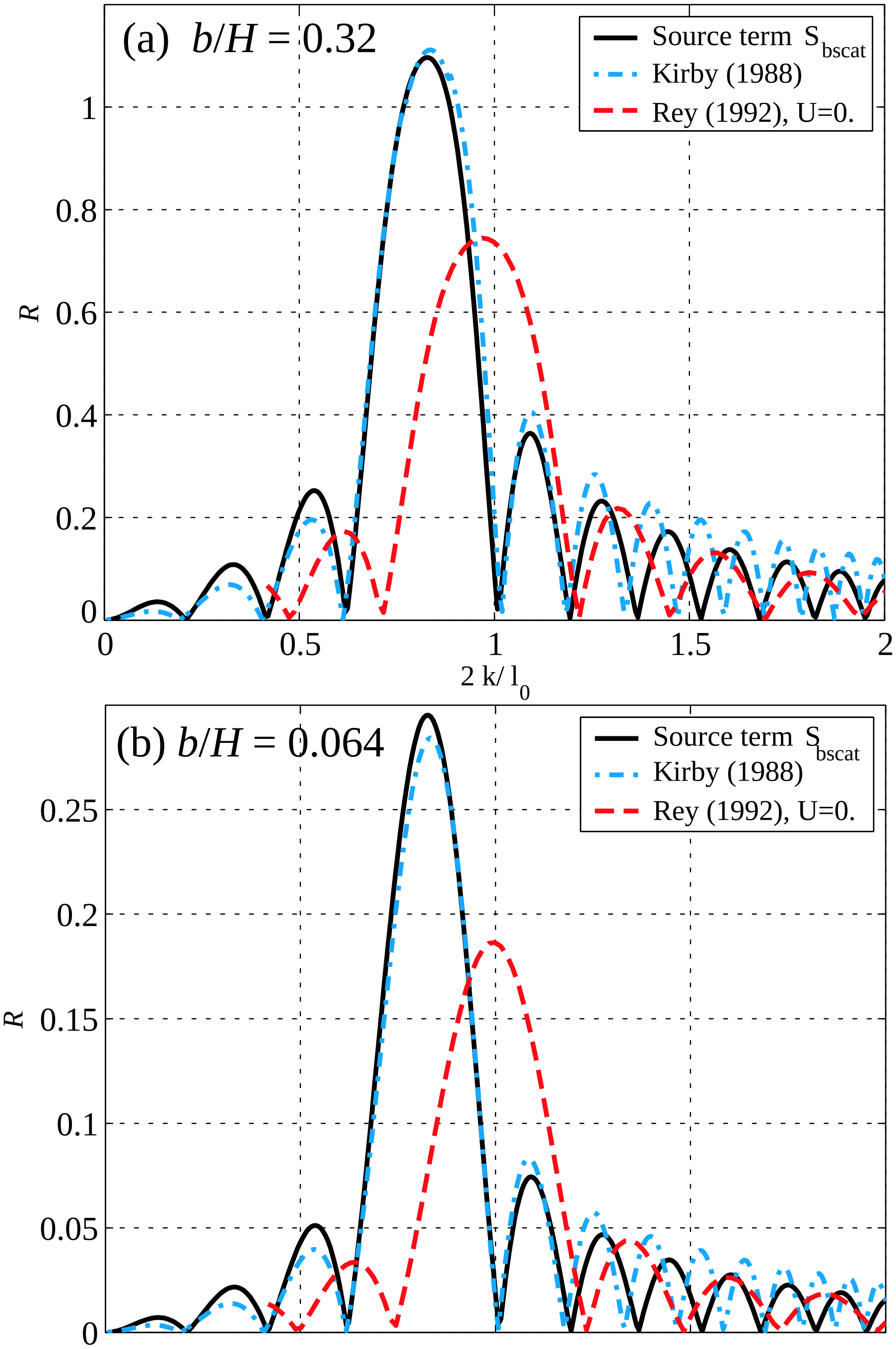

FIG. 7.4 – Amplitude reflection coefficients for monochromatic waves over sinusoidal bars for the same settings as in figure 3 with $U = 0.2$ m s^{-1}. For reference the reflection coefficient without current, as given by the exact model of Rey (1995), is also shown.

to quasi-stationary conditions with spatial gradients in at least one dimension. In this situation the simple solutions found above for 2D topography are not physical with a 3D bottom because the scattering along the transversal direction y tends to increase the wave energy propagating in that direction, and this energy will increase in time up to the point where it becomes as large as the incident wave energy, which can take a very long time. Therefore the source term is now introduced in a non-stationary wave model based on the wave action evolution equation (7.46) in which the time derivative on the left hand side is now a Lagrangian derivative following a wave packet in physical and spectral space. In practice the source term S_{bscat} was introduced in the version 2.22 of the wave model WAVEWATCH-III (Tolman 2002, see Magne 2005 for details on the implementation and more results with other wave-current configurations). The effects of a mean current on wave scattering are now examined using a real bathymetry spectrum that is estimated from a detailed bathymetric survey of an area located on the crest of a sand dune, in the southern North Sea (figure 7.5). In this region, tidal currents are known to generate a wide array of bedforms, from large scale tidal Banks to sand dunes and sand waves (e.g. Dyer & Huntley 1999, Hulscher & van den Brink 2001). Although sand dunes present a threat to navigation and are closely monitored (Idier *et al.* 2002), dunes are much larger than typical wind seas and swells wavelengths. In the surveyed area the shorter sandwaves present a peak wavelength of 250 m, and a variance of 3.1 m^2, which should lead to strong oblique scattering of waves with periods of 10 s and longer. The southern North Sea is also known for the attenuation of long swells, generated in the Norwegian Sea. This attenuation has been generally attributed to the dissipation of wave energy by bottom friction (Weber 1991).

The bottom spectrum of the area that we chose, like the spectra that were obtained by AH from the North Carolina shelf, roll off sharply at high wavenumbers, typically like l^{-4} for the two-dimensional spectrum. Here the maximum variance is found for bottom wavelengths of the order or larger than 250 m (figure 7.5). For a typical swell period of 10 s, this corresponds to 2 times the wavelength in 20 m depth, and thus a rather small scattering angle, 30° off from the incident direction. Swells propagating from a distant storm, with fixed absolute frequency $\omega = \sigma + \mathbf{k} \cdot \mathbf{U}$, should be reflected by bottom undulations with widely different variances as the current changes.

7.4.2 Scattering of waves normally incident on the sandwaves

To simplify the interpretation of the results, and the processing of the boundary conditions, a one dimensional (East/West) propagation grid is used for the

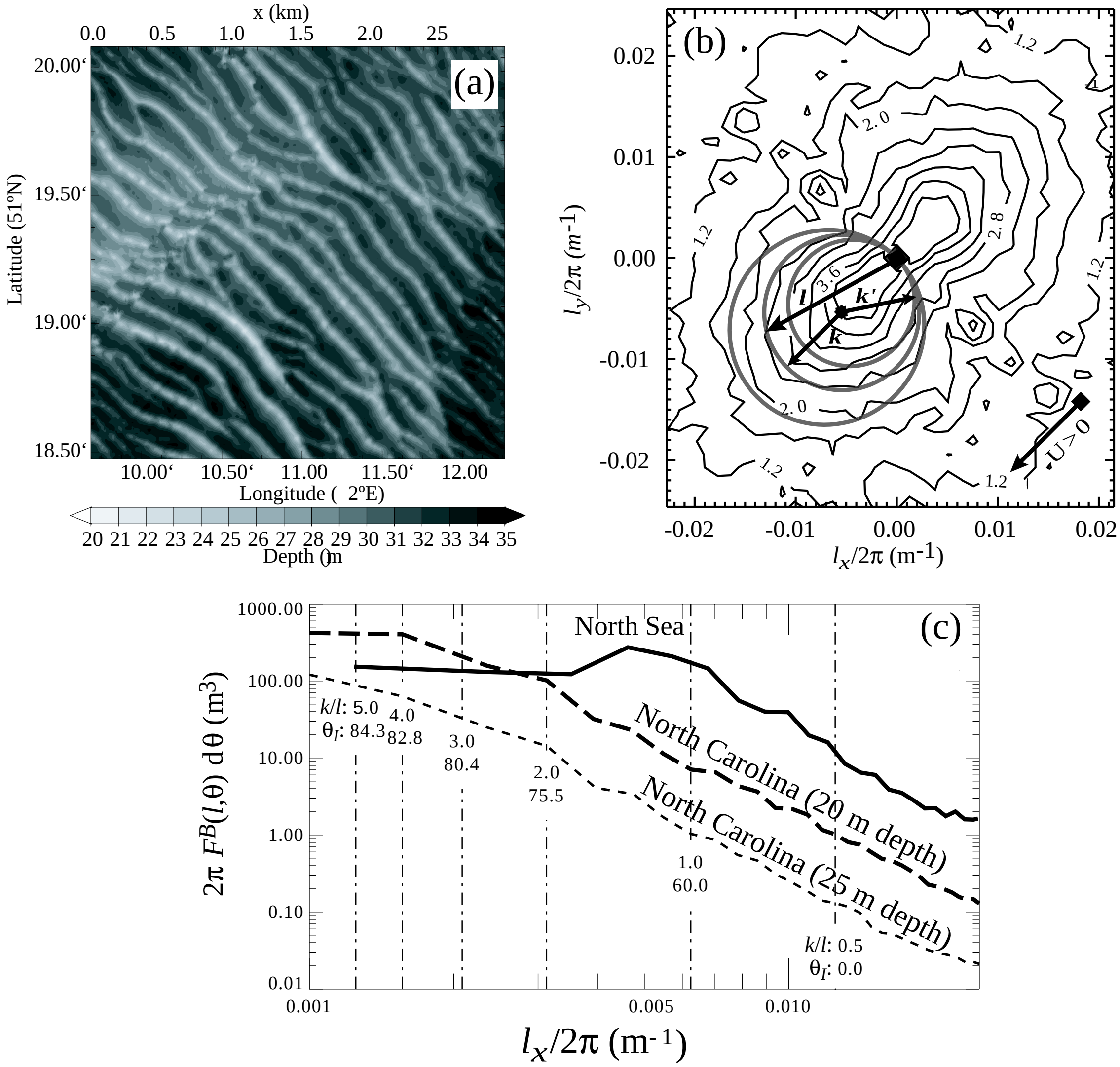

FIG. 7.5 – (a) high-resolution bathymetry of a sand wave field in the southern North Sea, and (b) corresponding bottom elevation spectrum with contour values representing $\log_1 0 \left(4\pi^2 F^B\right)$. The locus of the interacting bottom and surface wave components are indicated for a 12.5 s waves from the North-East in 25 m depth, with $U = 0$ (middle circle), $U = 2$ m s^{-1} (smaller ellipse), and $U = -2$ m s^{-1} (larger ellipse), U is positive from the North-East. (c) Direction-integrated bottom variance spectra from the North Carolina shelf and the southern North Sea. Vertical lines indicate k/l ratios and incident resonant incident directions θ_I in the case of sinusoidal bars, assuming an incident wave field of 12.5 s period in 25 m depth. For sinusoidal bars, the angle between incident and scattered waves is $180° - 2\theta_I$.

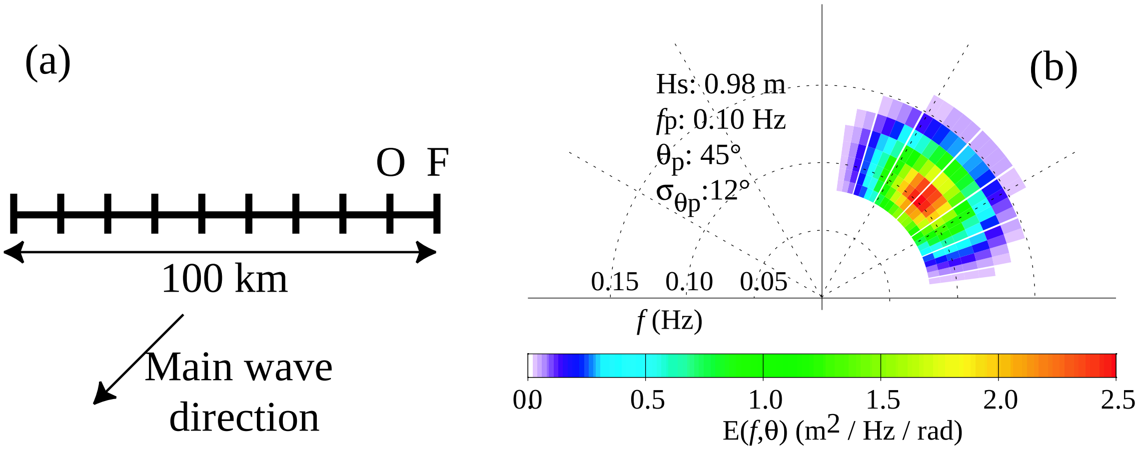

FIG. 7.6 – (a) Schematic of the model grid and (b) incident wave spectrum specified at point F. Model output is shown below for point O. Please note that waves are represented with their arrival direction (direction from, contrary to the standard wind sea convention).

computations, assuming that the wave field, still fully directional, is uniform in the North-South direction. The waves are propagated over a model grid 100 km long, with a mean depth of 20m, and a spatial grid step of 10 km (figure 7.6.a). As a result, scattering is probably stronger than in real conditions where the mean water depth is often larger than 20 m. The following results should still provide some understanding of the likely real effects.

A Gaussian incident surface wave spectrum is imposed, with a mean direction from the North-East, a narrow peak directional spread of 12°, and a peak frequency of 0.01Hz (figure 7.6.b). Bottom scattering is the only source term introduced in the present calculation. There is thus no transfer of wave action between frequencies. Still, the model was run with 25 frequencies ranging from 0.08 to 0.788 Hz which is a typical configuration. The source term is integrated with a time step of 120 s, and the advection in space uses a third order scheme with a time step of 120 s.

The scattering source term acts as a diffusion operator with a typical 3-lobe structure, negative at the peak of the wave spectrum and positive in directions of about 30° on both sides of the peak. This is identical, but with a larger magnitude, to the effect described by AH. In general the scattering effects are relatively stronger at the lowest frequencies, at least in the range of frequencies used here. For still lower frequencies the interaction coefficients decrease (see also AH) so that, on these spatial scales, very little scattering occurs for infra-gravity waves ($f < 0.05Hz$). In addition to this grazing-angle forward scattering the present case shows a significant back-scattering, in particular in the case of following currents.

For a wave frequency of 0.01Hz, the curves followed by the bottom resonant

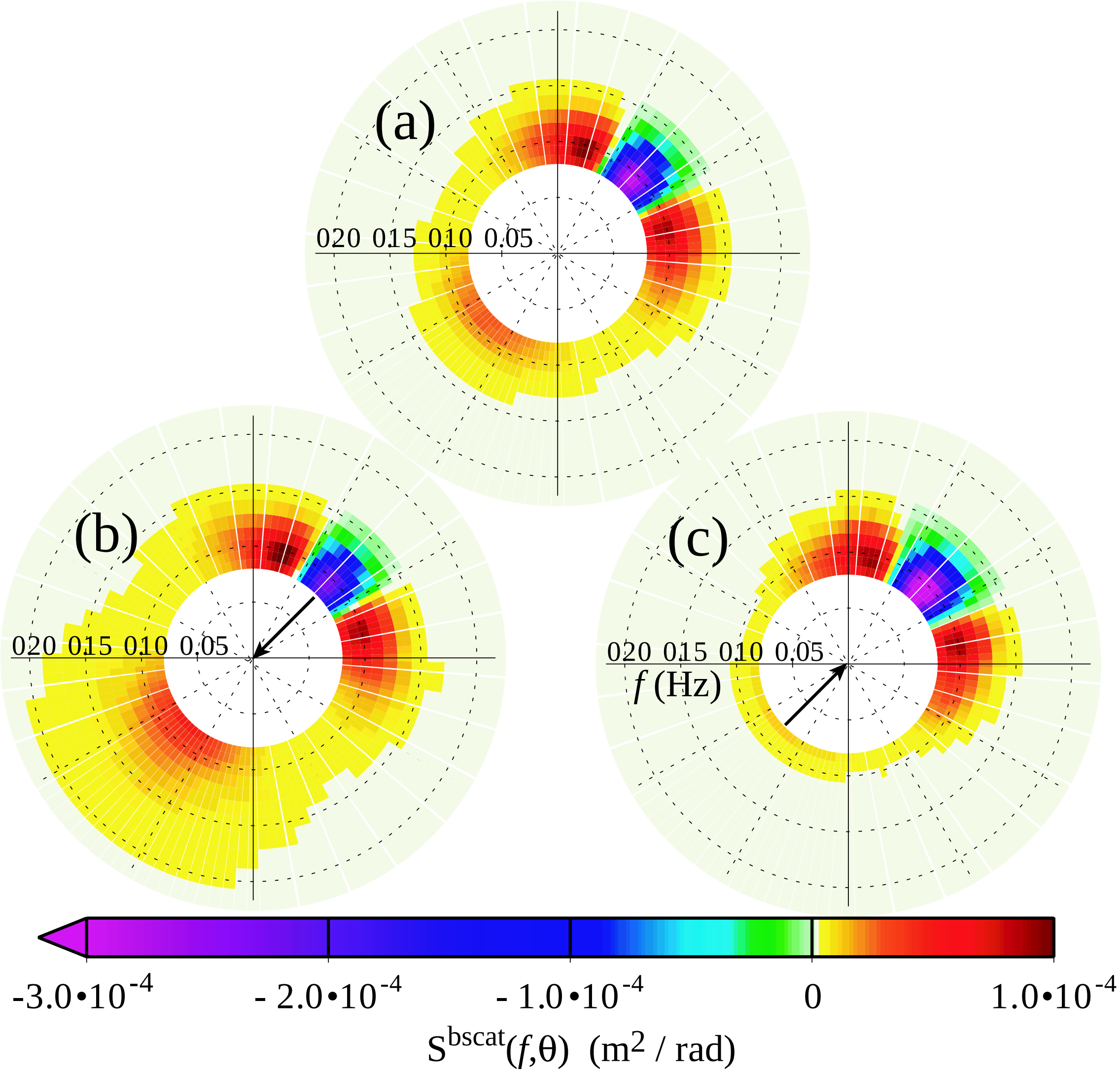

FIG. 7.7 – Computed source terms at the boundary forcing point F, (a) for $U = 0$, (b) for a following current $U = 2$ m s^{-1}, (c) for an opposing current $U = -2$ m s^{-1}.

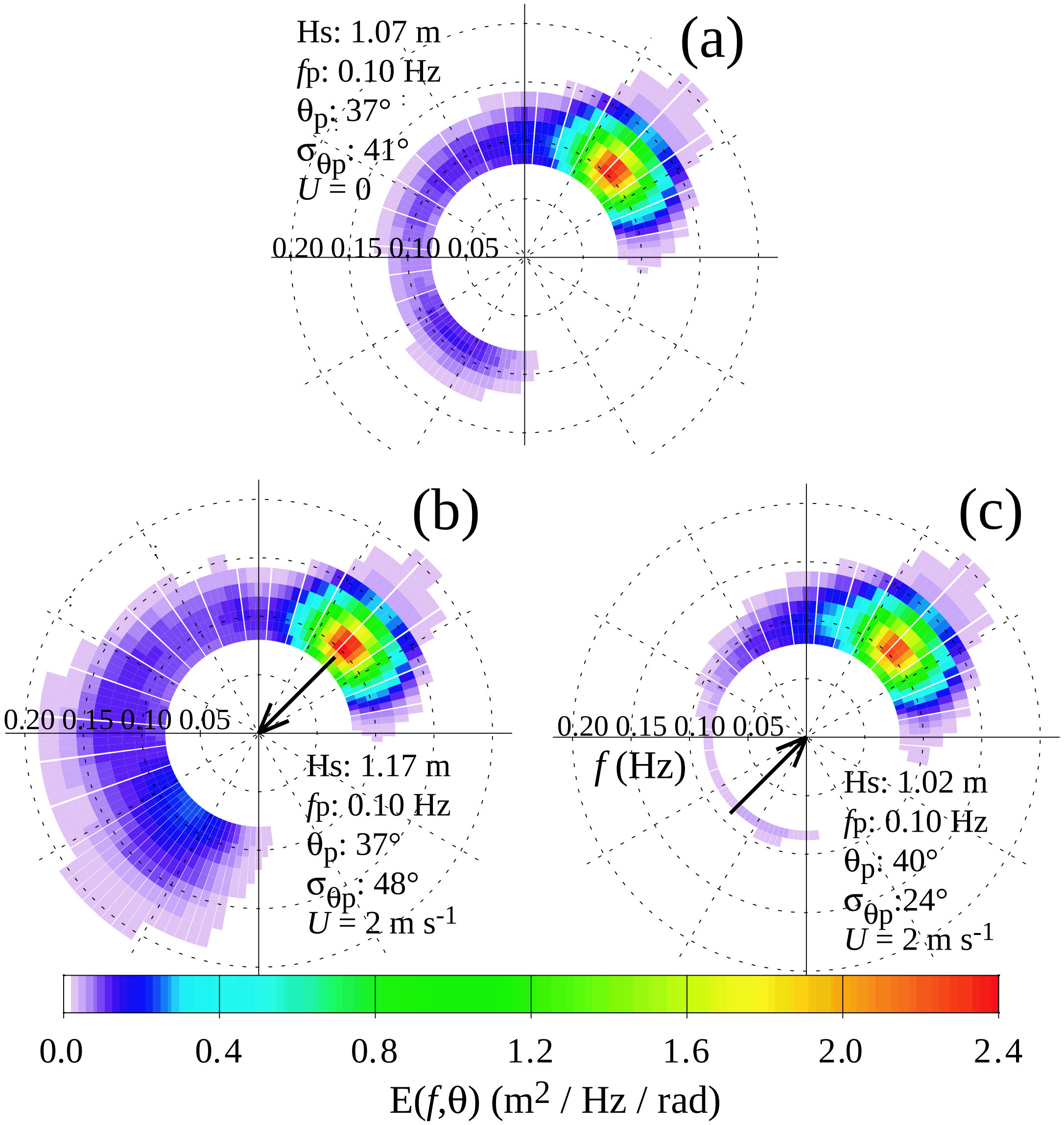

FIG. 7.8 – Computed wave spectra at point O, 10 km inside of the model domain (a) for $U = 0$, (b) for a following current $U = 2$ m s^{-1}, (c) for an opposing current $U = -2$ m s^{-1}.

wavenumbers are plotted over the contour plots of the seabed spectrum (figure 7.5 b). The wavenumbers $\mathbf{l}$ along these curves satisfy both the relations $\mathbf{k}' + \mathbf{l} = \mathbf{k}$ and $\sigma' = \sigma + \mathbf{l}.\mathbf{U}$. Without current the curve is exactly a circle which transforms to an ellipse for weak currents (Appendix C). The current shifts significantly the resonant configuration for the bottom and surface wavenumbers. A current opposed to the waves enlarges the ellipse towards higher wavenumbers, while a following current will lead to a 'sampling' of shorter wave numbers and longer bottom features. Since the bottom topography has the lowest variance at the largest wavenumbers, the scattering is strongest for following currents (figure 7.7). With our choice of parameters, there is about a factor 10 reduction in the bottom variance that causes backscatter as U is changed from 2 m s^{-1} to -2 m s^{-1}. Besides, as in the 2D case discussed above, the coupling coefficient $K(k', k, H)$ is increased in the case of a following current. Furthermore, a current opposed to the waves decreases the surface waves wavelength and favours resonant configuration such as $2k/l > 1$ corresponding to forward-scattering, so that the 3 lobes in the source term occupy a broader range of directions in the case of opposing currents.

The resulting wave spectra are further modified due to the conservation of the wave action flux that further enhances the resulting reflected wave energies, propagating more slowly with a velocity $U - C_g'$ for $U > 0$ (figure 7.8). Wave spectra are thus significantly broadened in directions, and that effect is most pronounced at the lowest frequencies. Without current or with following currents, spectra at the beginning of the model domain (figure 7.8) contain a large back-scattered energy, which increases the significant wave height and the directional spread on the up-wave side of the sandwave field. This effect should not be very sensitive to the directional spread of the incident wave field and should thus occur for a wide range of sea states. In contrast, it should be noted the initial spectral peak in figure (figure 7.8) is not much modified, because of the relatively short propagation distance from the forcing point (figure 7.6), but a significant broadening is predicted at the down-wave end of the model domain. That effect is small for relatively broad spectra (i.e. directional spreads $\sigma_{theta} > 30°$), as found by Ardhuin et al. (2003a) and Ardhuin and Herbers (2005). It was also found that this broadening of the main spectral peak is largest for waves propagating along the main sandwave crest directions (i.e. from the North-West in our case) due to the larger bottom variance at $\mathbf{l} = \boldsymbol{k} - \boldsymbol{k}'$ with $\boldsymbol{k} \simeq \boldsymbol{k}'$ (Magne 2005), with a significant modification of the mean direction.

Finally, without current, a wave height decrease along the grid is observed, indicating an attenuation due to wave-bottom scattering. In all cases a realistic bottom friction would likely induce a stronger decay, stronger than in the absence of scattering. Essentially the scattering increases the average time taken by wave energy to cross the domain, and bottom friction together with scattering would lead to a larger dissipation than friction alone because of that longer time (Ardhuin *et al.* 2003a,b).

7.4.3 Scattering of waves along the sandwaves crests

We now look at waves propagating along the sand wave crests. Again the resonant configuration of the bottom and surface wavenumber are overlaid on the contour plot of the bottom spectrum (Figure 7.9), for cases with and without current (the current vectors are identical to the previous case). Now that the current is perpendicular to main wave direction, the curve followed by the bottom wavenumber is shifted to the North-West or South-East depending on the current sign. Because most of the bottom variance lies along that axis, the different currents will favor forward-scattering to one side or the other of the main direction (the curves encounters large variances on one side or the other of the origin). On the contrary the current should not change too much the back-scattering because the variance is rather uniform at $l \approx 2k$ in this configuration. The initial North-West swell is shown in figure 7.10. Only the peak direction has changed compared to the South-West swell case, all other parameters of the simulations are unchanged. The corresponding scattering source terms are represented in figure 7.11abc, respectively without current, and a uniform current of 2m/s to the North-East or to the South-West. In the present case back-scattering is weak and the main effect of the source term is the diffusion around the peak direction, represented by a 3-lobe structure, negative at the peak direction and positive on the sides (figure 7.11). However, as expected from the interacting bottom components, the current introduces a marked asymmetry in the source term. When flowing to the North-East, the waves that propagate from the North are shortened by the current and thus interact less than in the opposite current, from the South-West. In that latter case the longer wavelengths from the North promote an interaction with bottom components that have a much larger variance. The opposite is true for waves from the West.

The resulting spectra after 6 hours of propagation are shown in figure 7.12 and 7.12abc, respectively at the beginning (the computation point just next to the boundary point) and at the end of the computational domain. The directional spread of the spectra at the beginning of the domain (Figure 7.12) shows considerable broadening, which thus occurs over a short distance (between the boundary and that point, namely 10 km). This initial rapid broadening is again consistent with the strong broadening of narrow spectral observed and modelled by Ardhuin et al. (2002b, 2003a), and negligible broadening of broader spectra. In a sense the directional wave spectrum relaxes to relatively broad spectrum, and this process is

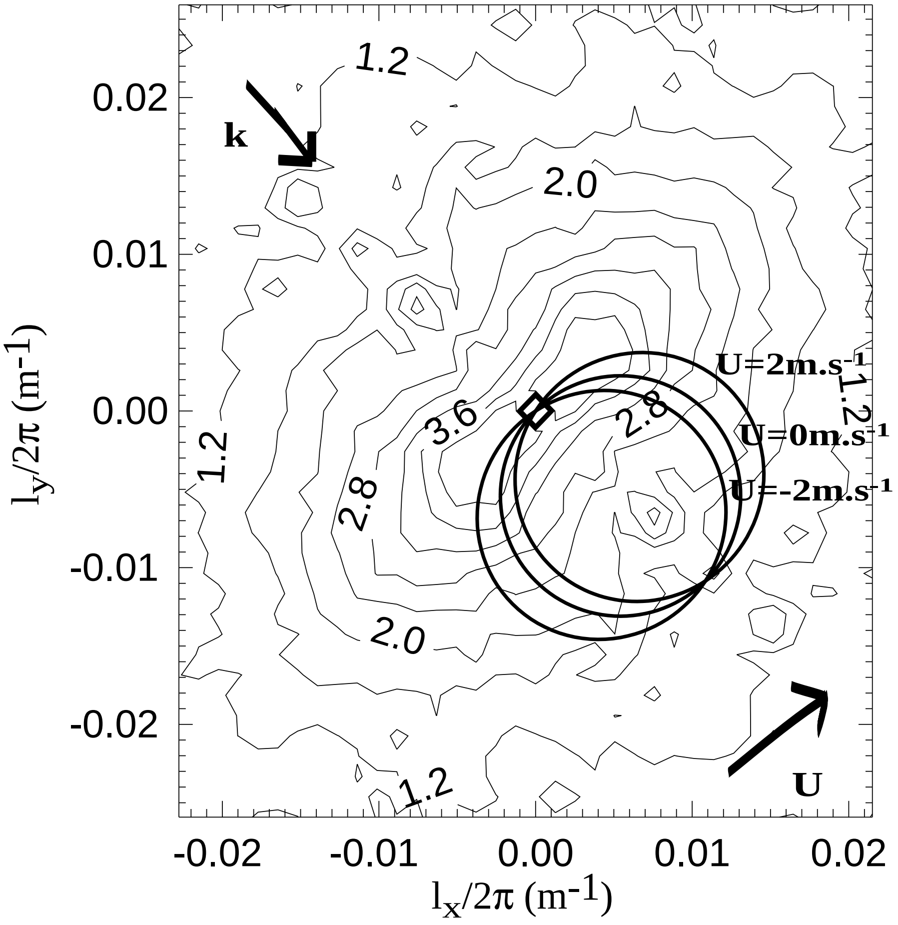

FIG. 7.9 – Same as figure 7.5 b, with circle and ellipses now indicating the bottom topography components that interact with waves arriving from the South-West with frequency 0.01 Hz, with ($U = \pm 2$ m/s) and without a South-West current.

relatively fast. This result should lead to the absence of wave spectra with directional spreads less than 25° in this area of the North Sea, except for strong refraction. The modelled mean directions are shifted towards to the North or to the West depending of the current sign, following the strength of the source term. No significant back scattering is found. At the end of the grid, the wave spectra are dramatically broadened(12° initially to about 40°). More specific to these cases is the shifted of the mean direction towards to the West, from 315 to 300° without current and 278° with current from the North-East.

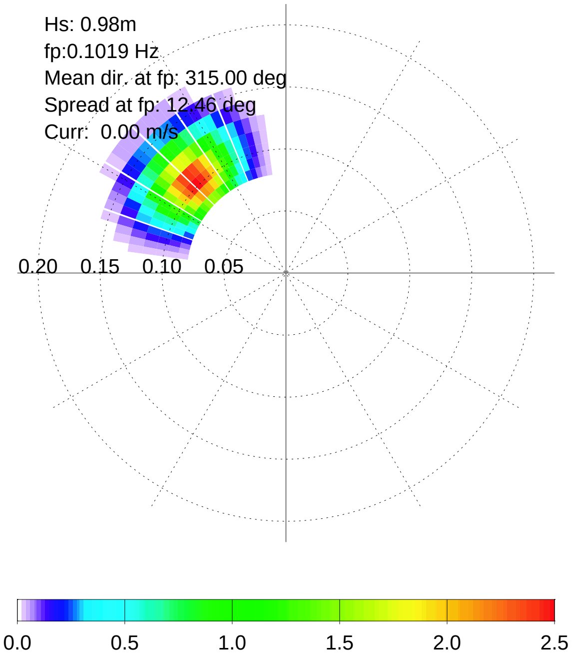

Fig. 7.10 – Incident surface spectrum.

7.5 Conclusion

The effect of a uniform current on the wave-bottom Bragg scattering was derived, extending the theory of Ardhuin & Herbers (2002). For deterministic 2D bathymetry such as a sinusoidal bottom and monochromatic waves, the source term converges to Mei's (1985) theory in absence of current and in the limit of the small bottom amplitudes. In the presence of a current, monochromatic wave results generally agree with Kirby's (1988) theory, but only converge in the limit of small Froude numbers. In two dimensions the main effect of a current is a Doppler-like shift of the resonant wave frequencies that undergo maximum reflection. For a given bottom topography this leads to a modification of the wave reflection coefficient that is sensitive to the

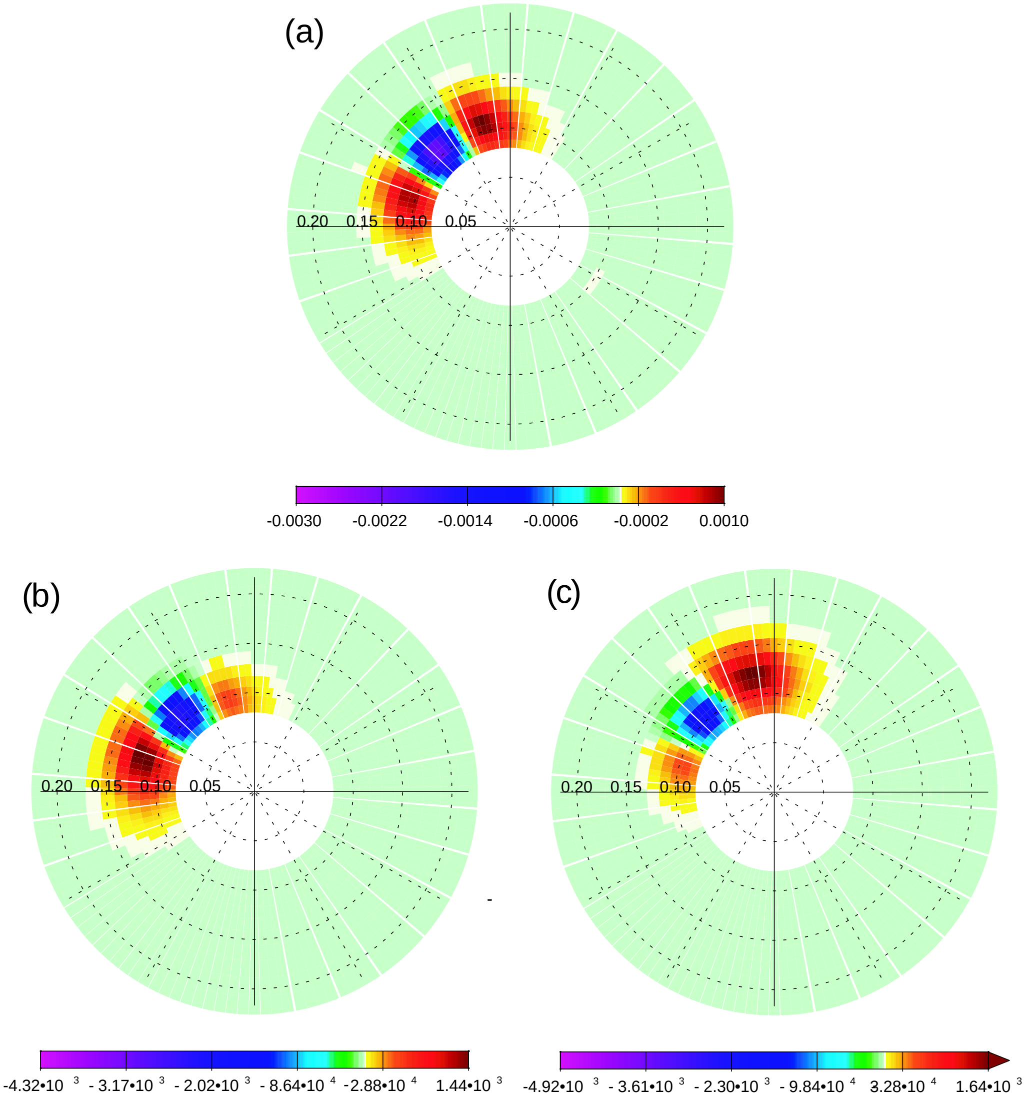

FIG. 7.11 – Source term corresponding to the incident surface spectrum, (a) $U = 0$, (b) $U = -2\text{m/s}$, (c) $U = 2\text{m/s}$.

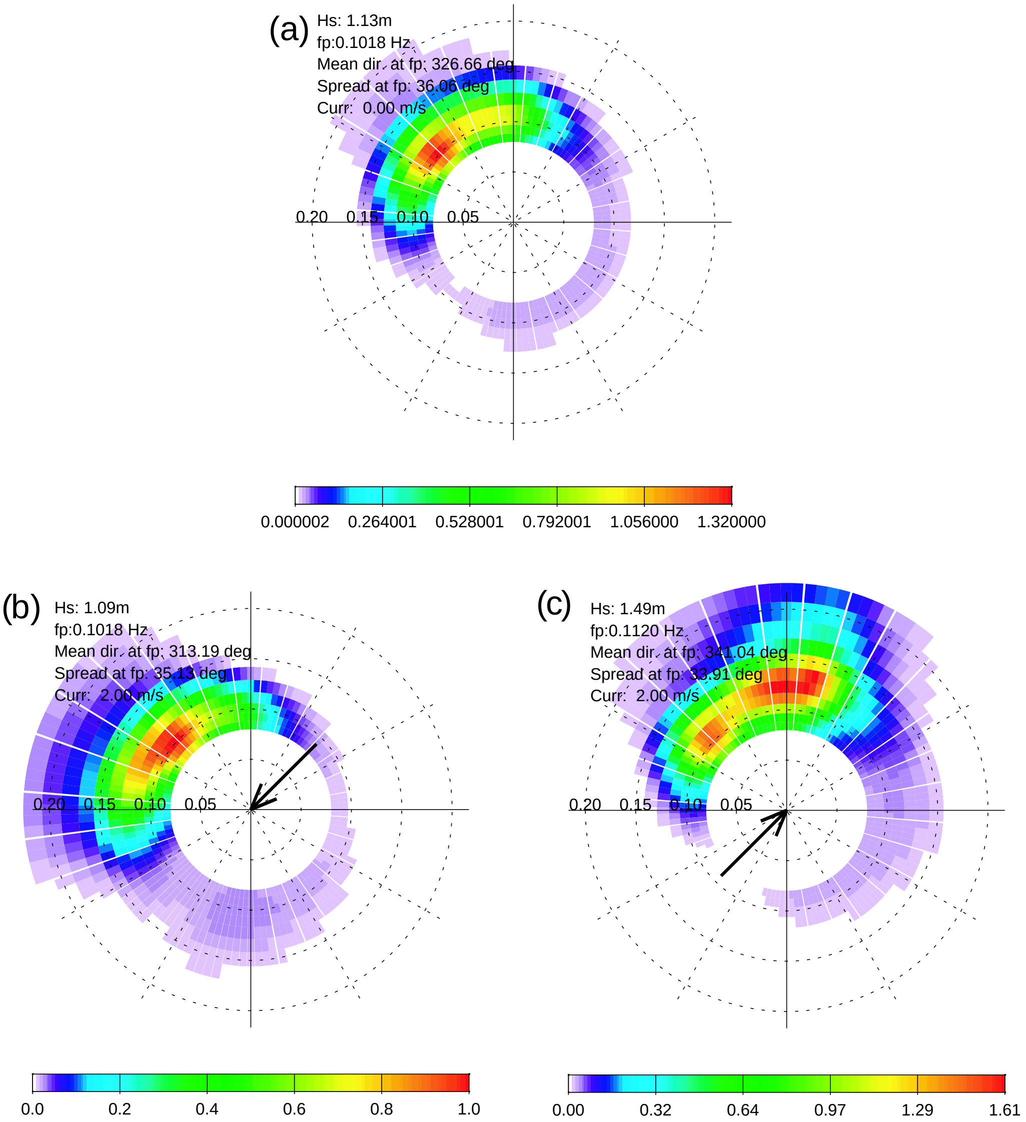

FIG. 7.12 – Surface spectra at the beginning of the grid (not the boundary point), (a) $U = 0$, (b) $U = -2\text{m/s}$, (c) $U = 2\text{m/s}$.

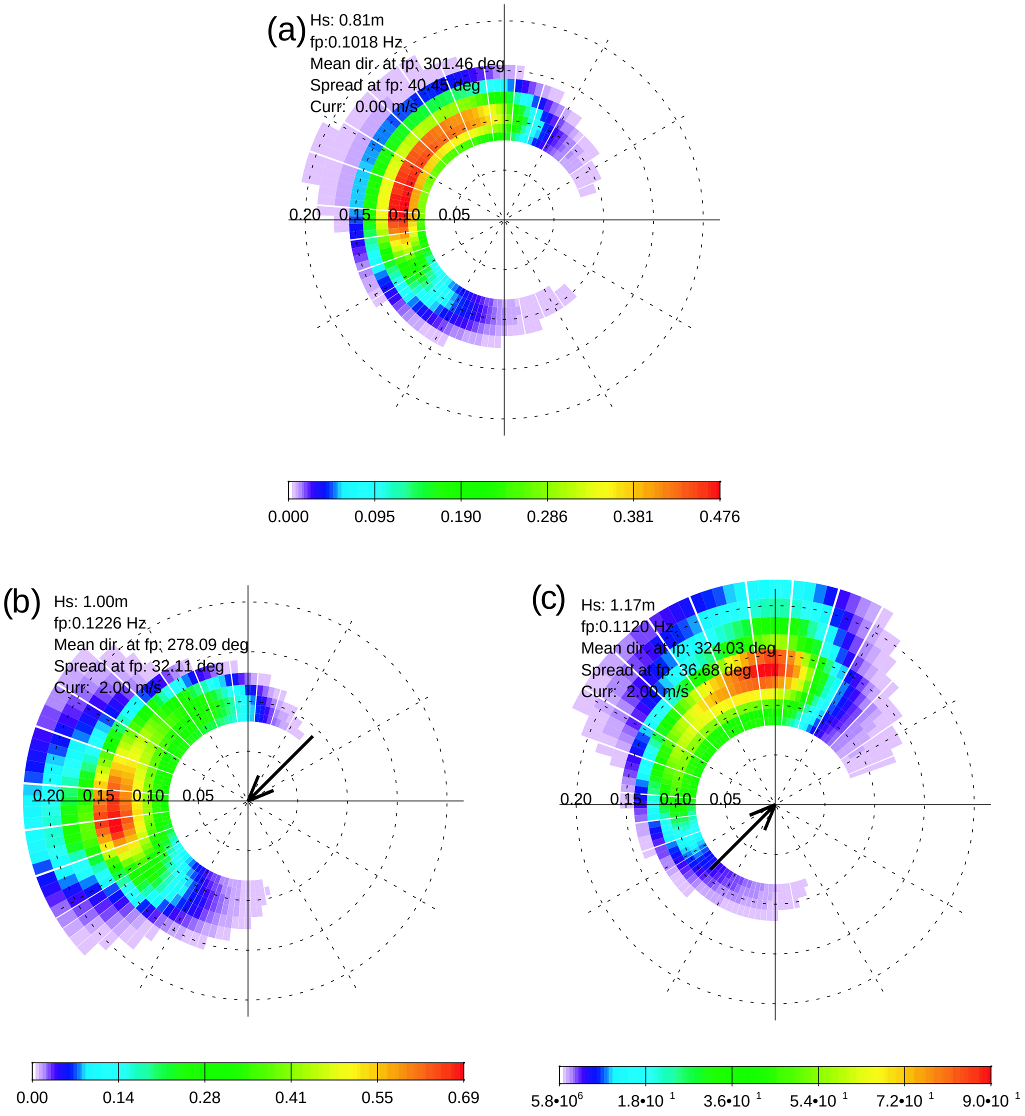

FIG. 7.13 – Surface spectra at the end of the grid , (a) $U = 0$, (b) $U = -2\text{m/s}$, (c) $U = 2\text{m/s}$.

current strength and direction. In these cases, the correlation of wave and bottom phases yields a negligible energy reflection, except for strong reflections.

In three dimension and over the shallow areas of the North Sea where large sand waves are found with strong tidal currents, wave scattering is expected to be significant and largely influenced by currents. Over natural topographies, the bottom typically de-correlates over scales shorter than the scattering-induced attenuation scales, so that the additional reflection due to a phase locking of the incident and reflected waves with the bottom may be neglected.

The wave scattering theory presented in this paper is thus one more piece in the puzzle of wave propagation over shallow continental shelves. Our representation of scattering as a source term in the action balance equation appears to be accurate in many conditions of interest and corresponds to the general use of phase-averaged models for engineering and scientific purposes when such large scales are involved. The alternative use of phase-resolving elliptic refraction-diffraction models (e.g. Berkhoff 1972 or Belibassakis et al. 2001), is much more expensive in terms of computer resources, and may not be much more accurate.

7.6 Acknowledgments

This research was supported by a joint grant from CNRS and DGA. Bathymetric data was acquired by the French Hydrographic and Oceanographic Service (SHOM). Discussions with Michael McIntyre, Kostas Belibassakis, Vincent Rey, and Thierry Garlan and gratefully acknowledged.

7.7 Appendix A. Harmonic oscillator equation for the second order potential

The harmonic oscillator equation (7.21) can be written as a linear superposition of equations of the type

$$\frac{d^2 f_1}{dt^2} + \omega^2 f_1 = \mathrm{e}^{\mathrm{i}\omega' t}. \tag{7.76}$$

In order to specify a unique solution to (7.76), initial conditions must be prescribed. In the limit of the large propagations distances, the initial conditions contribute a negligible bounded term to the solution. Following Hasselmann (1962), we choose $f_1(0) = 0$ and $df_1/dt(0) = 0$, giving the solution

$$f_1(\omega, \omega'; t) = \frac{\mathrm{e}^{\mathrm{i}\omega' t} - \mathrm{e}^{\mathrm{i}\omega t} + i(\omega - \omega') \sin(\omega t)/\omega}{\omega^2 - \omega'^2} \text{ for } \omega'^2 \neq \omega^2, \tag{7.77}$$

$$f_1(\omega, \omega'; t) = \frac{t\mathrm{e}^{\mathrm{i}\omega' t}}{2i\omega'} - \frac{\sin' \omega t)}{2i\omega' \omega} \text{ for } \omega' = \pm\omega \tag{7.78}$$

7.8 Appendix B. Harmonic oscillator equation and energy for the third order potential

Replacing ϕ_1 (7.18) in the surface boundary condition (7.42),

$$\left(\frac{d^2}{dt^2} + \sigma^2\right) \Phi^s_{2,\mathbf{k}}(t) = -gk\Phi^{si,s}_{2,\mathbf{k}} - \tanh(kH) \frac{\partial^2 \Phi^{si,s}_{2,\mathbf{k}}}{\partial t^2}, \tag{7.79}$$

and conserving only the non-bounded terms of $\Phi^s_{1,\mathbf{k}'}$, one obtains

$$\begin{aligned} &\frac{\partial^2 \Phi^{si,s}_{2,\mathbf{k}}}{\partial t^2} = \\ &-\sum_{\mathbf{k}',\mathbf{k}"} \frac{\mathbf{k}' \cdot \mathbf{k}}{k} \qquad \frac{\cosh(kH)}{\cosh(k'H)} M(\mathbf{k}', \mathbf{k}") G_{\mathbf{k}-\mathbf{k}'} G_{\mathbf{k}'-\mathbf{k}"} \Phi_{0,k"} \frac{\partial^2}{\partial t^2} \left(f_1(\sigma', \mathbf{k}'\mathbf{U} - s\omega")\mathrm{e}^{\mathrm{il.}\mathbf{U}t}\right). \end{aligned} \tag{7.80}$$

The amplitude $\Phi^s_{2,\mathbf{k}}$ satisfies a forced harmonic oscillator equation. Anticipating that only $k" = k$ will give a non-zero contribution due to the correlation $G_{\mathbf{k}-\mathbf{k}'} G_{\mathbf{k}'-\mathbf{k}"}$, we may simplify the notations in that equation as,

$$\left(\frac{\partial^2}{\partial t^2} + \sigma^2\right) \qquad \Phi^s_{2,\mathbf{k}}(t)$$

$$= \quad \sum_{\mathbf{k}'}\sum_{\mathbf{k}"} MM(\mathbf{k}',\mathbf{k}")G_{\mathbf{k}-\mathbf{k}'}G_{\mathbf{k}'-\mathbf{k}"}\Phi_{1,k"}f_1(\sigma',-\mathbf{l}'.\mathbf{U}-s\sigma")\mathrm{e}^{\mathrm{i}\mathbf{l}.\mathbf{U}t}, \tag{7.81}$$

with $\mathbf{l}'=(\mathbf{k}"-\mathbf{k}')\cdot\mathbf{U}$, and

$$M'=\frac{\mathbf{k}'\cdot\mathbf{k}}{k}\left[gk-\left(\sigma"^2-(\sigma'+\mathbf{l}.\mathbf{U})^2\right)\tanh(kH)\right]\frac{\cosh(kH)}{\cosh(k'H)}. \tag{7.82}$$

The second order potential potential amplitude must verify the equation

$$\left(\frac{d^2}{dt^2}+\sigma^2\right)\Phi^s_{2,\mathbf{k}}(t)=\sum_{\mathbf{k}'}\sum_{\mathbf{k}"} M'M(\mathbf{k}',\mathbf{k}")G_{\mathbf{k}-\mathbf{k}'}G_{\mathbf{k}'-\mathbf{k}"}\Phi_{0,k}f_1(\sigma',-\mathbf{l}'.\mathbf{U}-s\sigma")\mathrm{e}^{\mathrm{i}\mathbf{l}.\mathbf{U}t}, \tag{7.83}$$

thus we have to solve,

$$\left(\frac{d^2}{dt^2}+\sigma^2\right)f_2=f_1(\sigma',-\mathbf{l}'\cdot\mathbf{U}-s\sigma")\mathrm{e}^{\mathrm{i}\mathbf{l}.\mathbf{U}t}. \tag{7.84}$$

The solution f_2 may be written as

$$f_2=f_{2,a}+f_{2,b}, \tag{7.85}$$

where

$$f_{2,a}=-\frac{t\mathrm{e}^{-is\sigma"t}-\sin(\sigma"t)/\sigma"}{2is\sigma"\left[\sigma'^2-(\mathbf{l}'.\mathbf{U}+s\sigma")^2\right]}, \tag{7.86}$$

$$\begin{aligned} f_{2,b} \quad = \quad & -\frac{1}{2\sigma'(\sigma'-[\mathbf{l}'.\mathbf{U}+s\sigma"]))}\times \\ & \left[\frac{\mathrm{e}^{-i(\sigma'-\mathbf{l}'.\mathbf{U})t}}{\sigma"^2-(\sigma'-\mathbf{l}'.\mathbf{U})^2}-\frac{1}{2\sigma}\left(\frac{\mathrm{e}^{\mathrm{i}\sigma"t}}{\sigma"+(\sigma'-\mathbf{l}'.\mathbf{U})}+\frac{\mathrm{e}^{-i\sigma"t}}{\sigma"-(\sigma'-\mathbf{l}'.\mathbf{U})}\right)\right] \end{aligned} \tag{7.87}$$

The fourth order energy contribution from correlation between the first and third order velocity potential is given by,

$$F^{\Phi}_{2,0,\mathbf{k}}=F^{\Phi}_{0,2,\mathbf{k}}=2\langle\phi^+_{2,\mathbf{k}}\phi^-_{0,-\mathbf{k}}\rangle. \tag{7.88}$$

Then (7.81) becomes,

$$\frac{F^{\Phi}_{2,0,\mathbf{k}}}{\Delta\mathbf{k}}=\sum_{\mathbf{k}'}\sum_{\mathbf{k}''}M^2(\mathbf{k},\mathbf{k}')\frac{\langle G_{\mathbf{k}-\mathbf{k}'}G_{\mathbf{k}'-\mathbf{k}''}\rangle}{\Delta\mathbf{k}''}\frac{\langle\Phi^+_{1,\mathbf{k}}\Phi^-_{1,-\mathbf{k}}\rangle}{\Delta\mathbf{k}}\langle f_2\mathrm{e}^{\mathrm{i}\sigma t}\rangle\Delta\mathbf{k}''\Delta\mathbf{k}. \tag{7.89}$$

$$\langle f_2\mathrm{e}^{\mathrm{i}\sigma t}\rangle=\frac{\pi t}{8\sigma\sigma'}\delta\left[\sigma'-(\sigma''-\mathbf{l}''.\mathbf{U})\right]+O(1). \tag{7.90}$$

Changing the spectral coordinate from $\mathbf{k}''$ into σ'' and θ'' and taking the limit when $\Delta\mathbf{k} \rightarrow 0$, and anticipating that only $k'' = k$ gives a non null contribution from the bottom variance yields,

$$F^{\Phi}_{2,0}(t,\mathbf{k}) = -\int_{\mathbf{k}'}\int_{\mathbf{k}''}\frac{\pi t}{4\sigma''}M^2(\mathbf{k},\mathbf{k}')F^B(\mathbf{k}-\mathbf{k}')\frac{F^{\Phi}_{0,0}(\mathbf{k})}{\sigma'}\delta\left[\sigma' - (\sigma'' - \mathbf{l}''.\mathbf{U})\right]\mathrm{d}\mathbf{k}''d\mathbf{k}' + O(1). \tag{7.91}$$

$$F^{\Phi}_{2,0}(t,\mathbf{k}) = -\int_{\mathbf{k}'}\int_{\theta''}\int_{\sigma''}\frac{\pi t}{4\sigma''}M^2(\mathbf{k},\mathbf{k}')F^B(\mathbf{k}-\mathbf{k}')\frac{F^{\Phi}_{0,0}(\mathbf{k})}{\sigma'}\frac{k''}{C''_g}\delta\left[\sigma' - (\sigma'' - \mathbf{l}''.\mathbf{U})\right]\mathrm{d}\sigma''d\theta''d\mathbf{k}' + O(1). \tag{7.92}$$

$$F^{\Phi}_{2,0}(t,\mathbf{k}) = -\int_{\theta''}\frac{\pi t}{4\sigma''}M^2(\mathbf{k},\mathbf{k}')F^B(\mathbf{k}-\mathbf{k}')\frac{F^{\Phi}_{0,0}(\mathbf{k})}{\sigma'}\frac{k}{C_g}\mathrm{d}\theta'' + O(1). \tag{7.93}$$

$$F^{\Phi}_{2,0}(t,\mathbf{k}) = -\frac{\pi t}{4\sigma}\int_{\theta'}M^2(\mathbf{k},\mathbf{k}')F^B(\mathbf{k}-\mathbf{k}')\frac{F^{\Phi}_{0,0}(\mathbf{k})}{\sigma'}\frac{k'}{Cg}\frac{(Cg + \mathbf{k}.\mathbf{U})}{(Cg' + \mathbf{k}'.\mathbf{U})}\mathrm{d}\theta' + O(1). \tag{7.94}$$

7.9 Appendix C. Resonant wavenumber configuration for $U << C_g$

Under the assumption $U << C_g$, the resonant conditions

$$\sigma' - \sigma = l_x U = \Delta\sigma, \text{ and} \tag{7.95}$$

$$k' - k = \frac{\Delta k}{\Delta\sigma}\Delta\sigma + O(\Delta\sigma^2), \tag{7.96}$$

can be re-written as

$$k' - k = (k'_x - k_x)\frac{U}{C_g} + k\ O\left[\left(\frac{U}{Cg}\right)^2\right], \tag{7.97}$$

$$\frac{k - k'}{k_x - k'_x} = \frac{U}{C_g}. \tag{7.98}$$

We define, $r = k'$, $r_0 = k$, $r\cos\theta = k'_x$, with,

$$r = r_0 + \frac{U}{C_g}(r_0\cos\theta_0 - r\cos\theta), \tag{7.99}$$

$$r = \frac{r_0 + \frac{U}{C_g}r_0\cos\theta_0}{1 + \frac{U}{C_g}\cos\theta}, \text{ thus} \tag{7.100}$$

$$r = \frac{P}{1 + e\cos\theta}, \tag{7.101}$$

which is the parametric equation of an ellipse of semi-major axis a, semi-minor axis

b, c half the foci distance and eccentricity e, with, $P = r_0 + U/C_g r_0 \cos\theta_0 = b^2/a$ and $e = U/C_g = c/a$. The interaction between a surface wave with wavenumber $\mathbf{k}'$ and a bottom component with wavenumber $\mathbf{l}$ excites a surface wave with the sum wavenumber $\mathbf{k} = \mathbf{k}' + \mathbf{l}$. For a fixed $\mathbf{k}$ and current U, in the limit of $U << C_g$ the resonant $\mathbf{k}'$ and $\mathbf{l}$ follow ellipses described by their polar equation (7.101), that reduce to circle for $U = 0$.

Chapitre 8

Conclusion générale

Le travail présenté dans les chapitres précédents s'est concentré sur le phénomène de diffusion des vagues par une topographie sous-marine, faisant appel à différentes approches théoriques, avec confrontation à des données expérimentales et in situ.

Les prévisions de la diffusion des vagues par la topographie sous-marine, basées sur une équation spectrale d'évolution de l'énergie incluant un terme de source de diffusion de Bragg (Ardhuin et Herbers, 2002) sont comparées à une théorie déterministe, basée sur une décomposition du fond en marches successives avec continuité aux frontières (Rey, 1992). Pour de faibles amplitudes du fond, le terme de source est en accord avec la théorie déterministe pour un fond sinusoïdal modulé. Les résultats en réflexion de ce fond sont comparés à ceux d'un fond purement sinusoïdal et de même variance, calculé avec la méthode de Rey (1992). Dans la limite des faibles amplitudes du fond, les résultats sont identiques, confirmant que dans cette limite, la réflexion des vagues est entièrement déterminée par la variance du fond et ne dépend aucunement de la forme du fond. Ce résultat tient pour des fonds localisés comme une rampe ou une marche. Les travaux de Mei et Hancock (2003) confirment, que le terme de source, initialement dérivé pour des fonds aléatoires, est exact pour des fonds localisés, dans la limite des faibles amplitudes du fond. Le développement en perturbation à la base du terme de source utilise comme petit paramètre la pente du fond. Cependant, il semble que cette pente ne soit pas un facteur limitant, par contre l'amplitude du fond par rapport à la profondeur moyenne se révèle limiter l'application du terme de source. Pour une large gamme de topographies sous-marines rencontrées sur le plateau continental, le terme de source est une méthode précise et efficace pour représenter la diffusion des vagues dans les modèles de vagues spectraux en phase moyennée. Il serait intéressant de pousser l'expression analytique de ce terme aux ordres supérieurs pour surmonter certaines limitations comme les non-linéarités de surface, ou tout simplement pour pouvoir traiter des perturbations plus importantes.

Pour des variations topographiques plus marquées, ces approches en perturbations ne sont plus applicables. L'évolution des vagues au-dessus du Canyon sous-marin de Scripps, San Diego, Californie est étudiée dans le chapitre quatre. Des observations d'une longue houle sur ce canyon sont comparées à différents modèles de réfraction/diffraction, ainsi qu'au modèle couplé NTUA5 de Athanassoulis et Belibassakis (1999) et Belibassakis et al. (2001). NTUA5 et les modèles de réfraction/diffraction elliptiques ont tous mené à des résultats encourageants tandis que le modèle de réfraction/diffraction parabolique et le modèle de réfraction sur- et sous-estiment respectivement l'énergie des vagues en aval du canyon. Les différences entre ces modèles ont été clarifiées par des simulations 2D, en utilisant des profils transverses des Canyons de Scripps et La Jolla. La surestimation du modèle de réfraction peut être interprétée comme le résultat de diffraction ou de l'effet tunnel. Le modèle de réfraction prédit que toute l'énergie des vagues est piégée par le canyon pour des angles d'incidences élevés par rapport à la normale du canyon, alors qu'en réalité, une petite partie de l'énergie des vagues est transmise au-delà du canyon. Le modèle de réfraction/diffraction basé sur une approximation parabolique ne peut représenter des variations trop importantes du champ de vagues, ce qui mène à une sur-estimation de l'amplitude de l'onde transmise. Finalement, en fonction du profil du fond, les termes de pente du fond et de courbure, ainsi que les modes évanescents sont nécessaires pour une représentation correcte de la propagation des vagues au-dessus d'un canyon pour des angles d'incidences faibles.

L'effet du courant sur la réflexion des vagues par un fond sinusoïdal a été mis en évidence expérimentalement, pour des vagues régulières et irrégulières. Les théories de Rey (1992), incluant les modes évanescents et Kirby (1988), incluant les effets d'un courant ont été comparées aux résultats expérimentaux. Le décalage des fréquences résonantes dû au courant, ainsi qu'une légère amplification de la réflexion au niveau du pic principal de réflexion ont été prévus et observés. Cependant, l'amplitude de la réflexion diffère sensiblement entre les observations et les théories, suggérant un effet important de la réflexion de la plage, cumulé avec un effet de réfraction.

Le terme de source étudié dans le troisième chapitre, est étendu en présence de courant. Pour des bathymétries déterministes $2D$, comme des fonds sinusoïdaux, le terme de source donne des résultats en accord avec la théorie de Kirby en présence de courant, tant sur l'amplitude que sur le décalage en fréquence. Appliquée ensuite à des bathymétries réelles en Mer du Nord, caractérisées par des dunes sous-marines balayées par de forts courants, la théorie prévoit une diffusion des vagues très significative. Pour un spectre étroit ($\sigma_\theta = 12°$), la direction principale des vagues peut être décalée de 20 degrés, et l'étalement directionnel élargi de 30 degrés. Le courant agit comme un amplificateur ou un réducteur de ces phénomènes en fonction de sa direction et de son sens par rapport aux vagues et à la directionnalité du fond. Pour un couple $\mathbf{l}$ (nombre d'onde du fond), et $\mathbf{k}$ (nombre d'onde de surface) donné et sans courant, l'interaction résonante implique une composante $\mathbf{k}'$ qui diffuse le spectre (Fig .8.1a). Si on ajoute un courant dans le sens de propagation des vagues de composante $\mathbf{k}$, le nombre d'onde k est réduit, la diffusion s'oriente alors vers l'arrière, favorisant ainsi la réflexion des vagues (Fig.8.1b). Si on ajoute un courant opposé aux vagues (Fig.8.1c), le nombre d'onde k est amplifié, la diffusion des vagues s'oriente vers l'avant favorisant ainsi les interactions avec des composantes $\mathbf{k}'$ dans la direction des vagues incidentes (et du courant). L'étalement du spectre est réduit en se regroupant autour de la direction du courant. De manière plus générale, pour une fréquence de houle donnée, le courant modifie les composantes du fond interagissant de manière résonante. Ce décalage fait alors intervenir des niveaux de variances du fond pouvant être très différents en fonction du courant (figures 7.5 b et 7.9), ce qui favorise la diffusion dans des directions où la variance est la plus importante.

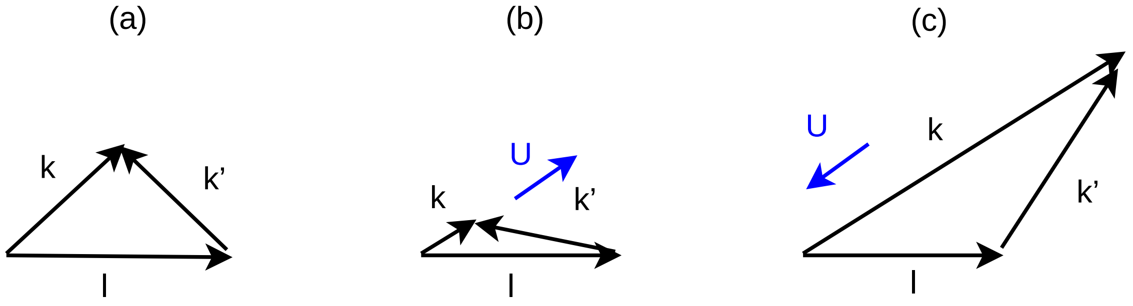

Fig. 8.1 – Influence du courant sur les interactions résonantes avec et sans courant

La diffusion des vagues par la topographie sous-marine a été étudiée dans cette thèse en confrontant plusieurs approches. L'importance de ce phénomène, largement influencé par le courant, a été mis en évidence pour des zones parsemées de dunes de sable et balayées par de forts courants de marée comme en Mer du Nord. Il est possible que cet effet ait échappé aux prévisionnistes qui accordent peu d'importance à l'étalement directionnel et parce que les modèles numériques présentent une diffusion artificielle qui peut en partie masquer le phénomène (Ardhuin et Herbers, 2005). L'approche spectrale, examinée et étendue en présence de courant via un terme de source, permet la représentation de la diffusion de Bragg dans les modèles de vagues spectraux, pour une large gamme de fonds présents sur le plateau continental, au même titre que les termes de source existants pour la génération des vagues par le vent, les interactions non-linéaires de vagues, la dissipation des vagues en surface et au fond. Une comparaison à des observations en Mer du Nord permettrait de valider en 3D le terme de source en présence de courant. De plus, l'étude de telles observations pourrait permettre de mieux comprendre l'atténuation de la houle observée en Mer du Nord, expliquée jusqu'à présent par le frottement au fond. Une partie importante de cette atténuation pourrait en fait être due au processus de diffusion des vagues tant au niveau des vagues rétro-diffusées qu'au temps de propagation allongé, accentuant le processus de friction par le fond. Cette forte diffusion agit également directement sur le comportement des vagues déferlant à la côte, favorisant un déferlement multi-pics à un déferlement uniforme suivant la crête des vagues. Ces effets sur le déferlement sont probablement à l'origine des différentes structures des barres d'avant plages obtenues, par modélisations numériques, avec différentes valeurs de l'étalement directionnel (Reniers et al., 2004). Cette approche spectrale permet de plus dans la limite des petites amplitudes du fond de représenter des fonds localisés, ce qui présente une alternative précise et efficace aux modèles déterministes. Le terme de source n'est cependant plus applicable pour des amplitudes du fond trop importantes relatives à la profondeur moyenne, comme l'illustre le cas du Canyon sous-marin de San Diego. Il est alors nécessaire d'utiliser des modèles déterministes capables de représenter la propagation des vagues pour des bathymétries aussi complexes et abruptes, sans négliger la réflexion des vagues, qui peut dans certains cas modifier la propagation des vagues au-dessus du canyon.

Bibliographie

Andrews D. G., McIntyre M. E. 1978 : On wave action and its relatives. *J. Fluid Mech.*, **89**,647–664 Corrigendum : vol. 95, p. 796

Ardhuin F., Herbers T. H. C. 2002 : Bragg scattering of random surface gravity waves by irregular seabed topography. *J. Fluid Mech.*, **451**,1–33

Ardhuin F., Herbers T. H. C. 2005 : Numerical and physical diffusion : Can wave prediction models resolve directional spread. *J. Atmos. Ocean Technol.* in press

Ardhuin F., Herbers T. H. C., Jessen P. F., O'Reilly W. C. 2003a : Swell transformation across the continental shelf. Part I : Attenuation and directional broadening. *J. Phys. Oceanogr.*, **33**,1921–1939

Ardhuin F., Herbers T. H. C., Jessen P. F., O'Reilly W. C. 2003b : Swell transformation across the continental shelf. Part II : Validation of a spectral energy balance equation. *J. Phys. Oceanogr.*, **33**,1940–1953

Ardhuin F., Herbers T. H. C., O'Reilly W. C. 2001 : A hybrid Eulerian-Lagrangian model for spectral wave evolution with application to bottom friction on the continental shelf. *J. Phys. Oceanogr.*, **31**(6),1498–1516

Ardhuin F., O'Reilly W. C., Herbers T. H. C., Jessen P. F. (2002) Spectral evolution of swell across the continental shelf. In : Proceedings of the 4th International Symposium Ocean Wave Measurement and Analysis. ASCE pp 744–753

Athanassoulis G. A., Belibassakis K. A. 1999 : A consistent coupled-mode theory for the propagation of small amplitude water waves over variable bathymetry regions. *J. Fluid Mech.*, **389**,275–301

Athanassoulis G., Belibassakis K. A., Georgiou Y. G. (2003) Transformation of the point spectrum over variable bathymetry regions. In : Proceedings of the 15th International Polar and Offshore Engineering Conference, Honolulu, Hawaii. ISOPE

Bailard J. A., Devries J. W., Kirby J. T. 1992 : Considerations in using Bragg reflection for storm erosion protection. *Journal of Waterway, Port, Coastal and Ocean Engineering*, **118**,62–74

Bailard J. A., Devries J. W., Kirby J. T., Guza R. T. (1990) Bragg reflection breakwater : a new shore protection method ? In : Proceedings of the 22th Coastal Eng. Conf. ASCE , New York, USA pp 1702–1715

Bal G., Chou T. 2002 : Capillary-gravity wave transport over spatially random drift. *Wave Motion*, **35**,107–124

Belibassakis K. A., Athanassoulis G. A., Gerostathis T. P. 2001 : A coupled-mode model for the refraction-diffraction of linear waves over steep three-dimensional bathymetry. *Applied Ocean Research*, **23**,319–336

Belzons M., Rey V. (1996) Dynamique de la redistribution d'un fond sédimentaire sous l'effet de nouvelles conditions de houle : une simulation de laboratoire. In : Actes des IVèmes Journées Nationales Génie Civil - Génie Côtier. , Dinard, France (in french) pp 69–76

Belzons M., Rey V., Guazzelli E. 1991 : Subharmonic bragg resonance for surface water waves. *Europhys. Lett.*, **16**,189–194

Benoit M. (1999) Extension de l'équation de réfraction-diffraction de berkhoff pour traiter des bathymétries rapidement variables. développement et validation d'un algorithme applicable aux cas mono-dimensionnels pour une houle linéaire. Technical Report HE-42/99/049/A Département Laboratoire National d'Hydraulique, Electricité de France

Berkhoff J. C. W. (1972) Computation of combined refraction-diffraction. In : Proceedings of the 13th international conference on coastal engineering. ASCE , Vancouver, Canada pp 796–814

Biesel F. 1950 : Etude théorique de la houle en eau courante. *La houille blanche*, **Numéro spécial A**,279–285

Booij N. 1983 : A note on the accuracy of mild-slope equation. *Coastal Engineering*, **7**,191–203

Booij N., Ris R. C., Holthuijsen L. H. 1999 : A third-generation wave model for coastal regions. 1. model description and validation. *J. Geophys. Res.*, **104**(C4),7,649–7,666

Brevik I., Aas. B. 1980 : Flume experiments on waves and currents, I. Rippled bed. *Coastal Engineering*, **3**,149–177

Chamberlain P. G., Porter D. 1995 : The modified mild slope. *J. Fluid Mech.*, **291**,393–407

Chandrasekara C. N., Cheung K. F. 1997 : Extended linear refraction-diffraction model. *Journal of Waterway, Port, Coastal and Ocean Engineering*, **123**(5),280–286

Chandrasekara C. N., Cheung K. F. 2001 : Linear refraction-diffraction model for steep bathymetry. *Journal of Waterway, Port, Coastal and Ocean Engineering*, **127**(3),161–170

Chao Y.-Y., Pierson W. J. 1958 : Experimental studies of the refraction of uniform wave trains and transient wave groups near a straight caustic. *J. Geophys. Res.*, **77**(24),4545–4554

Dalrymple R. A., Kirby J. T. 1986 : Water waves over ripples. *Journal of Waterway, Port, Coastal and Ocean Engineering*, **112**(2),309–319

Dalrymple R. A., Kirby J. T. 1988 : Models for very wide-angle water waves and wave diffraction. *J. Fluid Mech.*, **192**,33–50

Dalrymple R. A., Knoght R., Lambiase J. 1978 : Bedforms and their hydraulic stability relashionship in a tidal environement, bay of Fundy, Canada. *Nature*, **275**,100–104

Dalrymple R. A., Suh K. D., Kirby J. T., Chae J. W. 1989 : Models for very wide-angle water waves and wave diffraction. Part 2. Irregular bathymetry. *J. Fluid Mech.*, **201**,299–322

Davies A. 1980 : Some interactions between surface water waves and ripples and dunes on the seabed. *Inst. Oceanogr. Sci. Rep.*, p 108

Davies A. 1982 : The reflection of water-wave energy by undulations on the seabed. *Dynamics of Atmos. and Oceans*, **6**,207–232

Davies A. G., Heathershaw A. D. 1984*a* : Surface-wave propagation over sinusoidally varying topography. *J. Fluid Mech.*, **144**,419–443

Davies A., Heathershaw A. 1984*b* : Surface-wave propagation over sinusoidally varying topography. *J. Fluid Mech.*, **144**,419–443

Dobson R. S. (1967) Some applications of a digital computer to hydraulic engineering problems. Technical Report 80 Department of Civil Engineering, Stanford University

Dyer K. R., Huntley D. A. 1999 : The origin, classification and modelling of sand banks and ridges. *Continental Shelf Research*, **19**,1285–1330

Elfouhaily T. M., Guérin C.-A. 2004 : A critical survey of approximate scattering wave theories from random rough surfaces. *Waves in Random Media*, **14**,1–40

Elgar S., Raubenheimer B., Herbers T. H. C. 2003 : Bragg reflection of ocean waves from sandbars. *Geophys. Res. Letters*, **30**(1,1016),1–4

Elter J. F., Molyneux J. E. 1972 : The long-distance propagation of shallow water waves over an ocean of random depth. *J. Fluid Mech.*, **53**,1–15

Fredsøe J. 1974 : Rotational channel flow over small three-dimensional bottom irregularities. *J. Fluid Mech.*, **66**,49–66

Gelci R., Cazalé H., Vassal H. 1957 : Prévision de la houle, la méthode des densités spectroangulaires. *Bulletin d'information du Comité central d'Océanographie et d'Etude des Côtes*, **9**,416–435

Gerostathis T. (2004) Wave propagation in the nearshore/coastal environment using models appropriate for parallel processing. PhD thesis National Technical University of Athens

Guazzelli E., Rey V., Belzons M. 1992 : Higher-order Bragg reflection of gravity surface waves by periodic beds. *J. Fluid Mech.*, **245**,301–317

Hara T., Mei C. C. 1987 : Bragg scattering of surface waves by periodic bars : theory and experiment. *J. Fluid Mech.*, **178**,221–241

Hasselmann K. 1962 : On the non-linear energy transfer in a gravity-wave spectrum. *J. Fluid Mech.*

Hasselmann K. 1966 : Feynman diagrams and interaction rules of wave-wave scattering processes. *Rev. Geophys.*, **4**,1–32

Heathershaw A. D. 1982 : Seabed-wave resonance and sand bar growth. *Nature*, **296**,343–345

Heathershaw T. H. C., Hendrickson E. J., O'Reilly W. C. 2000 : Propagation of swell across a wide continental shelf. *J. Geophys. Res.*, **105**(C8),19729–19737

Herbers T. H. C., Orzech M., Elgar S., Guza R. T. 2003 : Shoaling transformation of wave-frequency directional spectra. *J. Geophys. Res.*, **108**(C1),3013 doi :10.1029/2001JC001304

Hulscher S. J. M. H., van den Brink G. M. 2001 : Comparison between predicted and observed sand waves and sand banks in the north sea. *J. Geophys. Res.*, **106**(C5),9327–9338

Idier D., Erhold A., Garlan T. 2002 : Morphodynamique d'une dune sous-marine du détroit du pas de calais. *Comptes rendus Géosciences*, **334**,1079–1085

Kim J. W., Bai K. J. 2004 : A new complementary mild slope equation. *J. Fluid Mech.*, **511**,25–40

Kirby J. T. 1986 : A general wave equation for waves over rippled beds. *J. Fluid Mech.*, **162**,171–186

Kirby J. T. 1986a : Higher-order approximations in the parabolic equation method for water waves. *J. Geophys. Res.*, **91**(C1),933–952

Kirby J. T. 1988 : Current effects on resonant reflection of surface water waves by sand bars. *J. Fluid Mech.*, **186**,501–520

Kirby J. T., Anton J. P. (1990) Bragg reflection of waves by artificial bars. In : Proceedings of the 22th Coastal Eng. Conf. ASCE , New York, USA pp 757–768

Kirby J. T., Chen T.-M. 1989 : Surface waves on vertically sheared flows : approximate dispersion relations. *J. Geophys. Res.*, **94**(C1),1013–1027

Kirby J. T., Dalrymple R. A. 1983*a* : Propagation of obliquely incident water waves over a trench. *J. Fluid Mech.*, **133**,47

Kirby J. T., Dalrymple R. A. 1983*b* : Propagation of obliquely incident water waves over a trench. *J. Fluid Mech.*, **133**,47–63

Knaapen M. A. F., Hulscher S. J. M. H. 2002 : Regeneration of sand waves after dredging. *Coastal Engineering*, **46**,277–289

Lee C., Park W. S., Cho Y., Suh K. D. 1998 : Hyperbolic mild-slope equations extended to account for rapidly varying topography. *Coastal Engineering*, **34**,243–257

Lee C., Yoon S. B. 2004 : Effect of higher-order bottom variation terms on the refraction of water waves in the extended mild slope equation. *Ocean Engineering*, **31**,865–882

Liu Y., Yue D. K. P. 1998 : On generalized Bragg scattering of surface waves by bottom ripples. *J. Fluid Mech.*, **356**,297–326

Long B. 1973 : Scattering of surface waves by an irregular bottom. *J. Geophys. Res.*, **78**(33),7,861–7,870

Longuet-Higgins M. S. 1957 : On the transformation of a continuous spectrum by refraction. *Proceedings of the Cambridge philosophical society*, **53**(1),226–229

Longuet-Higgins M. S. 1967 : On the trapping of wave energy around islands. *J. Fluid Mech.*, **29**,781–821

Lygre A., Krogstad H. E. 1986 : Maximum entropy estimation of the directional distribution in ocean wave spectra. *J. Phys. Oceanogr.*, **16**,2,052–2,060

Magne R., Ardhuin F., Herbers T. H. C., Rey V. 2005 : Topographical scattering of waves : a spectral approach. *J. Waterway, Port, Coastal and Ocean Eng.* in press. Available at http ://arxiv.org/abs/physics/0504148

Mahony J. J. 1967 : The reflection of short waves in a variable medium. *Quart. Appl. Math.*, (25),313–316

Massel S. R. 1993 : Extended refraction-diffraction equation for surface waves. *Coastal Eng.*, **19**,97–126

McWilliams J. C., Restrepo J. M., Lane E. M. 2004 : An asymptotic theory for the interaction of waves and currents in coastal waters. *J. Fluid Mech.*, **511**,135–178

Mei C. C. 1985 : Resonant reflection of surface water waves by periodic sandbars. *J. Fluid Mech.*, **152**,315 –335

Mei C. C. (1989) *Applied dynamics of ocean surface waves.* second edn World Scientific, Singapore 740 p.

Mei C. C., Black J. L. 1969 : Scattering of surface waves by rectangular obstacles in water of finite depth. *J. Fluid Mech.*, **38**,499 –515

Mei C. C., Hancock M. J. 2003 : Weakly nonlinear surface waves over a random seabed. *J. Fluid Mech.*, **475**,247–268

Meyer R. 1979 : Surface wave reflection by underwater ridges. *J. Phys. Oceanogr.*, **9**,150–157

Miles J. W. 1967 : Surface-wave scattering matrix for a shelf. *J. Fluid Mech.*, **28**,755–767

Munk W. H., Arthur R. S. 1952 : Wave intensity along a refracted ray. *Gravity Wave, U.S Nat. Bur. Stand.*, (Circ. 521),95–109

Munk W. H., Traylor M. A. 1947 : Refraction of ocean waves : a process linking underwater topography to beach erosion. *The Journal of Geology*, **LV**,1

Neuman J. N. 1965a : Propagation of water waves over a infinite step. *J. Fluid Mech.*, **23**,399–415

Neuman J. N. 1965b : Propagation of water waves past long two-dimensional obstacles. *J. Fluid Mech.*, **23**,23–30

O'Hare T. J., Davies A. G. 1992 : A new model for wave propagation over rapidly-varying bottom topography. *Coastal Engineering*, **18**,256–266

O'Hare T. J., Davies A. G. 1993 : Sand bar evolution beneath partially-standing waves : laboratory experiments and model simulations. *Continental Shelf Res.*, **13**,1149–1181

O'Hare T. J., Davies A. G. 1993a : A comparison of two models for wave propagation over rapidly-varying topography. *Applied Ocean Research*, **15**,1–11

O'Hare T. J., Davies A. G. 1993b : Sand bar evolution beneath partially-standing waves : laboratory experiments and model simulations. *Continental Shelf Res.*, **13**,1149–1181

O'Reilly W. C., Guza R. T. 1991 : Comparison of spectral refraction and refraction-diffraction wave models. *J. Waterway, Port, Coastal and Ocean Eng.*, **179**(3),199–215

O'Reilly W. C., Guza R. T. 1993 : A comparison of two spectral wave models in the Southern California Bight. *Coastal Engineering*, **19**,263–282

Peak S. D. (2004) Wave refraction over complex nearshore bathymetry. Master's thesis Naval Postgraduate School, Monterey

Phillips O. M. 1960 : On the dynamics of unsteady gravity waves of finite amplitude. Part1. *J. Fluid Mech.*, **9**,193–217

Phillips O. M. (1977) *The dynamics of the upper ocean.* Cambridge University Press, London 336 p.

Pihl J., Mei C. C., Hancock M. 2002 : Surface gravity waves over a two-dimensional random seabed. *Physical Review E*, **66**,016611

Porter D., Staziker D. J. 1965 : Extensions of the mild-slope equation. *J. Fluid Mech.*, **300**,367–382

Priestley M. B. (1981) *Spectral Analysis and Time series.* Academic Press, London 890 p.

Radder A. C. 1979 : On the parabolic equation method for water wave propagation. *J. Fluid Mech.*, **95**(1),159–176

Rayleigh L. (1896) *The theory of sound.* third edn Macmillan, London 890 p.

Reniers A. J. H. M., Roelvink J. A., Thornton E. B. 2004 : Morphodynamic modeling of an embayed beach under wave group forcing. *J. Geophys. Res.*, **109**,C01030 doi :10.1029/2002JC001586

Rey V. 1992 : Propagation and local behaviour of normally incident gravity waves over varying topography. *Eur. J. Mech. B,Fluids*, **11**,213–232

Rey V. 1995 : A note on the scattering of obliquely incident surface gravity waves by cylindrical obstacles in water of finite depth. *Eur. J. Mech., B/Fluids*, **14**(2),207–216

Rey V., Belzons M., Guazzelli E. 1992 : Propagation of surface gravity waves over a rectangular submerged bar. *J. Fluid Mech.*, **235**,453–479

Rey V., Capobianco R., Dulou C. 2002 : Wave scattering by a submerged plate in presence of a steady uniform current. *Coastal Engineering*, **47**(1),27–34

Rey V., Guazzelli E., Mei C. C. 1996 : Resonant reflection of surface gravity waves by one-dimensional doubly sinusoidal beds. *Phys. Fuids*, **8**(6),1525–1530

Richter K., Schmalfeldt B., Siebert J. 1976 : Bottom irregularities in the North Sea. *Deut. Hydrogr. Z.*, **29**,1–10

Schmitt T., Mitchell N. C., Ramsay A. T. S. (2004) Sediment transport pattern of two nearshore sandbanks inferred from time-lapse surveying of sand dunes. In :

MARID 2004, $2nd$ international workshop on Marine Sandwave and River Dune Dynamics. Service Hydrographique et Océanographique de la Marine pp 270–274

Smith R., Sprinks T. 1975 : Scattering of surface waves by a conical island. *J. Fluid Mech.*, **77**,373–384

Suh K. D., Lee C., Park W. S. 1997 : Time-dependent equations for wave propagation on rapidly varying topography. *Coastal Engineering*, **32**,91–117

Takano K. 1960 : Effets d'un obstacle parallélépipédique sur la propagation de la houle. *Houille Blanche*, **15**,247

Thomson J., Elgar S., Herbers T. 2005 : Reflection and tunnelling of ocean waves observed at a submarine canyon. *Geophysical Research Letters* in press.

Tolman H. L. (2002) User manual and system documentation of WAVEWATCH-III version 2.22. Technical Report 222 NOAA/NWS/NCEP/MMAB

Weber N. 1991 : Bottom friction for wind sea and swell in extreme depth-limited situations. *J. Phys. Oceanogr.*, **21**,149–172

White B. S. 1999 : Wave action on currents with vorticity. *J. Fluid Mech.*, **386**,329–344

Yu J., Mei C. C. 2000 : Do longshore bars shelter the shore. *J. Fluid Mech.*, **404**,251–268